Universidade de Aveiro
2024

Joana Nogueira Lagarinhos

Matrizes termoplásticas para componentes automóveis processados por T-RTM

Thermoplastic matrices for autoparts by T-RTM processing

2024

Universidade de Aveiro
2024

Joana Nogueira Lagarinhos

Matrizes termoplásticas para componentes automóveis processados por T-RTM

Thermoplastic matrices for autoparts by T-RTM processing

Tese apresentada à Universidade de Aveiro para cumprimento dos requisitos necessários à obtenção do grau de Doutor em Ciência e Engenharia de Materiais, realizada sob a orientação científica do Doutor José Martinho Marques de Oliveira, Professor Coordenador sem Agregação da Escola Superior de Design, Gestão e Tecnologias do Produção de Aveiro-Norte da Universidade de Aveiro.

Thesis submitted to the University of Aveiro for fulfilment of the necessary requirements leading to the Doctoral degree in Science and Materials Engineering, carried out under the scientific supervision of Doctor José Martinho Marques de Oliveira, Coordinator Professor without Aggregation of the School of Design, Management and Production Technologies, Aveiro North from the University of Aveiro.

Para o meu Pai,
que já não teve forças para me ver chegar até aqui.

Wherever you are, hope you are proud.

o júri

presidente

Prof.ª Doutora Susana Isabel Barreto de Miranda Sargento
Professora Catedrática da Universidade de Aveiro

vogais

Prof.ª Doutora Ana Vera Alves Machado Nóbrega
Professora Associada com Agregação da Universidade do Minho

Prof. Doutor Pedro Nuno Neves Lopes Simões
Professor Auxiliar da Universidade de Coimbra

Prof. Doutor Pedro Miguel Gonçalves Martinho
Professor Adjunto do Instituto Politécnico de Leiria

Prof. Doutor Vítor João Gomes da Silva Sencadas
Professor Auxiliar da Universidade de Aveiro

Prof. Doutor José Martinho Marques de Oliveira
Professor Coordenador da Universidade de Aveiro

agradecimentos

Gostaria de agradecer, em primeiro lugar, à minha família, pelo exemplo de trabalho e sem os quais isto não seria possível. Ao meu Pai, que apesar de já não estar connosco, sei que me ajudou a chegar até aqui. Tenho a certeza de que estás orgulhoso. À minha Mãe e à minha Irmã, pela paciência e por me terem ajudado a nunca desistir e a ir atrás dos meus sonhos.

Ao Professor Martinho, orientador deste trabalho de doutoramento, pela oportunidade e pelo conhecimento científico transmitido no decurso deste trabalho. Agradeço a boa disposição que prevaleceu ao longo destes anos e pela amizade.

Ao Grupo Simoldes pelo financiamento deste trabalho de doutoramento e sem os quais este trabalho não seria possível.

À Sara Silva agradeço todos os incentivos na busca pelo conhecimento e pelo encorajamento para fazer mais e melhor. Obrigada pela tua ajuda e apoio que foram fundamentais para a conclusão deste trabalho. A todos os colegas e funcionários da ESAN que se cruzaram comigo neste caminho, deixo um agradecimento pelo vosso apoio e companheirismo.

Ao João, não há palavras para descrever o teu apoio incondicional, paciência e amor. Obrigada por teres sido o meu porto seguro nos momentos mais difíceis e por me teres ajudado a ultrapassar todas as adversidades que comigo se cruzaram durante este percurso.

Aos meus amigos de Seia, Coimbra e Lisboa, que direta ou indiretamente me acompanharam neste caminho que escolhi para mim. Muitas vezes estiveram demasiado tempo longe da vista, mas nunca do coração. Uma palavra de carinho e agradecimento por fazerem parte da minha vida.

Ser-vos-ei eternamente grata! Um grande obrigada!

palavras-chave

poliamida 6, polimerização aniónica, *in situ*, T-RTM, materiais à base de grafeno, industria automóvel.

resumo

Hoje, a redução de emissões poluentes provenientes, nomeadamente aquelas provenientes do setor automóvel, é crucial. Uma solução eficaz para diminuir o consumo de combustível e, consequentemente, reduzir as emissões de dióxido de carbono (CO_2) é a redução de peso dos veículos. Nesse sentido, a indústria automóvel tem procurado soluções envolvendo compósitos, nomeadamente de matriz polimérica, como parte da estratégia para criar soluções inovadoras e ambientalmente mais sustentáveis.

As matrizes de natureza termoplástica são frequentemente utilizadas no desenvolvimento de compósitos envolvendo a incorporação de partículas e/ou de fibras curtas. A combinação de matrizes termoplásticas reforçadas com fibras longas exigiu novas tecnologias de moldação, nomeadamente aquelas que envolvem a moldação líquida. Esta tese focou-se no estudo e desenvolvimento de uma matriz termoplástica para processamento por moldação líquida de material termoplástico (T-RTM). Adicionalmente, foi estudado o efeito da adição de nanoplaquetas de grafeno (GNP) a esta matriz e o seu impacto nas propriedades físico-químicas dos nanocompósitos desenvolvidos. Com o objetivo de validação das formulações transformadas por T-RTM, foi ainda desenvolvido um protótipo de um componente automóvel.

Face à importância que a poliamida 6 (PA6) tem na tecnologia T-RTM, estudou-se a preparação e caracterização da PA6 por meio da polimerização aniónica por abertura de anel (AROP) do monómero ε-caprolactama (CL), com a adição do catalisador e ativador. Destacou-se a importância da escolha das matérias-primas, da formulação e da temperatura e tempo de polimerização, e como esses fatores afetam as propriedades finais da PA6.

O efeito da adição de nanoplaquetas de grafeno (GNP), de diferentes tamanhos, nas propriedades finais do compósito foi também estudado. As nanopartículas tendem a aglomerar, pelo que a seleção do método de homogeneização é uma das etapas críticas no desenvolvimento de nanocompósitos. Neste trabalho, o método selecionado envolveu o recurso a ultrassons e os resultados indiciam que as GNP podem atuar como agentes nucleantes na matriz PA6. Para baixas concentrações de GNP, os nanocompósitos obtidos apresentaram melhorias nas propriedades térmicas e mecânicas. No último capítulo é apresentado um estudo de caso baseado no desenvolvimento de um componente automóvel, de geometria tridimensional, com recurso aos parâmetros de processamento por T-RTM, anteriormente otimizados. As peças obtidas apresentaram boa qualidade embora se reconheça que é necessário melhorar o equipamento protótipo, de forma a permitir a aplicação de pressões mais elevadas que proporcionem produtos mais compactados.

Este trabalho contribuiu para incrementar o conhecimento sobre a tecnologia T-RTM, no sentido da sua consolidação como tecnologia alternativa para o processamento de materiais compósitos para a indústria, e em particular para o setor automóvel.

keywords

Polyamide 6, anionic polymerization, *in situ*, T-RTM, graphene-based materials, automotive industry.

abstract

Today, the reduction of pollutant emissions, especially those from the automotive sector, is crucial. An effective solution to decrease fuel consumption and, consequently, reduce carbon dioxide (CO_2) emissions is the reduction of vehicle weight. In this regard, the automotive industry has been seeking solutions involving composites, particularly those with a polymeric matrix, as part of the strategy to create innovative and environmentally more sustainable solutions.

Thermoplastic matrices are often used in the development of composites involving the incorporation of particles and/or short fibres. The combination of thermoplastic matrices reinforced with long fibres has required new moulding technologies, particularly those involving liquid moulding. This thesis focused on the study and development of a thermoplastic matrix for processing through Thermoplastic Resin Transfer Moulding (T-RTM). Additionally, the effect of adding graphene nanoplatelets (GNP) to this matrix and their impact on the physicochemical properties of the developed nanocomposites was studied. To validate the formulations transformed by T-RTM, a prototype of an automotive component was developed.

Given the importance of polyamide 6 (PA6) in T-RTM technology, the preparation and characterization of PA6 through anionic ring-opening polymerization (AROP) of the ε-caprolactam (CL) monomer, in the presence of a catalyst and an activator, were investigated. The importance of raw material selection, formulation, temperature, and polymerization time and how these factors affect the final properties of PA6 were highlighted.

The effect of adding GNP of different sizes on the final properties of the composite was investigated. Nanoparticles tend to aggregate, so the selection of the dispersion method is one of the critical steps in the development of nanocomposites. In this work, the selected method involved the use of ultrasonic, and the results indicate that GNP can act as nucleating agents in the PA6 matrix. For low GNP concentrations, the obtained nanocomposites showed improvements in thermal and mechanical properties.

The last part of this work presents a case study based on the development of a three-dimensional automotive component using the previously optimized T-RTM processing parameters. The parts obtained showed good quality, although it is acknowledged that it is necessary to improve the prototype equipment to allow the application of higher pressures for more compact products.

This work contributed to increasing knowledge about T-RTM technology, intending to consolidate it as an alternative technology for processing composite materials for the industry, particularly in the automotive sector.

Table of contents

List of Tables

List of Figures

Abbreviations

ABS	Acrylonitrile-butadiene-styrene
AROP	Anionic Ring-Opening Polymerization
BET	Brunauer-Emm-Teller
C1	ε-caprolactam magnesium bromide or Bruggolen® C1
C10	Sodium caprolactamate in ε-caprolactam or Bruggolen® C10
C20P	Hexamethylene-1,6-dicarbamoylcaprolactam in ε-caprolactam or Bruggolen® CP20
CBT	Cyclic Butylene Terephthalate
CF	Carbon Fibre
CL	ε-caprolactam
CLMgBr	ε-caprolactam Magnesium Bromide
CNC	Computer numerical control
CO_2	Carbon dioxide
DC	Conversion degree
DLS	Dynamic Light Scattering
DOC	Degree of Conversion
DOE	Design of experiments
DSC	Differential scanning calorimetry
DTG	Derivative thermogravimetric
EEA	European Environment Agency
EU	European Union
FRP	Fibre-reinforced Polymers
GBM	Graphene-based materials
GF	Glass Fibre
GNP	Graphene Nanoplatelets
ILO	International Labour Organization
LCM	Liquid Composite Moulding
LL	ω-laurolactam
LRI	Liquid Resin Infusion
NaCL	Sodium Caprolactamate
OEM	Original Equipment Manufacturer
PA	Polyamide
PA12	Polyamide 12
PA6	Polyamide 6
PBN	Polybuthylene naphhtalate

PBT	Polybutylene terephthalate
PC	Polycarbonate
PE	Polyethylene
PEEK	Polyetheretherketone
PEK	Polyetherketone
PEN	Polyethylene naphthalate
PES	Polyethersulfone
PET	Polyethylene terephthalate
PMMA	Polymethylmethacrylate
PP	Polypropylene
PPS	Polyphenylene sulfide
PS	Polystyrene
PU	Polyurethane
RIM	Resin Transfer Moulding
RIP	Reaction Injection Moulding
ROP	Ring-opening Polymerization
RSM	Response Surface Method
RTM	Resin Transfer Moulding
SEM	Scanning Electron Microscopy
SRIM	Structural Reaction Injection Moulding
TGA	Thermogravimetric analysis
TPU	Thermoplastic Polyurethane
T-RTM	Thermoplastic Resin Transfer Moulding
VARTM	Vacuum Assisted Resin Transfer Moulding
XRD	X-ray diffraction

Chapter 1

Framework

This chapter is a portrait of this work, motivated by a concern to reduce weight, costs and carbon footprint in automotive plastic parts.

1.1 Introduction

On December 12th 2015, 196 countries adopted the Paris Agreement to climate protection, to increase the global response to the climate change threat[1]. The goal of the agreement was to limit global warming to below 2 degree Celsius (°C), preferably to 1.5 °C, when compared to pre-industrial levels. In order to achieve these ambitious goals, the European Commission developed the European Green Deal[2]. The Green Deal is a set of strategies that aims to turn Europe the first continent to become carbon neutral by 2050. To this end, several measures are needed to be implemented in the areas of energy, industry, buildings and mobility, to reduce greenhouse gas emissions and increase resource efficiency[3].

The automotive sector is responsible of ≈25% for the carbon dioxide (CO_2) emissions in the European Union (EU). To achieve the Green Deal target, the automotive sector should reduce CO_2 emissions by 90% (compared to 1990 levels)[4].

In 2019, a passenger car showed an average emission of 122 g CO_2/km, 1 g CO_2/km higher than 2018, and 2g CO_2/km higher than 2017. However, this scenario was drop to 107 g CO_2/km in 2020, a decrease of 12% in a single year (Figure 1.1)[3].

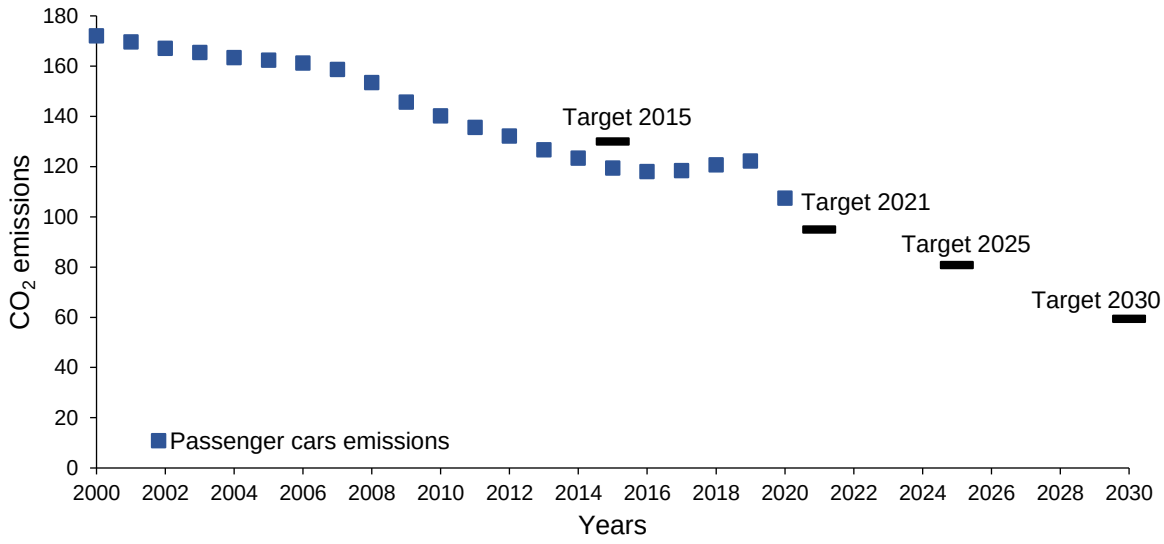

Figure 1.1 Evolution of CO_2 emissions from passenger cars per year, and emissions target for 2015 and 2021. Modified from reference 5.

The EU defined the emission limit target of 95 gCO_2/km to 2024 for new vehicles and the targets for 2025 and 2030 were also defined[6]. With sets stricter, EU defined a percentage reduction from 15% in 2025 on and 37.5% reduction from 2030 on[7]. Furthermore, each Member State is claimed should track data for each new passenger car registered to regulate CO_2 emissions, and excess emissions penalties were imposed on car manufacturers that do not meet these specific targets. Along with tightened regulation on emission pollutions, the automotive industry needs to increase efficiency in the vehicles it produces.

As a result of the regulatory constraints and an increase of the environmental awareness, the vehicle manufacturers have been pressured to take different strategies to have cars with high fuel efficiencies and low carbon footprint to abide by the strict vehicle emission standards.

Green car concepts have been emerging to increase fuel efficiency with the vision to achieve the strict CO_2 emission regulations. Toward producing more sustainable vehicles, automotive manufacturers have progressively invested in research and development for alternative fuel such as biodiesel, natural gas, hydrogen, and liquefied petroleum gas. New advanced powertrain technologies – fuel cell vehicle, hybrid electric vehicle, and plug-in hybrid electric vehicles – are also gaining prominence[8].

Electric vehicles have attracted widespread interest because of their ability to reduce energy consumption and emissions. When it comes to fully electric vehicle drive technology, the weight of the car is one crucial parameter to be considered for increasing the mileage of the battery. This can be achieved through usage of more lightweight plastics and compact space-saving structures made out of plastics and their composites[9].

According to a European Environment Agency (EEA) report, electric cars are clearly preferable to petrol or diesel cars, once emit less greenhouse gases and air pollutants over their entire life cycle[10]. The emissions are usually higher in the electric cars production phase, but these are more than offset over their lifetime. However, there seems to be a lot of doubts if this cars produce less CO_2 emissions that internal combustion engine vehicles, considering that the actual manufacturing as well as the disposing of battery electric vehicle, is less environmentally friendly than that of an internal combustion engine. Battery electric vehicles are not 100% clean, and probably, no vehicle never will be, but they are clearly a better choice for the environment, as no produce tailpipe emissions of air pollutants like nitrogen oxides and particles that affect the air quality[11]. For a battery electric vehicle to be truthfully accounted as producing zero emissions after manufacturing, is necessary to understand at where the energy that charges the vehicle comes from. Is the vehicle being charged with fossil fuel energy or renewable energy, it almost defeats the entire purpose of these new environmentally friendly vehicles[12].

Despite the emergence of these alternatives, higher production costs and the slow shift to new energy resources have hindered widespread adoption in the industry[13]. For this reason, manufacturers have focused on reducing the overall vehicle weight. Previous studies have shown the great potential of reducing fuel consumption through vehicle mass reduction, that lead to a reducing in their gaseous emissions[14–16].

Due to their lightness and rigidity, plastic composites have emerged in automotive industry as an alternative strategy, capable of maintaining the same mechanical properties of traditional composites, and at the same time, demonstrating environmental advantages and improvements on energy efficiency[17,18].

In this context, the present PhD thesis deals with the manufacturing of a thermoplastic material obtained from its precursor, as a preliminary approach towards lighter, cheaper, and more environmentally friendly automotive interior parts.

1.2 Plastics in automotive industry

The use of plastics in automotive sector is increasing rapidly and is estimated that automotive industry is the third largest consumer of the plastics globally[19]. Its use in a car body represents a weight reduction up to 35% lighter than aluminium and 60% lighter than steel, and an overall vehicle weight reduction of up to 10%[20]. The high absorption properties of plastics also allow the vehicle to meet stricter safety standards, while the use of engineering plastics allows for minimization of the mass of parts used in vehicles as they offer more design freedom compared to metals[21]. Plastic materials also offer the possibility to be formed in almost any shape, size, or colour.

The composition of a car has changed considerably in past decades, and consequently, car's weight has also been changing slightly. Until 1980s, the use of plastics in cars was less than 10%. Nowadays, the contribution of plastics materials is around 12-15% in a vehicle (representing 150-200 kg considering a total vehicle weight of ≈ 1300kg)[22]. In 2018, the automotive industry, was the third biggest plastic consumer in Europe[23].

A car is made of a huge variety of materials, ranging from glass and metals to plastic composites (Figure 1.2). Metals make a significant part of the vehicle weight; therefore, research efforts are underway to develop new advanced high-strength steels and aluminium to decrease parts' thickness and consequently, their weight. However, the use of such alternatives, possess disadvantages like the environmental impact, high costs and mechanical performance[20,24].

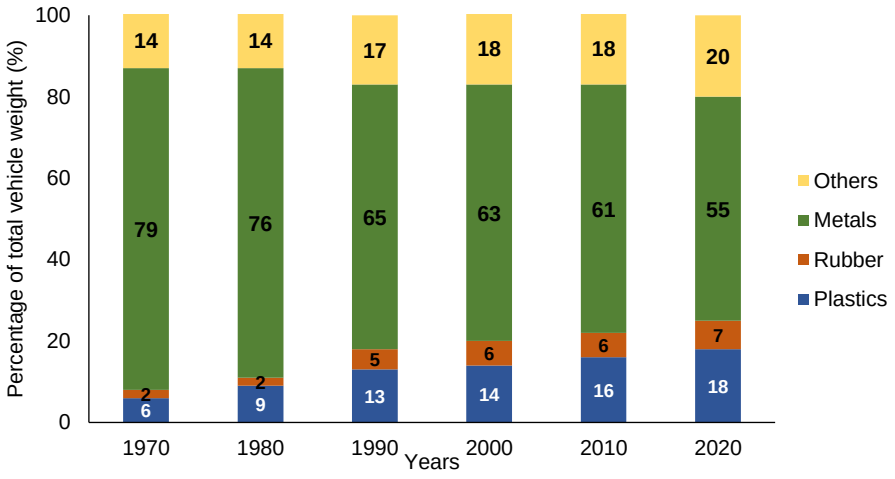

Figure 1.2 Materials distribution in a vehicle from 1970 to 2020. Adapted from reference 22.

Automotive producers are continuously focused on producing cost-effective lightweight vehicles by changing vehicle design and by using more advanced lightweight materials to replace conventional steels.

The gradual replacement of metal parts by plastic parts is always driven by the needs for reducing vehicle weight, increasing safety during an accident compared to an all-steel frame and are high performance materials (design freedom, flexibility in integrating components, comfort, and potential recyclability and composability)[21]. Initially, plastics were mainly used for interior finishing. Nowadays,

they are also used for exterior car parts, traditionally applied for steel and metal, such as fenders, bonnets, doors and even bumpers[25].

The application of different plastics in automobiles varies significantly due to the performance and the properties of the polymers. The contribution of different plastic materials used in automotive industry is shown in Figure 1.3.

Among different plastics used, polypropylene (PP) is by far the most employed polymer in automotive industry, followed by polyurethane (PU), polyamide (PA) and acrylonitrile-butadiene-styrene (ABS)[26]. As PP has a relatively good specific mechanical properties and low cost, is suitable for a wide range of applications, such as bumpers, wheel housings or defrost air channels. PU presents higher flexibility and is mainly used as flexible and rigid foams for seat cushions or impact energy absorbers. PA is an engineering polymer that combines excellent mechanical and thermal properties, and chemical resistance. It is mainly applied to replace metals in engine covers and electrical components. ABS is applied for aesthetic purposes due to the possibility to be painted and chromed. It is widely applied in interior panels and trims due to its reasonable dimensional stability, thermal and impact resistance[21]. Based on its final application and part performance requirements, the plastics are used in different ways: unfilled, glass fibre (GF), carbon fibre (CF), natural, coloured and so on.

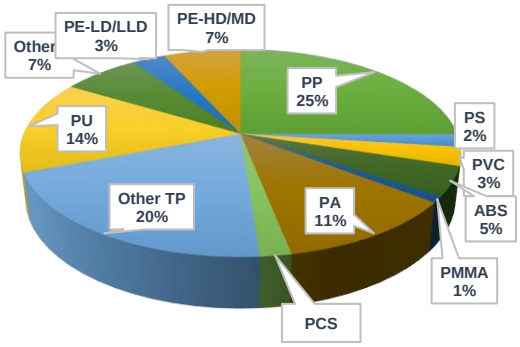

Figure 1.3 Percentages by weight of plastic materials used in cars per polymer type. Modified from 26.

Regarding to vehicle parts, plastic materials are predominantly employed in interior body of automobile, due to main aspects like, styling, surface quality, passenger comfort and safety, which are aspects that can be easily fulfilled by polymers. PP with talk particles or glass fibres are present in structural parts, while ABS or blended with polycarbonate (PC/ABS) are employed in parts with aesthetics functions. Typical exterior parts made of plastics are door handles (PC, polybutylene-terephthalate (PBT), or mirror housings (ABS, PC/ABS). Once car exterior is subjected to higher mechanical loads and environmental conditions, their production with thermoplastics is less common. Engineering plastics like PA or PBT are used surrounding the engine instead of metals, due to higher temperature stability, resistance to corrosive fluids and durability maintaining the surface properties[16,21].

Automotive plastics parts can be manufactured using different technologies, such as extrusion, injection moulding, thermoforming, rotational moulding, casting, compression moulding and resin transfer moulding (RTM)[27].

Innovative manufacturing technologies are needed to implement new materials strategies and to enable the production of lightweight parts. In that respect, Thermoplastic Resin Transfer Moulding (T-RTM) is an emergent liquid composite moulding technology and an evolution of the traditional low-pressure RTM. When compared with RTM technology, materials obtained through T-RTM technology can be produced in shorter cycle times. Due to the fast-chemical anionic polymerization reaction that characterize it, this technology can be employed for mass production of lighter composites. Due to the ease of production of lightweight composites and the fact that the final composite can be cheaper and recyclable, T-RTM is considered a promising technology.

The continuous development of plastic materials and technologies will further lead to lighter, higher performance, and more sustainable solutions. However, the increasing use of plastics shifts the environmental problem from the use phase of an automotive to the end of life vehicle stage (materials disposal). Whether light solutions lead in an overall reduction in environmental impact, the lightweight solutions would break even with negative end of life environmental impact. Even with the greenhouse emissions reduction, it is important to address and understand the end of life scenario and how the use of plastics in automotive sector can be truly[28,29].

One solution is to gradually increase the use of recycled plastics, although the recovery processes need to be improved to be more efficient and obtain high-quality end products at a cost that can compete with primary raw material prices. A major challenge concern the separation of different components of parts. The plastics parts used in automotive industry such as dashboards, bumpers and casings are mostly injection moulded. The recycling challenge here is that parts containing fillers such as glass or carbon fibres or plastic blend as well as two- or multi-component injection moulded parts are used, and thus is difficult to liberate for recycling[30].

Awareness of the automotive sector and commitment to technological innovation is moving towards sustainability in their products by introducing more sustainable approaches like recycled and natural materials in automotive parts to achieve their worn sustainability goals and target set by EU circular economy strategy[29,31]. Cars manufactures are actively seeking solutions that make automotive plastics economically recyclable. In the last couple of decades, the transition to bioplastics have begun. In light of dwindling fossil resources, the unpredictability of oil prices, and the need for more cost and fuel effective vehicles, bioplastics are hailed as also one of the best replacement materials for plastics[32,33].

Bioplastics can provide countless advantages in industry, including better recyclability, so the end-of-life process for vehicles made from bioplastic materials can yield other product and reduction in cost of manufacturing[34]. For instance, Lexus aims to make 95% of its cars recoverable and is exploring a range of new materials, including those produced from renewable plant sources, such as sweet potato, maize and sugarcane[35]. Jaguar Land Rover is exploring the opportunities to upcycle domestic waste plastic otherwise destinated for landfill or incinerators through chemical recycling.

This process can allow to transform end-of-life plastics into oil that can be used instead of virgin material to create a plastic product of comparable quality[36].

Overall, it is possible to note that the transformations in automotive industry will keep moving forwards to conserve the environment via a lowered carbon footprint. By 2030, it is expected plastics to be the preferred materials for automotive applications[37].

1.3 Simoldes overview

The automotive sector in Portugal is composed by 32.200 companies that produces automobiles and components. This sector accounts for 11% of total exports from Portugal and is a key performer in Portuguese economy, with national importance for employment and exports[38].

The automotive components industry in Portugal has grown 200% over the past 15 years and currently, is supplying carmakers with batteries, glass, plastic moulds, interiors, tires, metal works, cables and harnesses, car seats and electronics.

Portuguese moulds industry has been growing and consolidating its reputation in the international markets, driven by external demand, integrated competences and capabilities, as innovative solutions, which offers to its clients.

Simoldes Group was founded in 1959. This company comprises more than 20 companies, in 15 different countries, whose business is based into two distinct divisions – the production of moulds for plastic injection (Simoldes Tool division) and the production of plastic injection parts (Simoldes Plastic division). Currently, the turnover is in the order of 805 million euros, with over 6000 employees worldwide. Furthermore, Simoldes is among the world's leading manufacturers of moulds, particularly in the area of injection moulds for plastics (8th worldwide, 3rd in Europe)[39].

Simoldes Plastic division is responsible for the injection of the plastic into the mould, producing the final components that are sent to assemblers. With more than 30 years of experience, the company is able to develop products that make the mould making process easier, and the mainstream of revenues comes from this division[39].

Simoldes Plastics is one of the few companies in Europe able to support and produce for the automotive industry, being the main Original Equipment Manufacturer (OEM): Stellantis - former PSA, (Citroen, Peugeot, DS Automobiles, Opel), Renault Nissan Mitsubishi, VW Group (Volkswagen, Audi, Porsche, Seat, Skoda), BMW, Toyota, Scania, and Mercedes-Benz.

The company produces a wide variety of products for interior and exterior parts. Examples for interior parts are door panels, trunk, roof and seat components, trims, floor consoles, speed levers and dashboard components. For exterior parts the company produce flaps, side protector, door sash, bumper components, under covers, rood bar support and many others[39].

Research and development activities are a fundamental pillar for Simoldes (with 2.25% of turnover in R&D investment), which has allowed it to present innovative solutions in the market where it operates, resulting in sustained growth and market conquest, as well as in the broadening the knowledge and skills. As an international reference manufacturer of components for the automotive industry, it is faced with new challenges and opportunities arising from compliance with various

European directives and other more developed geographies related to the environmental sustainability of processes and products.

Thus, the technological objective from Simoldes refer to assert itself on the international scene as a leader in a process of innovation and development in new materials and processing technologies for the automotive industry. Besides it, Simoldes Plastics intends to acquire knowledge in new materials and technologies that allow the development of structural components. The company is committed to developing new products as well as ensuring their quality to continue to grow and respond to market challenges.

1.4 Thesis scope and outline

The initial work started in 2016 within the SIM T-RTM project. This project has been conducted with the collaboration between ESAN – University of Aveiro and Simoldes Plásticos SA, whose main aim was the development of new thermoplastic matrix composites and their transformation by the T-RTM process, to respond to the demands of the automobile market and, above all, to the world directives regarding sustainability, recyclability, and energy efficiency.

The aim of this thesis is to contribute towards the development of affordable high rate manufacturing processes with thermoplastic materials and their manufacturing technologies, through T-RTM technology. In this sense, the specific objectives of this work are:

1. Materials innovation – to develop polyamide (PA6) thermoplastic material from anionic polymerization of PA6 precursor (ε-caprolactam) as matrix, and graphene nanoplatelets as reinforcement using T-RTM technology. To the best of our knowledge, reactive processing of PA6 with graphene nanoplatelets through T-RTM, has never worked and represents the main motivation of this work;
2. Innovation in the T-RTM manufacturing process – technology and processing parameters optimization for future industrial production of structural components of the automobile;
3. Product innovation – to manufacture a prototype of an automotive bodywork component by T-RTM process, with a class A finish perspective, lighter, and equal mechanical performance when compared to the reference (composed by metal);

This thesis also has the objective of the economic strategy valorisation of the results and their impact for Simoldes Plastics. The company, as an international reference manufacturer of components for the automotive industry, is faced with new challenges arising from EU guidelines to respond to principal OEM. Thus, the outcomes that could be accomplish through this research work will be:

1. Increase company portfolio – This work will be a starting point for an expansion of thermoplastic components that Simoldes Plastics already supplies for automotive industry. The new materials will have the potential to replace body components previously produced in steel or aluminium;

2. Potentially competing solutions - Currently, the bodywork components remain mostly in steel and aluminium. However, there is a broad agreement in the scientific community that the potential gain in terms of density (and therefore weight reduction) will be much higher with composite materials produced by T-RTM technology;

3. New application sector – In addition to the automotive sector, Simoldes Plastics also identifies the aeronautical industry as a relevant future application sector;

4. New Markets – The geographic markets will be, essentially, those that are currently explored by Simoldes Plastics, following the geography of implantation of the industrial units of the main OEM customers of the company. Most relevant geographic markets: Spain, Portugal, Germany, Czech Republic, France, Poland, and United Kingdom. Most relevant clients: Stellantis Group, VW Group, Renault and Nissan;

5. Forefront R&D – With this work, the company will be at the forefront of T-RTM technology and producing components in advanced composite materials. Thus, Simoldes Plastics will aim to position itself in the market of thermoplastic components with a position of world technological leadership in terms of components in advanced composite materials processed by T-RTM, in terms of weight reduction and increased recyclability;

6. Brand new business – Based on current knowledge and given the expectation regarding the evolution of T-RTM technology, Simoldes Plastics admit that within 5 years will be able to create a new Business Unit, to produce and commercialize components obtained through T-RTM technology.

Combining both scientific and technological purposes, and to fulfil the objectives of this research work, the chapters of the dissertation are organized as follows (Figure 1.4):

- Chapter 1 describes the context and motivation of this dissertation;
- In Chapter 2, a literature review on reactive processing thermoplastic materials highlighting the advantages of reactive processing over more traditional methods is explained. The working principles required for suitable liquid composite moulding technologies are also included. Based on this review, strategies and objectives are also defined;
- Chapter 3 deals with the manufacturing parameters of the selected material, PA6, using a laboratorial T-RTM equipment. Different processing parameters on polymeric matrix are discussed;
- Chapter 4 focuses on testing procedures to manufacture PA6 with graphene-based materials recurring to T-RTM technology. The effect of graphene-based materials on the polymerization of PA6 is analyzed;
- Chapter 5 investigates the performance of the developed materials through the production of an automotive prototype;
- In Chapter 6, the main findings of the study are summarized, and future recommendations are provided.

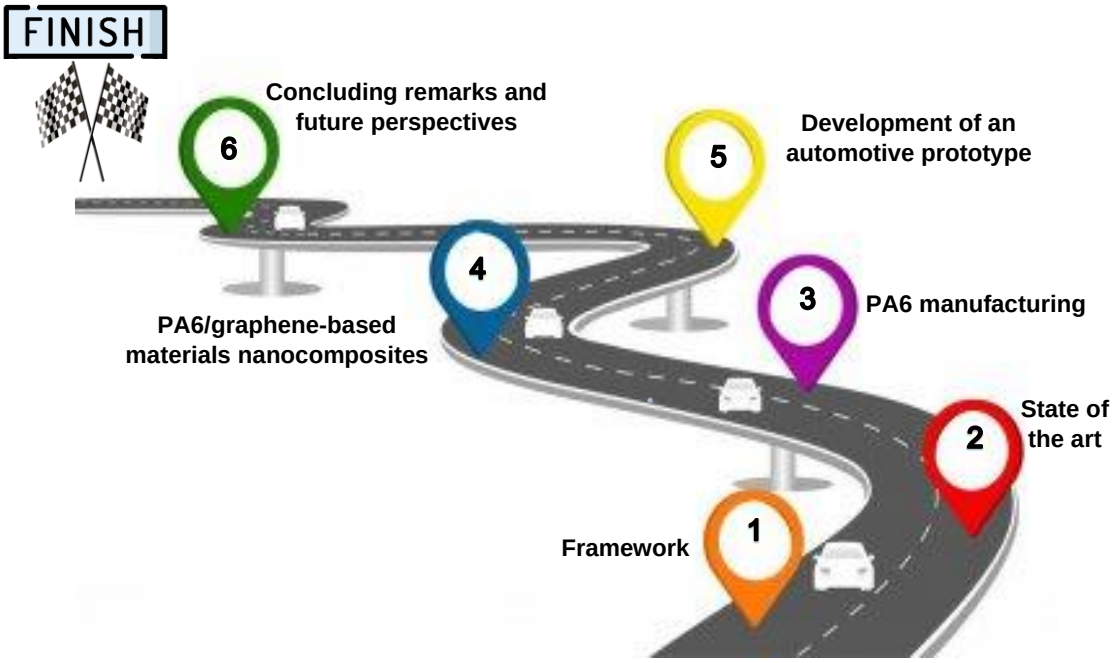

Figure 1.4 PhD roadmap with chapters.

References

1. Paris Agreement. United Nations Framework Convention on Climate Change. https://unfccc.int/process-and-meetings/the-paris-agreement/the-paris-agreement (2015).
2. Plan, A. Communication from the Commission to the European Parliament, the Council, the European Economic and Social Committee and the Committee of the Regions. *European Commission* (2011).
3. European Parliament. Regulation (EU) 2019/631 of the European Parliament and of the Council of 17 April 2019 setting CO2 emission performance standards for new passenger cars and for new light commercial vehicles, and repealing Regulations (EC) No 443/2009 and (EU) No 510/201. *Off. J. Eur. Union* **111**, 13–53 (2019).
4. European Commission. Sustainable and Smart Mobility Strategy. https://transport.ec.europa.eu/transport-themes/mobility-strategy_pt (2020).
5. European Environment Agency (EEA). *Monitoring CO2 Emissions from New Passenger Cars and Vans in 2017*. (2018).
6. Balakrishnan, V. S. & Seidlitz, H. Potential repair techniques for automotive composites: A review. *Composites Part B: Engineering* **145**, 28–38 (2018).
7. European Parliament. Regulation (EU) 2019/631 - Setting CO2 Emission Performance Standards for New Passenger Cars and for New Light Commercial Vehicles. *European Union Law. Available online: https://eur-lex. europa. eu/legal-content* (2019).
8. Panoutsou, C. *et al.* Advanced biofuels to decarbonise European transport by 2030: Markets, challenges, and policies that impact their successful market uptake. *Energy Strategy Reviews* **34**, 100633 (2021).
9. Shaheen, S. A. & Lipman, T. E. Reducing greenhouse emissions and fuel consumption: Sustainable approaches for surface transportation. *IATSS research* **31**, 6–20 (2007).
10. Pridemore, A. , *et al. Electric Vehicles from Life Cycle and Circular Economy Perspectives*. (2018).
11. Unterstaller, A. Electric vehicles: smart choice for the environment. *European Environment Agency* (2019).

12. Sergey Paltsev. *Are Electric Cars 'Green'? The Answer Is Yes, but It's Complicated*. (2021).
13. Fouquet, R. The slow search for solutions: Lessons from historical energy transitions by sector and service. *Energy policy* **38**, 6586–6596 (2010).
14. Friedrich, H. & Schumann, S. Research for a "new age of magnesium" in the automotive industry. *J Mater Process Technol* **117**, 276–281 (2001).
15. Koffler, C. & Rohde-Brandenburger, K. On the calculation of fuel savings through lightweight design in automotive life cycle assessments. *Int J Life Cycle Assess* **15**, 128–135 (2010).
16. Mallick P. Advanced materials for automotive applications: an overview. in *Advanced materials in automotive engineering* vol. 2 5–26 (Elsevier, 2012).
17. Volpe, V. *et al.* Lightweight High-Performance Polymer Composite for Automotive Applications. *Polymers* **11**, (2019).
18. Patil, A., Patel, A. & Purohit, R. An overview of polymeric materials for automotive applications. *Materials Today: Proceedings* **4**, 3807–3815 (2017).
19. Todor, M.-P. & Kiss, I. Systematic approach on materials selection in the automotive industry for making vehicles lighter, safer and more fuel–efficient. *Applied Engineering Letters* **1**, 91–97 (2016).
20. Pervaiz, M., Panthapulakkal, S., Sain, M., & Tjong, J. Emerging trends in automotive lightweighting through novel composite materials. *Materials Sciences and Applications* **7**, 26 (2016).
21. Davies, G. Materials for consideration and use in automotive body structures. in *Materials for automobile bodies* vol. 3 93–143 (Butterworth-Heinemann, 2012).
22. Emilsson, E. & Dahllöf, L. Plastics in passenger cars - A comparison over types and time. *IVL Swedish Environmental Research Institute Ltd* **454**, (2019).
23. Plastics Europe. Plastics - The Facts 2021 - An Analysis of European Plastics Production. *Demand and Waste Data* (2020).
24. Geck, P. Advanced High-Strength Steel Technology. in *Comparison of advanced high-strength steels* vol. 4 63–105 (SAE International, 2014).
25. Vadiraj, A., Abraham, M. & Bharadwaj, A. S. Trends in automotive light weighting. in *Light Weighting for Defense, Aerospace, and Transportation* 89–102 (Springer, 2019).
26. Plastics Europe. Automotive - the world moves with plastics (brochure). https://www.plasticseurope.org/en/resources/publications (2018).
27. Strong, A. B. *Plastics: Materials and Processing*. (Prentice Hall, 2006).
28. Yang, Y. *et al.* Recycling of composite materials. *Chemical Engineering and Processing: Process Intensification* **51**, 53–68 (2012).
29. Miller, L., Soulliere, K., Sawyer-Beaulieu, S., Tseng, S. & Tam, E. Challenges and alternatives to plastics recycling in the automotive sector. *Materials* **7**, 5883–5902 (2014).
30. Buekens, A. & Zhou, X. Recycling plastics from automotive shredder residues: A review. *Journal of Material Cycles and Waste Management* **16**, 398–414 (2014).
31. Ratiu, S. A. & Zgaverdea, A. C. The potential of using bio plastic materials in automotive applications. *Material Plastic* **56**, 901 (2019).
32. Samacke, P. & Reed, D. B. Automotive's bioplastic future. in *Proceedings of the Global Plastics Environmental Conference* (2004).
33. Rusu, D., Boyer, S., Lacrampe, M. F. & Krawczak, P. Bioplastics for automotive applications. *Handbook Bioplast Biocompos Eng Appl* **81**, 397 (2011).
34. Atiwesh, G., Mikhael, A., Parrish, C. C., Banoub, J. & Le, T.-A. T. Environmental impact of bioplastic use: A review. *Heliyon* **7**, e07918 (2021).
35. Renilde Becqué & Samuel Sharp. *Phasing out Plastics*. (2020).
36. Stephen Moore. Jaguar Land Rover trials chemical recycling process. *Plastics Today* (2019).
37. Council, A. C. *Automotive Plastics & Polymer Composites - a Roadmap for Future Mobility*. (2020).
38. ACAP. Associação Automóvel de Portugal - Estatísticas em Portugal. https://www.acap.pt/pt/estatisticas.
39. Simoldes company. https://www.simoldes.com/en/.

Chapter 2

Literature review

This chapter depicts the current state-of-the-art in reactive processing thermoplastic materials, namely relevant polymers features, materials selection, and available reactive manufacturing techniques.

2.1 Plastic composites

An adequate material selection involves a complex comparison of chemical, mechanical, and physical properties based on the requirements of each individual application[1]. Nowadays, there has been an effort in materials science to develop new materials, and the polymeric materials are one of the most used, driven by its proper combination of high strength and low weigh[2–4].

Polymers are macromolecules composed by chemical bonding of large numbers of smaller molecular, or repeating units, called monomer[5,6]. By combining a polymer with another material, it is often possible to obtain a polymer composite, with unique properties. The polymer usually acts as the continuous phase (matrix), and the nanofiller as the discontinuous phase[7]. Typically, composite materials are recognised for their specific mechanical properties and their potential for lightweight applications[8].

Of particular interest to automotive industry are fibre-reinforced polymers (FRP), that could be dispersed fibres with a specific aspect ratio or come in the form of woven fabric (typically carbon, glass, or a mixture of carbon/glass) that are embedded within a polymer matrix[9]. Commonly, FRP can contain randomly oriented fibres, oriented fibres, and continuous fibres, and can provide excellent performance while maintaining low weight and good processability of the resultant parts[10].

Generally, FRP are often divided into two types, based on their polymer matrix, which are thermoset composites and thermoplastic composites. The distinguishing principle is whether the chain of polymer is linear or not. There are mainly three different types of skeletal structure of a polymer molecule, which are linear, branched and network structures[11]. Thermoplastic polymer are both linear and brunched, because of their linear molecular chain, while thermoset polymer is formed by crosslinked of random molecular chains. Thermosetting polymer matrices are preferred for the manufacture of high performance FRP, once can confer especially high levels of strength and stiffness[12]. For instance, carbon fibre composites present a relative stiffness five times higher than steel[13]. Thus, many applications are ascribed for epoxy and polyester composites, such as car body components. The key advantage is that thermosets get a broader application in industry due to its easy-processing and cheap raw material[5].

However, thermoplastics offer certain advantages compared to thermosets, such as recyclability and could be re-processed into new less-demanding products[14]. Also, have a higher toughness and do not turn brittle at lower temperatures and have higher impact properties[9]. This features are particularly interesting for the automotive industry in colder temperatures. The processing time for melt processed thermoplastic parts is low compared to their thermosetting counterparts[15].

The use of thermoplastic composite materials is a growing trend for structural parts in the automotive, aeronautics, naval or wind power sectors[16]. Nevertheless, their development remains to this day hampered by their implementation, which is conditioned by the high melting temperature and the high viscosity of the thermoplastic matrices[17]. In the molten state, their viscosity is 100 to 1,000 times higher than that of thermosets, depending on the resin grade and the melt temperature, as shown in Figure 2.1.

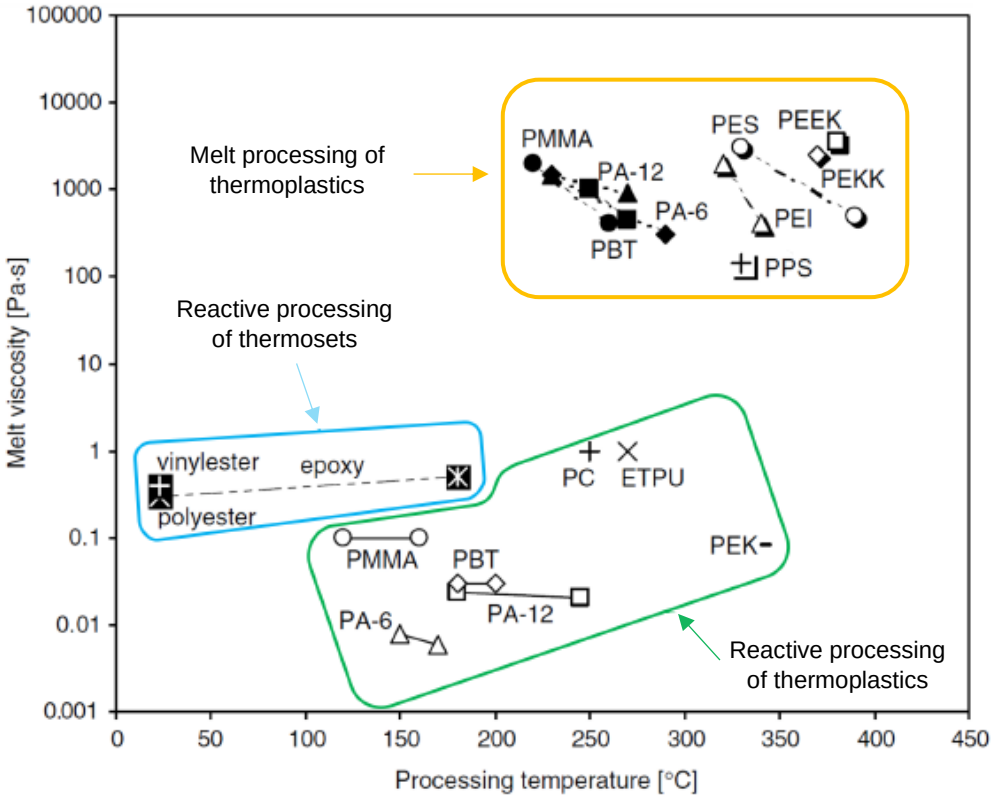

Figure 2.1 Melt viscosities and processing temperatures of various materials[18].

Due to this high melt viscosity, the introduction of a reinforcement phase in thermoplastics could be a current limitation, comparing to thermosets. To overcome the viscosity problem of the thermoplastic melt processing, the reactive processing of monomer and oligomer thermoplastic precursors represent a promising alternative for composites manufacturing.

2.2 Reactive thermoplastic resins systems

Traditionally, molten thermoplastic polymers have higher viscosities during processing, between 10^2-10^4, which requires higher temperatures and pressures[19]. The reactive thermoplastic resin systems are a solution available, whose processing is carried out in the liquid state (water like viscosity)[15].

Instead of injecting the high viscosity thermoplastic melt, the precursor materials from which the polymer is made from can be injected. The monomer and reactants are the precursors, that have much lower melt temperature and melt viscosity than the polymer which will produce[20]. Through reactive processing of thermoplastics, a better impregnation of fibres could be achieved and is a process that requires less energy (work and heat)[21].

To be compatible with liquid-based processes, the viscosity of the resin should not exceed 1 Pa·s during impregnation, due to the risk of hindering impregnation and favouring the appearance of porosities[22]. The resin must have minimal shrinkage to limit residual stresses in the final part and it

must solidify chemically (cross linking, polymerization) or physically (solidification, crystallization) in a reasonably short time[23–25].

Currently, there are several reactive thermoplastic precursor systems that follow these criteria. The most studied are polymethylmethacrylate (PMMA), polybutylene terephthalate (PBT), polyamide 6 (PA6) and polyamide 12 (PA12). Polyethylene terephthalate (PET), polycarbonate (PC), thermoplastic polyurethanes (TPU) and high performance thermoplastics such as, polyetheretherketone (PEEK), polyetherketone (PEK), polyethersulfone (PES), polyphenylene sulfide (PPS), polyethylene naphthalate (PEN) and polybuthylene naphhtalate (PBN) also follow the requirements, however, are less abundant in the literature[18,26].

2.3 Selection of reactive thermoplastic resin system

As observed, there are several thermoplastic resin systems which can be processed reactively. However, not all of them are able to fulfil the needs of a high-volume production of high-performance materials. The major properties of the reactive thermoplastic resins are summarized in Table 2.1, and are of great importance when it comes to the determination whether the thermoplastic material system is suitable for application in automotive parts. However, there are several criteria to consider when selecting the appropriate thermoplastic resin for automotive parts. These criteria ensure that the chosen material meets the necessary requirements for performance, durability, and safety in automotive applications. Some of these key criteria include:

- **Viscosity:** monomer viscosity should be <1000 mPa·s, to enable the reactive process and to further facilitates the impregnation of a reinforcement phase. Low melt viscosity allows to produce large thermoplastic parts in short times. Thereby, the low viscosity is a key material property when it comes to the determination of the process cycle time. The reactive processing of TPU and PMMA commonly involves a pre-polymerization step, during which the viscosity becomes too high for reactive process;
- **Processing temperature:** the processing temperature must be <200 ºC to minimize the costs of consumables and the thermal degradation of the reinforcement phase. In addition, high processing temperatures will also increase the costs of tooling and energy. It is clear that PA12, PBT, PC, TPU and PET present high processing temperatures. These factor exclude these polymers from further consideration in the current work. PA6 and PMMA processing temperatures are relatively low, which should lead to reduce the energy of the process;
- **Fast polymerization:** polymerization should occur as fast as possible, in order to reduce the process cycle time to a minimum. PMMA presented the higher polymerization time, which makes it unfeasible for process application;
- **Availability and price:** from a research and development industrial perspective, the development of a manufacturing process and detailed characterization requires a relatively large quantity of materials. The polymeric materials should be available in relevant quantities and not just in lab scale quantities. The materials price is of great importance when it comes to applications in automotive industry. Forming the main ingredient of the resin systems, the monomer largely

Table 2.1 Overview of properties of reactive thermoplastic polymers.

Material	Monomer/ Oligomer	T_m monomer (ºC)	T_m polymer (ºC)	Processing temperature (ºC)	Monomer viscosity (mPa·s)	Density polymer (g/cm^3)	Polymerization time (min)	Tensile strength (MPa)	Tensile modulus (GPa)
PMMA (Elium®)[27,28]	Methylmethacrylate	<40	130-140	20-100	<100	1.20	> 16hours	66	3.17
PA6[29–33]	Caprolactam	69	219-230	130-180	<5	1.15	3-60	85	2.0-3.8
PA12[29,34,35]	Laurolactam	180	175	180-240	23	1.04	1-10	50-60	1.4
PET[29,36–38]	Cyclic dimer	255	265	250-325	250-325	1.40	3-15	69	3
PBT[39–41]	Cyclic butylene terephthalate	147	225	180-260	20-150	1.30	30	85	1.8-2.7
TPU[29,42]	Low weight fraction TPU	270	140	300	~1000	1.20	-	40	0.2-2.3
PC[29,43]	Macrocyclic Bisphenol-A	200-210	300	250-300	250-300	1.20	2-5	60	2.2

determines the resin costs. And, for a higher matrix value, more expensive the car will be, which makes the costs of the polymer an important economic factor. PA6, PMMA, PBT and PC monomer are available for marketed in industrial scale, however the cost of PMMA monomer is higher. PA12 is industrially available but is produced in much lower quantities.

Considering the discussion above and the mentioned requirements, a range of criteria to adequate selection of monomer for in situ polymerization must be taken into account. Based on the previous requirements, it is possible to identify the most suitable reactive thermoplastic:

Table 2.2 Qualitative assessment of reactive materials.

Material	Precursor Viscosity	Processing temperature	Availability and price of precursor on market	Pass/Fail
TPU	XX	XX	No info available	X
PMMA	X	√	X	X
PA6	√√	√√	√√	√
PA12	√	X	√	√
PET	√	XX	√	X
PBT	√	X	√	√
PC	XX	XX	√	X

√ - advantage

X - disadvantage

Through materials qualitive assessment presented in Table 2.2, only the precursors of polyamides (PAs) and PBT prove to be suitable for all the above-mentioned requirements. PBT is not preferred, because these reactive systems are marketed by only one supplier (Cyclics Corporation, under the trend name Cyclics®)[44], and owing to paten exclusivity, can increase their prices. For this work, PA6 has been selected over PA12, for the following reasons:

(a) PA6 has higher performance/cost ratio than PA12. The LL monomer is more expensive than the ε-caprolactam (CL) monomer[45];

(b) High temperatures are associated with additional energy costs and tooling. As PA6 has a lower processing temperature, the additional costs can remain as little as possible;

(c) Lower viscosity of CL monomer, that will facilitate the impregnation of a reinforcement phase;

(d) Short cycle times and no generation of by-products. Shorter cycle times are essential in the production of high volumes parts for industrial applications.

2.4 Polyamide 6 (PA6) obtained from reactive system

PAs, commonly known as nylons, are widely used engineering polymers, with a large range of applications[46]. These polymers are able to cover a wide range of engineering polymers market, once they exhibit remarkable properties such high temperature resistance[47], toughness, hardness[47,48], high strength, resistance to warping and abrasion[47,48] and can also be dyed[49]. Due to their properties, the automotive industry is the major application[45,47]. PAs can be used in seat belts, tires and in car-bonnet application such as switch housing[47], air-intake manifold, and oil pans[50].

Polyamide 6 (PA6) or nylon 6 were invented by Wallace Hume Carothers in 1935[46]. At that time, Carothers was working for Du Pont, a chemical industry[51]. In the late 30's, the development of nylon was driven by the Japanese silk monopoly, from which a legend about the Nylon's acronym etymology was born "Now You're Lost, Old Nippon".

PA6 (melting temperature (T_m) between 210-220 °C) is a semi-crystalline polymer, which is composed by an amorphous phase and an ordered crystalline phase. PA6 has in its structure two crystalline forms (polymorphism): the α form and the γ form[52]. The α form is monocyclic, while the γ form is considered to be pseudo-hexagonal[53,54]. The two crystalline forms of PA6 have different properties due to their structural differences. The α form is characterized by a more rigid crystalline form due to antiparallel polymeric chains, while the γ-form presents a more rigid behaviour, due to the presence of parallel polymer chains[55].

2.4.1 PA6 polymerization from CL monomer

The monomer ε-caprolactam (CL) belongs to the lactam family. At room temperature, CL is a solid and present a low melting point of 69 °C[56]. Polymerization of CL can occur through several types of polymerization, which differ fundamentally in the initiation of the polymerization reaction. Basically, water produces hydrolytic polymerization, acids results in cationic polymerization and initiation leads in anionic polymerization[57,58]. All three mechanisms involve ring-opening of the monomer and assembly of a polymer chain. Thus, a ring-chain equilibrium exists, which can be shifted by the temperature or the addition of additives and also offers the possibility of recycling the PA6 through depolymerization[59,60].

The structural formulas of CL and PA6 are shown in Figure 2.2, where *n* indicates the degree of polymerization, i.e., the number of repeating units in PA6.

(a) **(b)**

Figure 2.2 Structural formulas: **(a)** CL monomer and **(b)** PA6.

Hydrolytic polymerization

Hydrolytic polymerization is one of the most common methods to obtain PA6 from CL monomer. Hydrolytic is generally conducted together with a small amount of water at higher temperatures (240 – 300 ºC) for 12-24 hours[57].

This route is the most important industrial approach for the PA6 production, however, the high reaction temperature and the long reaction time exclude this route from the compatibility criteria cited in subsection 2.3 for the large volume production of composites. Indeed, the generation of volatile products is not benefit, because it would cause porosity and voids in final parts. In addition, the very long reaction times and the additional purification step would significantly limit the possible rate of manufacture of final parts.

Cationic polymerization

Cationic polymerization is based on a polymerization initiated by acids[61]. In practice, this polymerization have very limited applications and is considered industrially uninteresting among the various polymerization processes. Low conversion rate and low molecular weight (Mw)[62,63] end products are generated through this polymerization, making its application unfeasible in 2.3 criteria.

Anionic polymerization

The anionic polymerization of CL, combined with a catalyst and an activator in PA6, is among one of the most developed forms of reactive processing of thermoplastics by anionic ring-opening polymerization (AROP)[63,64]. The anionic polymerization reaction is performed at temperatures between 130–170 ºC, and final conversions between 96% and 99% are possible to obtain, which means that the residual monomer content is low[33,65–67]. Moreover, polymerization and crystallization mechanisms can occur simultaneously resulting in a highly crystalline product[68,69]

Due to the sensitive to moisture (water could inhibit polymerization), the polymerization should be conducted under inert atmosphere (nitrogen is the inert gas preferred). The reaction mechanism for the anionic polymerization of PA6 is shown schematically on Figure 2.3.

The steps involved are as follows: catalyst dissociation at higher temperatures, to generate the anionic lactam. Strong bases such as alkaline metals or metal hydride, are used as catalyst[64]. Sodium caprolactamate is used as example, which was that used throughout this work (1). Ring-opening of the lactam, followed by the formation of an anionic N-acyllactam chain with the activator (2). Initiation is followed by rapid proton exchange between the caprolactam molecule and N-acyllactam group. Caprolactam deprotonation results in regeneration of the anion. Thus, the repeated acylation of the anion occurs during the reaction, resulting in subsequent chain growth to produce PA6 (3).

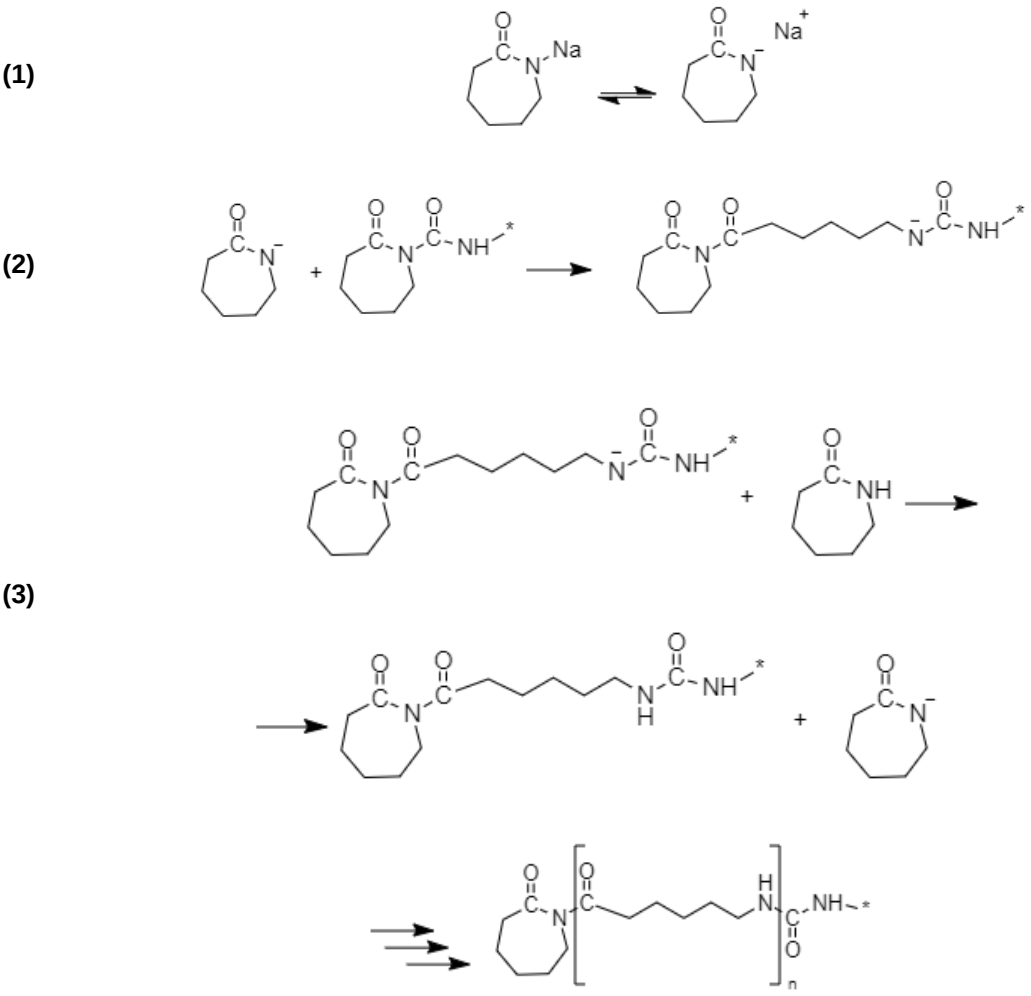

Figure 2.3 Steps of anionic polymerization of PA6.

The catalysts are predominantly salts (sodium) of lactams. The sodium caprolactamate (NaCL) is one of the most commonly used catalysts. Another commercial catalyst is caprolactam magnesium bromide (MgBrCL) which is being increasingly used because of its stability and functionality[70].

Currently, NaCL is commercialized under the trade names Addonyl® CR CATALYZE and Addonyl® KAT NL from Lanxess, Germany and, Bruggolen® C10, Nyrim® C1 and ε-caprolactam magnesium bromide (CLMgBr), from L. Brüggemann KG, Germany.

The activators, such as N-acetyl lactams and N-carbamoyl lactams are mainly used for CL polymerization[70,71]. Examples such N-acetyl-caprolactam (monofunctional) and hexamethylene-1,6-dicarbamoyl-caprolactam (bifunctional), are preferred with NaCL or CLMgBr catalyst[72].

Nowadays, the most common activators industrially available are Bruggolen® C20, that contains hexamethylene-1,6-dicarbamoylcaprolactam as active species in CL, Bruggolen® C235 with N-Ethyl-Pyrrolidon-free, both from L. Brüggemann KG, Germany, and Addonyl® ACTIVATE with CL-blocked isocyanate as active substance, Addonyl® 8101 and Addonyl® TT with N-carbamoyllactam precursor polyisocyanates from Lanxess, Germany. Polycarbodiimide-based

activators have also been commercialized under the trade name Addonyl® P, however, are less used.

Anionic polymerization route is the advantageous method for producing of PA6 matrix composites, owing to the commercial availability of the raw materials, low viscosity of the reactants and reaction rate at reasonably low temperatures. Thus, this route is compatible with the criteria defined in subsection 2.3 and is high interest for industrial processes to produce lightweight composite materials.

2.4.2 Processing parameters and its influence on PA6 properties

For industrial relevance and high-volume production, it is desirable to minimize the cycle time. One way to overcome this, is by using a fast catalyst and activator combination to reduce the polymerization time[73]. The addition of a catalyst and an activator accelerates the reaction rate of anionic polymerization of CL into PA6 and the combination of both components is fundamental because a catalyst alone promotes a slow reaction rate, and an activator alone cannot start the reaction. The type and concentration affect the polymerization in terms of molecular weight distribution, the presence of irregularities or branches within the polymer chain, the crystal structure and the morphology[67,71,74,75].

Catalyst and activator concentrations and their ratio also have a direct influence on the polymerization reaction[65,74,76,77]. Increasing the catalyst concentration leads to higher polymerization rates since more CL anions are formed. On the other hand, the addition of more catalyst can favour unwanted side reactions such as branching[67,74,78]. One reason is that for each catalyst molecule added, a cation is introduced that should be compensated by an CL anion. Thus, 100% conversion of the monomer is not achievable. Another reason for decreasing final conversion by adding more catalyst is due to the exothermic nature of polymerization reaction. As the reaction rate increases by adding more catalyst, the temperature increases, and the ring-chain equilibrium shifts to the monomer side[67]. Increasing the activator concentrations, increase the amount of growth centres, which increases the polymerization rate[70]. However, the length of the formed polymer chains decreases as more polymer chains start to grow simultaneously due to the higher amount of initiation points[70,78–80].

The polymerization temperature is another parameter that has a strong influence on PA6 properties such as crystallinity degree, conversion degree, average molecular weight, mechanical properties, and density of final polymer[61].

The influence of polymerization temperature on the polymer properties was extensively studied by Rijswijk *et al*.[33]. Increasing mould polymerization temperature, a higher reaction rate was achieved[66,81] and at temperatures above 160 °C, the polymerization occurs in only few minutes. In addition, increasing polymerization temperature, a sharply increase on average molecular weight was observed[33], leading to more branching reactions and thus, a broader molecular weight distribution. In reactions activated with N-carbamoyl lactam, the activators can decompose or deblock above 160 °C. This leads to the formation of an isocyanate group that can react with the amide of a growing chain and form a branch. This can occur with mono or

bifunctional N-carbamoyl lactams. In the latter case, the chain ends remain active and continue to polymerize or branch[33]. Calculated conversion degree reached a maximum at temperatures between 150 °C and 155 °C and decreased again with increasing polymerization temperature[33,79]. This can be due to ring-chain equilibrium of anionic polymerization that at high temperatures shifts towards to the monomer side. In addition, the branching reactions that occur at high temperatures can further reduce conversion, since the number of reactive chain ends is reduced by one with each branching point. For lower temperatures, such as about 140 °C, the conversion also decreases since the crystallization rate is higher here. Rapid crystallization can lead to the inclusion of CL in the crystals. This would decrease the concentration of the reactive species, reducing the final conversion[80,82] and a white coloration on the surface of PA6 can be observed[33].

The crystallization degree decreases as the polymerization mould temperature increases. This is due to lower crystallinity degree in equilibrium at higher polymerization temperatures, caused by the higher thermal movement of the polymer chains. Similarly, the tendency to crystallize is lower at higher temperatures, once need more time to reach this equilibrium. As the polymerization temperature increases, the polymer branches increase, which disrupts crystal formation and reduces the degree of crystallization[83,84]. Polymerization at around 145 °C to 150 °C gives the highest degree of crystallization of about 50%[67]. The denser packing in the crystalline phase leads to a higher density of PA6, which is a vantage for the mechanical properties[78].

As observed, there are a variety of parameters which influence the final properties of PA6, and several attempts are needed to be investigated to fill the lack for non-industrialization of the final parts. Thus, is important to evaluate the effect of different processing parameters and processing strategies on the properties of PA6.

2.4.3 Manufacturing technologies for reactive processing of PA6

Various reactive processes have been developed for the production of non-reinforced and reinforced PA6 materials. The selection of the manufacturing technology depends on the performance, economic and application requirements of the final component. The advantage of PA6 monomer low viscosity is the possibility of its application in a wide range of reactive processing technologies, therefore, new applications where thermosets were traditionally applied. But for successfully development of these materials, it is necessary to find the suitable manufacturing technology process that guarantees a good quality of the final product.

There are several manufacturing technologies for development of PA6 with and without reinforcement phase, such, polymerization casting[85–87], centrifugal[71,88] and rotational[66] moulding, reaction injection moulding[89–91] (RIM), reaction injection pultrusion[92–94] (RIP) and liquid composite moulding (LCM)[61,73].

However, not all of them are adequate for large-scale industrialization in automotive industry. For instance, polymer casting and rotational moulding are labour intensive, because each final part needs a postprocessing, increasing the final cost per part, and restricting its efficacy for higher volume applications[95,96]. These problems, coupled with a lack of research in this area, have been sufficient to limit their application for PA6 processing.

Regarding RIP, in the past, pultrusion has been applied only with PA12, however, in recent years, there has been an interest of develop pultrusion technology using PA6. One of the first industrial success applications was a cooperation between Hyundai (Korea), CQFD Composite (France) and Arkema (France). This project developed pultruded front bumper crash beam for Hyundai Motors (European Technical Centre), that contained unidirectional GF and PA6. This constructions helped to reduce 43% of the products weight[97]. At the best of our knowledge, no more information is available about this prototype, and probably, do not achieved industrial breakthrough in this field.

In recent years, the development of reactive processing has provided a means of enabling liquid composite moulding (LCM) of thermoplastics[73,98,99]. LCM technologies shows a clear analogy to the traditional resin transfer moulding (RTM), widely applied to produce thermoset composites. Due to monomer/oligomer low viscosity used, that allow for an increase in mechanical properties of final polymer, these materials have enormous potential in industry applications[99]. The LCM principle is in which a low viscosity resin is injected under pressure into a closed mould and preheated mould (that could contain predisposed reinforcements), and where the polymerization takes place to form a polymeric matrix[99].

Table 2.3 Qualitative assessment of reactive processing methods for PA6.

Technology	Production of complex shaped parts	Using of a reinforcement phase	Large scale production	Pass/Fail
Polymerization casting	√	X	√	X
Rotational moulding	√	X	X	X
RIM	√	√	X	X
RIP	√	√	√	√
LCM	√	√	√	√

As previous described and summarised in Table 2.3, among various processing technologies available for reactive processing of PA6, only RIP and LCM met the defined criteria and are capable of producing parts for automotive industry. However, RIP do not have the necessary features to bring the cycle time to the required level to fulfil the tough market requirements.

Through LCM processes, a production of large parts of composites could be assessed, as well as the production of complex shaped parts. Vacuum infusion/assisted RTM (VARTM) and thermoplastic RTM (T-RTM) have more or less similar process working, with some equipment differences that will be announced in the under subsections.

Vacuum infusion or vacuum assisted RTM (VARTM)

Similar to RTM, the first step of VARTM involves placing a dry fibre preform on the mould surface (in case of use a reinforcement phase). The second step consists of covering the mould with a flexible medium, i.e., a vacuum bag. After, the resin system is introduced by inlet valve, and then the resin is forced to flow toward the outlet port connected to the vacuum pump. Once the mould is completely fully, the inlet port is closed, and the part is left to polymerize before demoulding from the mould[31].

Vacuum infusion of thermoplastic composites, has not yet been used on an industrial scale, however, different systems were investigated over the past decade in the field of wind turbine blades[18,100]. By far, the most amount of detailed information available on this technology was carried out by Van Rijswijk from TU Delft using GF as reinforcement[33,67,101–103].

This work aimed the developing of a vacuum infusion process to manufacture thermoplastic wind turbine blades, using a reasonably low equipment investment. These studies centred mainly on the effects of processing temperature and different types and concentrations of catalysts and activator on the crystallinity, conversion degree and mechanical properties. As the final part as a large size, an appropriate selection of the catalyst and activator is necessary. Nyrim® C1 catalyst (less reactive) was used with Bruggolen® C20 activator to enable shorter cycle times[67]. The optimal processing parameters selected were 110 ºC melt temperature and 160 ºC polymerization mould temperature.

The authors concluded that the most important processing parameter was temperature, once it has impact on conversion and crystallinity[33]. Different fibre sizing's were studied to comparing interfacial properties of composites. The maximum conversion degree with GF achieved was 96%, with a crystallinity degree of 41%. It was proven that moisture, dirt and siloxyl groups on fibres have an inhibition effect on polymerization. Although the potential of results obtained by Van Rijswijk, which uncovered many of the unknows about AROP of CL into PA6, at the best of our knowledge, this reactive manufacturing process still not accomplish the industrial breakthrough. A plausible reason could be due to the sensitivity of the reactive systems and the climatic conditions that blades are exposed[104]. However, it is worth mentioned the composite wind blade (with 9 meters) developed by Arkema with Elium® acrylic resin[100].

The work from Yan *et al*.[105] also revealed the influence of manufacturing parameters, such, temperature, time, and raw materials concentrations on final properties of PA6 and continuous GF reinforced PA6 composites. Catalyst content and polymerization temperature have significant effects on both molecular weight and crystallinity degree of PA6 and PA6/GF composites that lead to a high mechanical properties of composites. Relevant developments related to post-heat treatments were further investigated. The authors revealed the influence of different post-heat treatments such quenching and annealing on mechanical properties. The results demonstrated a significantly reduction after quenching treatment, but an improvement after annealing.

As observed, there is some information in literature using vacuum infusion of PA6, however this technology is not suitable for high volume manufacturing. As previous mentioned, the resins used during process are almost water-like viscosity, making them sensitive to pressure changes

and difficulties to control using vacuum as the driving force. If vacuum pressure is low, polymerization may occur before reaches the outlet of the mould, and if vacuum is too high, the flow rate can be too fast that making infiltration of fibres poor. In particular, if the pressure goes bellow to atmospheric pressure, can induce the sublimation or evaporation of the monomer and creating voids[106,107]. Another disadvantage is related to vacuum bags and other consumables used, that are not reusable, and the process is considered less sustainable.

Due to the aforementioned reasons, VARTM is not suitable for high volume manufacturing, however, the results and know-how that came from previous works, can be applied in future research.

Thermoplastic resin transfer moulding (T-RTM)

More recently, T-RTM technology, that uses many features of VARTM, have emerged as a more controlled method for PA6 processing in terms of flow rate.

The processing is like a standard RTM process. A typical T-RTM equipment consist of a dosing machine, a mixing head, and a mould (Figure 2.4). The function of melting unit is to melt, pressurize, transport, and mix the reactive components. The melting unit has two tanks for melting the reactants: catalyst and activator each dissolved in the corresponding lactam (masterbatch)[99]. The use of several tanks is to separate the reactants, once in specific cases the polymerization reaction is too fast, leading to an increase in the mixture viscosity and avoid the injection step. The tanks are flushed with nitrogen to prevent the influence of moisture on the polymerization. Both mixtures can therefore be used over a longer period of time and can be circulated by a pump system in heated hoses[108].

The mixing head is placed between the tanks and mould, and the function is to improve the homogeneity of the system. After melted and mixed the raw materials in tanks, they flow through separate heated piped and are mixture through impingement on each other at very high speeds in a mixing head. Then, the reactive mixture is injected under pressure into the mould. When the reactive mixture enters the mould, the *in situ* chemical reaction occur[109,110]. After injection, the resin viscosity increases, and the polymerization occurs. The time between beginning of polymerization reaction to the complete solidification of the reactive mixture is denominated polymerization time[61].

The mould gives the product its final shape and is closed and heated to initiate the AROP reaction. The mould design is another parameters to considerer. A reduction in voids can be observed if a correct mould design is employed, as well as the strict control of parameters, such as injection pressure and curing time[110].

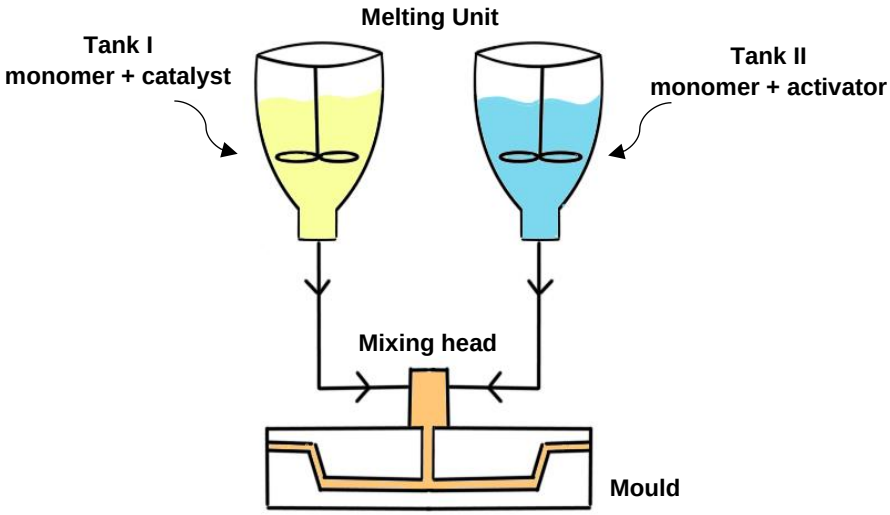

Figure 2.4 Schematic representation of T-RTM technology[111].

There are several parameters to considered: tank temperature and pressure, and stirring time have an influence on reactive mixture viscosity (Table 2.4). Polymerization kinetics, as well as the viscosity, is influenced by stirring time and speed. The tank pressure can also have an effect on viscosity. The higher temperatures on tanks, promote a resin more fluid, thus, the temperature is considered a major parameter[108,112].

The influence of temperature and the injection pressure can have a significant effect on the chemical reaction, and consequently in cycle time. The cycle time is one of the main characteristics to commercial feasibility of T-RTM process and should be as short as possible[108,113].

The effects of mould parameters, such mould temperature and residence time were investigated by Semperger *et al*.[108,114]. The relationships between crystallinity, mould temperature and residence time were detailed. The authors found out that crystallinity degree decreased as the temperature increases, and directly influences mechanical properties of material. It was reported that a high crystalline phase improved the mechanical properties. In contrast to literature data, the authors found out that residence time did not have a significant effect during T-RTM.

According to a study by Lee *et al*.[115], the curing temperature above the crystallization temperature (~170 ºC) is not suitable for T-RTM process. The authors studied the curing process from 120 to 200 ºC, with an interdigital dielectric sensor, and confirmed that at 160 ºC, polymerization and crystallization occurs simultaneously[116]. At 180 ºC, crystallization takes place after polymerization, and at 200 ºC, polymerization occurs very fast that crystallization do not have time to occur.

In another study, Choi and co-workers[112] studied the optimal polymerization conditions for PA6 and PA6/CF manufacturing. The authors used the response surface method (RSM) to optimize the experimental conditions of the process, using injection speed, catalyst, and activator concentrations as design variables. By optimizing the design variables with RSM, the authors identified the conditions to maximize the tensile strength and polymer conversion rate.

Table 2.4 Published studies regarding the development of PA6 using reactive technologies.

							Tensile properties		Flexural properties	
Monomer	**Catalyst/ Activator**	**Reinforcement**	**Technology**	**Production parameters**	**X_c (%)**	**DOC (%)**	**σ_{max} (MPa)**	**E_{max} (GPa)**	**σ_{max} (MPa)**	**E_{max} (GPa)**
CL[85]	C10/C20P	GF	Casting	T_{rect} = 120 ºC T_{mould} = 160 ºC Annealed for 30min	47	99	78	2.7	-	-
CL[71]	EtMgBr/ N-benzoyl e-capro-Lactam and N,N'-isophthaloyl-bis-caprolactam	-	Centrifugal	T_m = 90ºC t_{polym} = 20 min	36-47	66-98	-	-	-	2.3-3.1
CL[88]	Sodium bis[(2-methoxyethoxy) caprolactam/4,4 -diphenylmethane diisocyanate	GF	Centrifugal	T_{mA} = 85 ºC T_{mB}= 100 ºC T_{mould} = 140 – 190 ºC t_{polym} = 30 min	23-47	91-98	-	-	-	1.3-1.4
CL[33]	C1/C20	GF	VARTM	T_m = 110 ºC T_{mould} = 140 – 160 ºC	33-42	97	64-78	2.7-3.8	-	-
CL[117]	Sodium metal/HMDI	CF	VARTM	T_m = 110 ºC 120 ≤T_{mould} ≤ 200 ºC t_{polym} = 5 min	-	98-99	-	-	60-90	1-2
CL[118]	Addonyl CR/ Addonyl 8120	CF	T-RTM	T_m > 69 ºC T_{mould} = 150 ºC	26	98	268	19.5	218	1.1
CL[109]	sodium aluminum lactate/mixture of isocianates	CF and GF	T-RTM	T_m = 125 ºC T_{mould} = 165 ºC	43	97	48	0.8	-	-
CL[119,120]	C10/C20P	-	T-RTM	T_m = 98 ºC T_{mould} = 150 ºC t_{polym} = 5 min	44-50	~99	75-84	3.2-3.7	112-138	3.2-4.1

CL[21,121,122]	C10/C20P	GF	T-RTM	T_m = 100 ºC T_{mould} = 130 ºC t_{polym} = 15 min	42	94-95	83.2	2.8	102.7	3.2
CL[108,114]	C10/C20P	-	T-RTM	T_m = 110 ºC $T_{mix.\ head}$ =110 ºC T_{mould} = 150 – 175 ºC t_{polym} = 3-5 min	21-42	95-97	-	-	35-62	1.3-2.4
Addonyl CR activator Addonyl CR catalyst[115]		CF	T-RTM	T_m = 120 ºC T_{mould} = 120 – 200 ºC t_{polym} = 10 min	35-45	-	48-57	1.1-1.5	-	-

*DOC – Degree of Conversion

Minimizing the voids is another crucial achievement for obtaining good mechanical properties. Voids can act as stress concentrators and can cause an early rupture. An investigation on the void content was performed to minimizing voids to achieve sufficient quality and hence materials properties through tomography scan[121]. The presence of this voids was related to the air trapped, and the authors proposed a solution to reduce the voids, through using vacuum to reduce the quantity of air available. While this can easily be accomplished, however it is limited by caprolactam boiling at lower pressures, and reaction temperature is also a key factor.

An innovative work done by Osváth at *al*.[123], investigated the effect of post-polymerization heat on the monomer conversion and resulting molecular mass of PA6. Samples prepared without quenching revealed higher monomer conversion and molecular weights than for quenches samples, using the same reaction times. These findings can be used to improve the properties of PA6 produced using T-RTM technology.

In general, T-RTM demonstrates some advantages compared to other reactive thermoplastic manufacturing technologies, due to the possibility of obtaining high performance thermoplastics and thermoplastic composites with complex shapes, using different reinforcements, such as fibres or nanoparticles. However, this technology involves expensive equipment, but as is suitable for high volume production, and the equipment cost can be justified.

Regarding T-RTM equipment's availability, from mid-2010 some improvements from resin suppliers and injection system manufacturers have been achieved to develop an industrial-scale equipment's for processing reactive thermoplastic resins, notably with PA6 matrix[61,73,108–110,114,124–126]. There are only two known T-RTM equipment's available on trad, from Krauss Maffei[127] and from Engel[126,128], however based on the available literature both equipment's still have difficulties in the process domain, given by the complexity of the technology and the countless variables that affect the reaction.

Industrial partnerships have also demonstrated some improvements in this field. Automotive parts such as B-pillar[125], a hybrid roadster roof cover frame[124] and a mechanical subframes[129] have shown the success using highly sophisticated manufacturing process. A shovel was also fabricated, opened a new opportunity for the production of thermoplastics reinforced with fibres using T-RTM not only for automotive industry[126,130].

The obtained results, although promising, show the complexity of the T-RTM technology. It was found that we are not yet in the presence of a robust technology, verifying that there is no repeatability of the process that allows to produce parts from an industrial point of view. The large number of variables and the requirements that are necessary to control during the *in situ* reaction, reveal that it is still a challenge to obtain final products with quality.

As previous mentioned, the main motivation of the present thesis is to overcome the actual problems detected in industrial scale, giving the possibility of identifying the biggest challenges and obstacle in the industrialization of this technology, as well as potential strategies to overcome them. The potential of this technology has been strongly underestimated, however interesting developments in this field still may be expected.

References

1. Koronis, G., Silva, A. & Fontul, M. Green composites: A review of adequate materials for automotive applications. *Composites Part B: Engineering* **44**, 120–127 (2013).
2. Namazi, H. Polymers in our daily life. *Bioimpacts* **7**, 73–74 (2017).
3. Peters, E. N. Engineering thermoplastics—materials, properties, trends. in *Applied plastics engineering handbook* 3–26 (Elsevier, 2017).
4. Belgacem, M. & Gandini, A. Monomers, Polymers and Composites from Renewable Resources Monomers, Polymers and Composites from Renewable Resources. Preprint at (2008).
5. Peters, E. N. Engineering thermoplastics—materials, properties, trends. in *Applied Plastics Engineering Handbook* 3–26 (Elsevier, 2017).
6. Harper, C. Liquid Resin Processes. in *Handbook of plastic processes* vol. 18 529–572 (Wiley Online Library, 2006).
7. Bîrcă, A., Gherasim, O., Grumezescu, V. & Grumezescu, A. M. Introduction in thermoplastic and thermosetting polymers. in *Materials for biomedical engineering* 1–28 (Elsevier, 2019).
8. Mallick, P. K. Thermoplastics and thermoplastic–matrix composites for lightweight automotive structures. in *Materials, Design and Manufacturing for Lightweight Vehicles* 174–207 (Elsevier, 2010).
9. Scaffaro, R., Di Bartolo, A. & Dintcheva, N. T. Matrix and filler recycling of carbon and glass fiber-reinforced polymer composites: A review. *Polymers* **13**, 3817 (2021).
10. Jayan, J. S. *et al.* An introduction to fiber reinforced composite materials. in *Fiber Reinforced Composites* 1–24 (Elsevier, 2021).
11. Flory, P. J. *Principles of Polymer Chemistry*. (Cornell university press, 1953).
12. Parmar, H., Khan, T., Tucci, F., Umer, R. & Carlone, P. Advanced robotics and additive manufacturing of composites: towards a new era in Industry 4.0. *Materials and manufacturing processes* **37**, 483–517 (2022).
13. Hwang, H. Y. & Kim, J. K. Design and manufacture of a carbon fiber epoxy rotating boring bar. *Composite Structures* **60**, 115–124 (2003).
14. Goodship, V. Plastic recycling. *Science progress* **90**, 245–268 (2007).
15. Van Rijswijk, K. & Bersee, H. E. N. Reactive processing of textile fiber-reinforced thermoplastic composites–An overview. *Composites Part A: Applied Science and Manufacturing* **38**, 666–681 (2007).
16. Thori, P., Sharma, P. & Bhargava, M. An approach of composite materials in industrial machinery: advantages, disadvantages and applications. *International Journal of Research in Engineering and Technology* **2**, 350–355 (2013).
17. Mallick, P. K. Thermoset matrix composites for lightweight automotive structures. in *Materials, Design and Manufacturing for Lightweight Vehicles* 229–263 (Elsevier, 2021).
18. Van Rijswijk, K. Thermoplastic Composite Wind Turbine Blades: Vacuum Infusion Technology for Anionic Polyamide-6 Composites. *PhD Thesis* (Delft University of Technology, 2007).
19. Máirtín, P. Ó., McDonnell, P., Connor, M. T., Eder, R. & Brádaigh, C. M. Ó. Process investigation of a liquid PA-12/carbon fibre moulding system. *Composites Part A: Applied Science and Manufacturing* **32**, 915–923 (2001).
20. Murray, J. J. *et al.* Impact Performance of Thermoplastic Resin Transfer Moulded Carbon Fibre Composites. in *SAMPE Europe Conference* (2020).
21. Murray, J. J., Gleich, K., McCarthy, E. D. & Bradaigh, C. O. Properties of polyamide-6 composites using a low-cost thermoplastic resin transfer moulding system. in *ICCM22* 2013–2022 (2019).
22. Potter, K. RTM theory and Materials for RTM. in *Resin transfer moulding* 1–49 (Springer Science & Business Media, 2012).
23. Greaney, M. & Brádaigh, C. M. Ó. Development of a polyamide copolymer Resin Transfer Molding system for thermoplastic composites. in *7th International Conference on Flow Processes in Composite Materials (FPCM-7): Newark, Delaware, USA* 7–9 (2004).
24. Parton, H. & Verpoest, I. In situ polymerization of thermoplastic composites based on cyclic oligomers. *Polymer Composites* **26**, 60–65 (2005).
25. Luisier, A., Bourban, P. E. & Månson, J. A. E. Initiation mechanisms of an anionic ring-opening polymerization of Lactam-12. *Journal of Polymer Science, Part A: Polymer Chemistry* **40**, 3406–3415 (2002).
26. van Rijswijk, K. & Bersee, H. E. N. Reactive processing of textile fiber-reinforced thermoplastic composites – An overview. *Composites Part A: Applied Science and Manufacturing* **38**, 666–681 (2007).
27. ARKEMA. Liquid Thermoplastic Resin for Tougher Composites. Available online. https://www.arkema.com/global/en/products/product-finder/product-range/incubator/elium_resins/.

28. Bhudolia, S. K., Gohel, G., Joshi, S. C. & Leong, K. F. Manufacturing Optimization and Experimental Investigation of Ex-situ Core-shell Particles Toughened Carbon/Elium® Thermoplastic Composites. *Fibers and Polymers* **22**, 1693–1703 (2021).
29. Prabhakaran, R. T. D., Lystrup, A. & Andersen, T. L. Attribute based selection of thermoplastic resin for vacuum infusion process: A decision making methodology. in *Dynamic Methods and Process Advancements in Mechanical, Manufacturing, and Materials Engineering* 267–288 (IGI global, 2013).
30. BrüggemannChemical. Product data sheet AP-Nylon® Additives. https://www.brueggemann.com/.
31. Pillay, S., Vaidya, U. K. & Janowski, G. M. Liquid molding of carbon fabric-reinforced nylon matrix composite laminates. *Journal of Thermoplastic Composite Materials* **18**, 509–527 (2005).
32. Gong, Y., Liu, A. & Yang, G. Polyamide single polymer composites prepared via in situ anionic polymerization of ε-caprolactam. *Composites Part A: Applied Science and Manufacturing* **41**, 1006–1011 (2010).
33. Van Rijswijk, K., Bersee, H. E. N., Beukers, A., Picken, S. J. & Van Geenen, A. A. Optimisation of anionic polyamide-6 for vacuum infusion of thermoplastic composites: Influence of polymerisation temperature on matrix properties. *Polymer testing* **25**, 392–404 (2006).
34. Pini, N., Zaniboni, C., Busato, S. & Ermanni, P. Perspectives for reactive molding of PPA as matrix for high-performance composite materials. *Journal of Thermoplastic Composite Materials* **19**, 207–216 (2006).
35. Zingraff, L., Michaud, V., Bourban, P.-E. & Månson, J.-A. Resin transfer moulding of anionically polymerised polyamide 12. *Composites Part A: Applied Science and Manufacturing* **36**, 1675–1686 (2005).
36. Nagahata, R. *et al.* Thermal polymerization of uniform macrocyclic ethylene terephthalate dimer. *Polymer* **42**, 1275–1279 (2001).
37. Nagahata, R. *et al.* Solid-phase thermal polymerization of macrocyclic ethylene terephthalate dimer using various transesterification catalysts. *Journal of Polymer Science Part A: Polymer Chemistry* **38**, 3360–3368 (2000).
38. Youk, J. H., Kambour, R. P. & MacKnight, W. J. Polymerization of ethylene terephthalate cyclic oligomers with antimony trioxide. *Macromolecules* **33**, 3594–3599 (2000).
39. Baets, J., Godara, A., Devaux, J. & Verpoest, I. Toughening of isothermally polymerized cyclic butylene terephthalate for use in composites. *Polymer Degradation and Stability* **95**, 346–352 (2010).
40. Wu, W., Klunker, F., Xie, L., Jiang, B. & Ziegmann, G. Simultaneous binding and ex situ toughening concept for textile reinforced pCBT composites: Influence of preforming binders on interlaminar fracture properties. *Composites Part A: applied science and manufacturing* **53**, 190–203 (2013).
41. Abt, T. & Sánchez-Soto, M. A review of the recent advances in cyclic butylene terephthalate technology and its composites. *Critical Reviews in Solid State and Materials Sciences* **42**, 173–217 (2017).
42. Polymer Properties Database. Polyurethane. Available online. https://polymerdatabase.com/polymers/%0Ahexamethylenediisocyanatediethyleneglycol.html.
43. Salem, A. J., Stewart, K. R., Gifford, S. K. & Berenbaum, A. M. Fabrication of thermoplastic matrix structural composites by resin transfer molding of cyclic bisphenol-A polycarbonate oligomers. *SAMPE Journal* **27**, 17–22 (1991).
44. Balogh, G. Development of cyclic butylene terephthalate matrix composites . (University of Technology and Economics , Budapest, 2015).
45. Melvin, I. K. *Nylon Plastic Handbook*. *New York: Hanser* (1995).
46. Marchildon, K. Polyamides–still strong after seventy years. *Macromolecular reaction engineering* **5**, 22–54 (2011).
47. Platt, D. K. Overview of Engineering and High Performance Plastics. in *Engineering and high performance plastics market report: a Rapra market report* 9–14 (iSmithers Rapra Publishing, 2003).
48. Sastri, V. R. Engineering thermoplastics: acrylics, polycarbonates, polyurethanes, polyacetals, polyesters, and polyamides. *Plastics in medical devices* 121–173 (2010).
49. Silva, C., Cavaco-Paulo, A. & Nierstrasz, V. A. Enzymatic hydrolysis and modification of core polymer fibres for textile and other applications. in *Advances in Textile Biotechnology* 77–97 (Elsevier, 2010).
50. Solticzky, J. & Bíró, I. Motor-car industry as the main motivation of plastic-innovation. *Acta Technica Corviniensis-Bulletin of Engineering* **6**, 27 (2013).
51. Matthies, P. & Seydl, W. F. History and development of nylon 6. in *High Performance Polymers: Their Origin and Development: Proceedings of the Symposium on the History of High Performance Polymers* 39–53 (Springer, New York, 1986).
52. Holmes, D. R., Bunn, C. W. & Smith, D. J. The crystal structure of polycaproamide: Nylon 6. *Journal of Polymer Science* **17**, 159–177 (1955).
53. Wolanov, Y., Feldman, A. Y., Harel, H. & Marom, G. Amorphous and crystalline phase interaction during the Brill transition in nylon 66. *Express Polym. Lett* **3**, 452–457 (2009).

54. Pesetskii, S. S., Jurkowski, B., Olkhov, Y. A., Bogdanovich, S. P. & Koval, V. N. Influence of a cooling rate on a structure of PA6. *European polymer journal* **41**, 1380–1390 (2005).
55. Murthy, N. S. Metastable crystalline phases in nylon 6. *Polym. Commun* **32**, 301–305 (1991).
56. Kabo, G. J. *et al.* Thermodynamic properties of 6-aminohexanoic lactam (ε-caprolactam). *The Journal of Chemical Thermodynamics* **24**, 1–13 (1992).
57. Russo, S. & Casazza, E. Ring-opening polymerization of cyclic amides (lactams). (2012).
58. Dubois, P., Coulembier, O. & Raquez, J.-M. *Handbook of Ring-Opening Polymerization*. (John Wiley & Sons, 2009).
59. Merna, J., Chromcová, D., Brožek, J. & Roda, J. Polymerization of lactams: 97. Anionic polymerization of ε-caprolactam activated by esters. *European polymer journal* **42**, 1569–1580 (2006).
60. Šebenda, J. Polymerizability of lactams. in *Polymerization of Heterocycles (Ring Opening)* 329–334 (Elsevier, 1977).
61. Ageyeva, T., Sibikin, I. & Karger-Kocsis, J. Polymers and related composites via anionic ring-opening polymerization of lactams: Recent developments and future trends. *Polymers* **10**, 357 (2018).
62. Su, W.-F. Ring-opening polymerization. in *Principles of Polymer Design and Synthesis* 267–299 (Springer, 2013).
63. Roda, J. Polyamides. in *Handbook of Ring-Opening Polymerization* 165–195 (Wiley Online Library, 2009).
64. Sekiguchi, H., Ivin, K. J. & Saegusa, T. Ring-Opening Polymerization. *J., Saegusa, T., Eds.; Elsevier London UK* **2**, 809 (1984).
65. Russo, S., Imperato, A., Mariani, A. & Parodi, F. The fast activation of ε-caprolactam polymerization in quasi-adiabatic conditions. *Macromolecular chemistry and physics* **196**, 3297–3303 (1995).
66. Barhoumi, N., Maazouz, A., Jaziri, M. & Abdelhedi, R. Polyamide from lactams by reactive rotational molding via anionic ring-opening polymerization : Optimization of processing parameters. *Express Polymer Letters* **7**, 76–87 (2013).
67. Rijswijk, K. Van, Bersee, H. E. N., Jager, W. F. & Picken, S. J. Optimisation of anionic polyamide-6 for vacuum infusion of thermoplastic composites : choice of activator and initiator. *Composites Part A: Applied Science and Manufacturing* **37**, 949–956 (2006).
68. Karger-Kocsis, J. & Kiss, L. Attempts of separation of the polymerization and crystallization processes by means of DSC thermograms of activated anionic polymerization of ε-caprolactam. *Die Makromolekulare Chemie: Macromolecular Chemistry and Physics* **180**, 1593–1597 (1979).
69. Khodabakhshi, K., Gilbert, M., Fathi, S. & Dickens, P. Anionic polymerisation of caprolactam at the small-scale via DSC investigations. *Journal of Thermal Analysis and Calorimetry* **115**, 383–391 (2014).
70. Udipi, K., Davé, R. S., Kruse, R. L. & Stebbins, L. R. Polyamides from lactams via anionic ring-opening polymerization: 1. Chemistry and some recent findings. *Polymer* **38**, 927–938 (1997).
71. Rusu, G., Ueda, K., Rusu, E. & Rusu, M. Polyamides from lactams by centrifugal molding via anionic ring-opening polymerization. *Polymer* **42**, 5669–5678 (2001).
72. Piskun, Y. A., Vasilenko, I. V, Gaponik, L. V & Kostjuk, S. V. Activated anionic ring-opening polymerization of ε-caprolactam with magnesium di (ε-caprolactamate) as initiator: Effect of magnesium halides. *Polymer bulletin* **68**, 1501–1513 (2012).
73. Sibikin, I. & Karger-Kocsis, J. Toward industrial use of anionically activated lactam polymers: Past, present and future. *Advanced Industrial and Engineering Polymer Research* **1**, 48–60 (2018).
74. Bessell, T. J., Hull, D. & Shortall, J. B. The effect of polymerization conditions and crystallinity on the mechanical properties and fracture of spherulitic nylon 6. *Journal of Materials Science* **10**, 1127–1136 (1975).
75. Kim, K. J., Kim, Y. Y., Yoon, B. S. & Yoon, K. J. Mechanism and kinetics of adiabatic anionic polymerization of ε-caprolactam in the presence of various activators. *Journal of applied polymer science* **57**, 1347–1358 (1995).
76. Russo, S., Biagini, E. & Bonta, G. Novel synthetic approaches to poly (ε-caprolactam)-based materials. in *Makromolekulare Chemie. Macromolecular Symposia* vol. 48 31–46 (Wiley Online Library, 1991).
77. Malkin, A. Y., Beghishev, V. P. & Bolgov, S. A. The exothermal effects of superimposed processes of activated anionic polymerization of ε-caprolactam and crystallization of the polymer formed. *Polymer* **23**, 385–390 (1982).
78. Ueda, K. *et al.* Synthesis of high molecular weight nylon 6 by anionic polymerization of ε-caprolactam. *Polymer journal* **28**, 446–451 (1996).
79. Ricco, L., Russo, S., Orefice, G. & Riva, F. Anionic poly (ε-caprolactam): Relationships among conditions of synthesis, chain regularity, reticular order, and polymorphism. *Macromolecules* **32**, 7726–7731 (1999).
80. Davé, R. S., Kruse, R. L., Stebbins, L. R. & Udipi, K. Polyamides from lactams via anionic ring-opening polymerization: 2. Kinetics. *Polymer* **38**, 939–947 (1997).

81. Casazza, E., Ricco, L., Russo, S. & Scamporrino, E. Nature of a low molar mass peak in anionic poly (ε-caprolactam). Its identification as macrocyclic ensemble. *Macromolecules* **40**, 739–745 (2007).
82. Maazouz, A., Lamnawar, K. & Dkier, M. Chemorheological study and in-situ monitoring of PA6 anionic-ring polymerization for RTM processing control. *Composites Part A* **107**, 235–247 (2018).
83. Humphry, J. *et al.* Process modelling in Anionically Polymerised Polyamide-6 (APA6) for the in situ polymerisation of composite matrices. *Composites Communications* **8**, 111–114 (2018).
84. Mateva, R., Delev, O. & Kaschcieva, E. Structure of poly (ε-caprolactam) obtained in anionic bulk polymerization. *Journal of applied polymer science* **58**, 2333–2343 (1995).
85. Engelmann, G., Gohs, U. & Ganster, J. Monomer cast polyamide 6 composites and their treatment with high-energy electrons. *Journal of Applied Polymer Science* **123**, 1201–1211 (2012).
86. Horský, J., Kolařík, J. & Fambri, L. Composites of alkaline poly (6-caprolactam) and short glass fibers: one-step synthesis, structure and mechanical properties. *Die Angewandte Makromolekulare Chemie* **264**, 39–47 (1999).
87. Miscevic, M., Catic, I. & Sercer, M. Production of nylon-6 castings by anionic polymerisation of epsilon-caprolactam. *International Polymer Science and Technology(UK)* **20**, (1993).
88. Rusu, G. H., Rusu, M., Rusu, E., Stoleriu, A. & Teaca, C. A. Direct centrifugal molding of nylon 6-based products from ϵ-caprolactam. *Polymer-Plastics Technology and Engineering* **39**, 233–247 (2000).
89. Sibal, P. W., Camargo, R. E. & Macosko, C. W. Designing Nylon-6 polymerization systems for RIM. *Polymer process engineering* **1**, 147–169 (1983).
90. Ning, X. & Ishida, H. RIM-pultrusion of nylon-6 and rubber-toughened nylon-6 composites. *Polym Eng Sci* **31**, 632–637 (1991).
91. Hedrick, R. M., Gabbert, J. D. & Wohl, M. H. Nylon 6 RIM. in *Reaction Injection Molding* vol. 10 135–162 (ACS Publications, 1985).
92. Luisier, A., Bourban, P.-E. & Månson, J.-A. Reaction injection pultrusion of PA12 composites: process and modelling. *Compos Part A Appl Sci Manuf* **34**, 583–595 (2003).
93. Luisier, A., Bourban, P. E. & Månson, J. A. E. In-Situ Polymerization of Polyamide 12 for Thermoplastic Composites. in *Proceedings of 12th international conference on composite materials (ICCM-12), Paris/France* (Paris, France, 1999).
94. Luisier, A., Bourban, P. & Månson, J. Initiation mechanisms of an anionic ring-opening polymerization of lactam-12. *J Polym Sci A Polym Chem* **40**, 3406–3415 (2002).
95. Formlabs. Guide to Manufacturing Processes for Plastic. https://formlabs.com/blog/guide-to-manufacturing-processes-for-plastics/ (2020).
96. Barhoumi, N., Lamnawar, K., Maazouz, A., Jaziri, M. & Abdelhedi, R. Reactive rotational molding process of PP/PA6 bilayer systems: experimental investigations. *International Journal of Material Forming* **1**, 671–674 (2008).
97. Ringenbach, S., Richeton, J. & Coulton, J. Hyundai's breakthrough front bumper crash beam. *JEC Compos. Mag* **98**, 39–41 (2015).
98. Cassagnau, P., Bounor-Legaré, V. & Fenouillot, F. Reactive processing of thermoplastic polymers: a review of the fundamental aspects. *International Polymer Processing* **22**, 218–258 (2007).
99. Miranda Campos, B., Bourbigot, S., Fontaine, G. & Bonnet, F. Thermoplastic matrix-based composites produced by resin transfer molding: A review. *Polym Compos* **43**, 2485–2506 (2022).
100. Murray, R. *et al. Manufacturing a 9-Meter Thermoplastic Composite Wind Turbine Blade*. (2017).
101. van Rijswijk, K., Lindstedt, S., Vlasveld, D. P. N., Bersee, H. E. N. & Beukers, A. Reactive processing of anionic polyamide-6 for application in fiber composites: A comparative study with melt processed polyamides and nanocomposites. *Polymer Testing* **25**, 873–887 (2006).
102. Van Rijswijk, K., Teuwen, J. J. E., Bersee, H. E. N. & Beukers, A. Textile fiber-reinforced anionic polyamide-6 composites. Part I: The vacuum infusion process. *Composites Part A: Applied Science and Manufacturing* **40**, 1–10 (2009).
103. Van Rijswijk, K., Van Geenen, A. A. & Bersee, H. E. N. Textile fiber-reinforced anionic polyamide-6 composites. Part II: Investigation on interfacial bond formation by short beam shear test. *Composites Part A: Applied Science and Manufacturing* **40**, 1033–1043 (2009).
104. Durai Prabhakaran, R. T. Are reactive thermoplastic polymers suitable for future wind turbine composite materials blades? *Mechanics of Advanced Materials and Structures* **21**, 213–221 (2014).
105. Yan, C. *et al.* Preparation and properties of continuous glass fiber reinforced anionic polyamide-6 thermoplastic composites. *Materials & Design* **46**, 688–695 (2013).
106. Matsuzaki, R., Seto, D., Todoroki, A. & Mizutani, Y. Void formation in geometry–anisotropic woven fabrics in resin transfer molding. *Advanced Composite Materials* **23**, 99–114 (2014).
107. Mehdikhani, M., Gorbatikh, L., Verpoest, I. & Lomov, S. V. Voids in fiber-reinforced polymer composites: A review on their formation, characteristics, and effects on mechanical performance. *Journal of Composite Materials* **53**, 1579–1669 (2019).

108. Semperger, O. V. & Suplicz, A. The Effect of the Parameters of T-RTM on the Properties of Polyamide 6 Prepared by in Situ Polymerization. *Materials* **13**, 4 (2020).
109. Zaldua, N. *et al.* Nucleation and crystallization of PA6 composites prepared by T-RTM: Effects of carbon and glass fiber loading. *Polymers* **11**, 1680 (2019).
110. Boros, R., Sibikin, I., Ageyeva, T. & Kovács, J. G. Development and Validation of a Test Mold for Thermoplastic Resin Transfer Molding of Reactive PA-6. *Polymers* **12**, 976 (2020).
111. Lagarinhos, J., Santos, L. & Oliveira, J. Effect of Catalyst and Activator on Properties of Polyamide 6 Prepared by Thermoplastic Resin Transfer Molding Technology. *J Mater Eng Perform* **31**, 7098–7103 (2022).
112. Choi, C.-W., Jin, J.-W., Lee, H., Huh, M. & Kang, K.-W. Optimal Polymerization Conditions in Thermoplastic-Resin Transfer Molding Process for Mechanical Properties of Carbon Fiber-Reinforced PA6 Composites Using the Response Surface Method. *Fibers and Polymers* **20**, 1021–1028 (2019).
113. Kovács, Z., Pomázi, Á. & Toldy, A. The flame retardancy of polyamide 6—prepared by in situ polymerisation of ε-caprolactam—for T-RTM applications. *Polymer Degradation and Stability* 109797 (2021).
114. Semperger, O. V. & Suplicz, A. The effect of titanium dioxide on the moisture absorption of polyamide 6 prepared by T-RTM. in *IOP Conference Series: Materials Science and Engineering* vol. 903 12009 (IOP Publishing, 2020).
115. Lee, J., Lim, J. W. & Kim, M. Effect of thermoplastic resin transfer molding process and flame surface treatment on mechanical properties of carbon fiber reinforced polyamide 6 composite. *Polymer Composites* **41**, 1190–1202 (2020).
116. Vicard, C., De Almeida, O., Cantarel, A. & Bernhart, G. Experimental study of polymerization and crystallization kinetics of polyamide 6 obtained by anionic ring opening polymerization of ε-caprolactam. *Polymer* **132**, 88–97 (2017).
117. Li, M.-X. *et al.* Effect of temperature on the mechanical properties and polymerization kinetics of polyamide-6 composites. *Polymers* **12**, 1133 (2020).
118. Kim, B. J., Cha, S. H. & Park, Y. Bin. Ultra-high-speed processing of nanomaterial-reinforced woven carbon fiber/polyamide 6 composites using reactive thermoplastic resin transfer molding. *Composites Part B: Engineering* **143**, 36–46 (2018).
119. Wilhelm, M., Wendel, R., Aust, M., Rosenberg, P. & Henning, F. Compensation of water influence on anionic polymerization of ε-caprolactam: 1. Chemistry and experiments. *Journal of Composites Science* **4**, 7 (2020).
120. Wendel, R., Thoma, B. & Henning, F. Influence of water during manufacturing of aPA6 in the thermoplastic RTM process. in *Conference of the Polymer Processing Society* 10–14 (2017).
121. Murray, J. J., Robert, C., Gleich, K., McCarthy, E. D. & Brádaigh, C. M. Ó. Manufacturing of unidirectional stitched glass fabric reinforced polyamide 6 by thermoplastic resin transfer moulding. *Materials & Design* **189**, 108512 (2020).
122. Murray, J. J. *et al.* Effect of glass fibre sizing on the interfacial properties of composites produced using in-situ polymerised Polyamide-6 transfer moulding. *Composites Part B: Engineering* **235**, 109743 (2022).
123. Osváth, Z. *et al.* Post-polymerization heat effect in the production of polyamide 6 by bulk quasiliving anionic ring-opening polymerization of ε-caprolactam with industrial components: A green processing technique. *Processes* **8**, 856 (2020).
124. Schmidhuber, S., Fries, E. & Zimmermann, P. It couldn't be more hybrid. Thermoplastic-matrix rtm on the roof frame of the roading roadter. *Kunstst. Int* 1–2 (2017).
125. Bitterlich et al., M. Tailored to Reactive Polyamide 6. *Kunststoffe International* **3**, 80–84 (2014).
126. N, M. T-RTM Components from Caprolactam–Performance Characteristics, Processing Aspects and In-line Testing, Employing Active Thermography. *SAMPE Europe* 1–8 (2017).
127. Reith, L., Weissinger, M., Mueller, N., Sperneder, G. & Schoefer, G. Method for the production of plastic parts. Preprint at (2018).
128. Sealy, C. Molding the future: Engel takes composite approach to composites. *Reinforced Plastics* **60**, 138–141 (2016).
129. Garcia Arrieta, S. & Palenzuela Gutierrez, L. Process and device for polymerizing lactams in molds. 1–12 (2016).
130. Müller, N. T-RTM technology and processing of thermoplastic tapes – two technologies managing a common challenge different raw materials lead to competitive products. in *Automotive Composites Conference & Exhibition* (2017).

Chapter 3

PA6 by T-RTM

This chapter focuses on the preparation and characterization of PA6 by anionic ring-opening polymerization. The focus is on how the choice of materials and polymerization conditions affect the final properties of PA6. A detailed analysis and description of these effects are presented throughout this chapter.

3.1 Overview

The main objective of this chapter is to review the AROP process of CL into PA6 and comprehensively examine its processing parameters.

As stated in the previous chapters, numerous parameters have a significant influence on the polymerization process. The nature of reactants used their concentrations, and the temperature are an example of key factors.

In order to define the most suitable processing conditions for producing PA6 using T-RTM technology, the chapter 3 has been thoughtfully divided into two distinct subsections, each addressing critical aspects of the investigation:

- **Formulations**: To achieve optimal PA6 formulations is required a careful balance between the types and concentrations of catalyst and activator. Section 3.2 reports the influence of different catalyst and activator concentrations on the properties of PA6 samples.

- **T-RTM technology:** The study and control of T-RTM manufacturing parameters are mandatory to produce PA6 parts. Section 3.3 reports the effects of mould temperature and polymerization time on the final properties of the produced parts. This study aims to define the optimal cycle time.

Each section focuses on a critical aspect, contributing to a deeper understanding of the synthesis, processing, and characterization of PA6, in order to evaluate its potential as a high-performance thermoplastic matrix. The in-depth study of these elements will provide a deeper insight into the interplay between polymerization, processing, and material properties, paving the way for advances in the field of composites.

3.2 Effect of Catalyst and Activator on Properties of Polyamide 6 Prepared by Thermoplastic Resin Transfer Moulding Technology

Joana Lagarinhos, Laura Santos and José Oliveira

Journal of Materials Engineering and Performance, 2022, 1-6.
(DOI: https://doi.org/10.1007/s11665-022-07044-4)

Abstract

Thermoplastic resin transfer moulding technology has attracted much attention due to the possibility of manufacturing recyclable structural thermoplastic-based composites. Polyamide 6 obtained from anionic ring-opening polymerization (AROP) of *ε*-caprolactam (CL) has been prepared using T-RTM technology. When suitable catalyst and activator are used, the transformation occurs at a significantly faster reaction rate. Four different formulations were prepared. The influence of catalyst and activator amount on chemical, thermal and mechanical properties were analysed. Higher monomer conversions and molecular weight were obtained for samples with lower catalyst and activator content, indicating a pronounced effect of concentrations on final samples properties. Mechanical analyses also corroborated this behaviour. Optimizing PA6 formulations is necessary, to achieve reproducible materials with desirable properties.

Keywords

Polyamide 6; ε-caprolactam; *in situ* polymerization; anionic ring-opening polymerization; thermoplastic; T-RTM technology-

Contributions

The author had contributed to the planning and execution of all experiments presented herein, as well as on the discussion, interpretation, and preparation of the manuscript. Laura Santos contributed to the experimental procedure related to the preparation of PA6 formulations. José Oliveira contributed to the conception, revision and editing of the entire manuscript.

1. Introduction

In order to answer to many of tomorrow's challenges related to the development of sustainable transportation solutions, innovative high performance lightweight materials are being developed[1]. Initially, the requirements for road transportation market were focused mostly on stiffness, strength, and low cycle time production. Nowadays, environmentally friendly material solutions and recyclability became a "must issue" that led to an important emphasis on thermoplastic resin solutions.

Thermoplastic is a class of polymers that can be softened and melted by heat application[2]. In addition to the recyclability advantage, some thermoplastics have higher impact strength and ductility than thermoset currently used[3]. However, the viscosity of a thermoplastic resin is typically higher than the viscosity of a thermoset and can hinder the impregnation process[4]. To overcome this shortcoming, the polymerization of low-viscosity monomers or oligomers through reactive processing techniques was investigated. Among suitable polymerization types, the ring-opening polymerization (ROP) is the most common and it involves cationic or anionic reaction mechanisms[5,6]. Anionic polymerization proceed through an activated monomer mechanism and is mainly used to manufacture polyamides (PA6, PA10, PA12) from the corresponding lactams[7,8]. This mechanism is commonly designated by anionic ROP (AROP). Cationic initiation is also possible but not so effective due to the low molecular weight and conversion rate of the resulting polyamides[9].

The anionic reactive polymerization of ε-caprolactam (CL), combined with a catalyst and an activator in polyamide 6 (PA6), is among one of the most developed forms of reactive processing of thermoplastics by AROP[9,10]. The CL polymerization into PA6 (Figure 3.2.1) is performed at temperatures between 130-180 ºC in short cycle times, thus increasing the energy efficiency of the process. This reactive processing method is also characterized by the occurrence of polymerization and crystallization simultaneously, once processing occurs below the melting and crystallization temperature of the polymer[3,11,12].

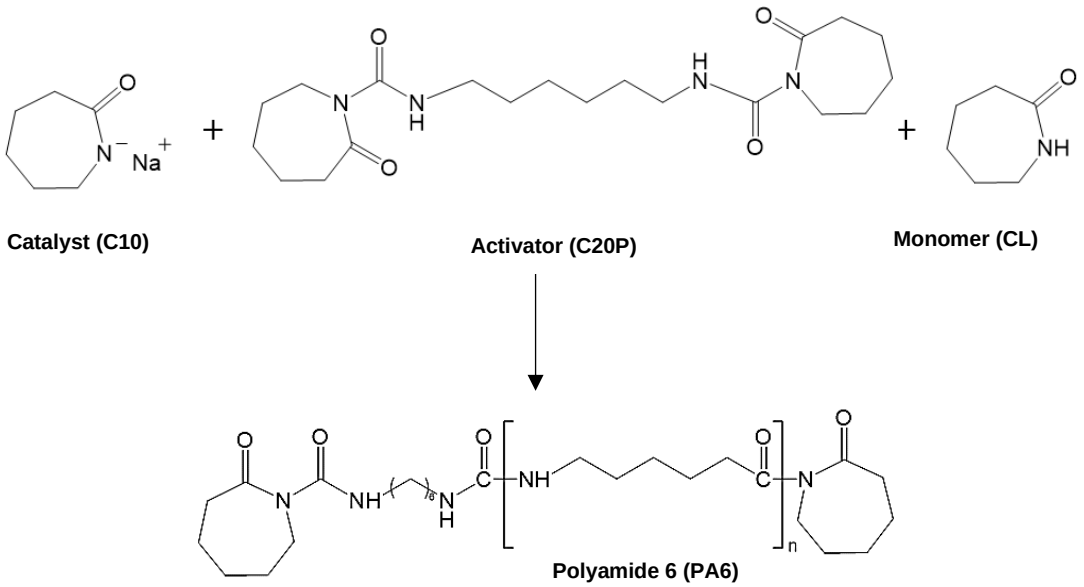

Figure 3.2.1. Anionic polymerization of CL into PA6, using C10 as catalyst and C20P as activator.

Regarding the processing technologies for AROP there are several approaches. Rijswijk *et al*. studied the vacuum infusion process using PA6 as matrix and glass fibre as reinforcement for wind turbines manufacturing[11,12]. The influence of polymerization conditions as well as the choice of catalyst and activator to produce PA6 matrix has been undertaken[3,13]. Gong *et al.*[14] managed to successfully produce reinforced composites with PA6 fibre and PA6 matrix via anionic polymerization of CL using an adapted resin transfer moulding (RTM) processing procedure. The influence of moulding temperature on thermal and mechanical properties was investigated. The authors achieved a high conversion degree and a low void fraction of samples. A strong interaction between PA6 matrix and fibre was also obtained.

Thermoplastic resin transfer moulding (T-RTM) is a promising technology with potential for the production of lightweight thermoplastic composites for automotive applications[4,15–18].

This technology is based in the injection of a reactive mixture (a low viscosity monomer with a suitable catalyst and activator) to a preheated mould, in which occurs a *in situ* polymerization[7,8]. Moreover, it allows the production of thermoplastic composites with relatively short mould cycle times. However, to achieve reproducible results there are a significant number of factors that could influence the final properties of a material obtained by T-RTM technology[4,16–20].

Semperger *et al.*[4] demonstrated the importance of investigate the effect of different parameters such as, polymerization time and mould temperature on morphological and mechanical properties of the final product. The obtained results demonstrated that monomer residual fraction and crystallinity degree were affected by increasing mould temperature. Mechanical performances and hardness were also influenced by tool temperature. The authors highlighted that mould temperature influenced the crystallinity, conversion degree and mechanical properties of the material and residence time had no significant effect during measurements.

Wilhelm *et al.*[20–22] evaluated the influence of moisture content on the AROP reaction. The authors introduced water into CL system, and the results revealed that polymerization was affected, slowing the reaction by deactivating the reactive components. During T-RTM, it is necessary to control the moisture content to achieve a good polymerization.

Other T-RTM studies demonstrated the potential of the technology to manufacture PA6 reinforced with carbon and glass fibres, and appropriate conditions are required[4,15,20–24].

Despite the research dedicated to thermoplastic-based composites, very few papers on the optimization of PA6 formulation from AROP of CL monomer have been performed. In AROP, the type and the amount of catalyst and activator chemically influence the polymer chains development. It is therefore necessary to find a balance between these factors to achieve the desirable properties.

This work focuses on the production of PA6 using a developed laboratory equipment designed for T-RTM technology. The aim is to investigate the effect of different concentrations of catalyst and activator on the properties of the produced PA6 samples.

2. Methodology

2.1. Materials

The PA6 samples were obtained from AROP of AP-Nylon® caprolactam monomer (melting point 69 ºC and density 0.6-0.7 g·cm^{-3}). Bruggolen® C10 (C10), that contains 17-19% sodium caprolactamate in caprolactam, was used as catalyst, and Bruggolen® C20P (C20P), a blocked diisocyanate in caprolactam with a cyanate (NCO) with approximately 17% of content, was used as activator. All chemical components employed in this work were purchased from L. Brüggemann GmbH and Co. KG, Germany. These components were stored and kept under vacuum overnight at 40 ºC to avoid moisture problems.

2.2. PA6 preparation through T-RTM

The AROP of CL into PA6 was performed in a semiautomatic T-RTM laboratory equipment. The scheme of T-RTM process is shown in Figure 3.2.2(a) as well as a scheme of the tensile test samples, Figure 3.2.2(b).

The laboratory T-RTM setup consists of a dosing unit with two tanks, a mixing head, a mould heating system, a pressure, and vacuum control system. The CL monomer was divided into two equal parts and placed into the two tanks. Catalyst (C10) was added to the one of the tanks and the activator (C20P) was added to the other tank. The melt temperature in each tank was set to 90 ºC under stirring.

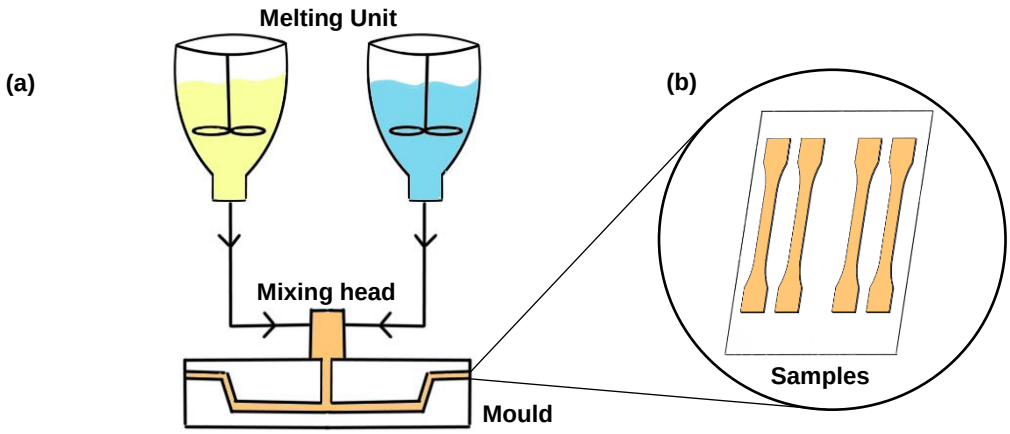

Figure 3.2.2. Schematic representation of T-RTM process **(a)** and mould shape **(b)** with tensile specimens employed.

After melting the components, the CL/C10 and CL/C20P flow through the different inlets into the mixing head (110 ºC) under controlled pressure and vacuum. Through impingement, the reactive mixture is injected into a preheated mould (160 ºC). The polymerization reaction occurs inside the mould. Following polymerization time (≈5 minutes), the plate (280mm x 150mm x 2mm) was demoulded, and samples prepared for further characterized.

Table 3.2.1 shows the compositions of the PA6 samples prepared by T-RTM.

Table 3.2.1. Chemical composition of the developed PA6 samples.

Samples	C10 (wt.%)	C20P (wt.%)	$\frac{C10}{C20P}$ (%)	CL (wt.%)	$\frac{C10+C20P}{CL}$ (%)
F1	6	4	1.5	90	11.1
F2	4.5	3	1.5	92.5	8.1
F3	3	2	1.5	95	5.3
F4	2.2	1.5	1.47	96.3	3.8

*wt. – percentage by weight

2.3. Differential scanning calorimetry (DSC) analyses

To determine the melting point (T_m) and crystallinity degree (X_c) of developed PA6 samples, a DSC equipment (Shimadzu DSC-60) was employed. During testing, two runs were carried out for each sample, and the second run was the one considered to determine the thermal properties. In the first run samples were heating from -25 ºC to 250 ºC at a scan rate of 10 ºC·min^{-1} and held for 2 min at this temperature to eliminate the thermal history and for self-seeding prevent of PA6[25]. After that, the samples were cooled again up to -25 ºC. In the second run, the cycle was repeated, and the data collected.

The X_c was determined according to equation 1:

$$\mathrm{Xc}\ (\%) = \frac{\Delta \mathrm{H_m}}{\Delta \mathrm{H_m^0}} \times 100 \qquad (1)$$

in which ΔH_m is the experimental heat of fusion, and ΔH_m^0 corresponds to the value for 100% of fully crystalline material (PA6 = 190 J·g^{-1})[26].

2.4. Viscosity average molecular weight

The viscosity average molecular weight (M_v) was measured according to DIN 51562-1 using a Ubbelohde viscosimeter, with a capillary diameter of 0.53 mm. The measurements were performed at 25 ºC, dissolving the samples in 85% formic acid with a concentration of 0.005 g·mL^{-1}. From the flow times (average of 5 measurements), the inherent viscosity (η_{inh}) was calculated according to equation 2:

$$\mathrm{n_{inh}} = \frac{\ln \frac{\mathrm{t}}{\mathrm{t_0}}}{\mathrm{c}} \qquad (2)$$

where *t* and t_0 are the flow time of the polymer solution and pure solvent respectively, through a capillary tube, and c is the concentration of the polymeric solution. For M_v calculation, it is assumed that the inherent viscosity is equal to the intrinsic viscosity ($\eta_{inh} = \eta_{int}$). Based on the results from η_{int} and using the Mark-Houwink equation (Equation 3), M_v can be calculated:

$$[\eta_{\mathrm{int}}] = \mathrm{K} \times \mathrm{M}_v^{\alpha} \qquad (3)$$

in which, *K* and *α* are the Mark-Houwink constants which depend on the specific combination of polymer-solvent used. In this polymer-solvent combination $K = 22.6 \times 10^{-3}$ $cm^3 \cdot g^{-1}$ and $\alpha = 0.82$[27].

2.5. Thermal analyses

Thermogravimetric analysis (TGA) was performed on a Hitachi STA300 equipment. A heating rate of 10 °C·min^{-1} was used from room temperature to 600 ºC, under N_2 atmosphere (flow rate of 100 mL·min^{-1}). TGA data and their corresponding first derivative (DTG) were collected to determine the thermal parameter's reaction. Conversion degree (DC) of CL through loss of mass, was calculated by following equation:

$$\mathrm{DC}\ (\%) = \frac{\mathrm{W_a}}{\mathrm{W_b}} \times 100\% \qquad (4)$$

where W_a is the weight measured at 240 ºC (inflexion point between monomer evaporation and polymer degradation), and W_b is the initial weight of the sample.

2.6. Mechanical analyses

The tensile tests were performed at room temperature on a universal testing machine Shimadzu AG-IS with a 10 kN load cell. Standard specimens of PA6 were cut out from the central part of plates according to ISO 527-2 standard (Type 1BA). A constant crosshead speed of 1 mm·min^{-1} was used. The tensile strength (σ_{max}) and elongation at break (ε_{max}) were taken from the maximum values from the stress-strain curve. The elongation of each specimen was measured using a video extensometer (DVE-101/201).

3. Results and Discussion

The influence of different amount of catalyst of activator was studied based on chemical, thermal and mechanical properties.

The DSC curves of the second run, in Figure 3.2.3, showed that the melting point has been influenced by the amount of catalyst and activator used in samples.

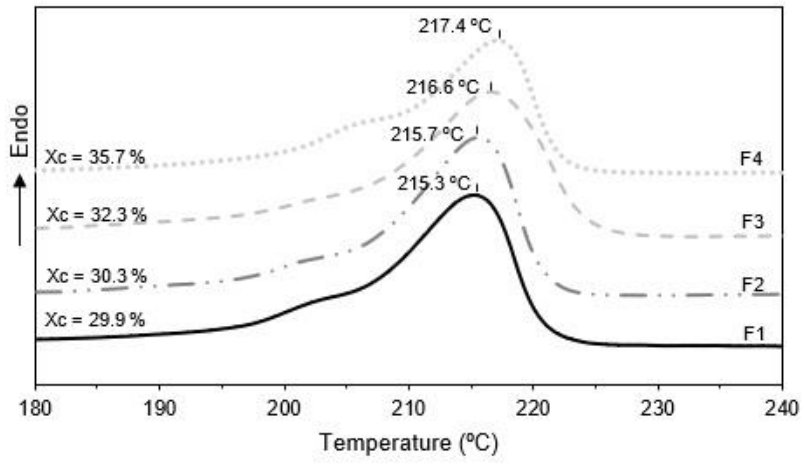

Figure 3.2.3. DSC curves of PA6 samples.

For higher concentrations of catalyst and activator, a lower melting point was achieved. This phenomenon has been explained by branching reactions that can occur during AROP[28,29]. Rijswijk *et al*.[3] reported that using difunctional and high concentration of activator, the monomer concentration depletes rapidly due to fast polymerization kinetics, characteristic of AROP reactions. Thus, the active amide anions on the polymer chain, attack the neighbouring polymer chains, causing branching. A transition in PA6 crystal structure can be also caused by branching, which may result in a decreasing of melting points. During synthesis of PA6 two types of crystals can appear: α-structure, which presents a $T_m = 220$ °C, and γ-structure, with a $T_m = 214$ °C[30]. If an excessive branching occurs, the γ-structure content can increase, thus reducing the melting point. Another explanation for the reducing of melting points is the residual CL monomer content that can remain in polymer after the polymerization process[3,31].

In Figure 3.2.3, it is also presented the crystallinity degree of the samples calculated according to equation 1. It can be observed that crystallinity degree also depends on the amount of catalyst of activator once it decreases gradually from 35.7% to 29.9% by increasing the amount of catalyst and activator. This behaviour is also due to the effect of branching, that changes the polymer chain and consequently, the formation of crystals is disturbed, affecting the crystallization process[3].

The decrease in crystallinity degree was attributed to the increase in molecular weight, which indicates that crystallization of PA6 was difficulted by the branching structures resulted from difunctional activator[32]. Table 3.2.2 showed the viscosity average molecular weights for PA6 samples. Higher amounts of catalyst and activator also influenced the molecular weight. The increasing of catalyst and activator concentrations, lead to a decreasing in molecular weight. As previously mentioned, using a difunctional activator, branching is more apparent. The macromolecular chains are not able to reorganize into perfect crystalline structures, thus reducing the molecular weight of the polymer[20,28,32]. This reduction is also accompanied by crystallinity and melting point reduction, as observed in Figure 3.2.3.

Table 3.2.2. Viscosity average molecular weight values of PA6 samples.

Sample	M_v (kg/mol)
F1	117.3 ± 2.7
F2	160.3 ± 2.2
F3	197.9 ± 1.5
F4	210.0 ± 2.0

In order to characterize the final conversion degree of the polymer, TGA was used to measure the evaporating residual amount of CL contained in samples. TGA thermograms and the corresponding first DTG graphs are presented in Figure 3.2.4.

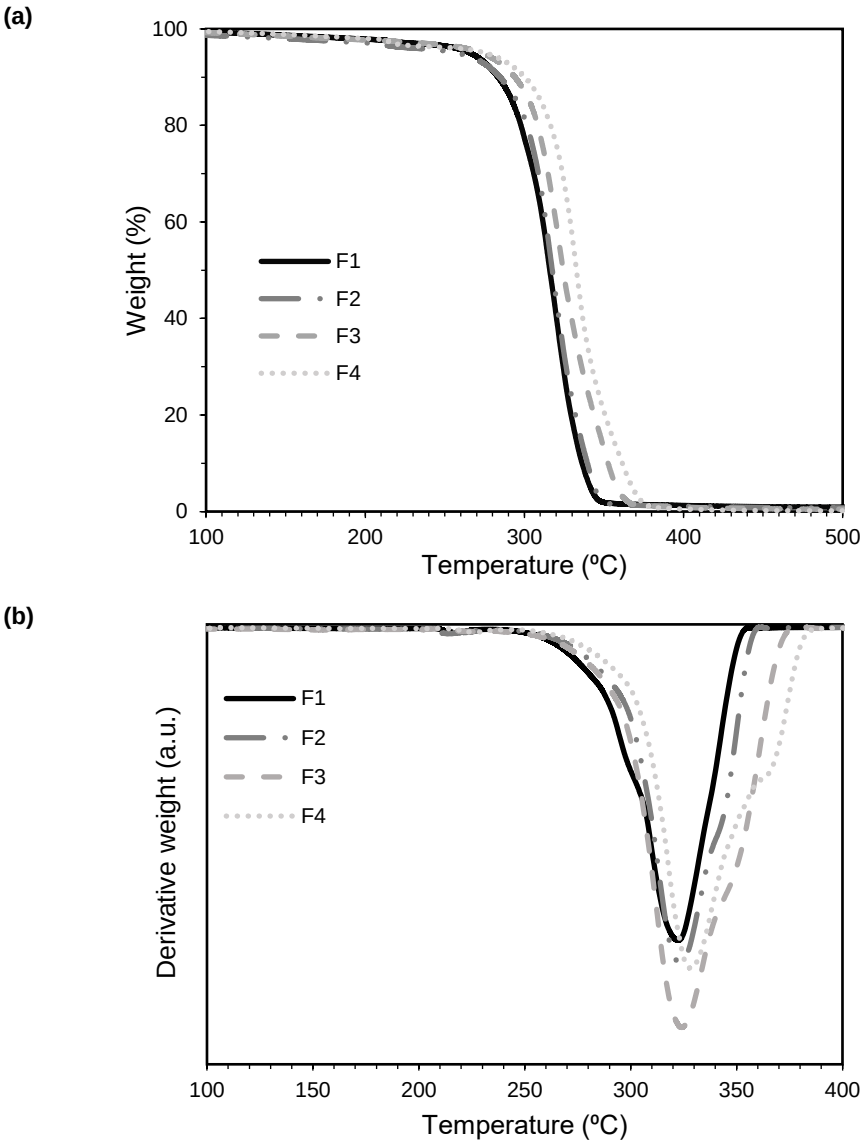

Figure 3.2.4. TGA **(a)** and DTG **(b)** curves of PA6 samples.

Two different ranges are observed on TGA curve. The first range between 100 and 240 ºC corresponds to residues of unconverted CL monomer evaporation[33]. As endothermic peak between 200 and 240 ºC revealed, the monomer evaporation occurs at the same time that PA6 melting. The second range started at around 260 ºC with a continuous weight loss, which refers to PA6 degradation. The thermal pattern showed that all samples were completely burnt under N_2 atmosphere before 400 ºC.

To analyse the thermal stability of PA6 materials to resist the action of heat, weight loss temperatures were monitored. $T_{5\%}$, $T_{10\%}$ and $T_{50\%}$ that corresponds to 5%, 10% and 50% weight loss occur, respectively, and T_{max} (temperature of maximum mass change) were noted from TGA thermograms (Table 3.2.3)[34]. The decomposition temperatures of samples increased with the decrease of catalyst and activator concentrations (from F1 to F4). This tendency revealed an improvement of thermal stability in samples with lower catalyst and activator levels. The derivate plots also corroborated this behaviour. The maximum weight loss rate was higher for samples with lower catalyst and activator content. Such an observation promotes the PA6 degradation in an early stage, as previous observed in TGA thermogram.

Table 3.2.3. Thermal data obtained from TGA and DTG curves of PA6 samples.

Sample	DC (%)	$T_{5\%}$ (ºC)	$T_{10\%}$ (ºC)	$T_{50\%}$ (ºC)	T_{max} (ºC)
F1	96.5 ± 0.2	266.4 ± 0.4	284.1 ± 0.5	316.4 ± 0.9	322.8 ± 1.5
F2	96.9 ± 0.1	271.3 ± 0.4	285.7 ± 0.4	318.3 ± 1.2	323.7 ± 0.9
F3	97.3 ± 0.1	273.6 ± 0.3	294.2 ± 0.4	324.2 ± 0.7	324.1 ± 1.0
F4	95.8 ± 0.4	275.8 ± 0.1	300.9 ± 0.2	333.1 ± 1.3	328.3 ± 1.2

DC values, calculated using equation 4, revealed a high conversion rate (between 96-97 wt.%), which mean that the polymerization was almost complete, and a low residual monomer content was achieved. This range is in good agreement with the literature[20,33].

The effect of different concentrations of catalyst and activator on the mechanical behaviour was investigated. The stress-strain curves of samples are presented in Figure 3.2.5. The tensile properties of the developed materials and its standard deviations, namely tensile strength (σ_{max}), strain at break (ε_{max}) and Young Modulus (E) are presented in Table 3.2.4.

Table 3.2.4.Tensile properties of PA6 samples.

Sample	$\sigma_{máx}$ (MPa)	$\varepsilon_{máx}$ (%)	E (GPa)
F1	59.3 ± 3.1	5.9 ± 0.9	2.4 ± 0.1
F2	63.1 ± 2.5	7.6 ± 2.3	2.4 ± 0.2
F3	63.5 ± 2.1	14.3 ± 3.5	2.6 ± 0.3
F4	65.9 ± 1.7	20.1 ± 2.9	2.7 ± 0.2

It can be seen from Figure 3.2.5, that tensile strength (σ_{max}) slightly increases with the decreasing of catalyst and activator concentrations. F4 sample shows the highest tensile strength (65.9 MPa). As observed, the tensile strength is weakened due to the loading of more amount of catalyst and activator concentrations.

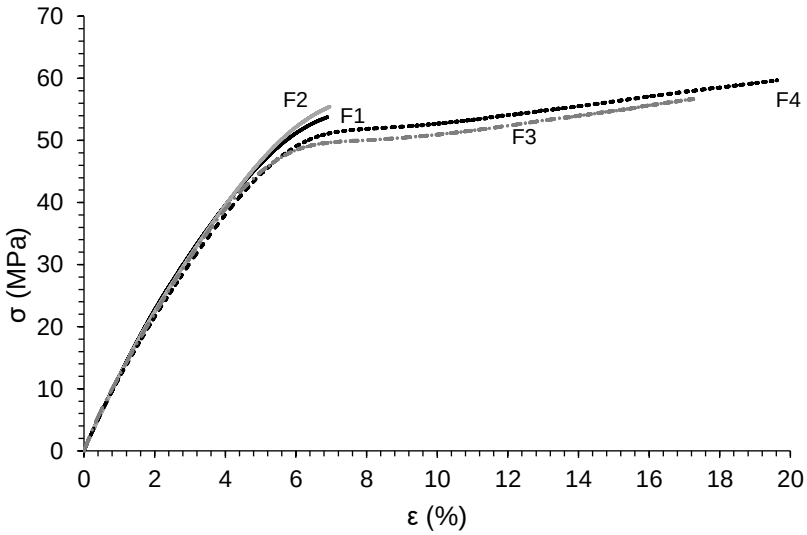

Figure 3.2.5. Tensile stress-strain curves of PA6 samples.

Samples F3 and F4 revealed an elastomeric behaviour given by a higher strain at break and a lower Young modulus. It can be also observed through Figure 3.2.5, that the elongation at break increases when the concentrations are lower. A slightly increase is also observed in Young modulus from 2.4 GPa to 2.7 GPa. As expected, higher crystallinity degree promotes a higher elastic modulus and tensile strength.

Comparing the obtained results with a commercial injection PA6, it can be concluded that the achieved results are higher. This behaviour is explained by high crystallinity degree and high molecular weight, characteristic of an anionic polymerized PA6[13].

4. Conclusions

The objective of this work was to develop an experimental investigation of several PA6 formulations obtained from in situ using a laboratorial equipment. AROP of CL was conducted by

using a C10 catalyst in combination with a C20P activator. Chemical, thermal, and mechanical data were investigated using a wide range of characterization techniques.

The results showed that the PA6 properties were affected by using different concentrations of catalyst and activator. The addition of higher concentrations of catalyst and activator resulted in a decrease in crystallinity degree of PA6 materials. Molecular weight measurements also clarified the influence of concentrations on molecular weight of the final PA6 polymer. As expected, the molecular weight increased with decreasing the amount of activator and catalyst. TGA revealed that higher thermal stability was achieved for samples with lower concentrations. However, a high conversion degree of 96-97% was reached for all samples, resulting in an almost complete polymerization and a low residual monomer content. Mechanical properties were predominantly influenced by crystallinity degree and conversion degree. The tensile properties revealed a more viscoelastic behaviour for lower catalyst and activator samples.

Based in the obtained results, PA6 samples demonstrated well-defined properties, determined by the concentrations of catalyst and activator. These findings also demonstrated the potential of the T-RTM to produce thermoplastic materials for industrial applications.

Acknowledgements

The authors would like to acknowledge to Simoldes Group for funding this research. This is a project in collaboration with Simoldes Plásticos, S.A. This work was also developed within the scope of the project CICECO-Aveiro Institute of Materials, UIDB/50011/2020 & UIDP/50011/2020, financed by national funds through the Portuguese Foundation for Science and Technology/MCTES. The authors would like to acknowledge Helder Morais for CNC specimen machining.

References

1. Mallick, P. K. Advanced materials for automotive applications: An overview. in *Advanced materials in automotive engineering* 5–27 (Elsevier, 2012).
2. Mallick, P. K. Thermoplastics and thermoplastic–matrix composites for lightweight automotive structures. in *Materials, design and manufacturing for lightweight vehicles* 187–228 (Elsevier, 2021).
3. Van Rijswijk, K., Bersee, H. E. N., Beukers, A., Picken, S. J. & Van Geenen, A. A. Optimisation of anionic polyamide-6 for vacuum infusion of thermoplastic composites: Influence of polymerisation temperature on matrix properties. *Polym Test* **25**, 392–404 (2006).
4. Semperger, O. V. & Suplicz, A. The Effect of the Parameters of T-RTM on the Properties of Polyamide 6 Prepared by in Situ Polymerization. *Materials* **13**, 4 (2020).
5. Šebenda, J. Polymerizability of lactams. in *Polymerization of Heterocycles (Ring Opening)* 329–334 (Elsevier, 1977).
6. Nuyken, O. & Pask, S. Ring-opening polymerization—an introductory review. *Polymers* **5**, 361–403 (2013).
7. Ageyeva, T., Sibikin, I. & Karger-Kocsis, J. Polymers and related composites via anionic ring-opening polymerization of lactams: Recent developments and future trends. *Polymers (Basel)* **10**, 357 (2018).
8. Sibikin, I. & Karger-Kocsis, J. Toward industrial use of anionically activated lactam polymers: Past, present and future. *Advanced Industrial and Engineering Polymer Research* **1**, 48–60 (2018).
9. Sekiguchi, H., Ivin, K. J. & Saegusa, T. Ring-Opening Polymerization. *J., Saegusa, T., Eds.; Elsevier London UK* **2**, 809 (1984).
10. Roda, J. Polyamides. in *Handbook of Ring-Opening Polymerization* 165 (2009).
11. Van Rijswijk, K., Teuwen, J. J. E., Bersee, H. E. N. & Beukers, A. Textile fiber-reinforced anionic polyamide-6 composites. Part I: The vacuum infusion process. *Compos Part A Appl Sci Manuf* **40**, 1–10 (2009).

12. van Rijswijk, K., Lindstedt, S., Vlasveld, D. P. N., Bersee, H. E. N. & Beukers, A. Reactive processing of anionic polyamide-6 for application in fiber composites: A comparative study with melt processed polyamides and nanocomposites. *Polym Test* **25**, 873–887 (2006).
13. Rijswijk, K. Van, Bersee, H. E. N., Jager, W. F. & Picken, S. J. Optimisation of anionic polyamide-6 for vacuum infusion of thermoplastic composites : choice of activator and initiator. *Compos Part A Appl Sci Manuf* **37**, 949–956 (2006).
14. Gong, Y., Liu, A. & Yang, G. Polyamide single polymer composites prepared via in situ anionic polymerization of ε-caprolactam. *Compos Part A Appl Sci Manuf* **41**, 1006–1011 (2010).
15. Murray, J. J., Robert, C., Gleich, K., McCarthy, E. D. & Brádaigh, C. M. Ó. Manufacturing of unidirectional stitched glass fabric reinforced polyamide 6 by thermoplastic resin transfer moulding. *Mater Des* **189**, 108512 (2020).
16. Zaldua, N. *et al.* Nucleation and crystallization of PA6 composites prepared by T-RTM: Effects of carbon and glass fiber loading. *Polymers (Basel)* **11**, 1680 (2019).
17. Boros, R., Sibikin, I., Ageyeva, T. & Kovács, J. G. Development and Validation of a Test Mold for Thermoplastic Resin Transfer Molding of Reactive PA-6. *Polymers (Basel)* **12**, 976 (2020).
18. Murray, J. J. *et al.* Thermoplastic RTM: Impact Properties of Anionically Polymerised Polyamide 6 Composites for Structural Automotive Parts. *Energies* **14**, 5790 (2021).
19. Barhoumi, N., Maazouz, A., Jaziri, M. & Abdelhedi, R. Polyamide from lactams by reactive rotational molding via anionic ring-opening polymerization : Optimization of processing parameters. *Express Polym Lett* **7**, 76–87 (2013).
20. Wilhelm, M., Wendel, R., Aust, M., Rosenberg, P. & Henning, F. Compensation of water influence on anionic polymerization of ε-caprolactam: 1. Chemistry and experiments. *Journal of Composites Science* **4**, 7 (2020).
21. Herzog, J. *et al.* Moisture Adsorption and Desorption Behavior of Raw Materials for the T-RTM Process. *Journal of Composites Science* **5**, 12 (2021).
22. Wendel, R., Thoma, B. & Henning, F. Influence of water during manufacturing of aPA6 in the thermoplastic RTM process. in *Conference of the Polymer Processing Society* 10–14 (2017).
23. Bitterlich et al., M. Tailored to Reactive Polyamide 6. *Kunststoffe International* **3**, 80–84 (2014).
24. Murray, J. J. *et al.* Impact Performance of Thermoplastic Resin Transfer Moulded Carbon Fibre Composites. in *SAMPE Europe Conference* (2020).
25. Sangroniz, L., Cavallo, D. & Müller, A. J. Self-nucleation effects on polymer crystallization. *Macromolecules* **53**, 4581–4604 (2020).
26. Cartledge, H. C. Y. & Baillie, C. A. Studies of microstructural and mechanical properties of nylon/glass composite Part I The effect of thermal processing on crystallinity, transcrystallinity and crystal phases. *Journal of Materials Science* **34**, 5099–5111 (1999).
27. Mattiussi, A., Gechele, G. B. & Francesconi, R. Polyamides in solution. III. Viscometry of linear polycaprolactam. *Journal of Polymer Science Part A-2: Polymer Physics* **7**, 411–422 (1969).
28. Udipi, K., Davé, R. S., Kruse, R. L. & Stebbins, L. R. Polyamides from lactams via anionic ring-opening polymerization: 1. Chemistry and some recent findings. *Polymer (Guildf)* **38**, 927–938 (1997).
29. Davé, R. S., Kruse, R. L., Stebbins, L. R. & Udipi, K. Polyamides from lactams via anionic ring-opening polymerization: 2. Kinetics. *Polymer (Guildf)* **38**, 939–947 (1997).
30. Rwei, S.-P., Ranganathan, P. & Lee, Y.-H. Isothermal crystallization kinetics study of fully aliphatic PA6 copolyamides: Effect of novel long-chain polyamide salt as a comonomer. *Polymers* **11**, 472 (2019).
31. Ricco, L., Russo, S., Orefice, G. & Riva, F. Anionic poly (ε-caprolactam): Relationships among conditions of synthesis, chain regularity, reticular order, and polymorphism. *Macromolecules* **32**, 7726–7731 (1999).
32. Rusu, G., Ueda, K., Rusu, E. & Rusu, M. Polyamides from lactams by centrifugal molding via anionic ring-opening polymerization. *Polymer (Guildf)* **42**, 5669–5678 (2001).
33. Zhang, C., Feng, L. & Hu, G. Anionic Polymerization of Lactams: A Comparative Study on Various Methods of Measuring the Conversion of ε-Caprolactam to Polyamide 6. *Journal of Applied Polymer Science* **101**, 1972–1981 (2006).
34. Król-Morkisz, K. & Pielichowska, K. Thermal decomposition of polymer nanocomposites with functionalized nanoparticles. in *Polymer Composites with Functionalized Nanoparticles* 405–435 (Elsevier, 2019).

3.3 Optimization of processing conditions in Thermoplastic Resin Transfer Moulding for PA6 production

Joana Lagarinhos[1,2], Sara Magalhães da Silva[1,2] and Martinho Oliveira[1,2]

[1]EMaRT Group – Emerging: Materials, Research, Technology, School of Design, Management and Production Technologies, University of Aveiro, Estrada do Cercal 449, 3720-509 Oliveira de Azeméis, Portugal

[2]CICECO - Aveiro Institute of Materials, University of Aveiro, Campus Universitário de Santiago, 3810-193 Aveiro, Portugal

Submitted to Journal of Materials Research

Abstract

Thermoplastic resin transfer moulding (T-RTM) technology is gaining prominence in the automotive industry for high-volume production of high-performance components. Therefore, there is a growing need for lightweight thermoplastic and easily recyclable. In this work, polyamide 6 (PA6) was produced from the low-viscosity monomer by anionic ring-opening polymerization using T-RTM technology. During the manufacturing process, there are parameters that need to be controlled to ensure a high process efficiency. The influence of mould temperatures, ranging from 130 ºC to 170 ºC and the polymerization times, ranging from 2 to 10 min, were evaluated. The results showed that crystallinity degree and molecular weight were predominantly influenced by the higher mould temperatures (between 150 ºC and 160 ºC). In addition, tensile and flexural properties were predominantly affected by crystallinity degree values. Furthermore, the polymerization time used did not have significantly influence on final results. From the conducted experimental work, it was defined 160 ºC as optimal mould temperature and 2 min for polymerization time.

Graphical Abstract

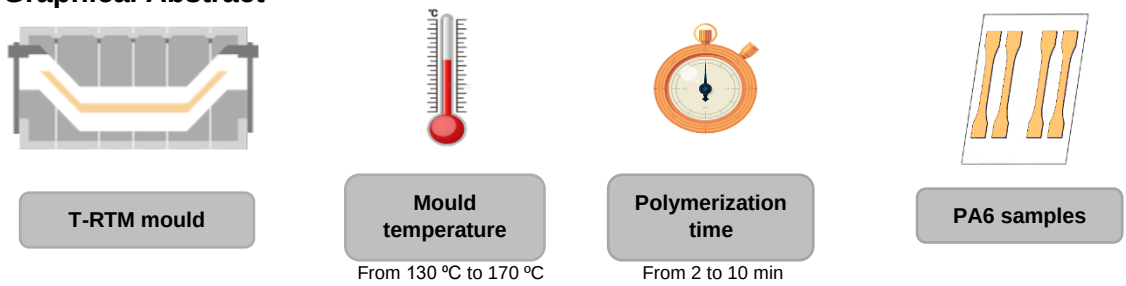

Contributions

The author had contributed to the planning and executing of all experiments presented herein, as well as on the discussion, interpretation, and preparation of all the manuscript. Sara Silva and José Oliveira contributed to the conception, revision and editing of the entire manuscript.

1. Introduction

Thermoplastics have caught the interest of industry in the last decades. This is mainly due to their unique properties, recyclable nature, manufacturing time and easily mouldable[1,2]. These features contribute to the use of thermoplastic materials in a wide range of applications, including aircraft, packaging, electronics, medical devices, automotive parts, and others[3–5].

The automotive industry is one of the major consumer sectors of thermoplastic materials[6,7]. Among different polymers used, polypropylene is by far the most employed polymer in vehicle production, followed by polyurethane and polyamide (PA). Thermoplastics are predominantly used for the production of interior components, owing to the ability to style to the surface quality, and to the easiness of being moulded[8]. In addition, thermoplastic usage in auto parts has shown steady growth due to the possibility of reducing vehicles' weight, which contributes to fuel saving and CO_2 emissions reduction, without impairing vehicles' comfort and safety[9].

Polyamide 6 (PA6) is an engineering thermoplastic used in the production of structural components for autoparts, exhibiting high mechanical performance together with thermal and chemical resistance properties[10–12]. Commercial PA6 is mainly synthesized by hydrolytic polymerization, due to its industrial viability, controllability, and polymerization stability for large-scale operation. However, this polymerization involves various steps[10,13]. On the other way, an anionic polymerization involves an activated monomer mechanism, where PA6 is obtained from the corresponding lactams[14,15]. The lactam polymerization can be an anionic reaction mechanism (initiated by a base) or a cationic reaction mechanism (initiated by an acid). However, cationic mechanisms are limited due to low conversions and low molar masses of the final products[15,16].

The anionic ring-opening polymerization (AROP) of ε-caprolactam (CL) into PA6 is among one of the most developed forms of reactive processing of thermoplastics. It is based on a polymerization mechanism in which the ring-shaped (cyclic) molecules are opened, giving rise to linear monomers or oligomers[15,16]. AROP is the fastest process for PA production, once it is characterized by short polymerization times, resulting in a faster cycle time and, consequently, a more efficient production (compared to thermosets). In addition to the monomer, a catalyst and an activator are needed to initiate and maintain the reaction[17]. This type of polymerization has emerged as a clean alternative to polymerization routes once it does not require hazardous solvents[13,18].

The short polymerization time of CL enables the production of PA6 via Thermoplastic Resin Transfer Moulding (T-RTM) technology[19–21]. T-RTM is an adapted version of resin transfer moulding (RTM), commonly used for thermoset composites. This technology involves the reaction of a monomer with low viscosity and the polymerization takes place directly inside the mould (*in situ*)[22,23]. T-RTM is considered a promising technology with the potential to be used for large-scale production by automotive and aerospace industries due to (1) the easiness of the production of lightweight composites; (2) lower production costs and (3) the ability to recycle[19,23,24]. However, to achieve reproducible results there are a significant number of factors that could influence the final properties

of a material obtained by T-RTM technology, namely, the mould temperature and polymerization time[13,25].

The polymerization mould temperature significantly and directly affects the crystallinity degree, conversion rate, and molecular weight, and in an indirect way also affects the thermomechanical properties[25,26]. This is due to the simultaneously occurrence of polymerization and crystallization of PA6 during AROP. An advantage of using a polymerization temperature (>120 ºC) bellow the melting temperature of PA6 (between 210 and 225 ºC) is the potential for shorter cycle times and increased energy efficiency in the process[27]. This leads to higher crystallinity degree (40-50%) and conversion rates (96-99%) of the material[11,13].

Rijswijk *et al*.[25], investigated the influence of varying the mould temperatures on the properties of PA6. The authors reported that increasing the mould temperature a higher polymerization rate and branching degree, is achieved. Nevertheless, a lower crystallinity degree is also attained. It is important to note that a higher branching degree is linked to reduced final conversion and lower melting point. The relationship between mechanical properties and temperature was also assessed. At low polymerization temperatures, the crystallization rate increased, which causes the mechanical properties and the overall conversion to be reduced.

Maazouz *et al*.[28] developed an isothermal time-temperature-transformation (TTT) diagram through experiments with different mould temperatures below the melting temperature, namely 180, 190 and 200 ºC and, also, above the melting temperature, 230 and 240 ºC. The authors determined the effect of temperature on the induction time, i.e., polymerization time, and viscosity profile. The results highlight that increasing the temperature reduced the polymerization time. As a result of a low polymerization temperature (190 ºC), a slow increase in viscosity was observed, whereas the higher the temperature, the faster the reaction. The temperature range employed was bellow T_c (which is around 180 ºC), and within this range, the lower the temperature, the faster was the crystallization.

More recently, Semperger and Suplicz[26], examined the relationship between crystallinity, mould temperature and polymerization time, also known as residence time. Three mould temperatures (150, 165 and 170 ºC) and three polymerization times (120, 180 and 240s) were employed. At 150 ºC for 120s, a crystallinity degree of 43% was achieved. However, for the same polymerization time and a mould temperature of 175 ºC, the crystallinity degree dropped by 20%. The crystallinity degree decreased as temperature increased, and directly impacting material's mechanical properties. Interestingly, unlike what is found in the literature, the authors determined that polymerization time did not significantly affect the T-RTM process.

In the case of PA6 produced using T-RTM technology, comprehending how temperature and polymerization time influence AROP is crucial. This study examines the impact of polymerization temperatures, ranging from 130 ºC to 170 ºC, and the polymerization times from 2 to 10 min, with 2 min interval. The analysis of the crystallinity degree, monomer conversion, density, molecular weight, tensile and flexural properties were conducted to define the optimal polymerization conditions.

2. Methodology

2.1. Materials

PA6 samples were produced using a monomer, ε-caprolactam (CL) – AP-Nylon®, which has low melt viscosity (3–5 mPa·s), a catalyst, a sodium caprolactamate in caprolactam (C10) – Bruggolen® C10 and an activator, a blocked diisocyanate in caprolactam (C20P) – Bruggolen® C20P. All these raw materials were obtained from L. Brüggemann GmbH and Co. KG, Germany. Before use, these materials were kept dried (Carbolite AX 60) at 35 ºC to avoid moisture. It is known that these components are sensitive to moisture and suffer significant changes in the presence of moisture[29].

2.2. PA6 preparation

A specially designed prototype of T-RTM was used to conduct the experimental work, as described on a previous work[30]. The concentrations used in this study were 95% of CL, 3% of C10 and 2% of C20P based on the aforementioned optimization[30].The polymerization occurred through the mixing of two distinct tanks. One containing the CL monomer and C20P (Figure 3.3.1a – tank A), and the second one filled with CL monomer and C10 (Figure 3.3.1a – tank B). Both tanks were at 90 ºC. A nitrogen (N_2) line was connected to each tank for purging the moisture from tanks and the injection lines. Also, the N_2 line was used to flush the system after injection to prevent the occurrence of polymerization within the heated parts. After mixing the precursors, the resulting liquid mixture was injected into a preheated mould (Figure 3.3.1b) with a plate geometry of 280 x 150 x 2 mm^3. Subsequently, the plates were removed from the mould at room temperature.

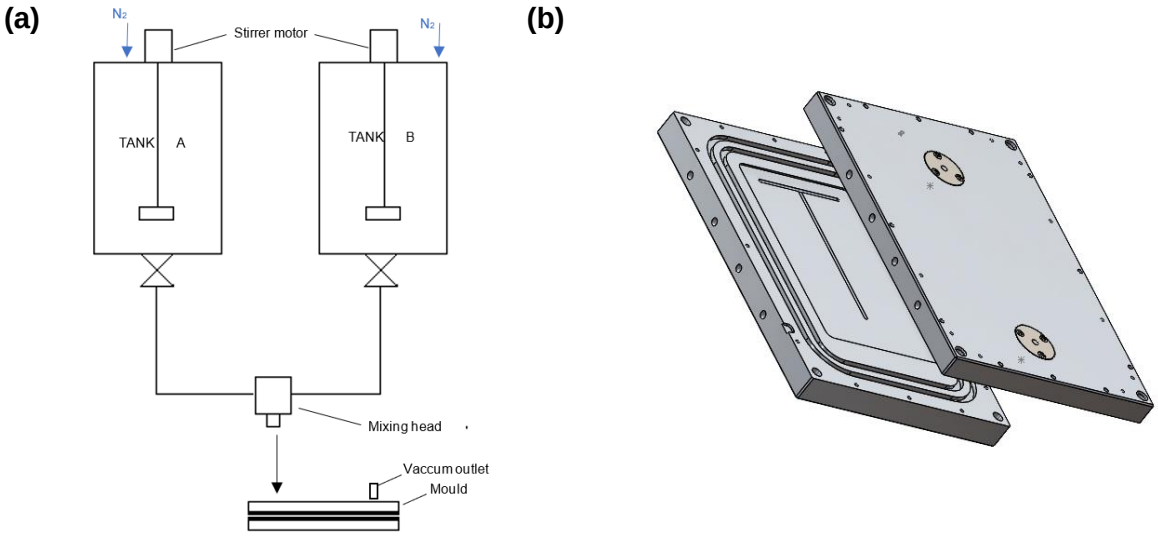

Figure 3.3.1. (a) Schematic diagram of prototype T-RTM equipment and **(b)** CAD image of the mould.

2.3. Processing parameters analysis

During PA6 polymerization, the temperature is a crucial factor that demands careful consideration. Such variations not only influence the polymerization rate, but also impact the properties of the resulting polymer. The literature indicates that the most suitable temperature range is 130-170 ºC and the polymerization time can range from 2 to 10 minutes[25,31].

The experiments were conducted using two independent variables: mould temperature and polymerization time. Mould temperature pertains to the temperature of the tool during the polymerization of samples. Polymerization time initiates at the injection of materials into the mould until the removal of the final parts. Throughout the polymerization process, both mould temperature and polymerization time play a significant role in shaping the morphological structure of the resulting material. This encompasses factors such as molecular weight and crystalline structure, which in turn influence the material's chemical, thermal, and mechanical properties.

The initial phase of the experiments involved the variation of the mould temperature, from 130 to 170 °C, while maintaining the polymerization time constant at 6 min. Subsequently, for the selected mould temperature, the polymerization time varied from 2 to 10 min, with 2 min interval.

2.4. Thermal analyses

Differential scanning calorimetry (DSC) studies were performed using a Shimadzu DSC-60 equipment. A heating/cooling rate of 10 ºC·min^{-1} was set. Sample weight was maintained constant (8-10 mg). Two consecutive heat-cool cycles were conducted ranging from -25 ºC to 250 ºC. The first scan was performed to eliminate any prior thermal history of samples. The crystallinity degree (X_c) of the samples was calculated using the equation 1:

$$Xc\ (\%) = \frac{\Delta H_m}{\Delta H_m^0} \times 100 \qquad (1)$$

, where ΔH_m is the melting enthalpy of the samples and ΔH_m^0 is the melting enthalpy for 100% crystalline PA6 ($\Delta H_m^0 = 190\ J.g^{-1}$)[32].

Thermogravimetric analysis (TGA) was performed using a Hitachi STA-300 thermal analyzer. Samples weighing between 5-7mg were heated up to 600 ºC, using a heating rate of 10 ºC·min^{-1} in an inert atmosphere of nitrogen (flow rate of 100 mL·min^{-1}). TGA curves provided insight into the residual monomer content within the samples, representing the unreacted monomer resulting from the polymerization process. Degree of Conversion (DC) of CL through loss of mass, was calculated according to equation 2:

$$DC\ (\%) = \frac{W_a}{W_b} \times 100\% \qquad (2)$$

where W_a is the weight measured at 240 ºC (inflexion point between monomer evaporation and polymer degradation), and W_b is the initial weight of the sample.

2.5. Viscosity measurements

The viscosity average molecular weight (M_v) was determined using a Ubbelohde viscosimeter with a capillary diameter of 0.53 mm. The M_v values were obtained through samples dissolved in formic acid at 85% for the preparation of solutions with concentrations of 0.005 g·mL^{-1}. The M_v was calculated using Mark-Houwink equation:

$$[\eta] = K \times M_v^a \quad (3)$$

, where constants K and α are equal to 22.6 x 103 and 0.8, respectively[33],and $[\eta]$ is the intrinsic viscosity in dL·g^{-1}. An average of 5 measurements were performed for each sample at 25 ± 0.1 ºC.

2.6. Mechanical analyses

Samples for mechanical analyses underwent a cutting process utilizing a computer numerical control (CNC) machine. The CNC machine (Deckel Maho, DMU 50) operated at a speed of 2500 RPM and a feed rate of 230 mm/min under end milling conditions. It is important to note that all specimens were subjected to precise and accurate cutting, after which they were stored in a desiccator until the testing phase.

The specimens were cut in accordance with ISO 527 type 1BA and ISO 178 for tensile and 3-point bending tests, respectively (Figure 3.3.2). Then, mechanical analyses were performed using a Shimadzu AG-IS universal testing machine equipped with a load cell of 10 kN.

Tensile tests were performed on the samples employing a constant crosshead speed of 1 mm·min^{-1}. To determine the Young's modulus (E), the extension of the specimens during the tensile test was monitored through a video extensometer (Shimadzu DVE 101/201). The tensile strength (σ_{max}) and elongation at break (ε_{max}) were recorded from the maximum values of the stress-strain curve. For the 3-point bending tests, samples were tested with a span length of 32 mm. A constant crosshead speed of 1 mm·min^{-1} was applied to all specimens.

Each sample underwent testing at room temperature, and an average of at least five specimens for each sample type were tested.

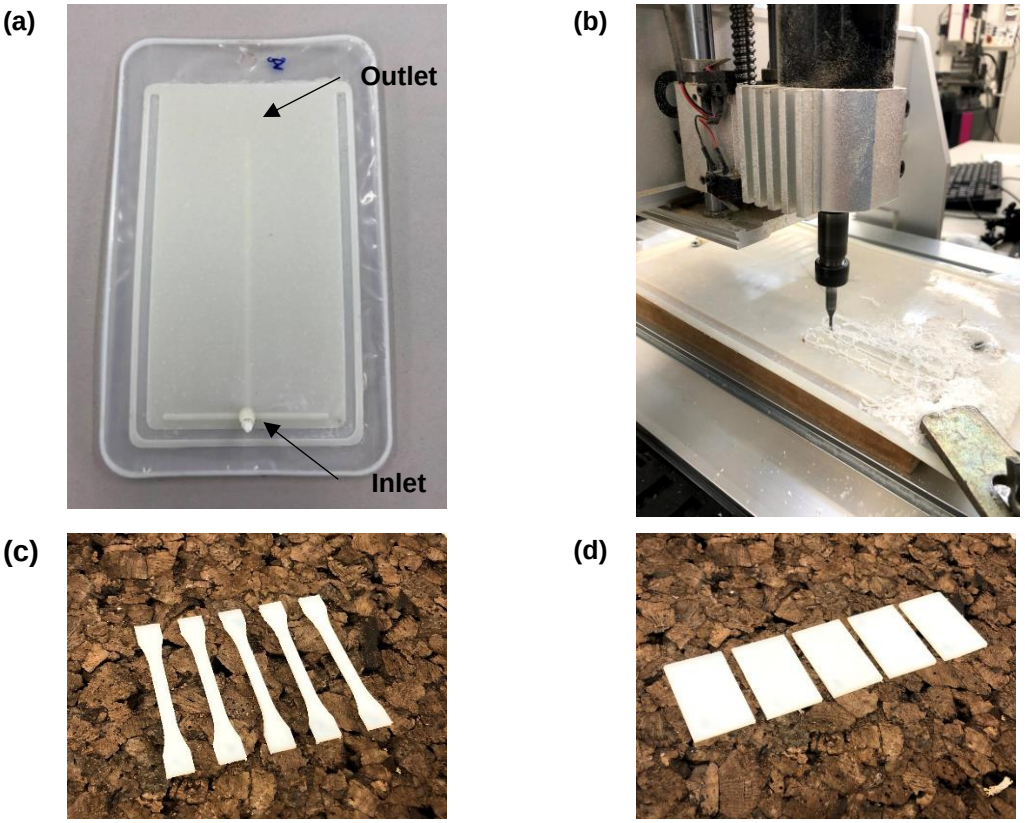

Figure 3.3.2. (a) PA6 plate; **(b)** CNC machining; **(c)**Tensile and **(d)** 3-point bending specimens.

2.7. Dimensional accuracy and density

The analysis of sample thickness and density distribution along the plate was conducted to demonstrate the effects of shrinkage and flow during polymerization. Machining conditions used were the same as for the mechanical tests. Thickness measurements were made from 25 different locations (Figure 3.3.3) ensuring even distribution across each produced plate. These measurements were acquired using an Insize digital calliper with a precision of 0.02mm. Density measurements were carried out at 8 distinct locations (Figure 3.3.3) in accordance with ISO 1183-1: 2019 Method A. The determination of density for each sample was executed using an analytical balance (Ohaus Explorer Pro-210), equipped with a density apparatus.

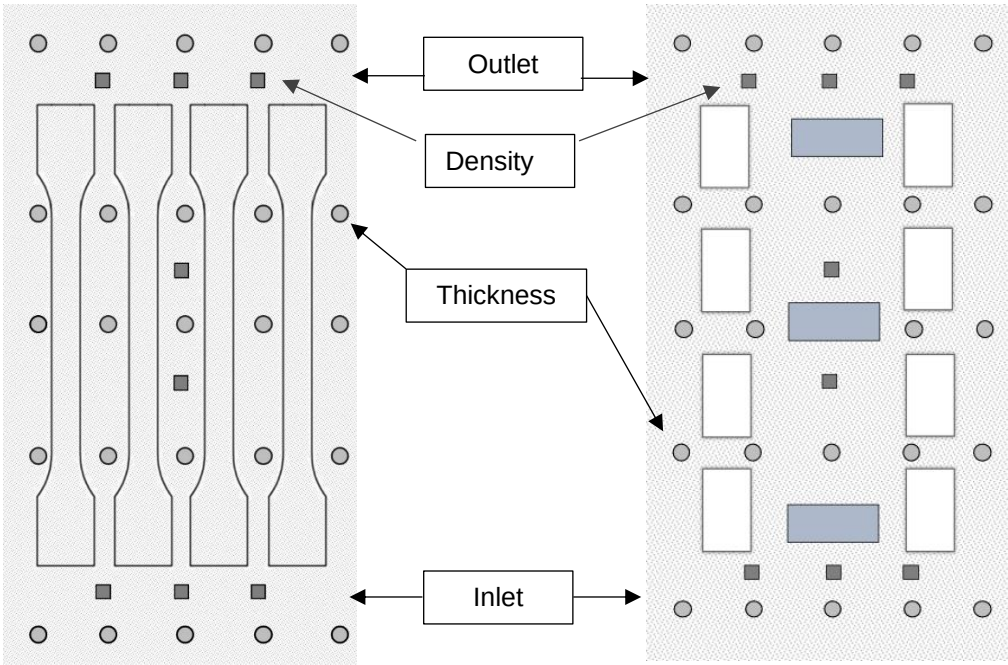

Figure 3.3.3. Layout of density and thickness samples.

3. Results and Discussion

3.1. Influence of polymerization temperature

The impact of mould temperature on the X_c can be seen in Figure 3.3.4. The X_c values decrease from 40.8% to 28.8% as the mould temperature increased. This trend can potentially be attributed to the fact that as the mould temperature is higher, the thermal motion of polymer chains intensifies, rendering it more challenging for the polymeric structure's hydrogen bridge bonds to form[31,34]. Another contributing factor could be the higher temperatures used, that facilitate an increase in branching reactions. Consequently, the number of irregular polymer chains also increases, impeding the crystallization process[25,35].

Furthermore, a noteworthy observation pertains to the higher X_c for the first heating in comparison to the second heating cycle. Crystallization occurs in two different phases – nucleation of the crystal nuclei and the ensuing crystal growth. It is known that higher temperatures hinder the formation of crystal nuclei[36]. The X_c reached its maximum at 130 ºC, where the crystallization during the polymerization process unfolds at an accelerated pace, primarily due to the presence of smaller-sized nuclei. As the mould temperature increases, the X_c values diminish, as the smaller-sized crystal nuclei do not exhibit substantial growth[37]. The explanation for X_c values after the second heating can be attributed to the fact that the samples were already polymerized, and their crystal growth rate had already tapered, rendering them nearly identical across various mould temperatures. This observation underscores the implication for the recyclability of the final material.

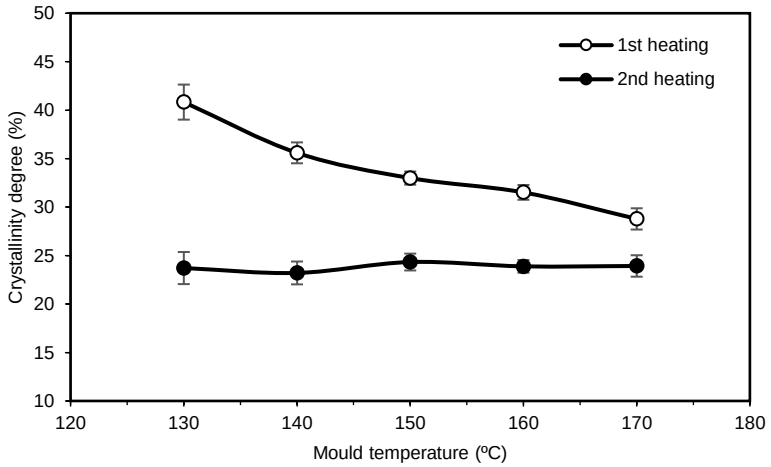

Figure 3.3.4. Effects of polymerization temperature on the X_c of samples.

The influence of mould temperature on the DC and the M_v was also investigated. It is evident that as the mould temperature increases, the M_v of the samples rises from 97000 g/mol to 120000 g/mol (Figure 3.3.5). This phenomenon can be attributed to the elevated polymerization temperature, which accelerates the polymerization rate and, consequently, leads to an increase in the M_η. This behaviour is in alignment with previous observations[25].

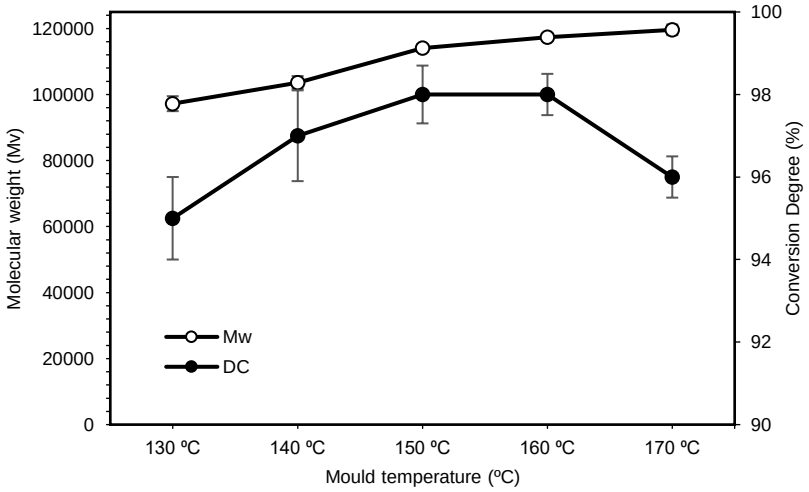

Figure 3.3.5. Effect of mould temperature on M_v and DC of samples.

The residual monomer content remaining in samples after polymerization and the evaluation of thermal stability was assessed by TGA. The presence of residual monomer is indicative of unreacted monomers from the polymerization process, which could subsequently decrease the final conversion rate. Excessive monomer content, exceeding 4-5%, can exert a plasticizing effect that influences the final mechanical properties[31,38]. Therefore, the removal of such content from the polymer becomes necessary[26]. Figure 3.3.6 presents a typical PA6 TGA curve for all studied samples. A previous work has indicated that the unconverted CL monomer tends to evaporate within the temperature range of

100 to 240 ºC[30]. At approximately 250 ºC, a discernible shift occurs, marking the onset of material degradation, culminating in complete degradation around 400 ºC.

From the TGA results it was possible to determine the thermal stability of the samples with respect to heat resistance, associated at 5% ($T_{5\%}$), 10% ($T_{10\%}$) and 50% ($T_{50\%}$) weight loss[39]. The DC was also determined, and the results are summarized in Table 3.3.1. When comparing the different mould temperatures used, it was noticeable that when higher mould temperatures were used, the decomposition temperatures of the samples increased, indicating an improvement in thermal stability.

For 130 ºC, samples exhibited lower $T_{10\%}$, indicating that initial degradation started for lower temperatures. This can be attributed to the lower polymerization temperature, which reduces the development of crystals. Consequently, not only does thermal stability decrease, but the measured DC also drops to 94%, with decreasing mould temperatures[40]. Samples exhibiting a high conversion rate of approximately 97-98%, despite variations in mould temperature within the range of 140 to 160 ºC, demonstrated low residual monomer content. This range is consistent with previously reported results[30,31,41].

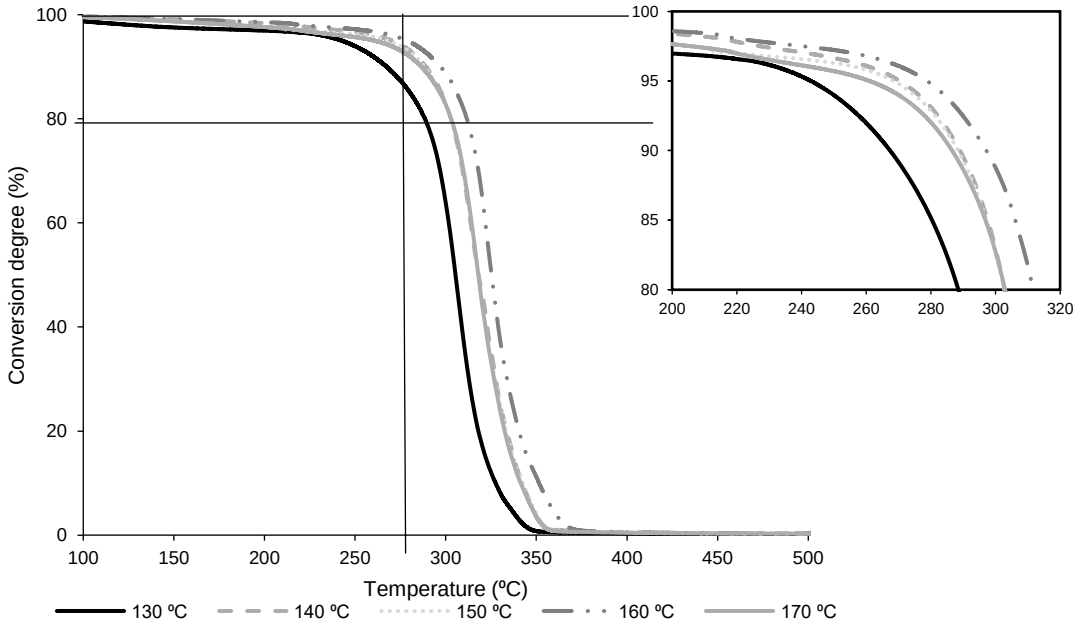

Figure 3.3.6. TGA curves of samples for different mould temperatures of samples.

Table 3.3.1. Thermal data obtained from TGA curves of PA6 samples.

Sample	DC (%)	$T_{5\%}$ (ºC)	$T_{10\%}$ (ºC)	$T_{50\%}$ (ºC)
130 ºC	94.3 ± 1.9	242.4 ± 1.2	267.6 ± 1.4	305.4 ± 1.7
140 ºC	97.2 ± 0.5	260.7 ± 0.7	286.5 ± 0.8	318.3 ± 1.0
150 ºC	98.0 ± 0.4	269.0 ± 0.5	288.8 ± 0.6	318.0 ± 0.9
160 ºC	98.1 ± 0.3	279.0 ± 0.2	297.3 ± 0.4	325.6 ± 0.5
170 ºC	95.8 ± 0.8	270.9 ± 1.3	287.4 ± 1.3	318.0 ± 1.2

The impact of polymerization temperature on the tensile properties of PA6 was also evaluated and it can be observed in Figure 3.3.7. The tensile strength exhibited an increase from 46.5 MPa (130 °C) to 77.3 MPa (160 °C). At 170 °C there is a slight decrease compared to the tensile properties obtained at 160 °C. A similar trend was observed for tensile modulus, which undergoes minimal variation in response to changes in polymerization temperature. Curiously, the X_c does not show the expected trend for tensile strength and Young's modulus. It is likely that the high X_c observed at 130 ºC, leads to the entrapment of CL in crystals. Thus, resulting in the formation of a brittle polymer, as can be supported by the results in Table 3.3.2. In general, a higher X_c in a polymer is associated with increased tensile strength, but sometimes the opposite behaviour can occur. Several factors can contribute to this counterintuitive relationship, namely defects and imperfection in the crystal, molecular weight, or processing conditions[42,43]. Imperfections act as stress concentration points and can weaken the overall structure, reducing tensile strength[44]. The molecular weight of the polymer chains can also influence both crystallinity and tensile strength. In this case, very high molecular weight PA6 may not pack efficiently into a crystalline structure, affecting both crystallinity and strength[45]. At very least, the processing conditions under which PA6 is processed, such as temperature and pressure, can also influence the crystalline structure[46].

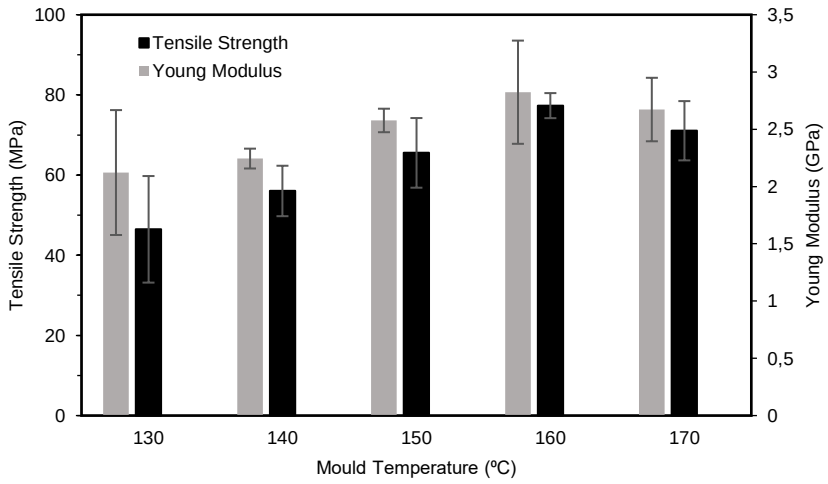

Figure 3.3.7. Tensile properties of samples for different mould temperatures.

Flexural properties are given in Figure 3.3.8 and Table 3.3.2. It was observed the same tendency of those observed for the tensile properties. For the temperature range of 130 - 160 ºC, an increase in flexural strength was obtained from 101 MPa (130 ºC) to 124 MPa (160 ºC). An analogous increase in the flexural modulus was also achieved, from 1.9 (130 ºC) to 2.7 GPa (160 ºC). A reduction in the flexural properties was also observed for the highest mould temperature. These findings could be explained by considering the influence of unreacted monomer content within the matrix on mechanical properties. Similar to many semi-crystalline polymers, the mechanical properties are predominantly governed by the DC rather than M_η or branching degree[25,47].

Table 3.3.2. Mechanical properties of samples as function as mould temperature.

	Tensile Properties			Flexural Properties		Hardness
Mould temp.	**σ_{max} (MPa)**	**ε_{max} (%)**	**E (GPa)**	**σ_{max} (MPa)**	**E (GPa)**	**Shore D**
130 ºC	46.5 ± 13.3	7.6 ± 3.9	2.1 ± 0.5	101.1 ± 3.7	1.9 ± 0.2	75.5 ± 0.1
140 ºC	56.0 ± 6.3	17.1 ± 12.5	2.2 ± 0.1	104.1 ± 3.0	2.2 ± 0.5	78.3 ± 0.9
150 ºC	65.5 ± 8.7	22.8 ± 4.3	2.6 ± 0.1	121.0 ± 5.1	2.3 ± 0.8	78.1 ± 0.8
160 ºC	77.3 ± 3.1	25.1 ± 3.8	2.8 ± 0.5	124.3 ± 5.6	2.7 ± 0.2	78.1 ± 0.6
170 ºC	71.1 ± 7.4	25.0 ± 15.4	2.7 ± 0.3	99.9 ± 2.9	2.5 ± 0.5	77.4 ± 0.4

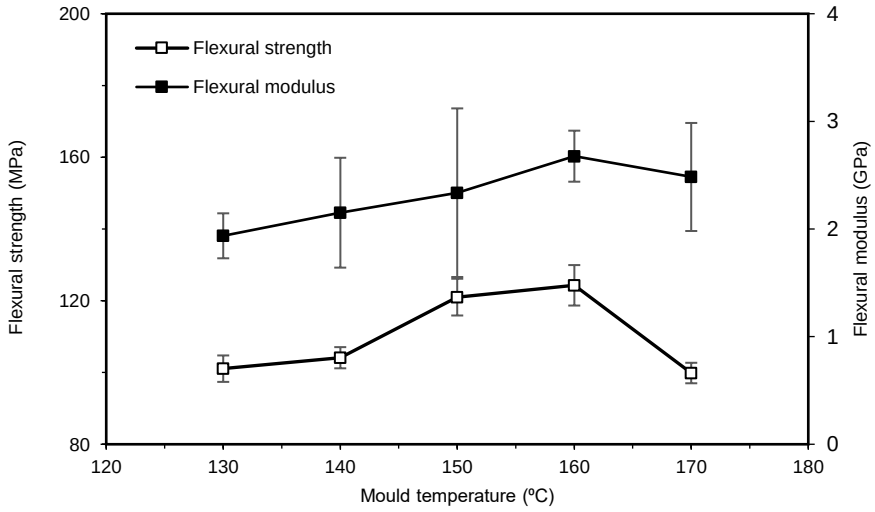

Figure 3.3.8. Flexural properties of samples at different mould temperatures.

PA6 samples processed at mould temperatures from 140 ºC and 160 ºC revealed the highest hardness values (79 Shore D). However, at 130 ºC and 170 ºC, a more pronounced reduction in hardness was observed. These findings are consistent with DC results. As previously discussed, the

higher unreacted monomer content in these samples contributes not only to diminished thermal stability but also to a decline in mechanical properties.

3.2. Influence of polymerization time

The influence of polymerization time was analysed while maintaining the mould temperature at 160 ºC. The selection of this temperature was based on an optimal balance between the X_c, monomer conversion and mechanical properties.

The polymerization time was systematically increased from 2 to 10 min using 2-min increments. The impacts of this variation on the M_v and X_c of PA6 are depicted in Figure 3.3.9. It is notable that the M_v exhibited marginal changes in response to polymerization time. Similarly, the X_c remained also unaffected by variations in polymerization time. After a duration of 6 minutes, the M_v of PA6 samples appear to stabilize and remain consistent.

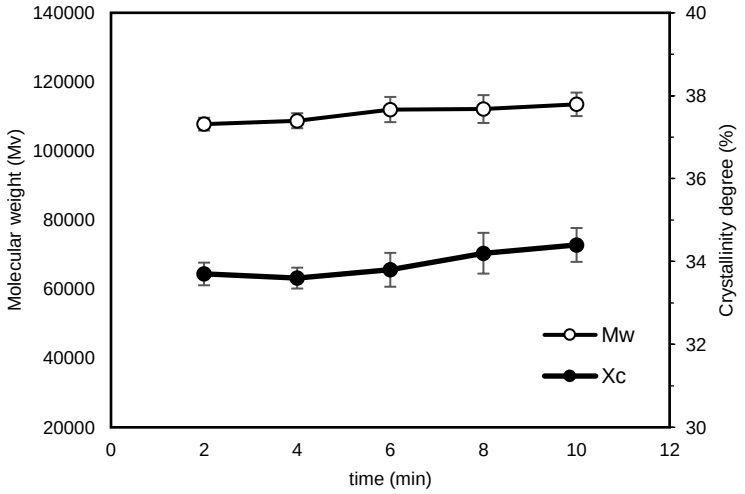

Figure 3.3.9. Effects of polymerization time on the viscosity average M_v and X_c of PA6 samples.

The effects of polymerization time on the mechanical properties are presented in Table 3.3.3. The tensile properties exhibited a relatively consistent behaviour across varying polymerization times. This trend is mirrored in the flexural properties, with values remaining unchanged despite the increase in the polymerization time. A similar behaviour was also reported by Zaldua *et al.*[26]. Additionally, the Shore D analysis also indicated that polymerization time does not influence the hardness results.

Table 3.3.3. Mechanical properties of samples as function as polymerization time.

	Tensile Properties			Flexural Properties		Hardness
Polym. time	**σ_{max} (MPa)**	**ε_{max} (%)**	**E (GPa)**	**σ_{max} (MPa)**	**E (GPa)**	**Shore D**
2 min	80.1 ± 3.2	33.8 ± 4.5	2.7 ± 0.2	117.8 ± 6.1	2.6 ± 0.7	77.7 ± 0.1
4 min	71.1 ± 7.4	25.0 ± 15.4	2.7 ± 0.3	120.5 ± 6.6	2.7 ± 0.6	78.1 ± 0.5
6 min	81.0 ± 8.5	23.8 ± 5.3	2.9 ± 0.3	125.1 ± 6.2	2.7 ± 0.5	77.9 ± 0.5
8 min	76.4 ± 3.8	20.4 ± 7.3	2.9 ± 0.2	129.6 ± 6.7	2.7 ± 0.6	78.0 ± 0.6
10 min	77.3 ± 3.1	25.1 ± 3.8	2.8 ± 0.5	124.3 ± 5.6	2.7 ± 0.2	78.1 ± 0.6

Based on the previous results, it can be concluded that viable PA6 parts can be produced by T-RTM using a mould temperature at 160 ºC and a polymerization time of 2 min. The acquired findings also demonstrated that at this specific temperature, a short cycle reaction time can be achieved.

3.3. Thickness and density distribution

A particular emphasis was placed on quality control and improving the accuracy and consistency of the process. Based on the above optimization (mould temperature set at 160 ºC and polymerization time of 2 min), the distribution and density of the material produced by T-RTM were determined. The calculated average density value was 1.14 ± 0.01 g/cm^3.

Figure 3.3.10(a) visually illustrates that there is no significant variability in the density values between the different locations of the measurements along the plates. In general, less densities are observed in areas closer to the outlet, as the injected material is exposed to lower temperatures over time.

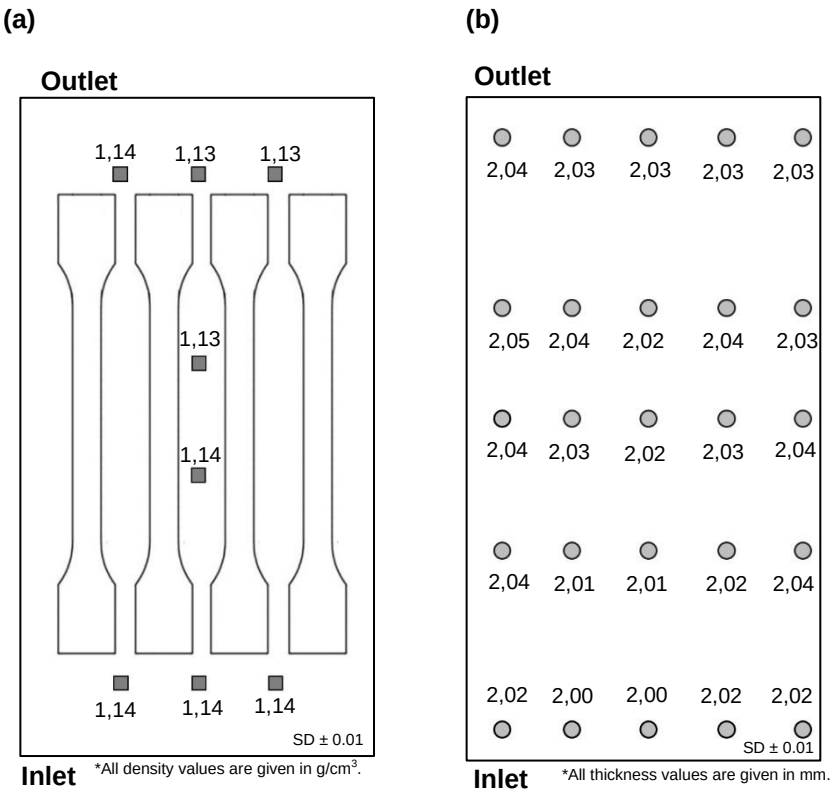

Figure 3.3.10. Density **(a)** and thickness **(b)** values for plate (according to Figure 3.3.3).

The thickness distribution across the plates is represented in Figure 3.3.10(b). The average thickness was 2.03 ± 0.01 mm. The deviation from the mould cavity (2 mm thickness) was small, but a slight change in thickness was observed in the areas near the edges and towards the outlet. This is likely due to the fact that in the edge areas the reactive mixture polymerizes first. Material closer to the outlet is exposed to lower temperatures over time compared to the inlet, promoting slightly thicker and less dense material (as stated before). In general, the obtained results demonstrate a uniform heating along the mould and a homogeneous distribution of the mixture as it is injected into the mould.

4. Conclusions

PA6 was prepared trough *in situ* AROP using a T-RTM equipment. The effect of two processing conditions were analysed, namely different mould temperatures (130 ºC to 170 ºC) and polymerization times (2 to 10 minutes).

Mould temperature revealed the influence on both the X_c and M_v of the samples. Samples exhibited higher monomer conversion and improved thermal stability at mould temperatures of 150 ºC and 160 ºC. As expected, the mechanical properties (tensile and flexural) were affected by the M_v

and by the X_c. At 160 ºC was attained the highest tensile and flexural strength, along with corresponding modulus.

In the case of the polymerization time, it was shown that this processing parameter does not impact the X_c, DC and mechanical performance. Based on the previous results, a mould temperature of 160ºC and a polymerization time of 2 min can be defined as the optimal processing conditions to favour the reaction development. These findings highlight the potential for achieving shorter reaction times for the T-RTM technology

Ultimately, the key conclusion drawn from the study is that mould temperature revealed to have a pronounced influence on the final properties of PA6 samples.

Acknowledgements

The authors would like to acknowledge to Simoldes Group for partial funding this research. This is a project in collaboration with Simoldes Plásticos, S.A. This work was also developed within the scope of the project CICECO-Aveiro Institute of Materials, UIDB/50011/2020, UIDP/50011/2020 & LA/P/0006/2020, financed by national funds through the FCT/MEC (PIDDAC).

References

1. Kim, B. J., Cha, S. H. & Park, Y. Bin. Ultra-high-speed processing of nanomaterial-reinforced woven carbon fiber/polyamide 6 composites using reactive thermoplastic resin transfer molding. *Compos B Eng* **143**, 36–46 (2018).
2. Stewart, R. Thermoplastic composites - Recyclable and fast to process. *Reinforced Plastics* **55**, 22–28 (2011).
3. Ben, G. & Sakata, K. Fast fabrication method and evaluation of performance of hybrid FRTPs for applying them to automotive structural members. *Compos Struct* **133**, 1160–1167 (2015).
4. Malpot, A., Touchard, F. & Bergamo, S. Fatigue Behaviour of a Thermoplastic Composite Reinforced with Woven Glass Fibres for Automotive Application. *Procedia Eng* **133**, 136–147 (2015).
5. Xiaoyin, W. *et al.* Lightweight design of automotive wheel made of long glass fiber reinforced thermoplastic. *Proc Inst Mech Eng C J Mech Eng Sci* **230**, 1634–1643 (2016).
6. Melvin, I. K. *Nylon Plastic Handbook*. *New York: Hanser* (1995).
7. Platt, D. K. *Engineering and High Performance Plastics Market Report: A Rapra Market Report*. (iSmithers Rapra Publishing, 2003).
8. Davies, G. Materials for consideration and use in automotive body structures. in *Materials for automobile bodies* vol. 3 93–143 (Elsevier, 2012).
9. Tobalina-Baldeon, D. *et al.* Feasibility analysis of bolted joints with composite fibre-reinforced thermoplastics. *Polymers (Basel)* **13**, 1904 (2021).
10. Rahman, M. A., Renna, L. A., Venkataraman, D., Desbois, P. & Lesser, A. J. High crystalline, porous polyamide 6 by anionic polymerization. *Polymer (Guildf)* **138**, 8–16 (2018).
11. Sibikin, I. & Karger-Kocsis, J. Toward industrial use of anionically activated lactam polymers: Past, present and future. *Advanced Industrial and Engineering Polymer Research* **1**, 48–60 (2018).

12. Mondal, A., Sohel, M., Mohammed Arif, P., Thomas, S. & SenGupta, A. Effect of ABS on non-isothermal crystallization kinetics of polyamide 6. *J Therm Anal Calorim* **146**, 2489–2501 (2021).
13. Ageyeva, T., Sibikin, I. & Karger-Kocsis, J. Polymers and related composites via anionic ring-opening polymerization of lactams: Recent developments and future trends. *Polymers (Basel)* **10**, 357 (2018).
14. Šebenda, J. Polymerizability of lactams. in *Polymerization of Heterocycles (Ring Opening)* 329–334 (Elsevier, 1977).
15. Sekiguchi, H., Ivin, K. J. & Saegusa, T. Ring-Opening Polymerization. *J., Saegusa, T., Eds.; Elsevier London UK* **2**, 809 (1984).
16. Roda, J. Polyamides. in *Handbook of Ring-Opening Polymerization* 165 (2009).
17. Kovács, Z., Pomázi, Á. & Toldy, A. The flame retardancy of polyamide 6—prepared by in situ polymerisation of ε-caprolactam—for T-RTM applications. *Polym Degrad Stab* 109797 (2021).
18. Barhoumi, N., Maazouz, A., Jaziri, M. & Abdelhedi, R. Polyamide from lactams by reactive rotational molding via anionic ring-opening polymerization : Optimization of processing parameters. *Express Polym Lett* **7**, 76–87 (2013).
19. Zaldua, N. *et al.* Nucleation and crystallization of PA6 composites prepared by T-RTM: Effects of carbon and glass fiber loading. *Polymers (Basel)* **11**, 1680 (2019).
20. Choi, C.-W., Jin, J.-W., Lee, H., Huh, M. & Kang, K.-W. Optimal Polymerization Conditions in Thermoplastic-Resin Transfer Molding Process for Mechanical Properties of Carbon Fiber-Reinforced PA6 Composites Using the Response Surface Method. *Fibers and Polymers* **20**, 1021–1028 (2019).
21. Murray, J. J. *et al.* Thermoplastic RTM: Impact Properties of Anionically Polymerised Polyamide 6 Composites for Structural Automotive Parts. *Energies (Basel)* **14**, 5790 (2021).
22. Wilhelm, M., Wendel, R., Aust, M., Rosenberg, P. & Henning, F. Compensation of water influence on anionic polymerization of ε-caprolactam: 1. Chemistry and experiments. *Journal of Composites Science* **4**, 7 (2020).
23. Murray, J. J., Robert, C., Gleich, K., McCarthy, E. D. & Brádaigh, C. M. Ó. Manufacturing of unidirectional stitched glass fabric reinforced polyamide 6 by thermoplastic resin transfer moulding. *Mater Des* **189**, 108512 (2020).
24. Boros, R., Sibikin, I., Ageyeva, T. & Kovács, J. G. Development and Validation of a Test Mold for Thermoplastic Resin Transfer Molding of Reactive PA-6. *Polymers (Basel)* **12**, 976 (2020).
25. van Rijswijk, K., Bersee, H. E. N., Beukers, A., Picken, S. J. & van Geenen, A. A. Optimisation of anionic polyamide-6 for vacuum infusion of thermoplastic composites: Influence of polymerisation temperature on matrix properties. *Polym Test* **25**, 392–404 (2006).
26. Semperger, O. V. & Suplicz, A. The Effect of the Parameters of T-RTM on the Properties of Polyamide 6 Prepared by in Situ Polymerization. *Materials* **13**, 4 (2020).
27. Lee, J., Lim, J. W. & Kim, M. Effect of thermoplastic resin transfer molding process and flame surface treatment on mechanical properties of carbon fiber reinforced polyamide 6 composite. *Polym Compos* **41**, 1190–1202 (2020).
28. Maazouz, A., Lamnawar, K. & Dkier, M. Chemorheological study and in-situ monitoring of PA6 anionic-ring polymerization for RTM processing control. *Composites Part A* **107**, 235–247 (2018).
29. Lagarinhos, J., Magalhães da Silva, S. & Martinho Oliveira, J. Non-Isothermal Crystallization Kinetics of Polyamide 6/Graphene Nanoplatelets Nanocomposites Obtained via In Situ Polymerization: Effect of Nanofiller Size. *Polymers (Basel)* **15**, (2023).
30. Lagarinhos, J., Santos, L. & Oliveira, J. Effect of Catalyst and Activator on Properties of Polyamide 6 Prepared by Thermoplastic Resin Transfer Molding Technology. *J Mater Eng Perform* **31**, 7098–7103 (2022).
31. Semperger, O. V. & Suplicz, A. The Effect of the Parameters of T-RTM on the Properties of Polyamide 6 Prepared by in Situ Polymerization. *Materials* **13**, 4 (2020).

32. Udipi, K., Davé, R. S., Kruse, R. L. & Stebbins, L. R. Polyamides from lactams via anionic ring-opening polymerization: 1. Chemistry and some recent findings. *Polymer (Guildf)* **38**, 927–938 (1997).
33. Mattiussi, A., Gechele, G. B. & Francesconi, R. Polyamides in solution. III. Viscometry of linear polycaprolactam. *Journal of Polymer Science Part A-2: Polymer Physics* **7**, 411–422 (1969).
34. Bhattacharyya, D., Maitrot, P. & Fakirov, S. Polyamide 6 single polymer composites. *Express Polym Lett* **3**, 525–532 (2009).
35. Mateva, R., Delev, O. & Kaschcieva, E. Structure of poly (ε-caprolactam) obtained in anionic bulk polymerization. *J Appl Polym Sci* **58**, 2333–2343 (1995).
36. Zhuravlev, E., Schmelzer, J. W. P., Wunderlich, B. & Schick, C. Kinetics of nucleation and crystallization in poly(ε-caprolactone) (PCL). *Polymer (Guildf)* **52**, 1983–1997 (2011).
37. Ben, G., Hirabayashi, A., Sakata, K., Nakamura, K. & Hirayama, N. Evaluation of new GFRTP and CFRTP using epsilon caprolactam as matrix fabricated with VaRTM. *Science and engineering of composite materials* **22**, 633–641 (2015).
38. Semperger, O. V. & Suplicz, A. The effect of titanium dioxide on the moisture absorption of polyamide 6 prepared by T-RTM. in *IOP Conference Series: Materials Science and Engineering* vol. 903 12009 (IOP Publishing, 2020).
39. Król-Morkisz, K. & Pielichowska, K. Thermal decomposition of polymer nanocomposites with functionalized nanoparticles. in *Polymer composites with functionalized nanoparticles* 405–435 (Elsevier, 2019).
40. Iobst, S. A. Polymerization and crystallization behavior of anionic nylon 6. *Polym Eng Sci* **25**, 425–430 (1985).
41. Nakamura, K., Ben, G. & Hirayama, N. Effect of molding condition on impact property of glass fiber reinforced thermoplastics using in-situ polymerizable polyamide 6 as the matrix. in *Proceedings of the 18th international conference on composites materials.* (2011).
42. Starkweather, H. W., Moore, G. E., Hansen, J. E., Roder, T. M. & Brooks, R. E. Effect of crystallinity on the properties of nylons. *Journal of Polymer Science* **21**, 189–204 (1956).
43. Andjelić, S. & Scogna, R. C. Polymer crystallization rate challenges: The art of chemistry and processing. *J Appl Polym Sci* **132**, (2015).
44. Galeski, A. Strength and toughness of crystalline polymer systems. *Prog Polym Sci* **28**, 1643–1699 (2003).
45. Su, K.-H., Lin, J.-H. & Lin, C.-C. Influence of reprocessing on the mechanical properties and structure of polyamide 6. *J Mater Process Technol* **192–193**, 532–538 (2007).
46. Yebra-rodriguez, A., Alvarez-lloret, P., Cardell, C. & Rrodriguez-Navarro, A. Crystalline properties of injection molded polyamide-6 and polyamide-6/montmorillonite nanocomposites. *Appl Clay Sci* **43**, 91–97 (2009).
47. Van Rijswijk, K. Thermoplastic Composite Wind Turbine Blades: Vacuum Infusion Technology for Anionic Polyamide-6 Composites. *PhD Thesis* (Delft University of Technology, 2007).

Chapter 4

PA6/graphene-based nanocomposites

This chapter begins with an overview of the theoretical basis of graphene-based polymer nanocomposites, focusing on the preparation of PA6 with graphene nanoplatelets. Different strategies to enhance the interaction between the polymer matrix and the nanofiller were explored. The subsequent investigation includes the nucleation effect, the crystallization kinetics under non-isothermal conditions and the influence of the nanofiller on the final properties of the nanocomposite produced by the T-RTM technology.

4.1 Overview

Chapter 3 successfully demonstrated the reproducible production of PA6 parts obtained by AROP. However, a crucial aspect remains unexplored: is it viable the production of PA6-based nanocomposites using T-RTM technology? The novelty of the present work lies in the development of PA6 nanocomposites reinforced with graphene nanoplatelets (GNP), whereas the main emphasis relies on fostering a robust interfacial interaction between the polymer matrix and the nanofiller. The overarching objective is to enhance the final properties, such as thermal stability and mechanical properties of PA6 from the resultant nanocomposites.

In this Chapter, several studies will be conducted, namely (1) GNP characterization (size, geometry, and particle characterization); (2) dispersion within the PA6 matrix; (3) PA6-GNP formulations; and (4) processing conditions. At the end, the main goal is to provide a proof of concept, demonstrating the feasibility of producing PA6 nanocomposites using the T-RTM technology. This research opens the boundaries of materials innovation and engineering through the integration of advanced nanofillers. In pursuit of these goals, this Chapter is divided into five distinct sub-chapters:

- **Sub-chapter 4.2** – **Current state-of-the-art in carbon-based materials, namely, GNP:** explores the existing carbon-based materials, with a particular focus on graphene nanoplatelets (GNP). This section also looks at different processing methods for their incorporation into polymers, with a focus on their application in the context of PA6;
- **Sub-chapter 4.3** – **Selection of GNP and Dispersion Strategy:** Based on the knowledge acquired in the previous 4.2, the sub-chapter 4.3 describes the selection of two different commercial GNP with different particle sizes (D90 < 50 μm (defined as GN) and D90 <70 μm (defined as GP). These selected GNP were further characterized to ensure their quality. Subsequently, a comprehensive analysis for the dispersion strategies of GNP into PA6 monomer was outlined. The loading levels of GNP chosen for the study cover a range of 0.1, 0.25, 0.5, 0.75 and 1 wt.%;
- **Sub-chapter 4.4** – **Nucleation Effect on Thermal Behaviour:** It is dedicated to understanding the effect of GNP on the thermal behaviour of PA6. The nanocomposites featuring 0.1 wt.% of GNP are selected for an in-depth investigation into the nucleation effect of GNP;
- **Sub-chapter 4.5** – **Crystallization Kinetics Under Non-Isothermal Conditions:** Here, the focus shifts to the evaluation of the influence of different GNP sizes on the crystallization kinetic behaviour of PA6 under non-isothermal conditions to mimic the T-RTM process. The nanocomposite with 0.5 wt.% GNP is subjected to a thorough analysis, using different kinetic models to understand the crystallization behaviour of PA6 in the presence of GNP;
- **Sub-chapter 4.6** – **Effect of GNP on Thermal and Mechanical Properties:** This sub-chapter marks the culmination of the study, where different loadings 0.1, 0.25, 0.5, 0.75 and 1.0 wt. %) of GNP are incorporated into the PA6 matrix. Even at low GNP loadings (0.1 and 0.25 wt.%), significant improvements in mechanical properties were observed when compared to pure PA6. In addition, the impact of GNP size variations on both thermal and mechanical properties is also studied.

4.2 Graphene-based materials

The search for novel materials has led to a remarkable transformation in the area of composite materials over the last few decades. As a result, a new class of advanced materials known as polymer nanocomposites, has emerged. These materials have improved physical and mechanical properties that can be applied in a wide range of applications. In particular, the thermal and electrical properties of polymer nanocomposites are a direct result of the skilful combination of properties exhibited by their constituent components. Consequently, the research and development of nanocomposites have attracted considerable interest, particularly for use in areas where lightweight components are required.

The incorporation of a reinforcement phase into a polymeric matrix to create a composite material results in significant improvements over unfilled polymers[1,2]. These improvements include enhanced mechanical properties, increased thermal stability and improved electrical properties, all of which can be achieved with relatively low filler content[3,4]. The discovery of nanoscale particles such as fullerenes[5], carbon nanotubes[6] and graphene[7] has unlocked the potential for a new range of nanocomposite materials with specific and superior properties.

PA6 is a material widely used in several applications, from engineering and automotive industry[8–10]. In this context, carbon based materials are emerging as a way to combine the inherent properties of PA6 with their unique features[11–13]. While carbon nanotubes (CNTs) offer exceptional mechanical properties and thermal conductivity, their complex and expensive production methods, often leaving toxic metal residues, can be tricky[14,15]. As a result, graphene-based materials (GBM) are emerging as an attractive alternative for the production of nanocomposites. GBM offer an appealing prospect due to their exceptional properties and the abundance of their precursor, graphite. In addition, the straightforward and cost-effective physicochemical methods employed in the production of GBM further contribute to their viability[16,17].

GBM are currently emerging as promising nanofillers for enhancing the mechanical, thermal, and electrical properties of polymers[18–20]. Due to their promising properties, GBM nanocomposites have been used in a wide range of applications, including automotive, electronics, packaging, aerospace, military, buildings, and constructions[3,20,21]. However, in order to fully exploit the remarkable potential of GBM nanocomposites, a significant challenge must be addressed: the tendency of graphene sheets to agglomerate within a polymer matrix[22]. The inherent properties of graphene sheets, characterized by their strong cohesiveness and large surface area (2630 $m^2 \cdot g^{-1}$)[23] cause a major challenge when attempting to develop graphene-based polymer nanocomposites. The main challenge here is the effective dispersion and interaction of these graphene sheets within the polymer matrix[24]. It emerges from the tendency of graphene sheets to stack on top of each other, leading to the formation of numerous defect sites such as agglomerates or aggregates in the resulting nanocomposites. These defects significantly reduce the reinforcing effect of GBM, causing deformation that culminate in premature failure.

In recent years, there has been a remarkable upsurge in the research of PA6/GBM nanocomposites[25–29]. There is available a large amount of information, so it is important to collect, compare and withdraw conclusions. The scientific community has extensively investigated the synthesis, production, application, and properties of PA6 and GBM, however, there is a noticeable gap[30–32]. To date, there has not been a comprehensive investigation specifically focused on PA6/GBM nanocomposites prepared by the innovative T-RTM technology using PA6 obtained from AROP. This is due to the complexity of T-RTM technology, which has contributed to the lack of such research.

The present work takes a role of a pioneer, as it represents a substantial contribution to this dynamic field. This research introduces novelty by both addressing the PA6 synthesis via AROP and the incorporation of GBM using the T-RTM technology. Following this fundamental exploration, the obtained results will be compared to the current progress made in the field of PA6/GBM production and the resulting properties will be benchmarked, ranging from chemical properties to thermal and mechanical behaviour. The aim is to elucidate and consolidate valuable insights that can potentially shape the trajectory of future research and applications in this field.

4.2.1 Graphene

Graphene structure emphasises a single atom thick 2D sheet of sp^2 hybridized carbon atoms, forming a hexagonal ring structure (Figure 4.2.1) through covalent bonds with a carbon-carbon bond length of 0.142 nm (1.42 Â)[1,33]. It is often addressed as "the material of the future". The versatility of graphene is evident as it can be manipulated into different forms: compressed into zero-dimensional (0D) fullerenes, rolled into one-dimensional (1D) nanotubes, or stacked into three-dimensional (3D) graphite structures (Figure 4.2.2)[34].

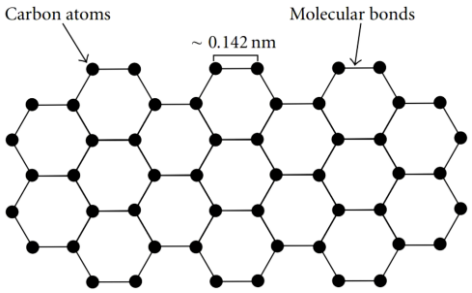

Figure 4.2.1. 2D Carbon structure of graphene[35].

From a structural point of view, graphene is classified as a macromolecule with a molecular weight typically in the range of 10^6-10^7 g/mol[36]. Theoretical calculations indicate a density of 1.822 g/cm^3 for this material. Its mechanical performance includes a Young's tensile modulus of about 1 TPa and a tensile strength of about 130 GPa when measured in the planar direction[37]. Graphene also has a thermal conductivity (~5000 $Wm^{-1}K^{-1}$) 14 times greater than cooper[38], and an electrical conductivity (ranging from 80 to 100 MS/m) comparable to silver at room temperature[39,40]. These properties,

combined with its large surface area (theoretically up to 2630 m^2/g), make graphene an ideal reinforcement for lightweight and high-strength nanocomposite materials.

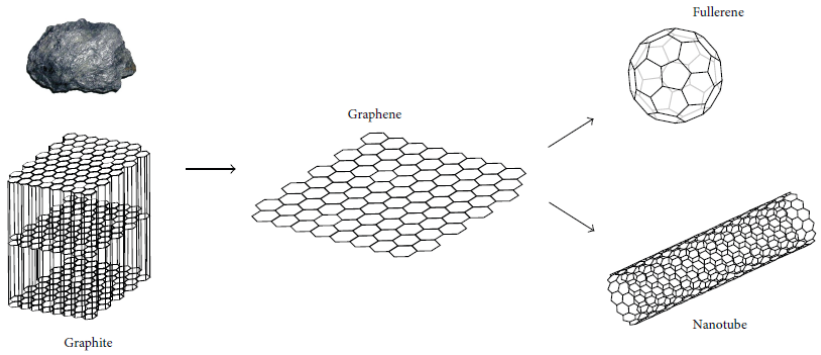

Figure 4.2.2. Graphite is a common mineral found in nature. Graphene serves as the basic building block for other carbon materials: fullerenes and carbon nanotubes. Reprinted from reference 41.

Graphene production methods can be categorized into two main approaches: top-down and bottom-up techniques[42]. The first approach involves the gradual reduction in the size of a bulk material (often graphite) until it reaches the nanoscale, resulting in the production of graphene. The second approach relies on carbon atoms sourced from specific precursors, such as hydrocarbon gases or solid carbides, to build graphene from the ground up[42,43]. The top-down approach involves the production or modification of graphene by the separation or cleavage of graphite or GO derivatives. Top-down methods are particularly suitable for producing significant amounts of graphene sheets, which is valuable for applications such as polymer nanocomposites where significant amounts of nanofillers are required. Examples of this approach include techniques such as micromechanical exfoliation, also known as “scotch tape”, method[44], direct sonication[45], electrochemical sonication[46], and super-acid dissolution of graphite[47]. While the bottom-up approach is capable of producing large-area graphene sheets (>100 cm^2), it is generally insufficient to produce sufficiently abundant and cost-effective quantities for applications such as polymer nanocomposites[43]. Graphene sheets produced by these methods are primarily targeted at electronic applications[48]. Bottom-up techniques include chemical vapour deposition (CVD)[49], arc discharge[50], epitaxial growth on silicon carbide[51,52], chemical conversion[53] and self-assembly of surfactants[54].

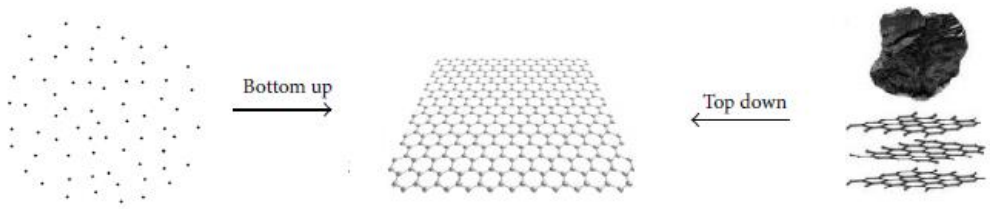

Figure 4.2.3. Schematic representation of bottom-up and top-down approaches for graphene synthesis. Adapted from reference 55**.**

The use of graphene as a nanofiller offers the advantage of improving the properties of existing materials used in common products. The incorporation of nanomaterials into polymeric materials results in nanocomposite materials with improved performance that is often unattainable using traditional fillers such as carbon or glass fibres. This improvement is due not only to the unique properties of these nanofillers, but also to the extensive interfaces formed between the nanofillers and the host polymers[2].

To fully exploit the potential of graphene as a reinforcement phase, there is a critical need for advances in the large-scale production of high-quality graphene. In particular, the structure and properties of graphene, including factors such as quality, and lateral size, are strongly influenced by the chosen production method. In addition, graphene material obtained by different synthetic approaches can differ significantly from its original form due to the presence of defects, resulting in different behaviour and consequently different performance in the final application.

4.2.2 Graphene Nanoplatelets (GNP)

The production of single-layer graphene remains costly, making it impractical for large-scale applications. Moreover, the use of high quality single-layer graphene in composites raises concerns about its efficacy due to challenges such as agglomeration and bonding issues between graphene and polymer matrix[56]. However, a cost-effective alternative and suitable for scalable production is the use of graphene nanoplatelets (GNP), also known as graphite nanosheets or exfoliated or expanded graphite[57]. These nanoflake powders can be produced in quantities up to 140 tonnes per year, providing a highly scalable material positioned between single graphene layers and bulk graphite (Figure 4.2.4)[58].

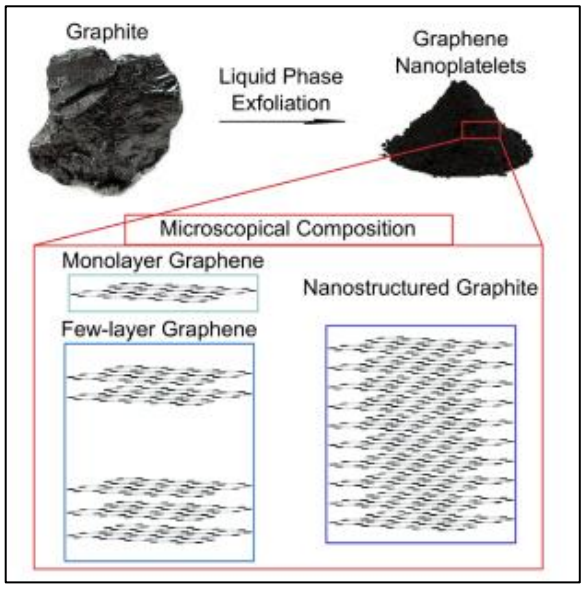

Figure 4.2.4. Schematic representation of GNP manufacture having graphite as the starting point[59].

The distinction between the term's "graphene", "GNP" and "graphite" has become somewhat blurred. In terms of morphological characteristics, the graphene family can be divided into single-layer graphene, few-layer graphene (consisting of 2 to 10 layers), and graphite nano- and micro-platelets. Commercially available GNP are composed of a mixture of single layers, few layers and nanostructured graphite, resulting in variations of GNP from 0.34 to 100 nm within the same production batch[60,61]. It is worth noting that graphite is generally considered to be 2D, when the number of layers is less than 10[56]. The structural configuration of GNP is similar to that of graphene, and their mechanical and electrical properties lie between those of graphene and graphite (Table 4.2.1). The effectiveness of graphene-like materials decreases as the number of layers in a stack increase[62].

Table 4.2.1. Properties of carbon allotropes[7,37,63,64].

Carbon allotrope	Density ($g \cdot cm^{-3}$)	Young Modulus (GPa)	Tensile strength (GPa)	Electrical conductivity ($S \cdot m^{-1}$)	Thermal conductivity ($W \cdot mK^{-1}$)
Graphite Bulk	1.6-1.7	7-17	0.006	13.79	19-20
Graphene	2.27	1000	130	10^8	2000-4000
GNP	2.2	-	-	10^7	3000

GNP are typically obtained by the liquid phase exfoliation method, often without additional centrifugation steps[65]. The liquid phase exfoliation process involved the conversion of graphite or multilayer graphene into single or few layer graphene by overcoming the van der Walls forces between individual sheets[66]**.** Various techniques can be employed to modify and control the diameter, thickness, and surface area of GNP, including oxidation, intercalation, ball-milling[65], microwave radiation shear exfoliation[65], and wet jet milling[67].

The combination of properties possessed by GNP, including their lightweight, ultra-high aspect ratio, remarkable flexibility, excellent electrical conductivity, thermal stability, and toughness, positions them as an ideal carbon nanofillers for enhancing the properties of polymer matrices in a wide range of applications[68]. However, it is important to recognise the challenges that still needed to be overcome when using GNP as a reinforcement phase. It is important to understand how GNP can be effectively dispersed within a polymer matrix and how these dispersion affects the final properties of the resulting nanocomposites.

4.2.3 Processing methods of graphene-based polymer nanocomposites

Numerous studies have been carried out to explore the potential of polymer graphene-based nanocomposites. It is crucial to develop and understand the chosen processing method prior to their production, in order to achieve adequate performance of the developed nanocomposites.

Such improvements can be related to the mechanical strength, thermal stability and/or electrical conductivity. Various processing techniques have been documented for dispersing graphene and

graphene-derived nanofillers into polymer matrices. As already referred, the chemical interactions between the filler and the polymer matrix plays a key role in determining the final properties of the nanocomposites. The establishment of covalent bonds between the polymer matrix and the nanofiller is a major challenge, mainly due to the limited presence of functional groups on the surface of GBM. This dispersion is influenced by factors such as the nature of the polymer, the functional groups present on the filler and the interactions between filler and polymer.

Several common processing methods are used for polymer nanocomposites, including solution mixing, melt mixing and *in situ* polymerization[69–72]. Solution mixing is the most widely used technique, offering a simple and rapid process. It consists of dispersing the GBM particles in a polymer solution, followed by solvent removal through evaporation to obtain a composite polymer film. Careful attention to solvent selection is essential to achieve optimum compatibility between the polymer and the nanofiller[73]. In general, this method provides satisfactory nanofiller dispersion and is versatile due to the ability to use different solvents for polymer dissolution and nanofiller dispersion. Notable successes include the mixing of polymers such as polystyrene (PS)[74,75], polymethyl methacrylate (PMMA)[76] and polyurethane (PU)[77] with modified GNM using the solution mixing approach. Melt mixing is a practical and versatile technique that is widely used in industry to produce thermoplastic nanocomposites, mainly due to its cost-effectiveness. This method involves melting the polymer at elevated temperatures and applying shear forces to uniformly disperse GBM powder in thermoplastic polymer matrices while in the molten state[78]. High temperatures facilitates the integration of the reinforcing phase. A drawback, however, is the shear forces required, which can potentially lead to buckling or fracture of the GBM sheets. Notably, this process does not require the use of solvents, making it an economical and environmentally friendly means of producing GBM thermoplastic nanocomposites on a large scale[33]. A wide range of thermoplastics, including polyethylene (PE)[79], polypropylene (PP)[80,81] and PU[82], have achieved improved mechanical properties through this process. However, it is important to note that this technique is less efficient at dispersing nanofillers than solution mixing, particularly as the filler content increases. This is due to the increased viscosity caused by the increasing filler concentration. Another challenge with melt blending is the low bulk density of graphene in its dry powder state, which makes it difficult to feed into the extruder.

The *in situ* polymerization technique involves the polymerization of monomers in the presence of GBM[18]. In this approach, either graphene or its derivative is allowed to swell in the liquid monomer along with a suitable reactive initiator. After dissociation of the initiator by heat or irradiation, the GBM can be mixed or cross-linked with the polymer chains, promoting interactions between the nanofiller and the polymer through covalent bonding[33]. This is attributed to the intercalation of monomers into the layered structure of GBM, leading to an expansion of the interlayer spacing and subsequent exfoliation of the graphene platelets[72,73,83].

4.2.4 PA6/graphene-based nanocomposites

GBM-filled PA6 materials hold great promise for creating a new class of high-performance materials by facilitating the fusion of the polymer matrix with GBM. As previously discussed, the choice of processing technique depends on ensuring uniform dispersion of the GBM, effective exfoliation and favourable interfacial interaction between the GBM and the polymer. Given the focus of this work on the development of PA6 via AROP, *in situ* polymerization emerges as the most suitable approach for the preparation of PA6/graphene-based nanocomposites.

Numerous research publications report *in situ* polymerization studies of graphene-reinforced PA6 and its derivatives, however, these studies have predominantly been carried out in a laboratory scale. Remarkably, as far as we know, there are no documented investigations involving the application of T-RTM technology in this field. This highlights the urgent need for a comprehensive understanding of the processing requirements and technical details associated with T-RTM technology. The main goal is to take the knowledge gained from *in situ* polymerization and extend its application to the field of T-RTM technology. By bridging the gap between *in situ* polymerization and T-RTM technology, this approach has the potential to usher in ground-breaking advances. It will require a careful adaptation of established methodologies to the unique challenges and parameters of T-RTM. This combination of techniques is in line with the overarching objective of developing PA6/graphene-based nanocomposites through a challenging technology-driven route.

The primary aim of reinforcing GBM in PA6 is to improve the properties of composites for potential applications in several industries, however, there are some challenges in the development of these nanocomposites that should be considered.

The morphology of the GBM is essential to observe the state of dispersion and the structure-property relationships for the polymer nanocomposite material[84]. The uniform distribution of GBM in the polymer is the main challenge due to the size of the nanofiller, the surface area and the experimental conditions, which could lead to a decrease in the load carrying capacity between the polymer matrix and the reinforcing phase[85]. An efficient dispersion of GBM within the polymer is also an important factor that influences the performance of the developed nanocomposites.

As property improvements are strongly correlated with the nanocomposite microstructure, effective characterization of the morphology is important to establish structure-property relationships for these materials[30].

Melting temperature (T_m), crystallization temperature (T_c) and crystalline structure play an important role in determining the thermal behaviour of polymers. The presence of graphene-based nanofillers has been shown to influence the melting temperature, and it is well known that these factors together influence polymer properties[86]. In the case of PA6, it has been documented that exists three different crystal forms: the α form, which is thermodynamically more stable; the β form, an unstable configuration; and the γ form[87]. A study by Gong *et al*. investigated the effect of incorporating GO into PA6. After analysing the DSC curves of PA6, they observed a peak at around 221 ºC along with a minor peak at around 215 ºC, indicating the coexistence of both α and β forms

of PA6[88]. However, in the case of PA6/GO nanocomposites, the DSC curves showed two distinct melting peaks. As the GO content was increased, the crystallinity of the nanocomposites decreased, indicating insufficient dispersion of GO within the PA6 matrix. Furthermore, the inclusion of GO sheets induced an increase in T_c. This phenomenon was attributed to the influence of these 2D nanofillers on the crystallization process of PA6. The introduction of GO facilitated heterogeneous nucleation and thus contributed to the observed increase in T_c[89]. The incorporation of graphene-based nanofillers also revealed a nucleating activity. An increased nucleating activity can lead to shorter industrial cycles and reduced manufacturing costs. Fu, X. *et al.*[28], carried out a study on the effect of multilayer graphene on PA6, showing that its addition acts as a nucleating agent, promoting crystallization and accelerating the crystallization rate of PA6 nanocomposites. Similar trends were observed by Zhang, F., and co-workers[90], in their study of the *in situ* non-isothermal crystallization kinetics of PA6/graphene composites. The presence of graphene introduced nucleation sites that modified the nucleation mechanism and crystallite growth in PA6. The thermal stability is indeed a critical property for PA6-based nanocomposites, considering their potential application as high-performance engineering plastics[91]. If the polymer matrix degrades at lower temperatures, will limit their application in high-temperature environments. This limitation becomes particularly when comparing polymers with materials such as metals or ceramics, which tend to withstand higher temperatures without significant degradation[33]. The degradation behaviour of polymers can be addressed by three main parameters: the onset temperature, which is the temperature at which a chemical begins to react; the degradation temperature, where the maximum degradation rate occurs; and the degradation rate, which gives an indication of the total degradation time. Numerous studies have confirmed that the incorporation of carbon nanofillers can improve the thermal stability of polymers. This is attributed to the ability of nanofillers to act as thermal barriers, preventing the heat transfer generated by the external environment within the polymer matrices[92–95]. The improved thermal stability of PA6/GBM nanocomposites is generally attributed to the high surface area, effective dispersion, and interactions of the nanofillers with the PA6 matrix[1,96]. In a study by Lui, Y. *et al.*[93] in which PA6/graphite oxide nanocomposites were synthesized using a delamination/absorption technique, the addition of 5 wt.% graphite oxide resulted in a significant 53 ºC improvement in the maximum decomposition temperature compared to the PA6 pure matrix. Similarly, Fu, X., and co-workers[28] investigated the thermal and mechanical properties of PA6 nanocomposites containing low levels of unmodified multilayer graphene. As expected, the incorporation of multilayer graphene led to an improvement in the thermal stability of PA6. The authors proposed that when nanofillers are introduced, these particles can infiltrate the intricate polymer structure, thereby modifying it in a way that increases the thermal stability of the nanocomposite. This modification effectively delays matrix degradation[97].

Most of the work into GBM/polymer nanocomposites has been focused on exploiting their improved mechanical properties, as a consequence of GBM larger specific area, results, and unique properties[24]. Several studies into the mechanical properties of graphene-based polymer nanocomposites have shown an increase in modulus with increased loading fraction[27,98–100]. For

example, Zhang, X. *et al*.[89] found that the incorporation of 1.0 wt.% GO resulted in an 88.0% increase in tensile strength and a 66.5% increase in Young's modulus for PA6/GO nanocomposites. This improvement in tensile properties can be attributed to the well-dispersed GO sheets and the robust interaction between these sheets and the PA6 matrix. However, a significant decrease in elongation at break was observed with increasing GO content, indicating that the nanocomposites became more brittle compared to pure PA6. This behaviour could be attributed to the molecular weight distribution of PA6. The obtained PA6 was prepared directly by *in situ* polymerization without removing the large amount of oligomer, which may result in higher polydispersity of PA6. Therefore, the large amount of oligomer in the products may reduce intermolecular interactions between the polymers and lead to a reduction in the elongation at the break of PA6. Zhuang, Y. *et al*.[101] reported the development of PA6/graphene nanocomposites with various graphene loadings (0.1, 0.5, 0.8, 1.0 wt.%). Nanocomposites were prepared using a pre-dispersion method to ensure uniform distribution of graphene within the PA6 matrix. They concluded that the use of the pre-dispersion method for graphene in PA6 resulted in an improvement in the mechanical properties of the nanocomposites compared to the absence of such a method. The tensile and bending strength reached the maximum (105% and 114%) when the amount of graphene was 0.5 wt.%, and the impact strength of the nanocomposites increased by 53% with 0.8 wt.% graphene loading. In another study, Vasiljevic, J. *et al*.[102] analyzed the feasibility of producing PA6/graphene composite fibres using commercially available few-layer graphene nanoplatelets and incorporated them into the PA6 matrix via *in situ* polymerization approach, followed by the pilot-scale melt spinning process. The GNP were pre-dispersed in molten ε-caprolactam at concentrations of 1 and 2 wt. %. The authors reported that the incorporated did not significantly affect the T_m of PA6, but did affect the crystallization temperature, crystallinity, and mechanical properties. Young's modulus and tenacity decreased by 7% and 56%, respectively for PA6/GNP 1 wt.%, and by 61% and 85%, respectively for PA6/GNP 2 wt.%, due to clogging of the filter in the spinning pack, and, consequently, reduced tensile properties. This reduction led the authors to suggest the need to optimize the parameters used in the process.

In general, the final properties of PA6/GBM nanocomposites are influenced by several factors that need to be considered. These factors include the preparation method, the type of nanofiller, the nanofillers' content and size, and, consequently, the dispersion within the polymeric matrix. This research aims to fill a gap in the existing literature in this area. In addition, it is important to recognise the technical challenges that still need to be overcome in the context of T-RTM, particularly in relation to the equipment solutions available on the market.

References

1. Verdejo, R., Bernal, M. M., Romasanta, L. J. & Lopez-Manchado, M. A. Graphene filled polymer nanocomposites. *J Mater Chem* **21**, 3301–3310 (2011).
2. Keledi, G., Hari, J. & Pukanszky, B. Polymer nanocomposites: structure, interaction, and functionality. *Nanoscale* **4**, 1919–1938 (2012).
3. Koo, J. H. *Polymer Nanocomposites: Processing, Characterization, and Applications*. (McGraw-Hill Education, 2019).
4. Mago, G., Kalyon, D. M., Jana, S. C. & Fisher, F. T. Polymer nanocomposite processing, characterization, and applications. *J Nanomater* **2010**, 1–2 (2010).
5. Kroto, H. W., Heath, J. R., O'Brien, S. C., Curl, R. F. & Smalley, R. E. C60: Buckminsterfullerene. *Nature* **318**, 162–163 (1985).
6. Iijima, S. Helical microtubules of graphitic carbon. *Nature* **354**, 56–58 (1991).
7. Geim, A. K. & Novoselov, K. S. The rise of graphene. in *Nanoscience and technology: a collection of reviews from nature journals* 11–19 (World Scientific, 2010).
8. Kim, B. J., Cha, S. H. & Park, Y. Bin. Ultra-high-speed processing of nanomaterial-reinforced woven carbon fiber/polyamide 6 composites using reactive thermoplastic resin transfer molding. *Compos B Eng* **143**, 36–46 (2018).
9. Zaldua, N. *et al.* Nucleation and crystallization of PA6 composites prepared by T-RTM: Effects of carbon and glass fiber loading. *Polymers (Basel)* **11**, 1680 (2019).
10. Murray, J. J., Robert, C., Gleich, K., McCarthy, E. D. & Brádaigh, C. M. Ó. Manufacturing of unidirectional stitched glass fabric reinforced polyamide 6 by thermoplastic resin transfer moulding. *Mater Des* **189**, 108512 (2020).
11. Zhou, L., Liu, H. & Zhang, X. Graphene and carbon nanotubes for the synergistic reinforcement of polyamide 6 fibers. *J Mater Sci* **50**, 2797–2805 (2015).
12. Khan, Z. U., Kausar, A. & Ullah, H. A review on composite papers of graphene oxide, carbon nanotube, polymer/GO, and polymer/CNT: Processing strategies, properties, and relevance. *Polym Plast Technol Eng* **55**, 559–581 (2016).
13. Wei, C., Akinwolemiwa, B., Yu, L., Hu, D. & Chen, G. Z. Polymer composites with functionalized carbon nanotube and graphene. in *Polymer Composites with Functionalized Nanoparticles* 211–248 (Elsevier, 2019).
14. Liu, X., Guo, L., Morris, D., Kane, A. B. & Hurt, R. H. Targeted removal of bioavailable metal as a detoxification strategy for carbon nanotubes. *Carbon N Y* **46**, 489–500 (2008).
15. Liu, Y., Zhao, Y., Sun, B. & Chen, C. Understanding the toxicity of carbon nanotubes. *Acc Chem Res* **46**, 702–713 (2013).
16. Das, T. K. & Prusty, S. Graphene-based polymer composites and their applications. *Polym Plast Technol Eng* **52**, 319–331 (2013).
17. Huang, X., Qi, X., Boey, F. & Zhang, H. Graphene-based composites. *Chem Soc Rev* **41**, 666–686 (2012).
18. Potts, J. R., Dreyer, D. R., Bielawski, C. W. & Ruoff, R. S. Graphene-based polymer nanocomposites. *Polymer (Guildf)* **52**, 5–25 (2011).
19. Kuilla, T. *et al.* Recent advances in graphene based polymer composites. *Prog Polym Sci* **35**, 1350–1375 (2010).
20. Zhang, M., Li, Y., Su, Z. & Wei, G. Recent advances in the synthesis and applications of graphene–polymer nanocomposites. *Polym Chem* **6**, 6107–6124 (2015).
21. Elmarakbi, A. & Azoti, W. State of the art on graphene lightweighting nanocomposites for automotive applications. *Experimental Characterization, Predictive Mechanical and Thermal Modeling of Nanostructures and their Polymer Composites* 1–23 (2018).
22. Kim, H., Abdala, A. A. & Macosko, C. W. Graphene/polymer nanocomposites. *Macromolecules* **43**, 6515–6530 (2010).
23. Zhu, Y. *et al.* Graphene and Graphene Oxide: Synthesis, Properties, and Applications. *Advanced Materials* **22**, 3906–3924 (2010).
24. Stankovich, S. *et al.* Graphene-based composite materials. *Nature* **442**, 282–286 (2006).
25. Gong, L., Yin, B., Li, L. & Yang, M. Nylon-6/Graphene composites modified through polymeric modification of graphene. *Compos B Eng* **73**, 49–56 (2015).

26. O'Neill, A., Archer, E., McIlhagger, A., Lemoine, P. & Dixon, D. Polymer nanocomposites: In situ polymerization of polyamide 6 in the presence of graphene oxide. *Polym Compos* **38**, 528–537 (2017).
27. Kiziltas, A., Liu, W., Tamrakar, S. & Mielewski, D. Graphene nanoplatelet reinforcement for thermal and mechanical properties enhancement of bio-based polyamide 6, 10 nanocomposites for automotive applications. *Composites Part C: Open Access* **6**, 100177 (2021).
28. Fu, X., Liu, Y., Zhao, X., Zhao, D. & Yang, G. A commercial production route to prepare polymer-based nanocomposites by unmodified multilayer graphene. *J Appl Polym Sci* **132**, (2015).
29. Xu, Z. & Gao, C. In situ polymerization approach to graphene-reinforced nylon-6 composites. *Macromolecules* **43**, 6716–6723 (2010).
30. Madhad, H. V & Vasava, D. V. Review on recent progress in synthesis of graphene–polyamide nanocomposites. *Journal of Thermoplastic Composite Materials* **35**, 570–598 (2022).
31. Kausar, A. Trends in graphene reinforced polyamide nanocomposite for functional application: a review. *Polymer-Plastics Technology and Materials* **58**, 917–933 (2019).
32. Faridirad, F., Ahmadi, S. & Barmar, M. Polyamide/Carbon Nanoparticles Nanocomposites: A Review. *Polym Eng Sci* **57**, 475–494 (2017).
33. Fu, X., Yao, C. & Yang, G. Recent advances in graphene/polyamide 6 composites: a review. *RSC Adv* **5**, 61688–61702 (2015).
34. Schedin, F. *et al.* Detection of individual gas molecules adsorbed on graphene. *Nat Mater* **6**, 652–655 (2007).
35. Roberts, M. W. *et al.* Continuum plate theory and atomistic modeling to find the flexural rigidity of a graphene sheet interacting with a substrate. *J Nanotechnol* **2010**, (2010).
36. Eigler, S. & Hirsch, A. Chemistry with graphene and graphene oxide—challenges for synthetic chemists. *Angewandte Chemie International Edition* **53**, 7720–7738 (2014).
37. Lee, C., Wei, X., Kysar, J. W. & Hone, J. Measurement of the elastic properties and intrinsic strength of monolayer graphene. *Science (1979)* **321**, 385–388 (2008).
38. Balandin, A. A. *et al.* Superior thermal conductivity of single-layer graphene. *Nano Lett* **8**, 902–907 (2008).
39. Du, X., Skachko, I., Barker, A. & Andrei, E. Y. Approaching ballistic transport in suspended graphene. *Nat Nanotechnol* **3**, 491–495 (2008).
40. Shinohara, H. & Tiwari, A. *Graphene: An Introduction to the Fundamentals and Industrial Applications*. (John Wiley & Sons, 2015).
41. Delsing, P. & Bergstrom, L. Nobel Prize in Physics-2010. (2010).
42. Zhang, Z., Fraser, A., Ye, S., Merle, G. & Barralet, J. Top-down bottom-up graphene synthesis. *Nano Futures* **3**, 42003 (2019).
43. Kumar, N. *et al.* Top-down synthesis of graphene: A comprehensive review. *FlatChem* **27**, 100224 (2021).
44. Novoselov, K. S. *et al.* Electric field effect in atomically thin carbon films. *Science (1979)* **306**, 666–669 (2004).
45. Bourlinos, A. B., Georgakilas, V., Zboril, R., Steriotis, T. A. & Stubos, A. K. Liquid-phase exfoliation of graphite towards solubilized graphenes. *small* **5**, 1841–1845 (2009).
46. Liu, N. *et al.* One-step ionic-liquid-assisted electrochemical synthesis of ionic-liquid-functionalized graphene sheets directly from graphite. *Adv Funct Mater* **18**, 1518–1525 (2008).
47. Behabtu, N. *et al.* Spontaneous high-concentration dispersions and liquid crystals of graphene. *Nat Nanotechnol* **5**, 406–411 (2010).
48. Arole, V. M. & Munde, S. V. Fabrication of nanomaterials by top-down and bottom-up approaches-an overview. *J. Mater. Sci* **1**, 89–93 (2014).
49. Wang, X. *et al.* Large-scale synthesis of few-layered graphene using CVD. *Chemical Vapor Deposition* **15**, 53–56 (2009).
50. Li, N. *et al.* Large scale synthesis of N-doped multi-layered graphene sheets by simple arc-discharge method. *Carbon N Y* **48**, 255–259 (2010).

51. Rollings, E. *et al.* Synthesis and characterization of atomically thin graphite films on a silicon carbide substrate. *Journal of Physics and Chemistry of Solids* **67**, 2172–2177 (2006).
52. De Heer, W. A. *et al.* Epitaxial graphene. *Solid State Commun* **143**, 92–100 (2007).
53. Yang, X. *et al.* Two-dimensional graphene nanoribbons. *J Am Chem Soc* **130**, 4216–4217 (2008).
54. Zhang, W. *et al.* A strategy for producing pure single-layer graphene sheets based on a confined self-assembly approach. *Angewandte Chemie* **121**, 5978–5982 (2009).
55. Skoda, M., Dudek, I., Jarosz, A. & Szukiewicz, D. Graphene: one material, many possibilities—application difficulties in biological systems. *J Nanomater* **2014**, (2014).
56. Novoselov, K. S., Colombo, L., Gellert, P. R., Schwab, M. G. & Kim, K. A roadmap for graphene. *Nature* **490**, 192–200 (2012).
57. Hope, J. T. *et al.* Scalable production of graphene nanoplatelets for energy storage. *ACS Appl Nano Mater* **3**, 10303–10309 (2020).
58. Gkourmpis, T. *et al.* Melt-mixed 3D hierarchical graphene/polypropylene nanocomposites with low electrical percolation threshold. *Nanomaterials* **9**, 1766 (2019).
59. Cataldi, P., Athanassiou, A. & Bayer, I. S. Graphene nanoplatelets-based advanced materials and recent progress in sustainable applications. *Applied Sciences* **8**, 1438 (2018).
60. Jang, B. Z. & Zhamu, A. Processing of nanographene platelets (NGPs) and NGP nanocomposites: a review. *J Mater Sci* **43**, 5092–5101 (2008).
61. Sengupta, R., Bhattacharya, M., Bandyopadhyay, S. & Bhowmick, A. K. A review on the mechanical and electrical properties of graphite and modified graphite reinforced polymer composites. *Prog Polym Sci* **36**, 638–670 (2011).
62. Chung, D. D. L. A review of exfoliated graphite. *J Mater Sci* **51**, 554–568 (2016).
63. Pop, E., Varshney, V. & Roy, A. K. Thermal properties of graphene: Fundamentals and applications. *MRS Bull* **37**, 1273–1281 (2012).
64. Lee, S.-M., Kang, D.-S. & Roh, J.-S. Bulk graphite: materials and manufacturing process. *Carbon letters* **16**, 135–146 (2015).
65. Young, R. J., Kinloch, I. A., Gong, L. & Novoselov, K. S. The mechanics of graphene nanocomposites: a review. *Compos Sci Technol* **72**, 1459–1476 (2012).
66. Allen, M. J., Tung, V. C. & Kaner, R. B. Honeycomb carbon: a review of graphene. *Chem Rev* **110**, 132–145 (2010).
67. Castillo, A. E. D. R. *et al.* High-yield production of 2D crystals by wet-jet milling. *Mater Horiz* **5**, 890–904 (2018).
68. Ranjbar, N., Mehrali, M., Mehrali, M., Alengaram, U. J. & Jumaat, M. Z. Graphene nanoplatelet-fly ash based geopolymer composites. *Cem Concr Res* **76**, 222–231 (2015).
69. Zhang, M., Li, Y., Su, Z. & Wei, G. Recent advances in the synthesis and applications of graphene–polymer nanocomposites. *Polym Chem* **6**, 6107–6124 (2015).
70. Moniruzzaman, M. & Winey, K. I. Polymer Nanocomposites Containing Carbon Nanotubes. *Macromolecules* **39**, 5194–5205 (2006).
71. Kamal, A., Ashmawy, M., S, S., Algazzar, A. M. & Elsheikh, A. H. Fabrication techniques of polymeric nanocomposites: A comprehensive review. *Proc Inst Mech Eng C J Mech Eng Sci* **236**, 4843–4861 (2022).
72. Potts, J. R., Dreyer, D. R., Bielawski, C. W. & Ruoff, R. S. Graphene-based polymer nanocomposites. *Polymer (Guildf)* **52**, 5–25 (2011).
73. Gonçalves, C., Gonçalves, I., Magalhães, F. & Pinto, A. Poly(lactic acid) Composites Containing Carbon-Based Nanomaterials: A Review. *Polymers (Basel)* **9**, 269 (2017).
74. Fang, M., Wang, K., Lu, H., Yang, Y. & Nutt, S. Covalent polymer functionalization of graphene nanosheets and mechanical properties of composites. *J Mater Chem* **19**, 7098–7105 (2009).
75. Ding, P. *et al.* Anisotropic thermal conductive properties of hot-pressed polystyrene/graphene composites in the through-plane and in-plane directions. *Compos Sci Technol* **109**, 25–31 (2015).
76. Hong, N. *et al.* Co-precipitation synthesis of reduced graphene oxide/NiAl-layered double hydroxide hybrid and its application in flame retarding poly (methyl methacrylate). *Mater Res Bull* **49**, 657–664 (2014).

77. Khanna, S. K. & Phan, H. T. T. High strain rate behavior of graphene reinforced polyurethane composites. *J Eng Mater Technol* **137**, 21005 (2015).
78. Vermant, J., Ceccia, S., Dolgovskij, M. K., Maffettone, P. L. & Macosko, C. W. Quantifying dispersion of layered nanocomposites via melt rheology. *J Rheol (N Y N Y)* **51**, 429–450 (2007).
79. Mittal, V., Luckachan, G. E. & Matsko, N. B. PE/Chlorinated-PE Blends and PE/Chlorinated-PE/Graphene Oxide Nanocomposites: Morphology, Phase Miscibility, and Interfacial Interactions. *Macromol Chem Phys* **215**, 255–268 (2014).
80. Li, C.-Q. *et al.* Mechanical and dielectric properties of graphene incorporated polypropylene nanocomposites using polypropylene-graft-maleic anhydride as a compatibilizer. *Compos Sci Technol* **153**, 111–118 (2017).
81. Ryu, S. H. & Shanmugharaj, A. M. Influence of hexamethylene diamine functionalized graphene oxide on the melt crystallization and properties of polypropylene nanocomposites. *Mater Chem Phys* **146**, 478–486 (2014).
82. Kang, S. *et al.* 2D reentrant micro-honeycomb structure of graphene-CNT in polyurethane: High stretchability, superior electrical/thermal conductivity, and improved shape memory properties. *Compos B Eng* **162**, 580–588 (2019).
83. Kim, H. *et al.* Graphene/polyethylene nanocomposites: Effect of polyethylene functionalization and blending methods. *Polymer (Guildf)* **52**, 1837–1846 (2011).
84. Dixon, D., Lemonine, P., Hamilton, J., Lubarsky, G. & Archer, E. Graphene oxide–polyamide 6 nanocomposites produced via in situ polymerization. *Journal of Thermoplastic Composite Materials* **28**, 372–389 (2015).
85. Fu, X., Yao, C. & Yang, G. Recent advances in graphene/polyamide 6 composites: a review. *RSC Adv* **5**, 61688–61702 (2015).
86. Du, N., Zhao, C., Chen, Q., Wu, G. & Lu, R. Preparation and characterization of nylon 6/graphite composite. *Mater Chem Phys* **120**, 167–171 (2010).
87. Ding, P. *et al.* Highly thermal conductive composites with polyamide-6 covalently-grafted graphene by an in situ polymerization and thermal reduction process. *Carbon N Y* **66**, 576–584 (2014).
88. Bhattacharyya, A. R., Pötschke, P., Häußler, L. & Fischer, D. Reactive compatibilization of melt mixed PA6/SWNT composites: mechanical properties and morphology. *Macromol Chem Phys* **206**, 2084–2095 (2005).
89. Zhang, X., Fan, X., Li, H. & Yan, C. Facile preparation route for graphene oxide reinforced polyamide 6 composites via in situ anionic ring-opening polymerization. *J Mater Chem* **22**, 24081–24091 (2012).
90. Zhang, F., Peng, X., Yan, W., Peng, Z. & Shen, Y. Nonisothermal crystallization kinetics of in situ nylon 6/graphene composites by differential scanning calorimetry. *J Polym Sci B Polym Phys* **49**, 1381–1388 (2011).
91. Chen, D., Zhu, H. & Liu, T. In situ thermal preparation of polyimide nanocomposite films containing functionalized graphene sheets. *ACS Appl Mater Interfaces* **2**, 3702–3708 (2010).
92. Ramanathan, T. *et al.* Functionalized graphene sheets for polymer nanocomposites. *Nat Nanotechnol* **3**, 327–331 (2008).
93. Liu, Y., Chen, Z. & Yang, G. Synthesis and characterization of polyamide-6/graphite oxide nanocomposites. *J Mater Sci* **46**, 882–888 (2011).
94. Zheng, D. *et al.* In situ thermal reduction of graphene oxide for high electrical conductivity and low percolation threshold in polyamide 6 nanocomposites. *Compos Sci Technol* **72**, 284–289 (2012).
95. Liu, H.-H., Peng, W.-W., Hou, L.-C., Wang, X.-C. & Zhang, X.-X. The production of a melt-spun functionalized graphene/poly (ε-caprolactam) nanocomposite fiber. *Compos Sci Technol* **81**, 61–68 (2013).
96. Salavagione, H. J., Gomez, M. A. & Martinez, G. Polymeric modification of graphene through esterification of graphite oxide and poly (vinyl alcohol). *Macromolecules* **42**, 6331–6334 (2009).

97. Liu, A., Xie, T. & Yang, G. Comparison of Polyamide-6 Nanocomposites Based on Pristine and Organic Montmorillonite Obtained via Anionic Ring-Opening Polymerization. *Macromol Chem Phys* **207**, 1174–1181 (2006).
98. Wang, R., Wu, L., Zhuo, D., Zhang, J. & Zheng, Y. Fabrication of polyamide 6 nanocomposite with improved thermal conductivity and mechanical properties via incorporation of low graphene content. *Ind Eng Chem Res* **57**, 10967–10976 (2018).
99. Li, C., Xiang, M. & Ye, L. Intercalation structure and highly enhancing tribological performance of monomer casting nylon-6/graphene nano-composites. *Compos Part A Appl Sci Manuf* **95**, 274–285 (2017).
100. Mayoral, B. *et al.* Melt processing and characterisation of polyamide 6/graphene nanoplatelet composites. *RSC Adv* **5**, 52395–52409 (2015).
101. Zhuang, Y. F. *et al.* Monomer casting nylon/graphene nanocomposite with both improved thermal conductivity and mechanical performance. *Compos Part A Appl Sci Manuf* **120**, 49–55 (2019).
102. Vasiljević, J. *et al.* Characterization of polyamide 6/multilayer graphene nanoplatelet composite textile filaments obtained via in situ polymerization and melt spinning. *Polymers (Basel)* **12**, 1787 (2020).

4.3 Dispersibility of graphene nanoplatelets in ε-caprolactam

Joana Lagarinhos[1,2], Martinho Oliveira[1,2]

[1]EMaRT Group – Emerging: Materials, Research, Technology, School of Design, Management and Production Technologies, University of Aveiro, Estrada do Cercal 449, 3720-509 Oliveira de Azeméis, Portugal

[2]CICECO - Aveiro Institute of Materials, University of Aveiro, Campus Universitário de Santiago, 3810-193 Aveiro, Portugal

To be Submitted

Abstract

Graphene nanoplatelets (GNP) are widely used to improve the final properties of polymers. This work focuses on the characterization of commercially available GNP with two different sizes prior to their incorporation into polymer nanocomposites, to ensure the feasibility of the manufactured components. Various characterization techniques, including Brunauer-Emm-Teller (BET) analysis, dynamic light scattering (DLS) for particle size distribution, thermogravimetric analysis (TGA), Raman spectroscopy, X-ray diffraction (XRD) and scanning electron microscopy (SEM), were used to thoroughly investigate the structure of the GNP. The interaction performance of the different GNP with ε-caprolactam (CL) monomer was evaluated by mechanical stirring and ultrasonication. The influence of GNP ranging from 0.1 to 1 wt.% and different time periods ranging from 5 to 60 min were evaluated. The results demonstrated that ultrasonication was a promising method for efficiently dispersing GNP and reducing the size of the agglomerates formed. The methodology applied revealed that GP required more time to achieve adequate dispersion compared to GN. The results obtained effectively address the dispersion challenges of GNP and facilitate the development of PA6 nanocomposites, ensuring the quality of the final components.

Keywords

graphene nanoplatelets; ε-caprolactam; dispersibility; nanocomposites.

Contributions

The author had contributed to the planning and execution of all experiments. The definition of the most adequate dispersion parameters used as well as on the discussion, interpretation, and preparation of the manuscript was also performed by the author. Martinho Oliveira contributed to the conception, revision and editing of the entire manuscript.

1. Introduction

The realm of nanotechnology and materials science has attracted considerable attention with the emergence of graphene, often hailed as the “wonder” material with high scientific and technological potential[1]. Graphene is a flat molecule derived from graphite materials, comprising a pattern of carbon atoms arranged in hexagonal shape[2]. It has a high intrinsic mobility (200 000 $cm^2 v^{-1} \cdot s^{-1}$)[3,4], high Young’s modulus (~1.0 TPa)[5] and thermal conductivity (~5000 $Wm^{-1} \cdot K^{-1}$)[6], and its optical transmittance (~97.7%)[5] and good electrical conductivity merit attention for a wide range of applications, including energy storage, electronics, bio-applications, and composite materials[7].

Graphene-based materials (GBM) composites have attracted significant interest as a response to the increased growing market for lightweight and energy efficient vehicles[8]. According to Elmarakbi[8,9], the use of GBM as a reinforcement phase for automotive components could result in weight reductions of up to 50%. In addition to weight reduction, GBM can also improve mechanical strength, flexibility, thermal and electrical conductivities. Even at lower GBM contents (≤2.0 wt. %), these properties often exceed those observed in other carbon-based reinforced nanocomposites[10]. Graphene nanoplatelets (GNP) have emerged as a promising GBM reinforcing strategy to enhance mechanical and thermal properties[11,12]. GNP comprises multiple stacked graphene monolayers that are more economical to produce than fully exfoliated graphene sheets[13]. Although GNP are commercially available from various manufacturers, preliminary studies are needed to ensure the desired final properties and to elucidate the results of GNP-polymer nanocomposites. An increased interfacial interaction between GNP and polymeric matrices facilitate an efficient stress transfer, resulting in enhanced mechanical properties of the developed composites.

Polyamide 6 (PA6) is a widely used thermoplastic material in the automotive industry due to its high tensile strength, wear, and chemical resistance[14–16]. Anionic ring-opening polymerization (AROP) of ε-caprolactam (CL) provides a viable route for manufacturing PA6, due to its rapid polymerization rate, making it a favourable option for industrial applications. One way to produce structural PA6 through AROP is to use thermoplastic resin transfer moulding (T-RTM) technology, also known as *in situ* polymerization. The incorporation of GNP into the PA6 matrix gives PA6-based nanocomposites distinct performance characteristics[2,17]. However, several studies are being conducted to achieve a homogeneous dispersion of GNP within the PA6 matrix[18–20]. The distribution and dispersion of nanoscale fillers within the polymeric matrix are key features for achieving superior properties in PA6/GNP nanocomposites. Recently, numerous techniques have been used to achieve homogeneous dispersion of GNP, including surface modification of GNP through covalent and noncovalent functionalization[21], mechanical stirring and ultrasonic processing[22]. Mechanical stirring is considered a suitable method for GNP dispersion[23]. Nevertheless, Yang *et al.*[24] reported that mechanical stirring of GNP could lead to reaggregation between flakes. Among the commonly used methods for dispersing GNP, sonication holds a prominent position[25,26]. This approach includes two variations: sonication bath and probe sonication, with the latter demonstrating an efficient GNP dispersion[27]. In particular, probe sonication exhibits higher performance than bath sonication under

identical conditions[28]. Ultrasonication generates numerous cavitation bubbles within the solution, which rapidly collapse, generating shockwaves capable of disintegrating agglomerates and separating stacked graphene layers from each other[29]. Among the various ultrasonic techniques, the incorporation of solvents has gained widespread acceptance as one of the simplest methods of GNP dispersion. Solvents such as acetone[30], 1-propanol[31] or dimethylformamide[32] have been widely used. However, it is important to know that such dispersion processes require an additional step for solvent removal prior to further reactions. This introduces additional steps and increases the processing time, while it must also be considered that residual solvent can have a detrimental effect on the final properties of the nanocomposite material. In addition, certain solvents are both expensive and toxic, raising concerns about environmental impact and health and safety implications. While a lot of work is being conducted to produce high performance PA6/GNP nanocomposites, the study of GNP as reinforcement of PA6, obtained through *in situ* polymerization, using the T-RTM technology remains limited. Most studies[33–36] focus primarily on the microstructure and mechanical properties of the resulting GNP nanocomposites, leaving the extensive effects of parameters such as ultrasonic power and time relatively unexplored. The molten CL monomer, with its low melt viscosity (5 mPa·s) and isothermal processability provides an improved dispersion medium for an effective dispersion of GNP[37–39]. Therefore, the definition of the optimal dispersion parameters is essential to boost the performance of the produced nanocomposites[40].

The present study focuses on the characterization of commercially available GNP with two different particle sizes (D90 <50 µm (defined as GN) and D90 <70 µm (defined as GP) prior to their incorporation into polymer nanocomposites. Subsequently, the study investigates the addition of GNP to molten CL monomer using two different dispersion strategies, such as mechanical stirring and sonication, to improve the thermal and mechanical performance of PA6/GNP based nanocomposites obtained by T-RTM.

2. Experimental

2.1. Materials

In this work, CL monomer (AP-Nylon®) with a melting point of 69 ºC and a viscosity of 5 mPa·s from Brüggemann Chemicals was used. The selected nanofillers, namely GrapheneBlack™ 0X (GN) and GrapheneBlack™ 3X (GP) were supplied from NanoXplore, Canada. The main characteristics of GNP are outlined in Table 4.3.1:

Table 4.3.1. Main characteristics of GNP according to the supplier.

Property[1]	GN	GP
	Value	
Primary particle size	0.5-1 μm	1-2 μm
Agglomerate size	D10 < 5 μm D50 < 15 μm D90 < 50 μm	D10 < 10 μm D50 < 30 μm D90 < 70 μm
Number of layers	6-10	
Bulk density	0.2-0.3 g·cm^{-3}	
Synthesis method	Liquid exfoliation	
Oxygen content	< 1 wt.%	
Carbon content	> 97 wt.%	> 96 wt.%

[1] obtained from NanoXplore technical data sheet .

2.2. Characterization of GNP

Several characterization techniques were employed to the selected GNP. Brunauer-Emmett-Teller (BET) specific surface area analysis was performed by physical adsorption of nitrogen (N_2) gas using a Quantachrome Autosorb IQ2 surface analyser. Approximately, 0.1 g of sample was placed in the sample holder. After degassing for 20 h at 200 ºC, N_2 gas was injected, and the surface area was calculated using the multipoint BET method[41]. At least three measurements were made for surface area analysis.

Particle size distribution was determined using a Horiba Scientific instrument (model LA 960-V2) at 25 ºC through the dynamic light scattering (DLS) technique. The sample was gradually added to a tank of water until obscuration was achieved. All measurements were carried out without ultrasonication to preserve the inherent size of the carbonaceous particles. Refraction index values of 1.33 and 2.60 were assigned to the dispersant (deionized water) and the GNP, respectively. DLS plots were generated based on the median particle size by volume (D50). At least three measurements were taken for each sample.

Thermogravimetric analysis (TGA) was investigated using a Hitachi STA300 apparatus under an inert atmosphere (N_2 flow rate of 100 mL·min^{-1}). The heating rate was set at 10 ºC·min^{-1}, ranging from room temperature up to 1000 ºC.

Raman spectroscopy was also performed at room temperature using a FT Raman Bruker MultiRAM instrument. Spectra were recorded in the spectral range from 50 to 3600 cm^{-1} with a resolution of 4 cm^{-1} and a laser with a 1064 nm.

The crystalline structures of GNP were analysed by X-ray diffraction (XRD) using a Panalytical X'Pert Pro 3 diffractometer. Cu Kα radiation (λ = 1.5406 Å) was employed at room temperature. XRD measurements were directly performed on the powder samples in the 2θ range of 5º to 40º with a step time of 0.02º.

The distance between the layers of GNP sheets calculated using Bragg's law equation[42]:

$$\lambda = 2dsin\theta \quad (1)$$

where λ is the wavelength of the X-ray beam (1.5406 Â), d is the interlayer spacing between the GNP sheets or layers, and θ is the diffraction angle.

GNP size and morphology were assessed by scanning electron microscopy (SEM). Images were acquired using a Hitachi SU-70 electron microscope. Prior to analysis, the samples were assembled on conducting carbon tape and examined at an acceleration voltage of 15 kV.

2.3. Samples preparation

Two different dispersion methods were investigated to achieve a uniform and optimized dispersion of GNP within CL. The first method involved mechanical stirring at a rate of 300 rpm using a T-RTM prototype equipment (Figure 4.3.1a)[43–45]. The second one involved sonication, using a sonicator (Figure 4.3.1b). The sonication was performed in a 250 mL beaker with a solution volume of 100 mL. For stirring, a Hielscher UP 200 S ultrasonic processor (200 watts, frequency 24 kHz) and an ultrasonic horn was employed to disperse GNP.

For both methods, different times, ranging from 5 to 60 minutes, at a constant temperature of 80ºC, were employed to study the effect of time on the dispersibility of CL/GNP dispersions prepared with GNP concentrations ranging from 0.1 to 1.0 wt.%.

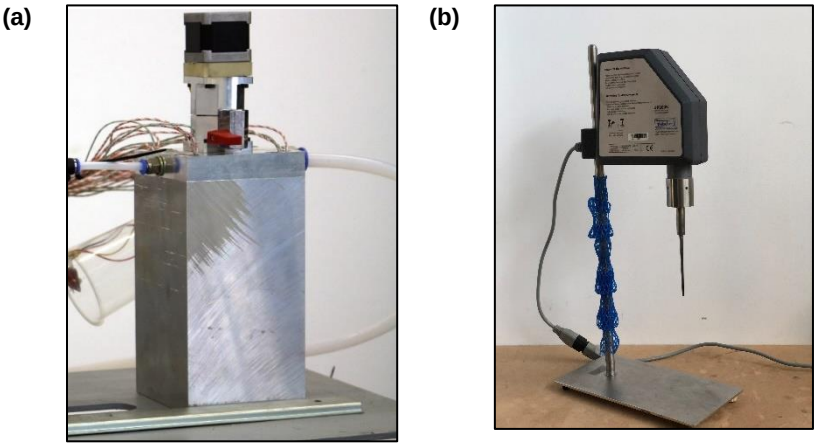

Figure 4.3.1. (a) T-RTM tank equipment and **(b)** sonicator.

For the sonification process, it is illustrated in Figure 4.3.2 a schematic representation of the sonication process used. Initially, the CL monomer is in the solid state (Figure 4.3.2a), and it is melted at 80 ºC (Figure 4.3.2b). Subsequently, a predetermined amount of GNP is introduced into the molten monomer (Figure 4.3.2c). The mixture is subjected to sonication for a specified time (Figure 4.3.2d). Following the sonication process, a careful analysis of the resulting mixture is conducted (Figure 4.3.2e).

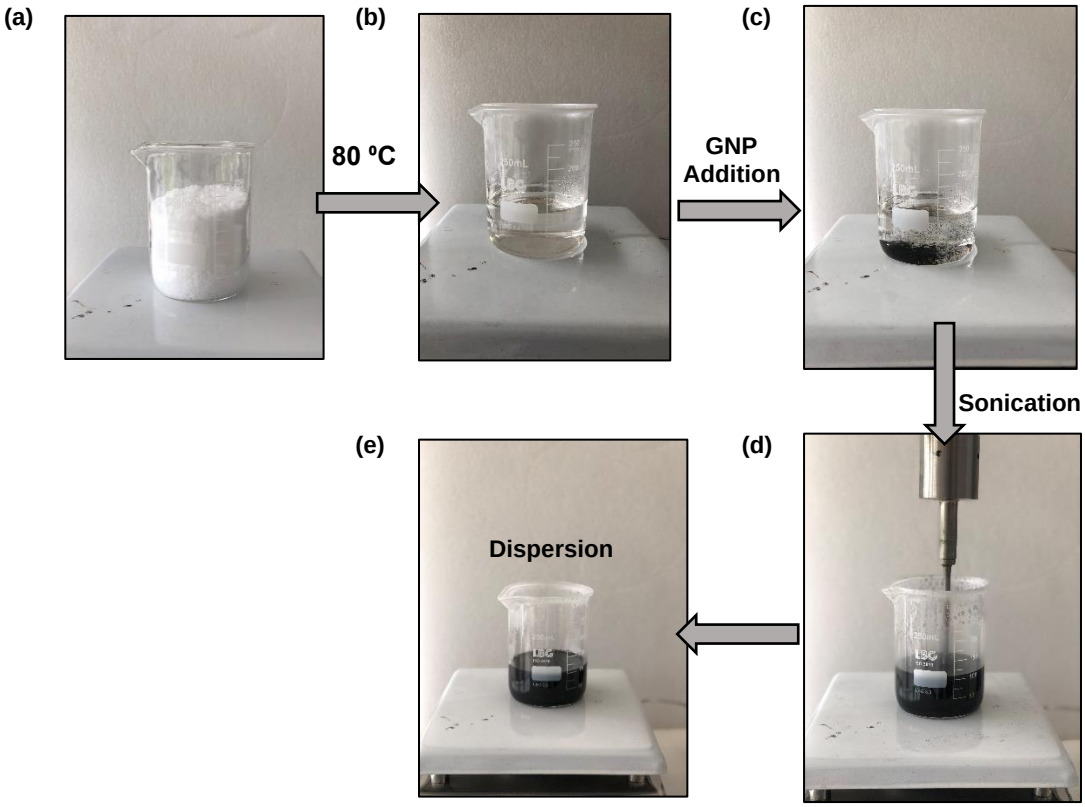

Figure 4.3.2. Schematic of the sonication dispersion process **(a)** solid CL monomer, **(b)** molten CL monomer; **(c)** GNP addition; **(d)** ultrasonic crusher and **(e)** dispersed mixture.

2.4. Characterization of GNP in molten CL monomer

To evaluate the distribution of GNP within the molten CL, observations were conducted using a reflected-light microscope (Nikon Eclipse L150) equipped with an HD Camera (Canon 100D). During the ultrasonic treatment, droplets were extracted directly from the liquid suspension using a pipette and deposited onto a microscope glass slide, which was positioned on a hot plate to keep the mixtures in a molten state.

3. Results and discussion

3.1. GNP characterization

Table 4.3.2 shows the BET surface area values for GN and GP. From Table 4.3.2, it can be seen that GN has a relatively lower specific surface area (9.0 ± 1.4 m^2/g), when compared to GP, which has a higher specific surface area of 16.8 ± 0.2 m^2/g.

Table 4.3.2. BET specific surface area parameters.

	Isotherm type (IUPAC)	BET surface area (m^2/g)	t-Plot method
GN	Types I-IV	9.0 ± 1.4	9.5 ± 1.7
GP	Types I-IV	16.8 ± 0.2	19.0 ± 0.2

The obtained N_2 adsorption-desorption isotherms (Figure 4.3.3) clearly show different adsorption profiles for GN and GP. The isotherm types (Types I-IV) revealed the presence of both micro- and mesoporosity in the GNP.

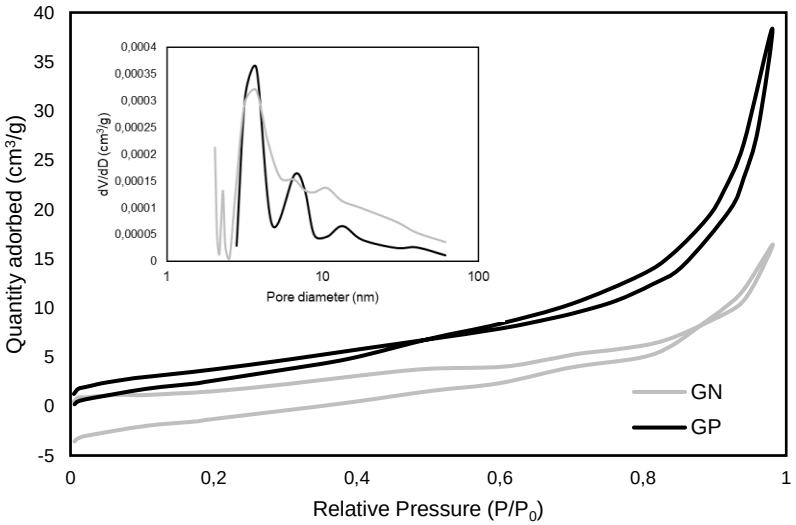

Figure 4.3.3. Nitrogen adsorption-desorption isotherms of GN and GP. Inset: pore size distribution for GNP.

A characteristic hysteresis cycle is evident during the desorption process which is indicative of mesoporosity within the structure of GNP. As expected, there are noticeable differences in the pore size distribution between GN and GP. The higher surface area GNP (GP) exhibit a greater number of mesopores (ranging from 2 to 50 nm) compared to GN, leading to a larger average pore diameter in GP. This difference can be attributed to the increased interlayer spacing present in GP.

The average particle size distributions of GN and GP were determined, using DLS, to validate the values provided in the technical data sheet. Figure 4.3.4 displays the distribution particle sizes as a function of percent intensity.

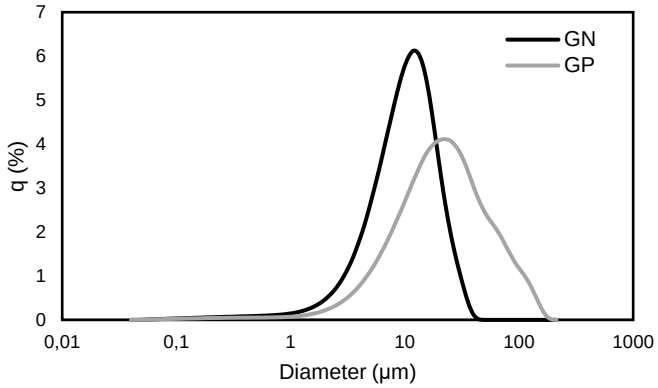

Figure 4.3.4. Particle size distribution curves of GN and GP.

It was observed that the median particle sizes distribution for GN and GP were found to be 10.6 ± 0.2 µm and 20.9 ± 1.6 µm, respectively, as showed in Table 4.3.3. The width of the peak indicates the range of particle sizes present in the sample and a narrower peak indicates a more uniform size distribution[46]. Both samples are characterized by a bell-shaped curve centred on a single peak. However, GN has a narrower peak compared to GP, which means that GP had a broad size distribution, indicating a less uniform size distribution compared to GN.

Table 4.3.3. DLS parameters.

Sample	D10 ± SE	D50 ± SE	D90 ± SE
GN	4.6 ± 1.3	10.6 ± 0.2	19.9 ± 2.7
GP	6.8 ± 1.2	20.9 ± 1.6	62.1 ± 11.8

*SE denotes standard error

The DLS values obtained are consistent with the range provided by the supplier. It is important to note that graphene-based materials are typically not composed of spherical particles and the diameters derived from the model do not necessarily reflect their actual size. The DLS results are primarily intended to illustrate the size differences between the two materials.

Thermal analyses were carried out to determine the presence of impurities and stability of the GNP. The TGA profiles up to 1000 ºC are depicted in Figure 4.3.5 (a) and the corresponding first derivative thermogravimetry (DTG) plots are provided bellow (Figure 4.3.5b).

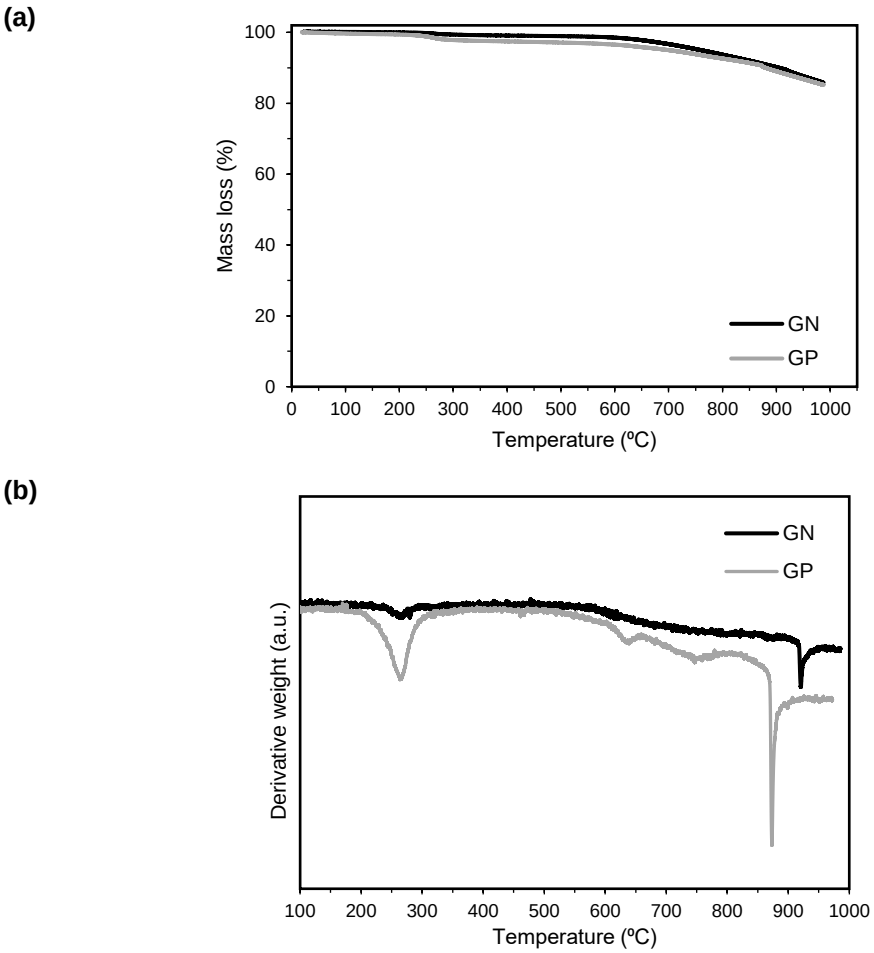

Figure 4.3.5. (a) TGA and **(b)** DTG curves of GN and GP.

As observed, both GNP exhibited a mass retention close to 100% due to their non-volatile composition[47]. A total weight loss of ~14% was observed for both samples. DTG plots demonstrated a single step mass loss during the thermal degradation for both GN and GP. As shown in the DTG graphs, the carbon combustion temperature was distinctly market by the temperature of maximum mass change rate (T_{max}), with GP undergoing carbon combustion at an earlier stage (T_{max} = 874 ºC) than GN (T_{max} = 921 ºC). This distinguished T_{max} can be attributed to the significant amount of external heat energy required to disrupt the robust bonding within their carbon lattice structure[47]. GN has higher T_{max} and requires a greater amount of heat energy to break down the sp^2 hybridized carbon atoms that are covalently bonded in a hexagonal carbon framework[48]. Consequently, these differences, could also be attributed to variations in the specific surface area of the GNP. A higher specific surface area corresponds to a greater number of edges and defects within the structure of the material, making it less stable at elevated temperatures. As the specific surface area increases, the decomposition temperature of GNP tends to decrease.

Raman spectroscopy was performed on the as-received GNP to investigate disorder and defects in nanostructured carbon materials[49]. The results for GN and GP are shown in Figure 4.3.6, with summarized data given in Table 4.3.4. Raman spectra enable the identification of the characteristic

D and G bands inherent to GNP materials[50]. The appearance of the D band is attributed to the introduction of disorder within the sp^2 bonded carbon structures, while the G band originates from the in-plane vibration of sp^2 carbon atoms within the graphene lattice[51]. For both GNP samples, prominent D (disordered carbon) and G (graphitic carbon) bands were observed at around 1285 cm^{-1} and 1587 cm^{-1}, respectively.

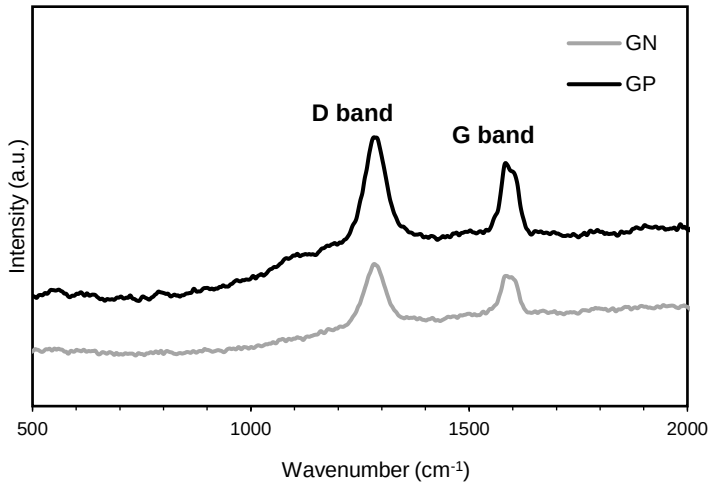

Figure 4.3.6. Raman spectra of **(a)** GP and **(b)** GN.

In addition, the intensity ratio between the D and G band (I_D/I_G) serves as a parameter to assess the extent of disorder or defects within the carbon materials[52]. An increase in I_D/I_G ratio indicates a higher degree of disorder or defects within the graphene layer structure[53]. For both samples, the I_D/I_G value was determined to be 0.81, indicating a moderate level of defects possibly resulting from the exfoliation process[54].

Table 4.3.4. Summarized Raman data obtained for GN and GP.

Sample	D band ± SE (cm^{-1})	G band ± SE (cm^{-1})	D/G Ratio ± SE (cm^{-1})
GN	1283 ± 0.5	1585 ± 0.4	0.81 ± 0.2
GP	1283 ± 0.3	1583 ± 0.7	0.81 ± 0.3

*SE denotes standard error

XRD analysis was also conducted to identify the structure of the crystalline units (d-spacing) within the GNP. The XRD patterns of GN and GP are shown in Figure 4.3.7 and revealed distinct diffraction peaks at 27º, which corresponds to the (002) graphite reflection[55]. This validates the presence of graphene within the samples and proves its crystalline. An interlayer spacing of 3.30 Â was calculated for both GNP.

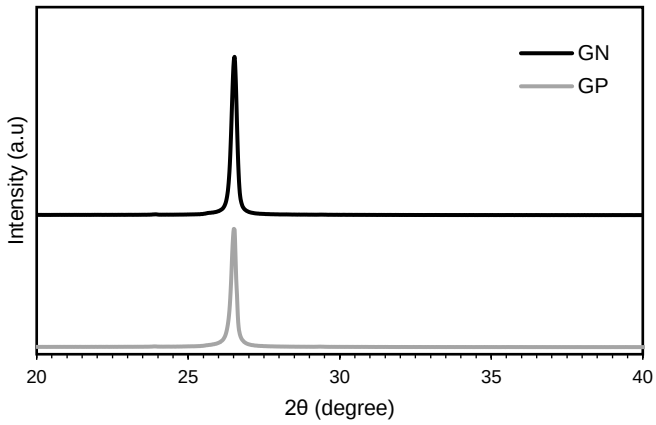

Figure 4.3.7. XRD spectra of GP and GN.

SEM analysis was employed to evaluate the morphology and distribution of the as-received GNP flakes (Figure 4.3.8). The GNP exhibited a platelet-like structure with irregularly shaped flakes and formed agglomerates.

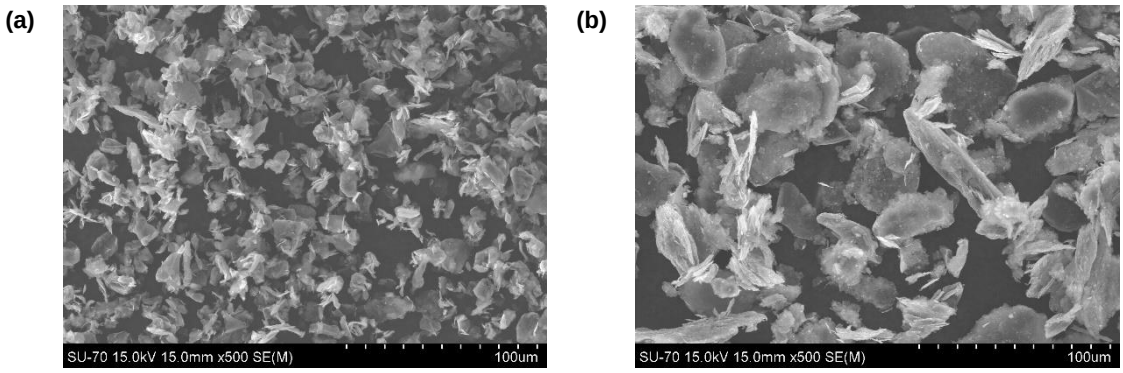

Figure 4.3.8. SEM images of as-received graphene nanoplatelets at **(a)** GN and **(b)** GP at 500x magnification.

Both GNP, GN and GP, exhibited layers of graphene stacked on top of each other and folded together. There is a clear tendency for stacking, with smaller particles adhering to the surface of the larger ones, as illustrated in Figure 4.3.8 (b).The particle size of GP is significantly larger than that of GN, as indicated in the manufacturer's data sheet. In addition, GP has a wider range of particle sizes, which is consistent with the DLS results (Figure 4.3.4). This could be of concern, particularly as uniform dispersion is important for the final application.

3.2. GNP dispersion into CL monomer

As mentioned above, one of the major challenges in the manufacturing process of nanocomposites is to ensure a homogeneous dispersion of nanoparticles within the polymeric matrix. It is widely recognized that only well-dispersed nanoparticles can offer unique properties to nanocomposites, including enhanced thermal and mechanical characteristics, even at very low filler concentrations[56].

The quality of GNP dispersion achieved through mechanical stirring was assessed using optical microscopy. Microphotographs of GN and GP, both at a concentration of 0.1 wt.% in molten CL, after 10 and 30 minutes of stirring are presented in Figure 4.3.9 (a), (c) and (b), (d), respectively. From the optical images, it is evident that even after 30 minutes of stirring, bundled GNP were still present, and the aggregates had not fully dispersed into smaller agglomerates or flakes.

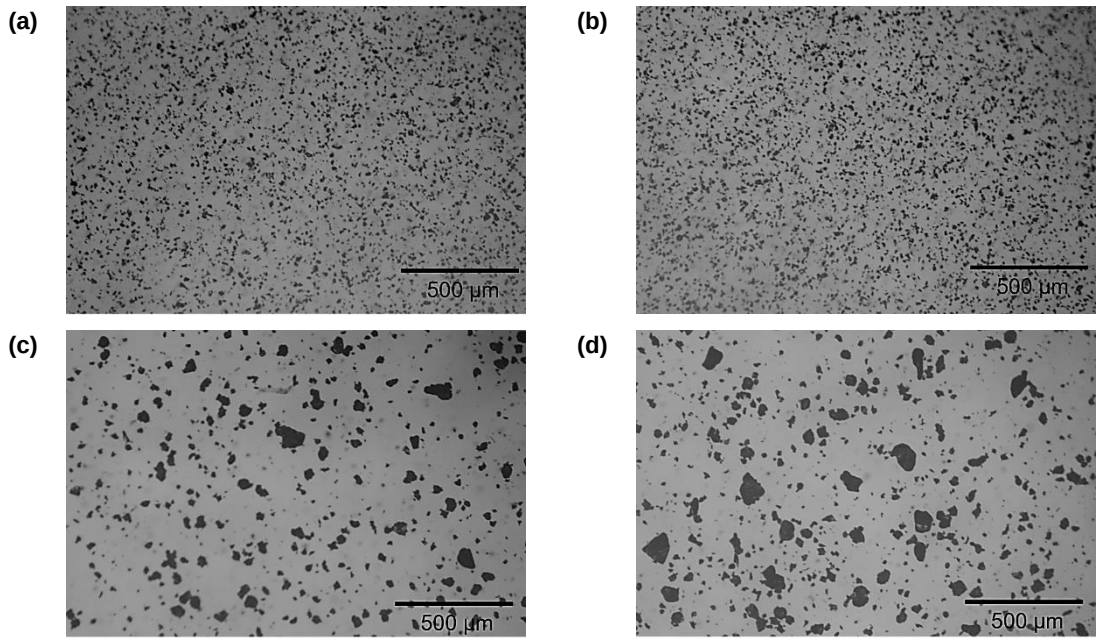

Figure 4.3.9. Optical microscopic analyses of: GN **(a)** after 10 min, **(b)** after 30 min; and GP **(c)** after 10 min **(d)** 30 min stirring.

The qualitative results indicate that the dispersion of graphene in molten CL using mechanical stirring is not efficient for achieving a proper dispersion of GNP. As a result, it was decided not to proceed with a design of experiments (DOE) at higher concentrations due to the ineffectiveness of mechanical stirring.

A straightforward and time-saving approach was studied and developed using ultrasonic cell in order to achieve effective GNP dispersion in molten CL. Microphotographs of GN and GP (0.1 wt.% loading) dispersed with sonication are presented in Figures 4.3.10 and 4.3.11, respectively. For GN, a non-uniform distribution is still evident after 5 minutes of sonication. However, after 10 minutes of sonication it is evident that the GNP have exfoliated and are uniformly distributed in the molten monomer (Figure 4.3.10c). This exfoliation behaviour can be attributed to the intense local shear forces generated during sonication. When the sonication time was increased to 15 minutes, a uniform exfoliation remained constant up to 60 minutes. It is noteworthy that there was no significant change in the dispersion state during this period, suggesting that maximum exfoliation was achieved, and the dispersion remained generally stable.

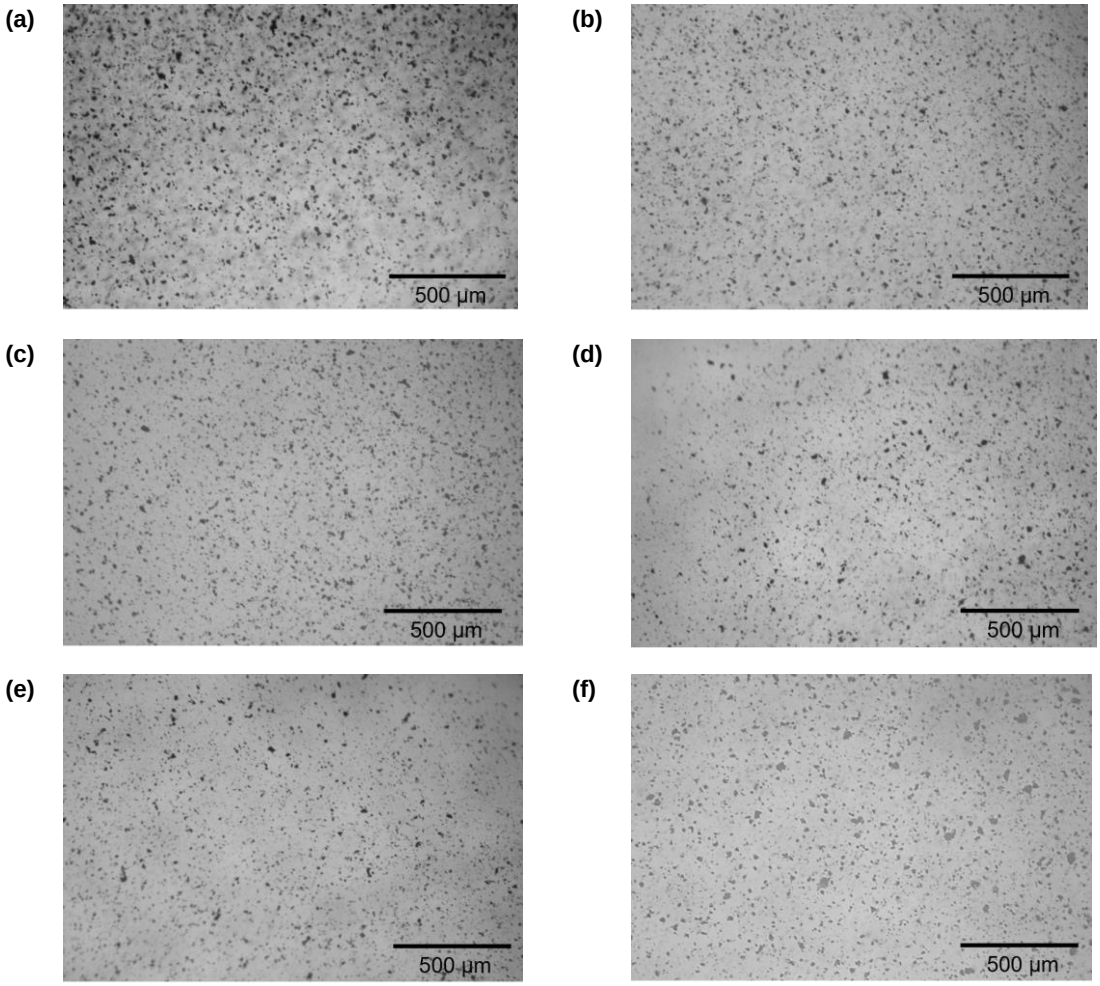

Figure 4.3.10. Optical microscope images of GN dispersions as function of time: **(a)** 5 min; **(b)** 10 min; **(c)** 15 min;**(d)** 20 min, **(e)** 30 min and **(f)** 60 min.

For GP (Figure 4.3.11), it becomes evident that achieving dispersion takes more time when compared to GN, primarily due to the larger particle size of GP (Figure 4.3.11). However, at 15 minutes sonication, the dispersion begins to improve and at 20 minutes a uniform distribution and disaggregation of GP is achieved. During this process, the aggregates are transformed into smaller agglomerates/flakes, which can be an indication of a successful dispersion and exfoliation.

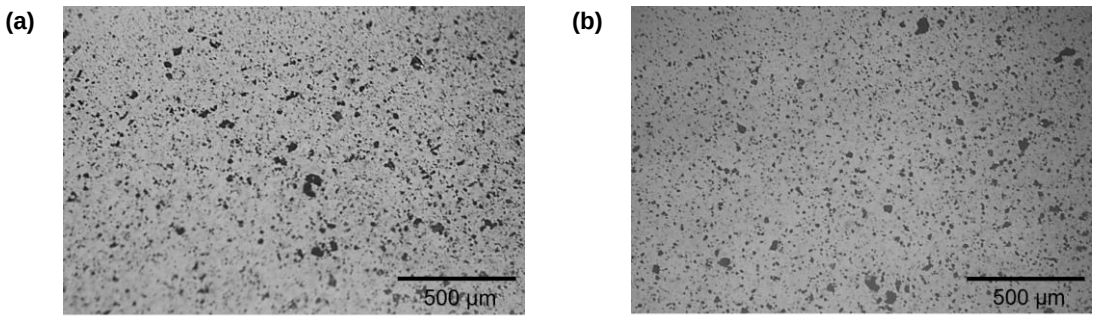

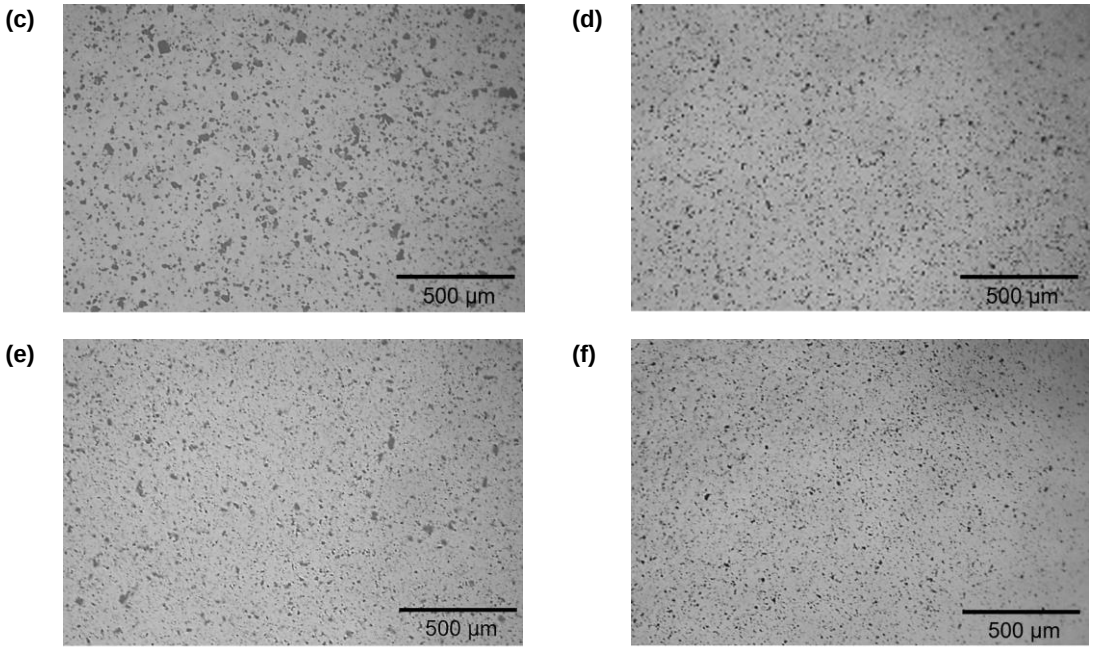

Figure 4.3.11. Optical microscope images of GP dispersions as function of time: **(a)** 5 min; **(b)** 10 min; **(c)** 15 min;**(d)** 20 min, **(e)** 30 min and **(f)** 60 min.

Similar observations were attained for other dispersion times and GNP concentrations (although not shown here). The optimal sonication time for each sample, along with their corresponding GN and GP concentrations, are summarized in Table 4.3.5.

Table 4.3.5. Optimal ultrasonic conditions.

GNP loading (wt.%)	Optimal ultrasonic time (min)	
	GN	GP
0.1	15	20
0.25	20	25
0.5	20	25
0.75	25	30
1.0	25	30

The data presented in Table 4.3.5, highlights a notable trend: as the concentration of GNP increases, achieving a uniform dispersion becomes more challenging, requiring longer sonication times to achieve proper dispersion. This phenomenon can be attributed to the proximity between dispersed GNP sheets at higher concentrations. The reduced interparticle distance makes it easier for GNP sheets to experience attractive forces, leading to a higher probability of reaggregation. This reinforces the need for longer sonication times to counteract this reaggregation behaviour and ensure effective dispersion of GNP at higher concentrations[57].

4. Conclusions

The evaluation of two different commercial references of GNP with different particle sizes was conducted to achieve a comprehensive understanding of how their inherent structure influence their dispersion with a low viscosity molten medium. As expected, the smaller particle size of GNP exhibited a reduced specific surface area compared to their larger counterpart. Consequently, these differences in specific surface area were manifested in the decomposition temperature of the GNP, where lower specific surface area correlated with improved thermal stability. The Raman spectroscopy results showed the characteristic D and G bands emblematic of the composition of GNP, while X-ray diffraction (XRD) analysis confirmed the presence of a distinct and intense diffraction peak, providing compelling evidence to confirm the graphene structure.

From the two analysed dispersion techniques, mechanical stirring proved to be an inefficient technique to achieve a homogeneous distribution of GNP within the molten CL. In contrast, ultrasonic technique proved to be a promising way of efficiently dispersing GNP and reducing the size of the agglomerates formed. A systematic investigation involving different sonication times and concentrations was carried out to evaluate the dispersion of GNP. The results showed that achieving adequate dispersion required more time for GP compared to GN, which can be attributed to the larger particle size of GP. In this work, using a loading of 0.5 wt.%, 20 minutes are required for GN to achieve adequate dispersion, and 25 minutes are required for GP.

Furthermore, the investigation highlighted the critical importance of investigating and understanding the dispersion characteristics of GNP in molten CL monomer. The methodological framework outlined in this study not only served as a fundamental step, but also has the potential to contribute significantly to the advancement of GNP reinforced PA6 for automotive applications.

Acknowledgements

This work was partially supported by Simoldes Group. This work was also developed within the scope of the project CICECO-Aveiro Institute of Materials, UIDB/50011/2020, UIDP/50011/2020 & LA/P/0006/2020, financed by national funds through the FCT/MEC (PIDDAC). Authors would also want to acknowledge Maria Celeste Azevedo for Raman measurements, Célia Miranda for XRD and BET patterns, Ana Ribeiro for DLS analysis, and Suzana Peripolli for the support during SEM analyses.

References

1. Skoda, M., Dudek, I., Jarosz, A. & Szukiewicz, D. Graphene: one material, many possibilities—application difficulties in biological systems. *J Nanomater* **2014**, (2014).
2. Geim, A. K. & Novoselov, K. S. The rise of graphene. in *Nanoscience and technology: a collection of reviews from nature journals* 11–19 (World Scientific, 2010).
3. Bolotin, K. I. *et al.* Ultrahigh electron mobility in suspended graphene. *Solid State Commun* **146**, 351–355 (2008).
4. Morozov, S. V. *et al.* Giant Intrinsic Carrier Mobilities in Graphene and Its Bilayer. *Phys Rev Lett* **100**, 016602 (2008).
5. Zhu, Y. *et al.* Graphene and Graphene Oxide: Synthesis, Properties, and Applications. *Advanced Materials* **22**, 3906–3924 (2010).
6. Balandin, A. A. *et al.* Extremely high thermal conductivity of graphene: Prospects for thermal management applications in silicon nanoelectronics. in *2008 IEEE Silicon Nanoelectronics Workshop* 1–2 (IEEE, 2008).
7. Galpaya, D. *et al.* Recent advances in fabrication and characterization of graphene-polymer nanocomposites. *Graphene* **1**, 30–49 (2012).
8. Elmarakbi, A. & Azoti, W. State of the art on graphene lightweighting nanocomposites for automotive applications. *Experimental Characterization, Predictive Mechanical and Thermal Modeling of Nanostructures and their Polymer Composites* 1–23 (2018).
9. Elmarakbi, A., El-Safty, S., Martorana, B. & Azoti, W. Nanocomposites for Automotive: Enhanced Graphene-based Polyer Materials and Multi-Scale Approach. *International Journal of Automotive Composites* **2**, 155–166 (2017).
10. Hu, K., Kulkarni, D. D., Choi, I. & Tsukruk, V. V. Graphene-polymer nanocomposites for structural and functional applications. *Prog Polym Sci* **39**, 1934–1972 (2014).
11. Irez, A. B., Bayraktar, E. & Miskioglu, I. Fracture toughness analysis of epoxy-recycled rubber-based composite reinforced with graphene nanoplatelets for structural applications in automotive and aeronautics. *Polymers (Basel)* **12**, 448 (2020).
12. Elmarakbi, A. *et al.* Effect of graphene nanoplatelets on the impact response of a carbon fibre reinforced composite. *Mater Today Commun* **25**, 101530 (2020).
13. Jiménez-Suárez, A. & Prolongo, S. G. Graphene Nanoplatelets. *Applied Sciences* **10**, (2020).
14. Sibikin, I. & Karger-Kocsis, J. Toward industrial use of anionically activated lactam polymers: Past, present and future. *Advanced Industrial and Engineering Polymer Research* **1**, 48–60 (2018).
15. Singh, R., Kumar, R., Ranjan, N., Penna, R. & Fraternali, F. On the recyclability of polyamide for sustainable composite structures in civil engineering. *Compos Struct* **184**, 704–713 (2018).
16. Begum, S. A., Rane, A. V. & Kanny, K. Applications of compatibilized polymer blends in automobile industry. in *Compatibilization of polymer blends* vol. 20 563–593 (Elsevier, 2020).
17. Fu, X., Liu, Y., Zhao, X., Zhao, D. & Yang, G. A commercial production route to prepare polymer-based nanocomposites by unmodified multilayer graphene. *J Appl Polym Sci* **132**, (2015).
18. Moniruzzaman, M. & Winey, K. I. Polymer Nanocomposites Containing Carbon Nanotubes. *Macromolecules* **39**, 5194–5205 (2006).
19. Coleman, J. N., Khan, U. & Gun'ko, Y. K. Mechanical reinforcement of polymers using carbon nanotubes. *Advanced Materials* **18**, 689–706 (2006).
20. Perumal, S., Atchudan, R. & Cheong, I. W. Recent Studies on Dispersion of Graphene–Polymer Composites. *Polymers (Basel)* **13**, 2375 (2021).
21. Assali, M. *et al.* Non-covalent functionalization of graphene sheets with surfactants and their antibacterial activity. *Palestinian Medical and Pharmaceutical Journal* **1**, 4 (2016).
22. Krishnamoorthy, K., Kim, G.-S. & Kim, S. J. Graphene nanosheets: Ultrasound assisted synthesis and characterization. *Ultrason Sonochem* **20**, 644–649 (2013).

23. Potts, J. R., Dreyer, D. R., Bielawski, C. W. & Ruoff, R. S. Graphene-based polymer nanocomposites. *Polymer (Guildf)* **52**, 5–25 (2011).
24. Yang, W., Widenkvist, E., Jansson, U. & Grennberg, H. Stirring-induced aggregation of graphene in suspension. *New Journal of Chemistry* **35**, 780–783 (2011).
25. Cai, X., Jiang, Z., Zhang, X. & Zhang, X. Effects of tip sonication parameters on liquid phase exfoliation of graphite into graphene nanoplatelets. *Nanoscale Res Lett* **13**, 1–10 (2018).
26. Yu, H. *et al.* Optimizing sonication parameters for dispersion of single-walled carbon nanotubes. *Chem Phys* **408**, 11–16 (2012).
27. Sandhya, M., Ramasamy, D., Sudhakar, K., Kadirgama, K. & Harun, W. S. W. Ultrasonication an intensifying tool for preparation of stable nanofluids and study the time influence on distinct properties of graphene nanofluids – A systematic overview. *Ultrason Sonochem* **73**, 105479 (2021).
28. Muthoosamy, K. & Manickam, S. State of the art and recent advances in the ultrasound-assisted synthesis, exfoliation and functionalization of graphene derivatives. *Ultrason Sonochem* **39**, 478–493 (2017).
29. Show, K.-Y., Mao, T. & Lee, D.-J. Optimisation of sludge disruption by sonication. *Water Res* **41**, 4741–4747 (2007).
30. Li, J., Wong, P.-S. & Kim, J.-K. Hybrid nanocomposites containing carbon nanotubes and graphite nanoplatelets. *Materials Science and Engineering: A* **483**, 660–663 (2008).
31. Choi, E.-Y., San Choi, W., Lee, Y. B. & Noh, Y.-Y. Production of graphene by exfoliation of graphite in a volatile organic solvent. *Nanotechnology* **22**, 365601 (2011).
32. Lamastra, F. R. *et al.* Poly (ε-caprolactone) reinforced with fibres of Poly (methyl methacrylate) loaded with multiwall carbon nanotubes or graphene nanoplatelets. *Chemical Engineering Journal* **195**, 140–148 (2012).
33. Wang, B. & Shuang, D. Effect of graphene nanoplatelets on the properties, pore structure and microstructure of cement composites. *Materials Express* **8**, 407–416 (2018).
34. Hassanzadeh-Aghdam, M. K., Ansari, R. & Deylami, H. M. Influence of graphene nano-platelets on thermal transport performance of carbon fiber-polymer hybrid composites: Overall assessment of microstructural aspects. *International Journal of Thermal Sciences* **171**, 107209 (2022).
35. Sheshmani, S., Ashori, A. & Arab Fashapoyeh, M. Wood plastic composite using graphene nanoplatelets. *Int J Biol Macromol* **58**, 1–6 (2013).
36. Rashad, M., Pan, F., Tang, A. & Asif, M. Effect of Graphene Nanoplatelets addition on mechanical properties of pure aluminum using a semi-powder method. *Progress in Natural Science: Materials International* **24**, 101–108 (2014).
37. Vasiljević, J. *et al.* Characterization of polyamide 6/multilayer graphene nanoplatelet composite textile filaments obtained via in situ polymerization and melt spinning. *Polymers (Basel)* **12**, 1787 (2020).
38. Kashani Rahimi, S. & Otaigbe, J. U. Polyamide 6 nanocomposites incorporating cellulose nanocrystals prepared by In situ ring-opening polymerization: Viscoelasticity, creep behavior, and melt rheological properties. *Polym Eng Sci* **56**, 1045–1060 (2016).
39. Ji, X., Xu, Y., Zhang, W., Cui, L. & Liu, J. Review of functionalization, structure and properties of graphene/polymer composite fibers. *Compos Part A Appl Sci Manuf* **87**, 29–45 (2016).
40. Wilhelm, M., Wendel, R., Aust, M., Rosenberg, P. & Henning, F. Compensation of water influence on anionic polymerization of ε-caprolactam: 1. Chemistry and experiments. *Journal of Composites Science* **4**, 7 (2020).
41. Mohan, V. B., Jayaraman, K. & Bhattacharyya, D. Brunauer–Emmett–Teller (BET) specific surface area analysis of different graphene materials: A comparison to their structural regularity and electrical properties. *Solid State Commun* **320**, 114004 (2020).
42. Kacher, J., Landon, C., Adams, B. L. & Fullwood, D. Bragg's Law diffraction simulations for electron backscatter diffraction analysis. *Ultramicroscopy* **109**, 1148–1156 (2009).
43. Lagarinhos, J. N. & Oliveira, M. The effect of graphene-based materials in polyamide 6 obtained by in situ thermoplastic resin transfer moulding (T-RTM) polymerization. in *Proceedings of the 20th European Conference on Composite Materials - Composites Meet*

Sustainability (Vol 1-6) (eds. Vassilopoulos, A. & Michaud, V.) 152–159 (EPFL Lausanne, Composite Construction Laboratory, 2022).
44. Lagarinhos, J., Santos, L. & Oliveira, J. Effect of Catalyst and Activator on Properties of Polyamide 6 Prepared by Thermoplastic Resin Transfer Molding Technology. *J Mater Eng Perform* **31**, 7098–7103 (2022).
45. Lagarinhos, J. & Oliveira, M. Nucleation Activity of Graphene in Polyamide 6-Based Nanocomposites Prepared by In Situ Polymerization. *Materials Proceedings* **8**, 83 (2022).
46. Hinterwirth, H. *et al.* Comparative method evaluation for size and size-distribution analysis of gold nanoparticles. *J Sep Sci* **36**, 2952–2961 (2013).
47. Farivar, F., Yap, P. L., Karunagaran, R. U. & Losic, D. Thermogravimetric analysis (TGA) of graphene materials: effect of particle size of graphene, graphene oxide and graphite on thermal parameters. *C (Basel)* **7**, 41 (2021).
48. Gadipelli, S. & Guo, Z. X. Graphene-based materials: Synthesis and gas sorption, storage and separation. *Prog Mater Sci* **69**, 1–60 (2015).
49. O'Neill, A., Archer, E., McIlhagger, A., Lemoine, P. & Dixon, D. Polymer nanocomposites: In situ polymerization of polyamide 6 in the presence of graphene oxide. *Polym Compos* **38**, 528–537 (2017).
50. Mohiuddin, T. M. G. *et al.* Uniaxial strain in graphene by Raman spectroscopy: G peak splitting, Grüneisen parameters, and sample orientation. *Phys Rev B* **79**, 205433 (2009).
51. Liu, H.-H., Peng, W.-W., Hou, L.-C., Wang, X.-C. & Zhang, X.-X. The production of a melt-spun functionalized graphene/poly (ε-caprolactam) nanocomposite fiber. *Compos Sci Technol* **81**, 61–68 (2013).
52. de Lima, L. R. M. *et al.* Characterization of commercial graphene-based materials for application in thermoplastic nanocomposites. *Mater Today Proc* **20**, 383–390 (2020).
53. Ferrari, A. C. & Robertson, J. Interpretation of Raman spectra of disordered and amorphous carbon. *Phys Rev B* **61**, 14095 (2000).
54. Gayathri, S., Jayabal, P., Kottaisamy, M. & Ramakrishnan, V. Synthesis of few layer graphene by direct exfoliation of graphite and a Raman spectroscopic study. *AIP Adv* **4**, 27116 (2014).
55. Rashad, M., Pan, F., Asif, M. & Chen, X. Corrosion behavior of magnesium-graphene composites in sodium chloride solutions. *Journal of magnesium and alloys* **5**, 271–276 (2017).
56. Hussain, F., Hojjati, M., Okamoto, M. & Gorga, R. E. Polymer-matrix nanocomposites, processing, manufacturing, and application: an overview. *J Compos Mater* **40**, 1511–1575 (2006).
57. Kim, H., Abdala, A. A. & Macosko, C. W. Graphene/polymer nanocomposites. *Macromolecules* **43**, 6515–6530 (2010).

4.4 Nucleation Activity of Graphene in Polyamide 6-Based Nanocomposites Prepared by In Situ Polymerization

Joana Lagarinhos and Martinho Oliveira

Materials Proceedings, 2022, 8.1: 83
(DOI: https://doi.org/10.3390/materproc2022008083)

Abstract

Graphene nanoplatelets (GNP) are growing attention in automotive industry, due to potential of development lightweight structure parts with superior mechanical performance and thermal conductivity. Two types of GNP with a fixed number of layers and with a particle size ranging from 0.5 to 2 μm were introduced in polyamide 6 (PA6) at a loading rate of 0.1 wt.% by *in situ* polymerization through thermoplastic resin transfer moulding (T-RTM) technology. T-RTM is a promising technology for mass manufacturing of lighter automotive parts.

A non-isothermal crystallization study was performed using differential scanning calorimetry (DSC) at four different rates (5, 10, 15, and 20 ºC·min^{-1}) to understand the influence of GNP on thermal behaviour of the prepared nanocomposites. Enhancement in melting and crystallization temperatures was observed due to nucleation effect of GNP. Dobreva and Gutzow method was applied to study the nucleation activity (Φ) of GNP in PA6 matrix. Results showed that GNP acted as an active surface by revealing Φ value lower than 1, suggesting that it acts as a nucleating agent during non-isothermal crystallization.

Keywords

Polyamide 6; graphene-based materials; *in situ* polymerization; nucleation activity; differential scanning calorimetry.

Contributions

The author had contributed to the planning and execution of the DSC analyses and modelling calculations herein presented, as well as on the discussion interpretation and preparation of the manuscript. Martinho Oliveira contributed to the revision and editing of the entire manuscript.

1. Introduction

The increasing demand for high performance materials has been driven by the proliferation of polymer nanocomposites, which often exhibit advanced thermal, electrical and mechanical properties due to the reinforcing influence of incorporated fillers[1].

Polyamide 6 (PA6) is one of the most widely used semi-crystalline polymers with a number of advantageous properties, including exceptional mechanical robustness and chemical resistance, making it suitable for a wide range of applications[2,3]. In addition to conventional synthesis techniques such as polycondensation, PA6 can also be synthesized by anionic ring opening polymerization (AROP) of its corresponding cyclic lactam, ε-caprolactam[4]. Nowadays, AROP of ε-caprolactam has emerged as the most industrially relevant route for the production of PA6, mainly due to its rapid polymerization kinetics, making it suitable for industrial use[5].

Thermoplastic resin transfer moulding (T-RTM) is technology in which the ring opening polymerization of ε-caprolactam is carried out in the mould to produce parts directly[6,7]. This approach facilitates the production of large and intricately structured components for automotive applications. The end product is often recyclable and the production schedule is accelerated due to the speed of chemical reaction based polymerization[8,9].

In an effort to enhance the properties of the base polymer, a variety of fillers have been incorporated into the PA6 matrix, resulting in composites with improved performance characteristics[10–12].

Graphene-based materials (GBM), have emerged as an outstanding class of reinforcing nanofillers due to their exceptional properties coupled with the advantages of large scale production and cost effectiveness[13]. Graphene, composed of a single graphite monolayer, has an impressive Young's modulus (≈1100 GPa), high fracture strength (≈125 GPa), remarkable electrical conductivity and optical properties[14,15]. However, its synthesis remains difficult and mass production remains a challenge.

Recently, graphene nanoplatelets (GNP), have emerged as a promising alternative for reinforcing polymer matrices[16]. GNP consist of stacked layers of graphite nanocrystals held together by van der Waals forces[17]. These nanoflakes have a high aspect ratio, planar geometry, commendable mechanical properties, and excellent thermal properties. The combination of these properties and the ability to disperse well in various polymer matrices has given rise to a burgeoning category of polymer nanocomposites.

Due to their inherent properties, GNP have attracted considerable attention in various applications, particularly in the automotive industry. This reinforcement strategy has the potential to simultaneously reduce vehicle weight, facilitate economical manufacturing and enable large-scale production[18,19].

The present study is part of a collaboration with a multinational company recognized as a leading European mould manufacturer. The overall objective is to develop thermoplastic matrices for automotive components by incorporating nanoparticles as structural reinforcements using T-RTM technology. Thorough investigations into the thermal behaviour of PA6/GNP are essential to improve

material processing, increase thermal resistance and enhance mechanical properties. Previous research[20–24], has shown that the introduction of a reinforcing phase into the PA6 matrix can significantly influence the crystallization process, primarily by increasing nucleation activity.

In this context, the study focuses on the preparation of PA6 and PA6/GNP nanocomposites via T-RTM technology, using *in situ* anionic ring opening polymerization of ε-caprolactam monomer. Two variants of GNP, characterized by a constant number of layers and particle sizes ranging from 0.5 to 2 μm, were selected as reinforcing phase.

The main objective is to evaluate the thermal behaviour of PA6 and PA6/GNP nanocomposites, and to investigate the nucleation activity of GNP within the PA6 matrix using the method Dobreva and Gutzow method[25,26]. For this, Differential Scanning Calorimetry (DSC) was used to investigate the non-isothermal crystallization behaviour of the samples.

2. Materials and Methods

2.1. Materials

For the preparation of PA6 from AROP, Brüggemann's Bruggolen system was used: ε-caprolactam (AP-Nylon®) as monomer, Bruggolen® C10 (sodium caprolactamate) as catalyst, and Bruggolen® C20P (N, N-hexane-1,6-diylbis (hexahydro-2-oxo-1H-azepine-1-carboxamide) as activator. The GNP used in this study were supplied by NanoXplore Inc., with 2 different particle sizes: GrapheneBlack 0X with a particle size of 0.5-1 μm (GN) and GrapheneBlack 3X with a particle size: 1-2 μm (GP), were used as reinforcements of the nanocomposites. The bulk density of both GNP fillers is reported to be 0.2-0.3 g/cm^3.

2.2. Samples preparation

Semi-automatic T-RTM laboratory equipment was used to prepare PA6 and PA6/GNP nanocomposites. Prior to its use, all the components involved in the process were carefully stored in a vacuum oven (Carbolite AX60 model) to avoid any potential problems due to exposure to moisture. The concentrations chosen for the synthesis of PA6 were determined based on the optimization process detailed in a previous work[27]. This optimization was crucial for ensuring the desired properties and characteristics of the resulting PA6 polymer. For the preparation of the PA6/GN and PA6/GP nanocomposites, a similar strategy was followed as for PA6. However, in this case, an additional step involved the incorporation of 0.1 wt.% of GrapheneBlack 0X for PA6/GNP and GrapheneBlack 3X for AP/GP nanocomposites, respectively[28].

2.3. DSC analysis

The thermal behaviour of the samples was evaluated using a Shimadzu DSC-60 instrument. Samples of approximately 7.0 mg were studied in aluminium pans. The analysis was performed using a non-isothermal procedure, in which the sample was initially heated from -25 ºC to 250 ºC at a scanning rate of 20 ºC·min^{-1}. This temperature was maintained for 2 minutes to erase any previous thermal history. Cooling scans were then performed at different rates: 5, 10, 15 and 20 ºC·min^{-1}. This

cycle was repeated, and only the data from the second run were used to analyse the melting temperature (T_m) and crystallization temperature (T_c) of samples.

3. Results

3.1. Non-isothermal behaviour

The thermal properties of PA6 and PA6/GNP samples are summarized in Table 4.41. It is noteworthy that the melting temperatures of PA6/GN and PA6/GP nanocomposites remained relatively unaffected by the variations in heating rates applied. However, in the case of the crystallization peaks, a different trend was observed with increasing cooling. The crystallization onset temperature decreases with higher cooling rates, indicating that the onset of crystallization occurs at lower temperatures under faster cooling conditions. For example, at a cooling rate of 5 ºC·min^{-1}, the crystallization peak of PA6 was observed at approximately 179°C, whereas at a cooling rate of 20 ºC·min^{-1} this peak occurred almost 13°C lower. Consequently, the range within which crystallization takes place becomes wider as the cooling rate increases.

This phenomenon can be attributed to the significant influence of temperature on both the nucleation and crystal growth processes. At lower cooling rates, there is sufficient time for the polymer chains to align themselves favourably for crystallization. Conversely, at higher cooling rates, a greater degree of supercooling is required to initiate crystallization, resulting in a reduction in T_c[20,29]. This behaviour was observed for both PA6/GN and PA6/GP nanocomposites.

Table 4.4.1. Non-isothermal crystallization parameters obtained by DSC.

Samples	φ (ºC·min^{-1})	T_m (ºC)	T_c (ºC)
PA6	5	219.09	179.37
	10	218.64	173.44
	15	218.38	168.99
	20	217.80	165.67
PA6/GN	5	218.15	185.50
	10	217.23	179.95
	15	217.60	175.84
	20	216.90	172.72
PA6/GP	5	219.43	185.83
	10	218.59	179.65
	15	217.71	172.02
	20	219.13	172.24

The crystallization peak for the nanocomposites, at a given cooling rate, was higher when compared with PA6. Specifically, GN, which has the smaller particle size, shifted the crystallization peak to higher temperatures compared to GP. As mentioned above, two main factors influence the crystallization process: nucleation and crystal growth. In a polymeric matrix, the polymer chains need

to overcome the free energy barrier for primary nucleation and create a new surface for crystal growth. The incorporation of GNP can reduce the free energy required for nucleation, leading to a faster crystallization process. As a result, more crystals are formed, resulting in a higher T_c. This indicates that the addition of GNP to the PA6 matrix acted as an effective nucleating agent.

3.2. Nucleating activity

The addition of a reinforcing fillers to polymers can significantly improve their mechanical properties and thermal stability[18,30]. Dobreva and Gutzow[25,26] developed a method to evaluate the nucleation activity of foreign substrates in a polymer melts using DSC measurements. Nucleation activity (Φ) represents the extent to which 3D nucleation is reduced by the addition of a foreign substrate. It is calculated from the ratio:

$$\Phi = \frac{\beta^*}{\beta}, \quad (1)$$

where β* is the nucleation parameter for heterogeneous nucleation and β is that for homogeneous nucleation. When Φ approaches to 0, the substrate is considered highly active, while an approach to 1 means that the filler is inert.

Both B and β* can be determined experimentally from the following equation:

$$\ln(\varphi) = A - \frac{\beta \ (or \ \beta^*)}{\Delta T_p^2}, \quad (2)$$

where φ is the cooling rate, A is the constant, and ΔT_p^2 represents the degree of supercooling (Equation 3):

$$\Delta T_p^2 = T_m - T_c, \quad (3)$$

The values of β and β* for PA6 and PA6/GNP can be obtained by plotting ln (φ) against ΔT_p^2, as shown in Figure 4.4.1. The plots show a clear linear relationship. The nucleation activity values are given in Table 4.4.2.

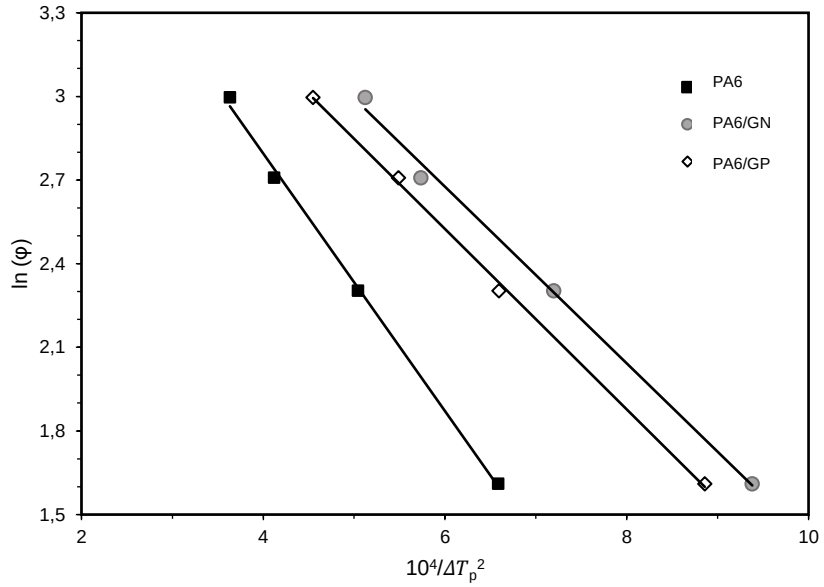

Figure 4.4.1. Plots of ln(φ) versus ΔT_p^2 for evaluating nucleating activity of GNP in PA6/GN and PA6/GP nanocomposites.

The slopes of these lines allowed the calculation of B and B* values for PA6, PA6/GN and PA6/GP, which were found to be 0.46, 0.30 and 0.32 respectively. The Φ values obtained for PA6/GN and PA6/GP are lower than 1, indicating that GNP acted as an effective nucleating agents within the PA6 matrix, creating an active surface for crystallization.

Table 4.4.2. Nucleating activity.

Samples	β	B^*	Φ	R^2
PA6	0.46	-	-	1.00
PA6/GN	-	0.30	0.65	1.00
PA6/GP	-	0.32	0.70	1.00

From these results, it can be concluded that the smaller particle size of PA6/GN allows for more effective nucleation activity within the PA6 matrix, enhancing the crystallization process. On the other hand, PA6/GP can create a higher energy barrier for the segments of the PA6 polymer to overcome during the crystallization process. This higher energy barrier can hinder the close packing of polymer chains, making it more difficult for them to arrange themselves into well-ordered crystalline structures or crystallites. As a result, the crystallization process in the PA6/GP nanocomposite may be less efficient or delayed compared to the PA6/GN nanocomposite, where the smaller-sized graphene nanoplatelets have a more favourable influence on nucleation and crystallization.

4. Conclusions

The current study focused on investigating the nucleation activity of GNP in a PA6 matrix through non-isothermal crystallization analysis. The experimental DSC data showed that the nanocomposites exhibited higher crystallization peak temperatures compared to pure PA6, suggesting that GNP acts as a nucleating agent for PA6.

The Dobreva and Gutzow method was effectively used to assess the nucleation activity, revealing the nucleating potential of the filler. Both types of GNP showed a nucleation activity of less than 1, indicating their role as surface active agents within the polymeric matrix, promoting the crystallization process. In particular, the influence of GNP was more pronounced in PA6/GN compared to PA6/GP. This enhanced nucleation activity can be attributed to the smaller particle size of the GNP structure.

These results have significant practical implications for the technological application of PA6 nanocomposite materials. The GNP-based PA6 nanocomposites have the potential to be used as lightweight materials in the automotive industry, meeting the demand for superior thermal and mechanical performance.

Acknowledgments

The authors would like to acknowledge to Simoldes Group for partially funding this research. This is a project in collaboration with Simoldes Plásticos, S.A. This work was also developed within the scope of the project CICECO-Aveiro Institute of Materials, UIDB/50011/2020 & UIDP/50011/2020 & LA/P/0006/2020, financed by national funds through the FCT/MEC (PIDDAC).

References

1. Zhang, M., Li, Y., Su, Z. & Wei, G. Recent advances in the synthesis and applications of graphene–polymer nanocomposites. *Polymer Chemistry* **6**, 6107–6124 (2015).
2. O'Neill, A., Bakirtzis, D. & Dixon, D. Polyamide 6/Graphene composites: The effect of in situ polymerisation on the structure and properties of graphene oxide and reduced graphene oxide. *European Polymer Journal* **59**, 353–362 (2014).
3. Xiang, M., Li, C. & Ye, L. In situ synthesis of monomer casting nylon-6 / reduced graphene oxide nanocomposites : Intercalation structure and electrically conductive properties. *Journal of Industrial and Engineering Chemistry* **50**, 123–132 (2017).
4. Miranda Campos, B., Bourbigot, S., Fontaine, G. & Bonnet, F. Thermoplastic matrix-based composites produced by resin transfer molding: A review. *Polym Compos* **43**, 2485–2506 (2022).
5. Ageyeva, T., Sibikin, I. & Karger-Kocsis, J. Polymers and related composites via anionic ring-opening polymerization of lactams: Recent developments and future trends. *Polymers (Basel)* **10**, 357 (2018).
6. Semperger, O. V. & Suplicz, A. The Effect of the Parameters of T-RTM on the Properties of Polyamide 6 Prepared by in Situ Polymerization. *Materials* **13**, 4 (2020).
7. Murray, J., Gleich, K., McCarthy, E. & Bradaigh, C. O. Properties of polyamide-6 composites using a low-cost thermoplastic resin transfer moulding system. in *22nd International Conference on Composite Materials (ICCM 2019)* 2013–2022 (RMIT University, 2019).

8. Murray, J. J. *et al.* Thermoplastic RTM: Impact Properties of Anionically Polymerised Polyamide 6 Composites for Structural Automotive Parts. *Energies (Basel)* **14**, 5790 (2021).
9. Boros, R., Sibikin, I., Ageyeva, T. & Kovács, J. G. Development and Validation of a Test Mold for Thermoplastic Resin Transfer Molding of Reactive PA-6. *Polymers (Basel)* **12**, 976 (2020).
10. Zaldua, N. *et al.* Nucleation and crystallization of PA6 composites prepared by T-RTM: Effects of carbon and glass fiber loading. *Polymers (Basel)* **11**, 1680 (2019).
11. Murray, J. J., Robert, C., Gleich, K., McCarthy, E. D. & Brádaigh, C. M. Ó. Manufacturing of unidirectional stitched glass fabric reinforced polyamide 6 by thermoplastic resin transfer moulding. *Mater Des* **189**, 108512 (2020).
12. Myalski, J., Godzierz, M. & Olesik, P. Effect of carbon fillers on the wear resistance of pa6 thermoplastic composites. *Polymers* **12**, 2264 (2020).
13. Rao, C. emsp14N emsp14R, Sood, A. emsp14K, Subrahmanyam, K. emsp14S & Govindaraj, A. Graphene: the new two-dimensional nanomaterial. *Angewandte Chemie International Edition* **48**, 7752–7777 (2009).
14. Papageorgiou, D. G., Kinloch, I. A. & Young, R. J. Mechanical properties of graphene and graphene-based nanocomposites. *Progress in Materials Science* **90**, 75–127 (2017).
15. Phiri, J., Gane, P. & Maloney, T. C. General overview of graphene: Production, properties and application in polymer composites. *Materials Science and Engineering: B* **215**, 9–28 (2017).
16. Galpaya, D. *et al.* Recent advances in fabrication and characterization of graphene-polymer nanocomposites. *Graphene* **1**, 30–49 (2012).
17. Jiménez-Suárez, A. & Prolongo, S. G. Graphene nanoplatelets. *Applied Sciences* vol. 10 1753 Preprint at (2020).
18. Elmarakbi, A., El-Safty, S., Martorana, B. & Azoti, W. Nanocomposites for Automotive: Enhanced Graphene-based Polyer Materials and Multi-Scale Approach. *International Journal of Automotive Composites* **2**, 155–166 (2017).
19. Elmarakbi, A. & Azoti, W. State of the art on graphene lightweighting nanocomposites for automotive applications. *Experimental Characterization, Predictive Mechanical and Thermal Modeling of Nanostructures and their Polymer Composites* 1–23 (2018).
20. Shi, J., Yang, X., Wang, X. & Lu, L. Non-isothermal crystallization kinetics of nylon 6 / attapulgite nanocomposites. *Polymer Testing* **29**, 596–602 (2010).
21. Liu, B., Hu, G., Zhang, J. & Wang, Z. The non-isothermal crystallization behavior of polyamide 6 and polyamide 6/HDPE/MAH/L-101 composites. *Journal of Polymer Engineering* **39**, 124–133 (2019).
22. Wu, B., Gong, Y. & Yang, G. Non-isothermal crystallization of polyamide 6 matrix in all-polyamide composites: Crystallization kinetic, melting behavior, and crystal morphology. *Journal of Materials Science* **46**, 5184–5191 (2011).
23. Liu, Y. & Yang, G. Non-isothermal crystallization kinetics of polyamide-6/graphite oxide nanocomposites. *Thermochimica Acta* **500**, 13–20 (2010).
24. Zhang, F., Peng, X., Yan, W., Peng, Z. & Shen, Y. Nonisothermal crystallization kinetics of in situ nylon 6/graphene composites by differential scanning calorimetry. *Journal of Polymer Science Part B: Polymer Physics* **49**, 1381–1388 (2011).
25. Dobreva, A. & Gutzow, I. Activity of substrates in the catalyzed nucleation of glass-forming melts. I. Theory. *Journal of non-crystalline solids* **162**, 1–12 (1993).
26. Dobreva, A. & Gutzow, I. Activity of substrates in the catalyzed nucleation of glass-forming melts. II. Experimental evidence. *Journal of non-crystalline solids* **162**, 13–25 (1993).
27. Lagarinhos, J., Santos, L. & Oliveira, J. Effect of Catalyst and Activator on Properties of Polyamide 6 Prepared by Thermoplastic Resin Transfer Molding Technology. *J Mater Eng Perform* **31**, 7098–7103 (2022).
28. Lagarinhos, J. N. & Oliveira, J. M. The effect of graphene-based materials in polyamide 6 obtained by in situ thermoplastic resin transfer moulding (T-RTM) polymerization. in *ECCM20 - Proceeding 20th European Conference on Composite Materials;* 3, 152–159 (2022).

29. Aziz, M. S. A., Saad, G. R. & Naguib, H. F. Non-isothermal crystallization kinetics of poly (3-hydroxybutyrate) in copoly (ester-urethane) nanocomposites based on poly (3-hydroxybutyrate) and cloisite 30B. *Thermochimica Acta* **605**, 52–62 (2015).
30. Korkees, F., Aldrees, A., Barsoum, I. & Alshammari, D. Functionalised graphene effect on the mechanical and thermal properties of recycled PA6/PA6, 6 blends. *Journal of Composite Materials* **55**, 2211–2224 (2021).

4.5 Non-isothermal crystallization kinetics of polyamide 6/graphene nanoplatelets nanocomposites obtained via *in situ* polymerization: effect of nanofiller size

Joana Lagarinhos, Sara Magalhães da Silva, Martinho Oliveira

Polymers, 2023, 15(20)

(DOI: https://doi.org/10.3390/polym15204109)

Abstract

Thermoplastic resin transfer moulding (T-RTM) technology was applied to synthesize graphene nanoplatelets-based nanocomposites via anionic ring-opening polymerization (AROP). Polyamide 6 was obtained by AROP and was used as the polymeric matrix of the developed nanocomposites. The non-isothermal crystallization behaviour of PA6 and nanocomposites was analysed by differential scanning calorimetry (DSC). Nanocomposites with 0.5 wt.% of graphene nanoplatelets (GNP) with two different diameter sizes were prepared. Results have shown that the crystallization temperature shifted to higher values in the presence of GNP. This behaviour is more noticeable for the nanocomposite prepared with smaller GNP (PA6/GN). The crystallization kinetic behaviour of all samples was assessed by Avrami and Liu's models. It was observed that GNP increased the crystallization rate, thus revealing a nucleating ability, and also validated the reduction of half-time crystallization values. Such tendency was also supported by the lower activation energy values determined by Friedman's method.

Keywords

Polyamide 6 (PA6); anionic ring-opening polymerization (AROP); thermoplastic resin transfer moulding (T-RTM); graphene nanoplatelets (GNP); nanocomposites; non-isothermal crystallization kinetics

Contributions:

The author had contributed to the design and execution of all DSC, SEM and POM analyses presented here, as well as to the discussion, interpretation, and drafting of the manuscript. Sara Magalhães da Silva and Martinho Oliveira contributed to the conceptualization, review and editing of the data presented.

1. Introduction

Polyamide 6 (PA6) is a thermoplastic material of particular interest in automotive applications, mainly in semi-structural parts, due to its excellent impact resistance, good strength properties and high resistance to most solvents and acids[1,2]. PA6 has emerged as an alternative to traditional automotive metal parts, capable of combining their unique mechanical properties with their lightness[3–5]. PA6 can be produced by hydrolytic polymerization, due to its industrial viability, controllability, and polymerization stability for large-scale operation. However, this polymerization involves various steps[1,6]. On the other hand, an anionic polymerization involves an activated monomer mechanism, where PA6 is obtained from the corresponding lactams[7,8]. The lactam polymerization can be an anionic reaction mechanism (initiated by a base) or a cationic reaction mechanism (initiated by an acid). However, cationic mechanisms are limited due to low conversions and the low molar masses of the final products[8,9].

The anionic ring-opening polymerization (AROP) of ε-caprolactam (CL) into PA6 is among one of the most developed forms of reactive processing of thermoplastics. It is based on a polymerization mechanism in which the ring-shaped (cyclic) molecules are opened, giving rise to linear monomers or oligomers[8,9]. AROP is the fastest process for PA6 production; it is characterized by short polymerization times, resulting in a faster cycle time, and, consequently, a more efficient production (compared to thermosets). In addition to the monomer, a catalyst, and an activator are needed to initiate and maintain the reaction[10]. This type of polymerization has emerged as a clean alternative to polymerization routes once it does not require hazardous solvents[1,11].

Thermoplastic resin transfer moulding (T-RTM) is a technology able to produce a thermoplastic material by combining a precursor with low viscosity, a catalyst, and an activator[12–14]. The reactive mixture is injected into a mold and polymerizes inside it (*in situ*). Ensuring appropriate processing conditions for polymerization *in situ*, namely, adequate temperature, polymerization time, and inert atmosphere, is necessary[3]. PA6 can be synthesized by AROP using the T-RTM technology, due to the characteristic low viscosity of ε-caprolactam combined with a fast polymerization rate[7–9]. PA6 synthesized by AROP was found to produce high molecular weights, which results in tougher materials that are adequate for industrial applications[15]. A superior mechanical performance was also observed, such as impact resistance, abrasion resistance, and strength properties, which were above those normally found in melt-processed PA6[3,13].

The diffusion of thermoplastics has aroused high interest in the development of composite materials. Thermoplastics reveal high impact resistance, short processing time, and recyclability[4,16,17]. Recently, for structural applications, several reinforcing fabrics, such as carbon[3,18] and glass fibers[19], aramid[20], attapulgite[21,22] or carbon nanotubes (CNTs)[23,24], are being used to reinforce thermoplastic composites. The incorporation of a reinforcement phase into a polymeric matrix to create a composite material results in significant improvements over unfilled polymers[25,26]. These improvements include enhanced mechanical properties, increased thermal stability, and improved electrical properties, all of which can be achieved with relatively low filler content[27,28]. In

the case of using PA6 as the polymeric matrix, the low viscosity of PA6 precursors enabled the reactive processing of thermoplastic composites by T-RTM. This has opened the door for new applications and materials development where thermosets have traditionally been used[29,30]. An example of such development is the study of graphene nanoplatelets (GNP) as a cost-effective filler in PA6-based nanocomposites[31,32]. GNP exhibit improved mechanical and thermal properties such as high Young's modulus, high fracture strength and thermal conductivity[33–35]. Due to their promising properties, GNP-based nanocomposites have been used in a wide range of applications, including automotives, electronics, packaging, aerospace, military, buildings, and construction[27,36,37]. GNP offer an appealing prospect due to their unique properties and the abundance of their precursor, graphite. In addition, the straightforward and cost-effective physicochemical methods employed in the production of GNP can further contribute to their viability[34,38].

Several studies have shown that the addition of nanofillers can influence properties, such as toughness, and impact performance, thermal stability, and electrical and thermal conductivity[39]. The study of crystallization behaviour is, therefore, an important tool for optimizing processing conditions, contributing to shorter industrial cycles, and reducing manufacturing costs. This trend was observed by Fu, X. *et al.*[40], who have studied the effect of multilayer graphene (MG) content of 0.01–0.5 wt.% on PA6. According to the authors, the addition of MG affected the crystallinity degree, which varied within a small range between 32.8 and 34.8%. This result was higher than that of the PA6 matrix (31.8%), indicating that MG can promote crystallization by acting as a nucleating agent. In addition, the crystallization peaks of composites become narrower compared to PA6, which means that MG loading can also increase the crystallization rate of PA6-based nanocomposites. Yang Chen and co-workers[41], prepared exfoliated graphite-filled PA6 composites and evaluated the influence of graphite (0–20 wt.%) on the thermal properties of the composites. The authors showed that all PA6/graphite composites had higher crystallization rates (varying from 2.97–5.08 min) than pure PA6 (6.28 min). However, the addition of 20 wt.% graphite slowed down the crystallization rate, as MG could induce a physical barrier and reduce the mobility of polymer chains. This behavior indicated the nucleating ability of graphite, which provided nucleation sites and facilitated the crystallization process when small amounts of graphite are used, while higher concentrations of graphite may hinder the growth of crystallites. Nevertheless, none of these studies are related to the study of non-isothermal crystallization behavior and kinetics of PA6-based nanocomposites prepared by T-RTM via AROP.

This work aims to investigate the effect of GNP, with different diameters, on the crystallization behavior of PA6 under non-isothermal conditions prepared by T-RTM technology. The crystallization was conducted at non-isothermal conditions to simulate the T-RTM process. It will provide significant information about the polymerization mechanisms and kinetics of PA6/GNP to guarantee parts with dimensional accuracy and reduced defects, such as warping[15,42,43]. Kinetic studies using Avrami[44,45] and Liu[46] models were carried out to evaluate the influence of GNP in the crystallization kinetics of PA6. The crystallization activation energy (E_c) was calculated using Friedman's methodology[47]. In addition, the morphology of GNP was observed by scanning electron microscopy (SEM) and the

dispersion and distribution of the GNP into PA6 was evaluated by polarized optical microscopy (POM).

2. Experimental

2.1. Materials

PA6 was prepared by T-RTM technology using the following materials: (1) monomer: ε-caprolactam (CL), AP-Nylon®; (2) catalyst: Bruggolen® C10; and (3) activator: Bruggolen® C20P. All chemical components were purchased from L. Brüggemann GmbH and Co. KG, Germany. The GNP fillers were supplied by NanoXplore (Canada), and two different sizes were considered, namely D90 < 50 μm (defined as GN) and D90 <70 μm (defined as GP). The bulk density of all GNP fillers is reported to be 0.2-0.3 $g \cdot cm^{-3}$ (data from technical datasheets).

2.2. PA6 and PA6/GNP nanocomposites preparation

PA6 was prepared using the same compositions and T-RTM laboratory system as described in a previous study[48].The nitrogen pressure (3 bar) and vacuum conditions (150 mbar) were carefully adjusted to reduce the existence of voids and to ensure the integrity of the manufactured parts. PA6/GNP nanocomposites were prepared by pre-dispersing 0.5 wt.% GN (PA6/GN) and GP (PA6/GP) in molten CL using a Hielscher ultrasonic device UP 200 S (200 watts, frequency 24 kHz) to achieve better dispersion of GNP in the PA6 matrix. The sonication time was set to 20 min for GN and 25 min for GP. Then, the catalyst and activator were added, and the polymerization process proceeded as previously described[48]. The selection of 0.5 wt.% as GNP concentration was previously investigated, where the influence of different concentrations of GNP on the final properties of the PA6 matrix were evaluated[49].

2.3. Thermal analyses

The thermal properties and the non-isothermal crystallization behavior and kinetics of PA6 and PA6/GNP were studied by differential scanning calorimetry (DSC). A Shimadzu DSC-60 equipment under air atmosphere was used. The thermal history of the samples was erased by heating from room temperature to 250 °C at 20 $°C \cdot min^{-1}$ and remaining at this temperature for 2 minutes. Non-isothermal crystallization behavior was investigated by cooling the samples from 250 °C to -20 °C at various cooling rates of 5, 10, 15 and 20 $°C \cdot min^{-1}$. This cycle was duplicated, and only the second run was used to evaluate the crystallization behavior. Crystallization temperature (T_c), crystallization enthalpy (ΔH_c) and melting temperature (T_m) were determined from the DSC thermograms. At least three measurements were made for each testing condition.

2.4. Morphological analyses

Morphological analyses were conducted to analyze the microstructure of GNP. An SEM Hitachi S4100 was used with an acceleration voltage of 15 kV. The GNP were assembled on a conducting carbon tape, and then the samples were sputter coated with AU/Pd for 3 min to enhance the image resolution and to prevent electrostatic charging. To evaluate the distribution of GNP into the PA6 matrix, a Nikon Eclipse L150 microscope equipped with a digital camera (Canon 100D) was used. The analyzed samples were obtained from the longitudinal section of the specimens. Both samples were melted between two glass slides at 230 °C for 5 min to obtain thin films and were kept at this temperature for 10 min.

3. Results and discussion

3.1. GNP and nanocomposites morphology

Figure 4.5.1 (a-b) shows the morphologies of the GNP used, under identical magnification for accurate comparison of the GNP size. Both GNP consist of platelet-shaped graphene layers stacked and folded together, with irregular morphology and opaque structure. The images also show that the diameter of each of the GNP corresponds to the average diameter reported by the manufacturer.

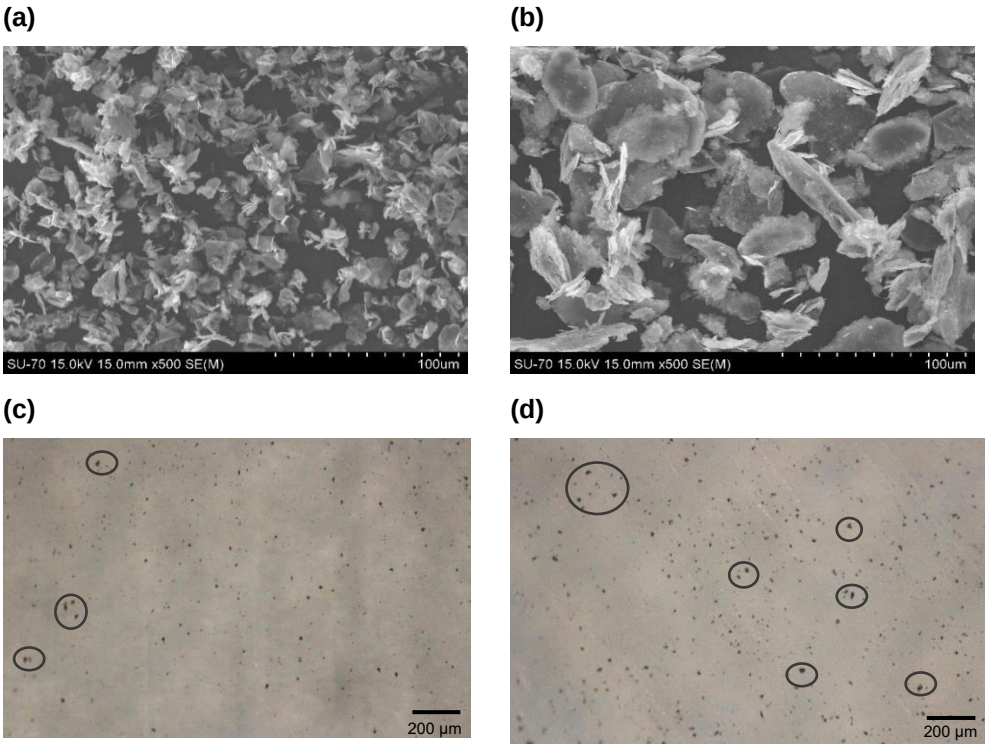

Figure 4.5.1. SEM images of **(a)** GN and **(b)** GP and optical micrographs of **(c)** PA6/GN and **(d)** PA6/GP nanocomposites (black circles highlight GNP agglomerates).

According to the technical data sheet of the GNP, functional groups such as carboxyl or hydroxyl groups are present at the edges of the nanoplatelets, which facilitates the distribution of GNP in the PA6 matrix. Optical micrographs of PA6/GNP after 10 min at 230 °C in a hot plate are shown in

Figure 4.5.1 (c-d). Each type of GNP was dispersed in the PA6 matrix, and it is possible to perceive the differences between the diameters of the two GNP used in this work. A good dispersion was observed for both nanocomposites, although some agglomerates can be noticed in Figure 4.5.1 (d) due to the larger size of GP. The nanocomposite PA6/GN shows better dispersion and less agglomeration of nanoplatelets than PA6/GP. Based on this observation, it can be assumed that a larger GNP diameter makes the dispersion difficult and promotes the formation of aggregates. Thus, GNP particle size can influence the mechanical properties, as reported previously[49], and the thermal properties of nanocomposites[50].

3.2. Non-isothermal crystallization behavior of PA6 and PA6/GNP nanocomposites

DSC measurements were conducted to investigate the effect of each GNP type on the non-isothermal crystallization behavior of the prepared nanocomposites. The exothermic curves of PA6, PA6/GN and PA6/GP at different cooling rates are shown in Figure 4.5.2. The resulting thermal parameters are listed in Table 4.5.1.

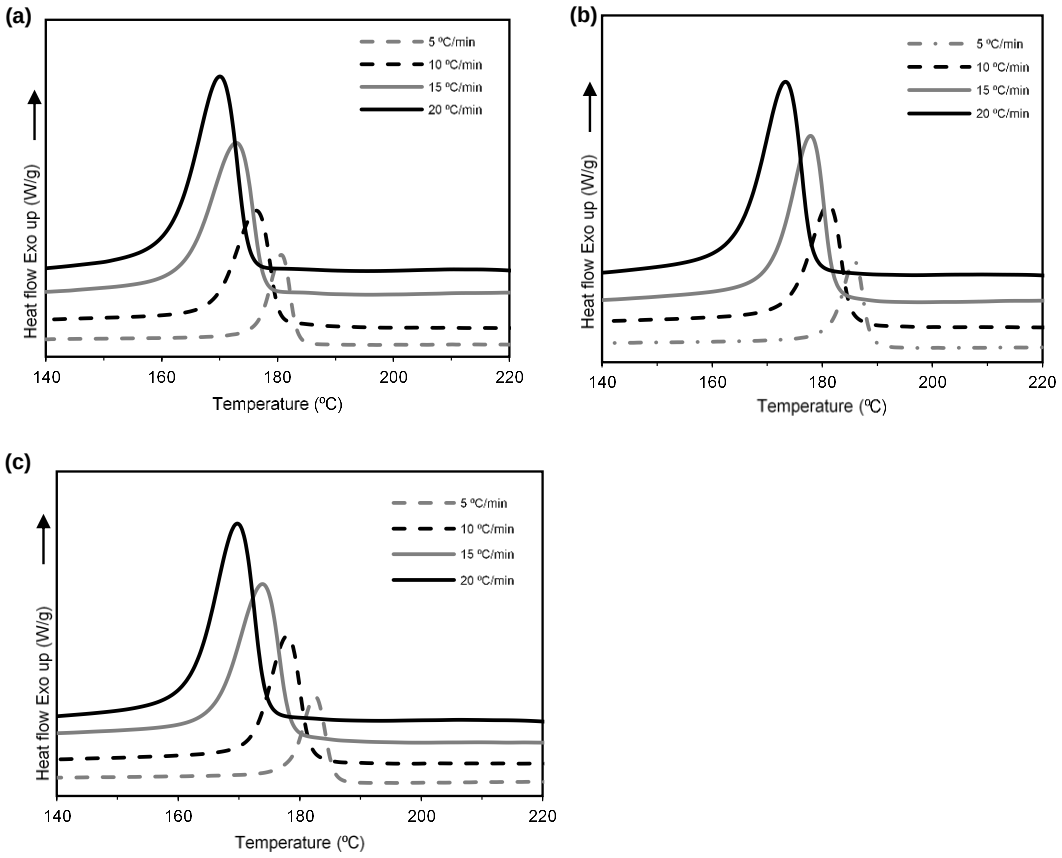

Figure 4.5.2. DSC curves at different cooling rates for **(a)** PA6, **(b)** PA6/GN and **(c)** PA6/GP.

Table 4.5.1. Non-isothermal crystallization parameters of PA6 and its nanocomposites.

Sample	φ (°C·min^{-1})	T_m (°C)	T_c (°C)	X_c (%)
PA6	5	218.9 ± 0.1	180.7 ± 0.4	38.6 ± 4.1
	10	219.1 ± 0.2	175.4 ± 0.3	39.4 ± 3.0
	15	218.9 ± 0.1	170.9 ± 0.7	40.8 ± 3.9
	20	218.8 ± 0.3	166.3 ± 0.5	41.6 ± 2.3
PA6/GN	5	219.1 ± 0.0	185.8 ± 0.6	39.6 ± 3.8
	10	219.2 ± 0.1	180.1 ± 0.4	40.9 ± 3.5
	15	219.0 ± 0.1	177.9 ± 0.4	41.5 ± 2.7
	20	218.9 ± 0.2	172.3 ± 0.3	42.4 ± 1.8
PA6/GP	5	218.8 ± 0.3	182.2 ± 0.8	39.0 ± 3.1
	10	218.8 ± 0.5	177.4 ± 0.7	40.6 ± 4.3
	15	218.6 ± 0.2	173.8 ± 0.7	41.3 ± 4.1
	20	218.1 ± 0.4	168.7 ± 0.9	41.9 ± 3.2

As can be seen from Table 4.5.1, the T_m of PA6 and its nanocomposites were unaffected by the selected cooling rate of samples. The cooling curves (Figure 4.5.2) show that the lowest cooling rates, 5 and 10 °C·min^{-1}, induce a rather narrow T_c, whereas the highest cooling rates, 15 and 20 °C·min^{-1}, induce broad crystallization curves. As expected, as the cooling rate increases, the curves, and thus the peak temperatures, shift towards lower temperatures where there is insufficient time to activate the nuclei at higher temperatures. PA6 and its nanocomposites showed a significant decrease in T_c of about 14 °C and 13 °C, respectively. The T_c values, for a given cooling rate, were higher for nanocomposites than for PA6. This behaviour can indicate that PA6 crystallized earlier in the presence of GNP, revealing a nucleation effect of GNP on the polymeric matrix[51]. In particular, PA6/GN nanocomposites, with smaller GNP, showed higher T_c values than PA6/GP. It can be assumed that lower surface area induces fewer interactions between GNP and PA6, which difficult the regular packing of PA6 polymer chains[52].

The X_c was assessed to better understand the effect of GNP on PA6 crystal formation. This parameter was calculated according to equation (1):

$$Xc\ (\%) = \frac{\Delta H_c}{(1-\alpha)\Delta H_m^0} \times 100 \quad (1)$$

,where ΔH_c was obtained by integrating the crystallization peak, ΔH_m^0 corresponds to the 100% crystalline form of PA6 (which is assumed to be 190 J·g^{-1}) [53] and α is the filler mass fraction. It was observed that the addition of GNP did not significantly affect the X_c values. The same behavior was

also previously reported[54–56]. Theoretically, the addition of GNP to PA6 can have two significant effects: heterogeneous nucleation, where GNP provide sites for polymer molecules to form crystalline structures; and, physical hindrance, where GNP can obstruct the movement of polymer molecules[57]. As a result, the process of crystal growth can be slowed down. In the literature, studies have reported that carbon-based fillers can reduce X_c[58,59], but it has also been found in other studies that an increase in X_c was detected[60–62]. In this case, the addition of GNP showed no significant changes in X_c. The 2D structure of GNP with a small thickness and high aspect ratio, could be a critical reason for its inhibitory effect. This structural uniqueness can interfere with the molecular movement and crystalline growth of the PA6 matrix in an irregular manner.

From the DSC thermograms, the evolution of the relative crystallinity degree (X_t), at a certain time (*t*) can be determined by equation (2):

$$X_t = \frac{\int_{T_0}^{T} \left(\frac{dH_c}{dT}\right) dT}{\int_{T_0}^{T_\infty} \left(\frac{dH_c}{dT}\right) dT} \quad (2)$$

, where T_0 and T_∞ are the temperatures at which crystallization begins and ends, respectively. In non-isothermal crystallization, the temperature (T) can be converted to the crystallization time[63], *t*, using the following equation:

$$t = \frac{T_0 - T}{\varphi} \quad (3)$$

, where T is the temperature at crystallization time and φ corresponds to the cooling rate. Thus, from equation (3), it is possible to convert $X_t = f(T)$ curves from non-isothermal DSC crystallization data into $X_t = f(t)$ curves. Figure 4.5.3 displays the X_t vs. *t* curves for all samples. All curves exhibited a sigmoidal shape with two non-linear parts. The early stage (first non-linear part) corresponds to fast primary crystallization attributed to the formation of nuclei; while the later stage (the second non-linear part) is described by a slow secondary crystallization, ascribed to the spherulitic impingement of the crystallization. The crystallization process starts at higher temperatures for slower cooling rates (5 °C·min^{-1}), and it occurs for a longer time. Although the crystallization process begins at lower temperatures at higher cooling rates (20 °C·min^{-1}), the duration is shorter. From these plots, the strong dependence of nucleation and growth processes on the cooling rate can be seen. When the cooling rate increases, the curves shift to the left position, indicating a faster crystallization rate. Other studies also have reported a similar trend[64–66].

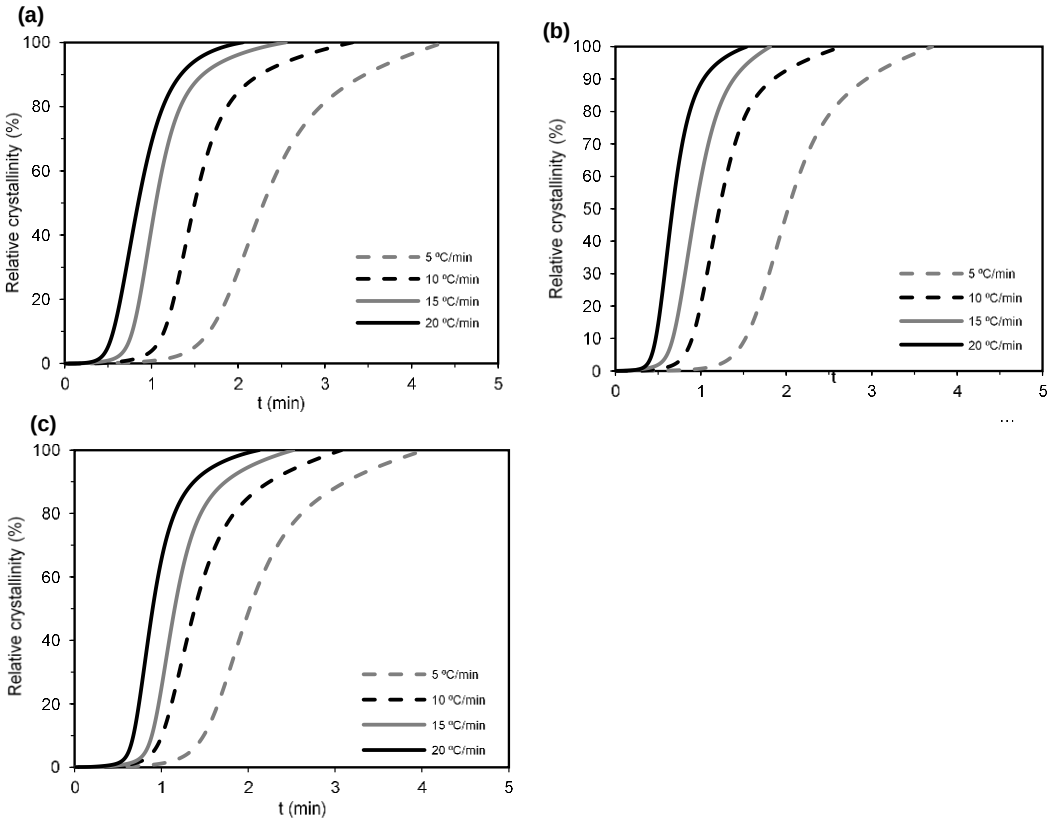

Figure 4.5.3. Curves of X_t vs t under different cooling rates for **(a)** PA6, **(b)** PA6/GN and **(c)** PA6/GP.

3.3. Non-isothermal crystallization kinetic behavior of PA6 and PA6/GNP nanocomposites

3.3.1. Avrami model

Avrami[44]equation has been commonly applied to analyze the non-isothermal kinetics of the nucleation and growth phases of polymers at a fixed crystallization temperature:

$$X_t = 1 - \exp(-Z_t t^n) \quad (4)$$

where Z_t is the growth rate constant that includes both nucleation and growth rate, *n* is the Avrami exponent, that depends on the shape of the crystalline units and on the nucleation process. It should be noted that these parameters affect the rates of both nucleation and spherulite growth caused by their temperature dependence. The linearized form of equation (4) can be written as follows:

$$\log[-\ln(1 - X_t)] = \ln(Zt) + n\ln(t) \quad (5)$$

Figure 4.5.4 shows the curves of $\log[-\ln(1 - X_t)]$ *vs* log (t) for PA6, PA6/GN and PA6/GP at different cooling rates. The Avrami exponent *n* and the parameter rate Z_t can be calculated, from

the slope and the interception of the lines, respectively. Avrami approach can reveal several fundamental aspects related to the crystallization mechanisms but is not able to properly describe the non-isothermal crystallization of the process, as a constant cooling rate can affect the parameters. Jeziorny *et al*.[67] adapted the adjustments to Avrami model, by replacing the rate parameter Z_t with Z_c to describe the non-isothermal kinetics:

$$\ln Z_c = \frac{\ln(Z_t)}{\varphi} \tag{6}$$

This correction is widely used to adjust Avrami' s theory to non-isothermal conditions. Avrami plots and kinetic parameters are show in Figure 4.5.4 and Table 4.5.2 respectively. X_t values between 10 and 80% were considered.

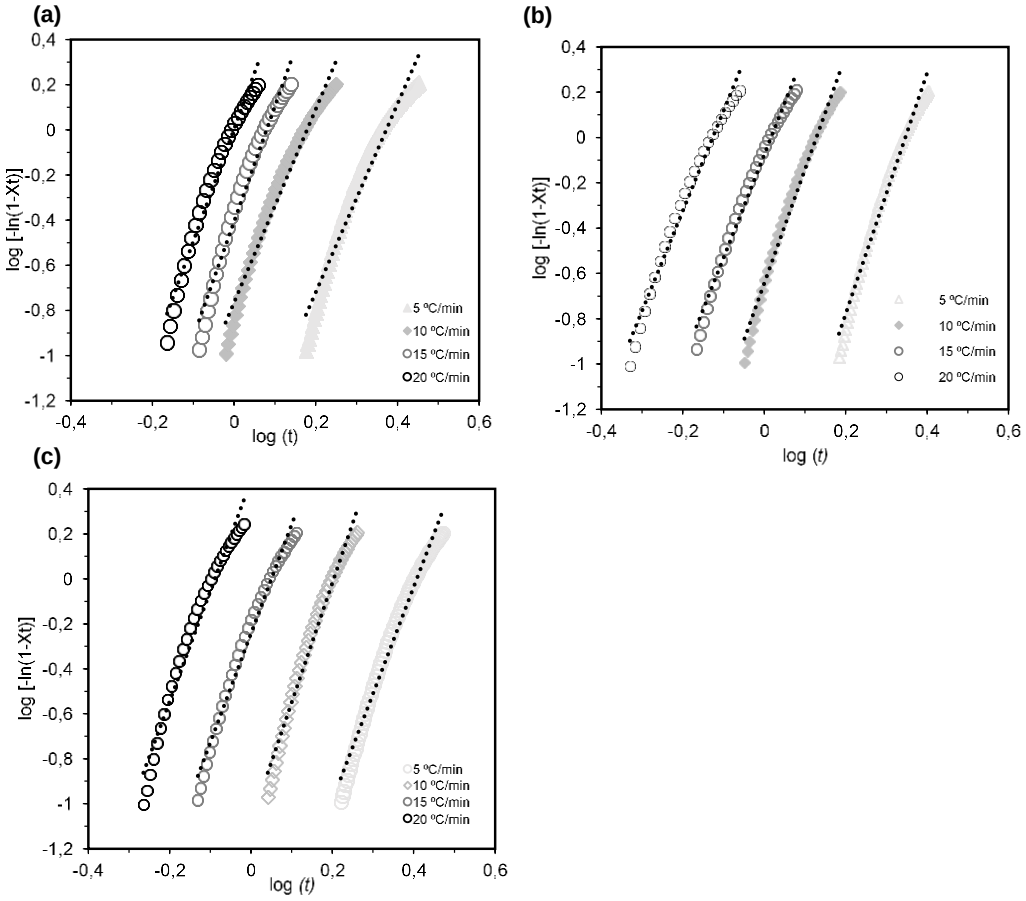

Figure 4.5.4. Avrami plots for **(a)** PA6, **(b)** PA6/GN and **(c)** PA6/GP.

The data presented in Table 4.5.2 showed that the presence of GNP did not affect the crystallization kinetics of PA6. The variation of Avrami parameter *n* with cooling rate revealed the presence of mixed nucleation and growth mechanisms. A crystallization process with *n* varying from 1 and 2 follows a one-dimensional crystal growth, and a value between 2 and 3 is a two-dimensional

growth. When the n value is between 3 and 4, the crystallization follows a three-dimensional (3D) growth and for a *n* value higher than 4, a complex multi-dimensional crystallization process is developed[68]. *n* values higher than 3 can be associated with developing a 3D growth crystallization process, implying that different growth mechanisms may occur simultaneously during the crystallization process[21]. Similar studies have reported an analogous behavior[66,69,70]. Comparing overall values of PA6 and PA6/GNP, it can be observed that marginal changes were noted at 0.5 wt.% GNP incorporation. Melo *et al*.[64] also observed a similar behavior when using the same amount of graphene oxide (GO) concentration. The authors observed that no significant changes in the nucleation rate were observed for 0.1 and 0.5 wt.% nanocomposites. However, when incorporating 1 and 5 wt.% GO, higher n values were observed with increasing cooling rates. This behavior suggests a change in the nucleation mechanism of the sample at higher nanofiller concentrations. On the other hand, increased amounts of GO, also caused an increase in Z_c values and an increase in $t_{1/2}$, indicating a slower crystallization rate for the nanocomposites due to the reduced mobility of the polymer chains in the presence of GO sheets.

Table 4.5.2. Half-time crystallization and Avrami kinetic parameters.

Sample	φ	$t_{1/2}$	Avrami		
	(°C·min^{-1})	(min)	*n*	Z_c (min^{-1})	R^2
PA6	5	2.33	4.92	0.68	0.98
	10	1.48	5.32	0.89	0.98
	15	1.04	4.84	0.98	0.98
	20	0.84	4.73	0.99	0.99
PA6/GN	5	2.01	4.66	0.82	0.98
	10	1.20	4.71	0.92	0.97
	15	0.95	4.52	1.01	0.97
	20	0.67	4.37	1.02	0.97
PA6/GP	5	2.04	4.28	0.73	0.98
	10	1.38	4.09	0.90	0.98
	15	1.14	3.97	0.97	0.99
	20	0.86	3.81	1.00	0.99

The time to reach 50% of X_t is defined as the half-time crystallization ($t_{1/2}$). This parameter is also an indicator of the crystallization rate and can be determined by equation (7):

$$t_{1/2} = \left(\frac{\ln 2}{Z_c}\right)^{1/n} \quad (7)$$

The $t_{1/2}$ values are also given in Table 4.5.2. It can be seen that the addition of GNP leads to a decrease in the $t_{1/2}$ values, indicating that the addition of GNP accelerated the crystallization rate. This can be an indication of the heterogeneous nucleation ability of GNP[71]. In the case of nanocomposites, PA6/GN achieved lower $t_{1/2}$ than PA6/GP. This can be due to the smaller diameter of GN, which provided more nuclei, thus promoting crystallization.

3.3.2. Liu model

The Liu[46] model was also applied to adjust the non-isothermal kinetic behavior of PA6 and nanocomposites. It was developed as an alternative method by combining the Avrami and Ozawa equations. From that, a new kinetic equation was obtained:

$$\log K(T) - m\log(\varphi) = \log Z_t + n\log(t) \quad (8)$$

Simplifying this equation:

$$\log(\varphi) = \log[F(T)] - b\log(t) \quad (9)$$

, where F(T) refers to the cooling rate required to reach X_t in a specific *t*, and *b* is the ratio between the exponents of Avrami (*n*) and Ozawa (*m*). According to equation (9), the kinetic parameters F(T) and the b values, can be determined from the intercept and the slope of the lines by plotting *log φ* against *log t*, respectively. Figure 4.5.5 shows the Liu curves for PA6 and PA6/GNP nanocomposites and in Table 4.5.3 is also presented Liu kinetic parameters.

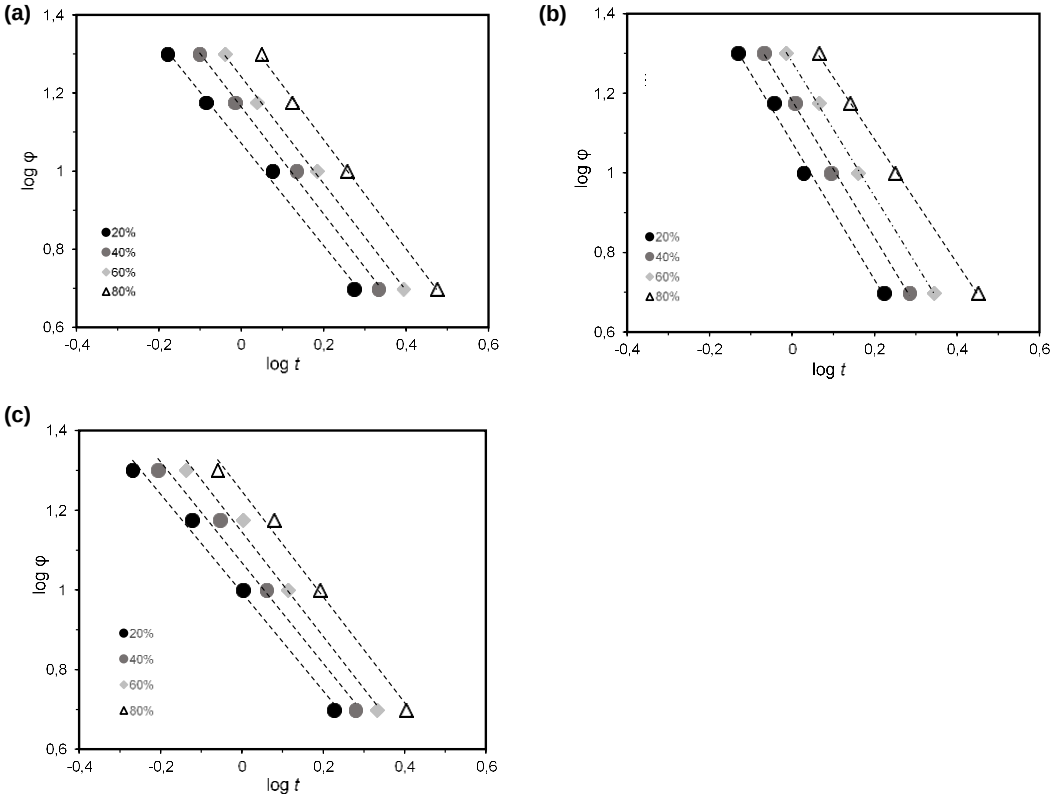

Figure 4.5.5. Liu plots for **(a)** PA6, **(b)** PA6/GN and **(c)** PA6/GP.

Parallel straight lines and linearity were attained for different X_t, indicating that Liu analysis can successfully describe PA6 and PA6/GNP kinetic behavior. For a given sample, F(T) increased with increasing X_t. Since F(T) is described as a cooling rate value, a decrease in F(T) indicates that a higher crystallization rate is required to reach a given crystallinity degree at a set time[72]. Comparing the F(T) values of PA6 with those of PA6/GNP samples, the nanocomposites presented lower values than the pure matrix. The presence of GNP increases the crystallization rate of the polymer and accelerates the process, implying that the GNP facilitate the crystallization process, also demonstrating their nucleation ability[73]. Furthermore, when comparing PA6/GN with PA6/GP, it can be seen that for PA6/GP, F(T) values are higher due to the filler diameter size. At larger sizes, the interparticle distance decreases and GNP are unable to disperse into the PA6 matrix, due to the resulting aggregation from weak intermolecular forces between them[72]. The kinetic parameter *b* is almost constant for each material at different X_t values, ranging from 1.31 and 1.59. These values imply that significant secondary crystal growth accompanies the primary crystallization during non-isothermal crystallization. The nucleation mechanism and crystal growth geometries are similar, indicating that the method used could describe the non-isothermal crystallization process of PA6 and its nanocomposites[74]. The results obtained from this model are in accordance with the DSC analysis, described in section 3.2 and $t_{1/2}$ parameter, described in the previous section.

Table 4.5.3. Liu kinetic parameters.

Sample	φ (°C·min^{-1})	Liu			
		Xt (%)	*b*	F(T)	R^2
PA6	5	20	1.31 ± 0.03	11.80 ± 0.11	0.99
	10	40	1.37 ± 0.01	14.58 ± 0.09	1.00
	15	60	1.37 ± 0.02	17.43 ± 0.14	1.00
	20	80	1.40 ± 0.03	22.93 ± 0.12	1.00
PA6/GN	5	20	1.43 ± 0.02	10.93 ± 0.16	0.99
	10	40	1.42 ± 0.02	13.18 ± 0.11	1.00
	15	60	1.46 ± 0.03	16.98 ± 0.17	1.00
	20	80	1.49 ± 0.01	21.91 ± 0.10	1.00
PA6/GP	5	20	1.47 ± 0.03	11.47 ± 0.21	0.99
	10	40	1.49 ± 0.02	14.01 ± 0.11	0.99
	15	60	1.31 ± 0.03	11.80 ± 0.11	0.99
	20	80	1.37 ± 0.01	14.58 ± 0.09	1.00

3.3.3. Friedman model

Friedman[47] and Vyazovkin[75] developed an isoconversional method to calculate the E_c of the non-isothermal crystallization process. This method can be used to evaluate the dependence of E_c on crystallinity and temperature. From equation (10), different activation energies can be calculated for each X_t:

$$ln\left(\frac{dX}{dt}\right)_{X,i} = constant - \frac{E_c}{RT_{X,i}} \quad (10)$$

, where ln (dX/dt)$_x$ is the instantaneous crystallization rate as a function of time for a given value of X_t, R is the universal gas constant, *i* corresponds to each applied heating rate and T_x is the temperature for a given scanning rate *i*. Ec can be calculated from plotting ln(dX/dt)$_x$ versus $1/T_x$.

Figure 4.5.6 shows the effective activation energy at a given crystallinity degree, and a regression coefficient of 0.99 was obtained for all samples.

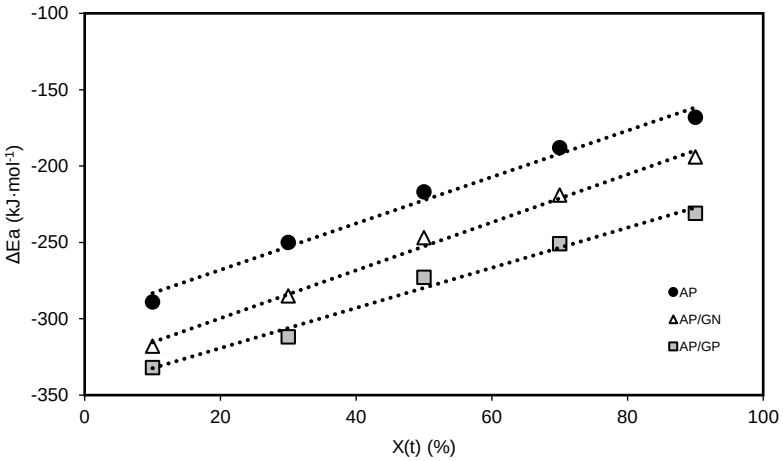

Figure 4.5.6. Friedman plots for PA6, PA6/GN and PA6/GP.

As X_t increased, the values of E_c also increased, which reflects the difficulty of PA6 to crystallize as the crystallization process occurs[76] Moreover, the E_c of PA6 decreased with the addition of GNP. This is indicative that GNP can act as nucleating agents to promote the initial stage of crystallization by inducing heterogeneous nucleation and, therefore, reducing the energy barrier. Comparing both nanocomposites, PA6/GN showed lower E_c than PA6/GP. These results are in accordance with those obtained previously for Avrami and Liu models. Similar results have been reported[65,77].

4. Conclusions

The use of T-RTM technology was found to be successful for the preparation of PA6 and PA6/GNP nanocomposites from AROP. The non-isothermal crystallization and kinetic behaviour of developed PA6 and its nanocomposites were investigated. GNP with two different sizes (GN and GP) were used. DSC trials were conducted at different cooling rates (5, 10, 15 and 20 °C·min^{-1}).

Results have shown that the incorporation of GNP affected the crystallization behaviour of PA6. Both GNP led to an increase of T_c, when compared to PA6, revealing the nucleation activity of the GNP. Avrami and Liu's models were selected to study the non-isothermal crystallization kinetics of all samples. Both models successfully described the behaviour of PA6 and PA6/GNP nanocomposites.

The addition of GNP increased the crystallization rate of PA6, and mixed growth mechanisms were observed ($n < 4$ and $b > 1$). Comparing both nanocomposites, the one prepared with GN (smaller diameter) exhibited a faster crystallization rate. These results were supported by Friedman's isoconversional method, where a lower E_c was obtained for PA6/GNP nanocomposites. Overall, these results indicated that all the kinetic models validated the nucleating effect of GNP. A lower energy is needed for crystallization to take place in the presence of GNP, which is more evidence for nanocomposites prepared with GN particles.

GNP size had a significant effect on the crystallization performance, and it is expected that this behaviour will affect the mechanical behaviour of the final parts. Further studies are needed to understand the influence of higher GNP concentrations on the crystallization behaviour of PA6.

Acknowledgements

The authors would like to acknowledge Simoldes Group for funding this research. This is a project in collaboration with Simoldes Plásticos, S.A. This work was developed within the scope of the project CICECO-Aveiro Institute of Materials, UIDB/50011/2020, UIDP/50011/2020 & LA/P/0006/2020, financed by national funds through the FCT/MEC (PIDDAC).

References

1. Ageyeva, T., Sibikin, I. & Karger-Kocsis, J. Polymers and related composites via anionic ring-opening polymerization of lactams: Recent developments and future trends. *Polymers (Basel)* **10**, 357 (2018).
2. Semperger, O. V. & Suplicz, A. The Effect of the Parameters of T-RTM on the Properties of Polyamide 6 Prepared by in Situ Polymerization. *Materials* **13**, 4 (2020).
3. Zaldua, N. *et al.* Nucleation and crystallization of PA6 composites prepared by T-RTM: Effects of carbon and glass fiber loading. *Polymers (Basel)* **11**, 1680 (2019).
4. Kim, B. J., Cha, S. H. & Park, Y. Bin. Ultra-high-speed processing of nanomaterial-reinforced woven carbon fiber/polyamide 6 composites using reactive thermoplastic resin transfer molding. *Compos B Eng* **143**, 36–46 (2018).
5. Ben, G. & Sakata, K. Fast fabrication method and evaluation of performance of hybrid FRTPs for applying them to automotive structural members. *Compos Struct* **133**, 1160–1167 (2015).
6. Rahman, M. A., Renna, L. A., Venkataraman, D., Desbois, P. & Lesser, A. J. High crystalline, porous polyamide 6 by anionic polymerization. *Polymer (Guildf)* **138**, 8–16 (2018).
7. Sebenda, J. Anionic ring-opening polymerization: lactams. *Pergamon Press plc, Comprehensive Polymer Science: the Synthesis, Characterization, Reactions & Applications of Polymers.* **3**, 511–530 (1989).
8. Sekiguchi, H., Ivin, K. J. & Saegusa, T. Ring-Opening Polymerization. *J., Saegusa, T., Eds.; Elsevier London UK* **2**, 809 (1984).
9. Roda, J. Polyamides. in *Handbook of Ring-Opening Polymerization* 165 (2009).
10. Kovács, Z., Pomázi, Á. & Toldy, A. The flame retardancy of polyamide 6—prepared by in situ polymerisation of ε-caprolactam—for T-RTM applications. *Polym Degrad Stab* 109797 (2021).
11. Barhoumi, N., Maazouz, A., Jaziri, M. & Abdelhedi, R. Polyamide from lactams by reactive rotational molding via anionic ring-opening polymerization : Optimization of processing parameters. *Express Polym Lett* **7**, 76–87 (2013).
12. Murray, J. J., Robert, C., Gleich, K., McCarthy, E. D. & Brádaigh, C. M. Ó. Manufacturing of unidirectional stitched glass fabric reinforced polyamide 6 by thermoplastic resin transfer moulding. *Mater Des* **189**, 108512 (2020).
13. Murray, J. J. *et al.* Thermoplastic RTM: Impact Properties of Anionically Polymerised Polyamide 6 Composites for Structural Automotive Parts. *Energies (Basel)* **14**, 5790 (2021).
14. Boros, R., Sibikin, I., Ageyeva, T. & Kovács, J. G. Development and Validation of a Test Mold for Thermoplastic Resin Transfer Molding of Reactive PA-6. *Polymers (Basel)* **12**, 976 (2020).
15. Miranda Campos, B., Bourbigot, S., Fontaine, G. & Bonnet, F. Thermoplastic matrix-based composites produced by resin transfer molding: A review. *Polym Compos* **43**, 2485–2506 (2022).
16. Höhne, C. *et al.* Hexaphenoxycyclotriphosphazene as FR for CFR anionic PA6 via T-RTM : a study of mechanical and thermal properties. *Fire Mater* **41**, 291–306 (2016).
17. Stewart, R. Thermoplastic composites - Recyclable and fast to process. *Reinforced Plastics* **55**, 22–28 (2011).
18. Uematsu, H. *et al.* Mechanical behavior of unidirectional carbon fiber-reinforced polyamide 6 composites under transverse tension and the structure of polyamide 6 among carbon fibers. *Polym J* **52**, 1195–1201 (2020).

19. Şanli, S., Durmus, A. & Ercan, N. Effect of nucleating agent on the nonisothermal crystallization kinetics of glass fiber- and mineral-filled polyamide-6 composites. *J Appl Polym Sci* **125**, (2012).
20. Li, H. *et al.* Interfacial adhesion and shear behaviors of aramid fiber/polyamide 6 composites under different thermal treatments. *Polym Test* **81**, 106209 (2020).
21. Shi, J., Yang, X., Wang, X. & Lu, L. Non-isothermal crystallization kinetics of nylon 6 / attapulgite nanocomposites. *Polym Test* **29**, 596–602 (2010).
22. Pan, B. *et al.* Non-Isothermal Crystallization Kinetics of PA6/Attapulgite Composites Prepared by Melt Compounding. *Journal of Macromolecular Science, Part B* **45**, 1025–1037 (2006).
23. Zhao, C. *et al.* Synthesis and characterization of multi-walled carbon nanotubes reinforced polyamide 6 via in situ polymerization. *Polymer (Guildf)* **46**, 5125–5132 (2005).
24. Meincke, O. *et al.* Mechanical properties and electrical conductivity of carbon-nanotube filled polyamide-6 and its blends with acrylonitrile/butadiene/styrene. *Polymer (Guildf)* **45**, 739–748 (2004).
25. Verdejo, R., Bernal, M. M., Romasanta, L. J. & Lopez-Manchado, M. A. Graphene filled polymer nanocomposites. *J Mater Chem* **21**, 3301–3310 (2011).
26. Keledi, G., Hari, J. & Pukanszky, B. Polymer nanocomposites: structure, interaction, and functionality. *Nanoscale* **4**, 1919–1938 (2012).
27. Koo, J. H. *Polymer Nanocomposites: Processing, Characterization, and Applications*. (McGraw-Hill Education, 2019).
28. Mago, G., Kalyon, D. M., Jana, S. C. & Fisher, F. T. Polymer nanocomposite processing, characterization, and applications. *J Nanomater* **2010**, 1–2 (2010).
29. Rijswijk, K. Van, Bersee, H. E. N., Jager, W. F. & Picken, S. J. Optimisation of anionic polyamide-6 for vacuum infusion of thermoplastic composites : choice of activator and initiator. *Compos Part A Appl Sci Manuf* **37**, 949–956 (2006).
30. Van Rijswijk, K., Bersee, H. E. N., Beukers, A., Picken, S. J. & Van Geenen, A. A. Optimisation of anionic polyamide-6 for vacuum infusion of thermoplastic composites: Influence of polymerisation temperature on matrix properties. *Polym Test* **25**, 392–404 (2006).
31. Kalaitzidou, K., Fukushima, H., Askeland, P. & Drzal, L. T. The nucleating effect of exfoliated graphite nanoplatelets and their influence on the crystal structure and electrical conductivity of polypropylene nanocomposites. *J Mater Sci* **43**, 2895–2907 (2008).
32. Ahmad, S. R., Xue, C. & Young, R. J. The mechanisms of reinforcement of polypropylene by graphene nanoplatelets. *Materials Science and Engineering: B* **216**, 2–9 (2017).
33. Geim, A. K. & Novoselov, K. S. The rise of graphene. in *Nanoscience and technology: a collection of reviews from nature journals* 11–19 (World Scientific, 2010).
34. Huang, X., Qi, X., Boey, F. & Zhang, H. Graphene-based composites. *Chem Soc Rev* **41**, 666–686 (2012).
35. Gomez, J., Villaro, E., Karagiannidis, P. G. & Elmarakbi, A. Effects of chemical structure and morphology of graphene-related materials (GRMs) on melt processing and properties of GRM/polyamide-6 nanocomposites. *Results in Materials* **7**, 100105 (2020).
36. Zhang, M., Li, Y., Su, Z. & Wei, G. Recent advances in the synthesis and applications of graphene–polymer nanocomposites. *Polym Chem* **6**, 6107–6124 (2015).
37. Elmarakbi, A. & Azoti, W. State of the art on graphene lightweighting nanocomposites for automotive applications. *Experimental Characterization, Predictive Mechanical and Thermal Modeling of Nanostructures and their Polymer Composites* 1–23 (2018).
38. Das, T. K. & Prusty, S. Graphene-based polymer composites and their applications. *Polym Plast Technol Eng* **52**, 319–331 (2013).
39. Bikiaris, D. N. *et al.* Preparation by melt mixing and characterization of isotactic polypropylene/SiO2 nanocomposites containing untreated and surface-treated nanoparticles. *J Appl Polym Sci* **100**, 2684–2696 (2006).
40. Fu, X., Liu, Y., Zhao, X., Zhao, D. & Yang, G. A commercial production route to prepare polymer-based nanocomposites by unmodified multilayer graphene. *J Appl Polym Sci* **132**, (2015).

41. Chen, Y., Zou, H. & Liang, M. Non-isothermal crystallization study of in-situ exfoliated graphite filled nylon 6 composites. *Journal of Polymer Research* **21**, 417 (2014).
42. Valente, M., Rossitti, I., Biblioteca, I. & Sambucci, M. Thermoplastic Composite Materials Approach for More Circular Components: From Monomer to In Situ Polymerization, a Review. *Journal of Composites Science* **6**, 132 (2022).
43. Beatrice, C. A. G., Branciforti, M. C., Alves, R. M. V & Bretas, R. E. S. Rheological, mechanical, optical, and transport properties of blown films of polyamide 6/residual monomer/montmorillonite nanocomposites. *J Appl Polym Sci* **116**, 3581–3592 (2010).
44. Avrami, M. Kinetics of phase change. I General theory. *J Chem Phys* **7**, 1103–1112 (1939).
45. Avrami, M. Kinetics of Phase Change . II Transformation-Time Relations for Random Distribution of Nuclei Kinetics of Phase Change . II Transformation-Time Relations for Random Distribution of Nuclei. *J Chem Phys* **8**, 212–224 (1940).
46. Liu, T., Mo, Z., Wang, S. & Zhang, H. Nonisothermal melt and cold crystallization kinetics of poly (aryl ether ether ketone ketone). *Polym Eng Sci* **37**, 568–575 (1997).
47. Friedman, H. L. Kinetics of thermal degradation of char-forming plastics from thermogravimetry. Application to a phenolic plastic. in *Journal of polymer science part C: polymer symposia* vol. 6 183–195 (Wiley Online Library, 1964).
48. Lagarinhos, J., Santos, L. & Oliveira, J. Effect of Catalyst and Activator on Properties of Polyamide 6 Prepared by Thermoplastic Resin Transfer Molding Technology. *J Mater Eng Perform* **31**, 7098–7103 (2022).
49. Lagarinhos, J. N. & Oliveira, M. The effect of graphene-based materials in polyamide 6 obtained by in situ thermoplastic resin transfer moulding (T-RTM) polymerization. in *Proceedings of the 20th European Conference on Composite Materials - Composites Meet Sustainability (Vol 1-6)* (eds. Vassilopoulos, A. & Michaud, V.) 152–159 (EPFL Lausanne, Composite Construction Laboratory, 2022).
50. Xu, Z. *et al.* Relationship between the structure and thermal properties of polypropylene/graphene nanoplatelets composites for different platelet-sizes. *Compos Sci Technol* **183**, 107826 (2019).
51. Lagarinhos, J. & Oliveira, M. Nucleation Activity of Graphene in Polyamide 6-Based Nanocomposites Prepared by In Situ Polymerization. *Materials Proceedings* **8**, 83 (2022).
52. Li, J., Wong, P.-S. & Kim, J.-K. Hybrid nanocomposites containing carbon nanotubes and graphite nanoplatelets. *Materials Science and Engineering: A* **483–484**, 660–663 (2008).
53. Liu, X. & Wu, Q. Non-isothermal crystallization behaviors of polyamide 6/clay nanocomposites. *Eur Polym J* **38**, 1383–1389 (2002).
54. Alvaredo, Á., Martín, M., Castell, P., Guzmán de Villoria, R. & Fernández-Blázquez, J. Non-Isothermal Crystallization Behavior of PEEK/Graphene Nanoplatelets Composites from Melt and Glass States. *Polymers (Basel)* **11**, 124 (2019).
55. Hou, X., Hu, Y., Hu, X. & Jiang, D. Poly (ether ether ketone) composites reinforced by graphene oxide and silicon dioxide nanoparticles. *High Perform Polym* **30**, 406–417 (2018).
56. Ahmed, A. K., Atiqullah, M., Al-Harthi, M. A., Abdelaal, A. F. & Pradhan, D. R. Non-isothermal crystallization of Ziegler Natta i-PP-graphene nanocomposite: DSC and new model prediction. *Can J Chem Eng* **98**, 1398–1410 (2020).
57. Kiziltas, A., Liu, W., Tamrakar, S. & Mielewski, D. Graphene nanoplatelet reinforcement for thermal and mechanical properties enhancement of bio-based polyamide 6, 10 nanocomposites for automotive applications. *Composites Part C: Open Access* **6**, 100177 (2021).
58. Karsli, N. G. & Aytac, A. Tensile and thermomechanical properties of short carbon fiber reinforced polyamide 6 composites. *Compos B Eng* **51**, 270–275 (2013).
59. Liu, H. *et al.* Functionalization of multi-walled carbon nanotubes grafted with self-generated functional groups and their polyamide 6 composites. *Carbon N Y* **48**, 721–729 (2010).
60. Jin, J., Rafiq, R., Gill, Y. Q. & Song, M. Preparation and characterization of high performance of graphene/nylon nanocomposites. *Eur Polym J* **49**, 2617–2626 (2013).

61. Caamaño, C., Grady, B. & Resasco, D. E. Influence of nanotube characteristics on electrical and thermal properties of MWCNT/polyamide 6,6 composites prepared by melt mixing. *Carbon N Y* **50**, 3694–3707 (2012).
62. Faghihi, M., Shojaei, A. & Bagheri, R. Characterization of polyamide 6/carbon nanotube composites prepared by melt mixing-effect of matrix molecular weight and structure. *Compos B Eng* **78**, 50–64 (2015).
63. Cebe, P. & Hong, S.-D. Crystallization behaviour of poly (ether-ether-ketone). *Polymer (Guildf)* **27**, 1183–1192 (1986).
64. Melo, C. C. N. de, Beatrice, C. A. G., Pessan, L. A., de Oliveira, A. D. & Machado, F. M. Analysis of nonisothermal crystallization kinetics of graphene oxide - reinforced polyamide 6 nanocomposites. *Thermochim Acta* **667**, 111–121 (2018).
65. Liu, Y. & Yang, G. Non-isothermal crystallization kinetics of polyamide-6/graphite oxide nanocomposites. *Thermochim Acta* **500**, 13–20 (2010).
66. Hemlata & Maiti, S. N. Nonisothermal crystallization kinetics of PA6 and PA6/SEBS-g-MA blends. *Journal of Polymer Research* **19**, 9926 (2012).
67. Jeziorny, A. Parameters characterizing the kinetics of the non-isothermal crystallization of poly(ethylene terephthalate) determined by d.s.c. *Polymer (Guildf)* **19**, 1142–1144 (1978).
68. Allen, J. L., Jow, T. R. & Wolfenstine, J. Kinetic Study of the Electrochemical FePO4 to LiFePO4 Phase Transition. *Chemistry of Materials* **19**, 2108–2111 (2007).
69. Balamurugan, G. P. & Maiti, S. N. Nonisothermal crystallization kinetics of polyamide 6 and ethylene-co-butyl acrylate blends. *J Appl Polym Sci* **107**, 2414–2435 (2008).
70. Weng, W., Chen, G. & Wu, D. Crystallization kinetics and melting behaviors of nylon 6/foliated graphite nanocomposites. *Polymer (Guildf)* **44**, 8119–8132 (2003).
71. Hay, J. N. & Mills, P. J. The use of differential scanning calorimetry to study polymer crystallization kinetics. *Polymer (Guildf)* **23**, 1380–1384 (1982).
72. Tarani, E. *et al.* Effect of graphene nanoplatelets diameter on non-isothermal crystallization kinetics and melting behavior of high density polyethylene nanocomposites. *Thermochim Acta* **643**, 94–103 (2016).
73. Lv, Q. *et al.* Crystallization of Poly(ε-caprolactone) composites with graphite nanoplatelets: Relations between nucleation and platelet thickness. *Thermochim Acta* **612**, 25–33 (2015).
74. Liu, B., Hu, G., Zhang, J. & Wang, Z. The non-isothermal crystallization behavior of polyamide 6 and polyamide 6/HDPE/MAH/L-101 composites. *Journal of Polymer Engineering* **39**, 124–133 (2019).
75. Vyazovkin, S. & Dranca, I. Isoconversional Analysis of Combined Melt and Glass Crystallization Data. *Macromol Chem Phys* **207**, 20–25 (2006).
76. Ferreira, C. I., Dal Castel, C., Oviedo, M. A. S. & Mauler, R. S. Isothermal and non-isothermal crystallization kinetics of polypropylene/exfoliated graphite nanocomposites. *Thermochim Acta* **553**, 40–48 (2013).
77. Run, M., Song, H., Yao, C. & Wang, Y. Crystal morphology and nonisothermal crystallization kinetics of short carbon fiber/poly(trimethylene terephthalate) composites. *J Appl Polym Sci* **106**, 868–877 (2007).

4.6 The effect of graphene nanoplatelets size in polyamide 6 nanocomposites obtained by *in situ* T-RTM polymerization

Joana Lagarinhos and Martinho Oliveira

Proceedings of the 20th European Conference on Composite Materials (ECCM), 2022, 3, 152-159 [1]
(DOI: https://doi.org/10.5075/epfl-298799_978-2-9701614-0-0)

Abstract

Polyamide 6 (PA6) and PA6 reinforced with graphene nanoplatelets (PA6/GNP) were developed by an *in situ* anionic ring opening polymerization of ε-caprolactam through thermoplastic resin transfer moulding (T-RTM) technology. In low viscosity raw materials, the dispersion of nanoparticles namely graphene, is a demanding challenge. Two types of GNP with different sizes were pre-dispersed in molten ε-caprolactam monomer at loading rates of 0.1, 0.25, 0.5, 0.75 and 1.0 wt.%. Differential Scanning Calorimetry (DSC), Thermogravimetric Analysis (TGA) and Scanning Electron Microscopy (SEM) techniques were used to understand the crystallization, thermal and structural behaviour of the prepared nanocomposites. Mechanical properties were also determined. The prepared nanocomposites exhibit improved thermal stability based on the determination of the temperature at 10% weight loss ($T_{10\%}$) and the temperature at 50% weight loss ($T_{50\%}$). An increase in crystallization temperatures (T_c) is observed due to a nucleation effect of GNP. An improvement in mechanical strength is observed with GNP loading for both grades. In general, the mechanical performance of the polymer matrix was improved in the presence of GNP, however, the GNP with smaller particle size is more advantageous in improving the polymer properties. Overall, the smaller the size, the better the dispersion and the lower the agglomeration.

Keywords

Polyamide 6; anionic ring opening polymerization; *in situ*; graphene nanoplatelets; nanocomposite; thickness effect.

Contributions

The author had contributed to the planning and execution of all experiments present herein, as well as on the discussion, interpretation, and preparation of the manuscript. Martinho Oliveira contributed to the conceptualization, review and editing of the data presented

[1] This paper, presented at the *European Conference on Composite Materials,* showed a study with only one type of the selected GNP. Here, another type of GNP has been included to provide a more complete study of the influence of different GNP sizes on the final properties of PA6.

1. Introduction

The use of plastic materials in automotive parts have arouse great interest in the industry[1]. Some automotive structures are based on thermoset matrices, but nowadays, global market is slowly replacing the thermosets with thermoplastic matrices looking for better environment performance[2].

Thermoplastic resin transfer moulding (T-RTM) is an efficient processing technology for large-scale production of thermoplastics via *in situ* polymerization[3,4]. This technology is based in the injection of a reactive mixture (low viscosity monomer with suitable catalyst and activator) to a preheated mould, in which a *in situ* polymerization occurs[5,6] Anionic polymerization of ε-caprolactam monomer combined with a catalyst and activator system can be used to produce PA6 *via* T-RTM[7]. This is possible since anionic polymerization occurs at relatively low temperatures with short mould cycle times[8].

Polyamide 6 (PA6) obtained from T-RTM shows relatively high molecular weight, high crystallinity and superior mechanical performance which enable to replace metallic materials of structural components in automotive industry[9,10]. However, its mechanical performance, such as strength and elasticity modulus, can limits its applications[11]. To expand the use of PA6 in areas with increasing performance demands, many attempts have been made to improve its mechanical properties.

The incorporation of nanofillers, such graphene-based materials have been studied, with special focus on the improvement of mechanical properties[12–14]. Graphene, a two dimensional honeycomb layer of sp^2 bonded carbon, has a high potential to be an effective filler to prepare high performance nanocomposites. Its electrical, thermal, and mechanical properties can substantially increase the performance of composites[15–17]. It has been reported as the strongest material tested with an ultimate strength of 130 GPa and Young modulus of 1 TPa[18].

Graphene nanoplatelets (GNP) are formed by graphite nano crystals in several layer that exist by virtue of van der Waals forces. Polymer nanocomposites with GNP have generated enormous interest in a wide range of applications due to its intrinsic properties. Several studies have focused on the effect of GNP on PA6 performance[19–21]. The scientific literature reveals that PA6 nanocomposites reinforced with GNP augments both mechanical and thermal behaviour. However, the dispersion of GNP within low viscosity raw materials and its interfacial adhesion are a key factor to determine the properties of the final nanocomposites[22].

Several approaches to achieve of uniformly nano dispersed GNP has been reported[23,24]. Although, *in situ* polymerization has been proven to be a more efficient method due to the reduced processing time[25]. Furthermore, the low monomer viscosity, turn it a better medium for dispersing GNP allowing a more efficient retention of its properties[26–28].

Herein, a simple and effective method to prepare PA6 and PA6 reinforced with GNP via *in situ* polymerization by using T-RTM technology is reported. An attempt has been made to deep

explanation of the effect of GNP size and loading rates on various physicochemical properties of its nanocomposites with PA6.

2. Materials and preparations

2.1. Materials

The monomer AP-Nylon® caprolactam (CL), mixed with a catalyst Bruggolen® C10 (C10) and activator Bruggolen® C20P (C20P) were used for anionic polymerization of PA6. These components were purchased from L. Brüggemann GmbH and Co. KG, Germany. In this study, a formulation of 95% CL, 3% C10 and 2% C20P, was developed[29]. Powder graphene nanoplatelets (GNP) was purchased from NanoXplore company (Canada). This study used two different sizes of GNP, GN with D90 < 50µm, and GP with D90 < 70µm.

2.2. PA6 and PA6/GNP preparation

PA6 and PA6/GNP samples were prepared by *in situ* ring-opening polymerization of CL monomer using a semiautomatic T-RTM laboratory equipment[29]. The laboratory T-RTM setup consists of a dosing unit with two tanks, a mixing head, and a mould system equipped with a heating, a pressure, and a vacuum control units.

For PA6 preparation, the CL was divided into two equal parts and placed into the two tanks. C10 was added to one of the tanks and C20P was added to the other. The temperature in each tank was set to 90 ºC under stirring, at a speed of 350 rpm for a period of 7 min. After melting the components, the CL/C10 and CL/C20P flow in separated channels into the mixing head (110 ºC) under controlled pressure. Through impingement, the reactive mixture was injected into a preheated mould (160 ºC), under vacuum. The polymerization reaction occurs inside the mould. Following polymerization time (≈6 min), a plate (280mm x 150mm x 2mm) was demoulded at room temperature, and samples prepared for further characterization.

For the preparation of PA6/GNP nanocomposites, the GNP loadings were pre-dispersed in the molten ε-caprolactam using a sonicator. The sonication time used to disperse the GNP was based on a previous optimization process[30]. The catalyst and activator were then added, and the polymerization process followed in the same way as for PA6.

The chemical compositions of the different formulations developed are described in Table 4.6.1:

Table 4.6.1. Compositions of the developed PA6 and PA6/GNP nanocomposites.

Filler (wt.%)	PA6 (wt.%)	Sample code
0	100.0	PA6
GN		
0.1	99.9	PA6/GN1
0.25	99.75	PA6/GN2
0.5	99.5	PA6/GN3
0.75	99.25	PA6/GN4
1.0	99.0	PA6/GN5
GP		
0.1	99.9	PA6/GP1
0.25	99.75	PA6/GP2
0.5	99.5	PA6/GP3
0.75	99.25	PA6/GP4
1.0	99.0	PA6/GP5

3. Materials characterization

3.1. Thermal analyses

The thermal behaviour of nanocomposites was studied by DSC and TGA experiments. The DSC analysis was carried out using a Shimadzu DSC-60 equipment. Samples were heated from room temperature to 250 ºC at a heating rate of 20 ºC·min^{-1} and held for 2 min to eliminate the thermal history. Then, the samples were cooled to -25 ºC, and reheated to 250 ºC at 10 ºC·min^{-1}. Various thermal properties such as melting (T_m) and crystallization (T_c) temperatures and degree of crystallinity (X_c) were traced from DSC analysis. The X_c was determined using equation (1):

$$Xc\ (\%) = \frac{\Delta H_m}{\Delta H_m^0\,(1-\varphi)} \times 100 \qquad (1)$$

where ΔH_m is the melting enthalpy of sample, φ is the weight fraction of GNP, and ΔH_m^0 corresponds to the melting enthalpy of PA6 in 100% crystalline state (PA6 = 190 J·g^{-1})[31].

The thermal stability of the nanocomposites was analysed by performing TGA experiments using a Hitachi STA300 instrument. The samples were heated in a nitrogen environment at a flow rate of 100 mL·min^{-1}. Each sample was heated from room temperature to 600ºC at a rate of 10ºC·min^{-1} to analyse its degradation behaviour.

3.2. Mechanical measurements

Tensile and flexural properties were performed on an Autograph AG-IS (Shimadzu) universal testing machine with a 10kN load cell.

Tensile tests were measured according to ISO 527-2 standard (Type 1BA) with a constant crosshead speed of 1mm·min^{-1}. A video extensometer (Shimadzu DVE-101/201) was used to determine the elongation of each specimen. The flexural properties were assessed following ISO 178, with a crosshead speed of 1mm/min.

All above tests were performed at room temperature. Each group of samples contained, at least, five specimens, and the average and standard deviation values of the measured tensile and flexural properties have been used in the reported data.

3.3. Morphological analyses

Morphological analyses were carried out using a SEM Hitachi SU-70 equipment. Analysis was performed on the fracture surface after tensile testing. Samples were mounted on aluminium stubs and sputter coated with Au/Pd target for 2 minutes at 12 mA.

4. Results and Discussion

4.1. DSC analysis

The influence of GNP on melting (T_m) and crystallization (T_c) behaviour of PA6/GNP nanocomposites was analysed by DSC. The second heating and cooling thermograms of PA6 and PA6/GN and PA6/GP nanocomposites are shown in Figure 4.6.1 and Figure 4.6.2, respectively, and data are summarized in Table 4.6.2.

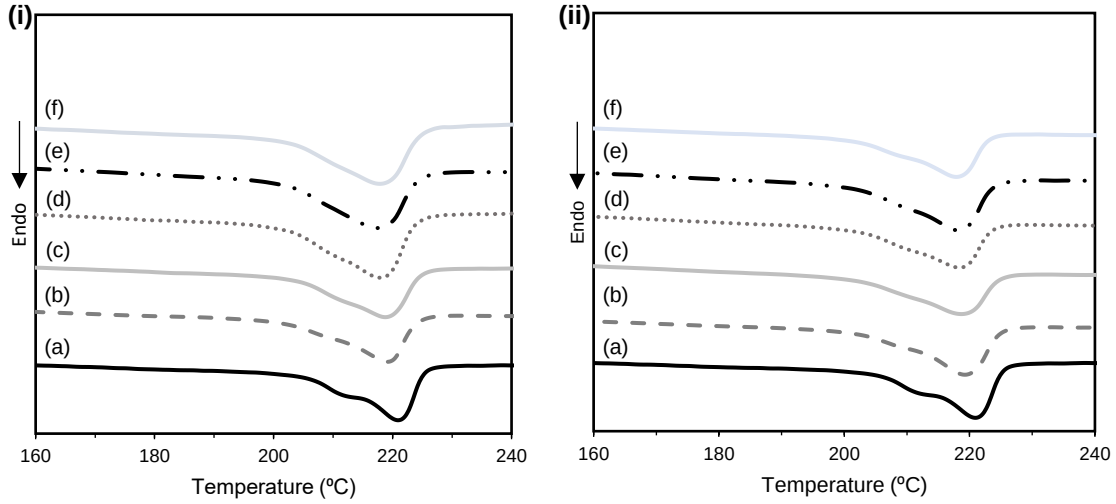

Figure 4.6.1. DSC heating scans of **(i)** GN nanocomposites: a) PA6; (b) PA6/GN1; (c) PA6/GN2; (d) PA6/GN3; (e) PA6/GN4; (f) PA6/GN5 and **(ii)** GP nanocomposites: (a) PA6; (b) PA6/GP1; (c) PA6/GP2; (d) PA6/GP3; (e) PA6/GP4; (f) PA6/GP5 (from bottom to top). The curves are vertically offset for clarity.

DSC heating curves showed that the addition of GNP had a slightly effect on melting temperature of PA6. It is well-known that PA6 has two crystal forms at least: α-form crystal, a more thermodynamically stable with hydrogen bonds between antiparallel chains, and γ-form crystal with hydrogen bonds between parallel chains[32], indicated by T_m peaks at 221 ºC and 212 ºC in DSC

curves, respectively. From nanocomposites heating curves it was possible to observe that with increasing GNP loading, T_{m2} peak was attenuated, suggesting a well-dispersed nanoparticles[33].

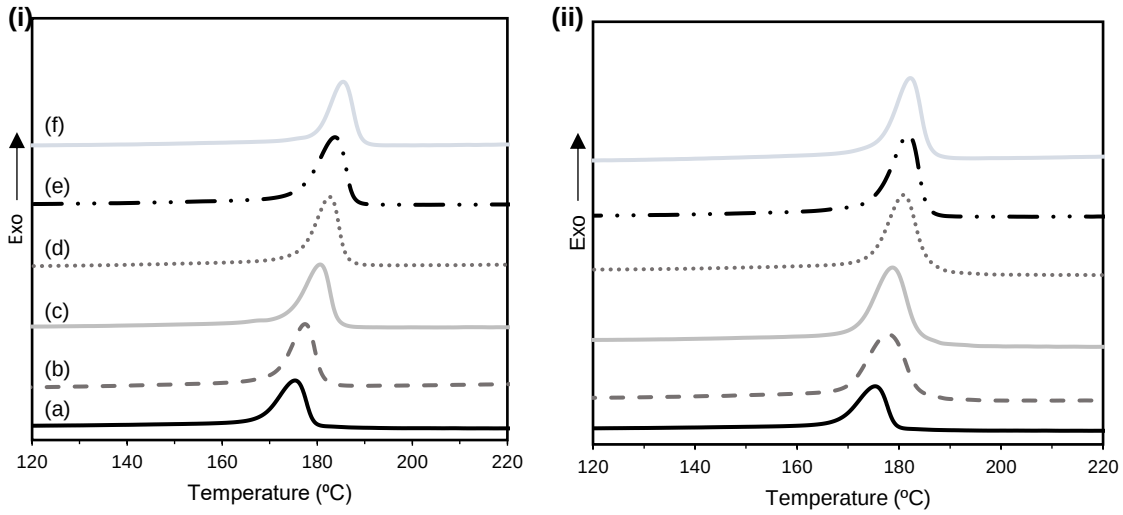

Figure 4.6.2. DSC cooling scans **(i)** GN nanocomposites: a) PA6; (b) PA6/GN1; (c) PA6/GN2; (d) PA6/GN3; (e) PA6/GN4; (f) PA6/GN5 and **(ii)** GP nanocomposites: (a) PA6; (b) PA6/GP1; (c) PA6/GP2; (d) PA6/GP3; (e) PA6/GP4; (f) PA6/GP5 (from bottom to top). The curves are vertically offset for clarity.

The addition of GNP significantly increases the T_c of nanocomposites. This is indicative of a strong nucleation effect of GNP during the crystallization of the PA6[11].

Table 4.6.2. Thermal parameters of PA6 and PA6/GNP nanocomposites.

Samples	T_m, ºC	T_c, ºC	ΔT, ºC	X_c, %
PA6	220.9	175.4	45.5	31.5
PA6/GN1	219.1	177.3	41.8	33.7
PA6/GN2	219.3	180.7	38.6	35.3
PA6/GN3	218.0	182.8	35.2	35.9
PA6/GN4	217.4	184.2	33.2	34.5
PA6/GN5	217.2	185.3	31.9	33.2
PA6/GP1	219.3	177.9	41.4	33.2
PA6/GP2	218.5	178.7	39.8	33.3
PA6/GP3	218.4	180.9	37.5	34.4
PA6/GP4	218.3	181.7	36.6	34.8
PA6/GP5	217.9	182.2	35.7	34.0

For 1 wt.% GNP content, T_c increased by 9.9 ºC for PA6/GN5, whereas PA6/GP5 increased T_c by 7.5 ºC. This is due of better dispersion promoted by GNP with a smaller particle size, hence facilitate the crystallization at higher temperatures[34].

The addition of GNP also increases X_c compared to the PA6 matrix. As mentioned above, GNP can promote crystallization by acting as a nucleating agent, thus facilitating crystallization. A slight decrease in X_c is observed in PA6/GN5, suggesting that the excess of nanoparticles can hinder the mobility of PA6 chains, thus reducing the crystallization growth[13].

The above results suggest that even at low amounts, GNP have a significant influence on the crystallization of nanocomposites, improving their crystallinity and increasing the rate of PA6 crystallization.

4.2. Thermal stability

The thermal stability of the PA6/GNP nanocomposites was studied, and the resulting curves are shown in Figure 4.6.3. The thermal parameters, such as, the temperatures corresponding to 5% weight loss ($T_{5\%}$), 10% weight loss ($T_{10\%}$), 50% weight loss ($T_{50\%}$), and residue at 500 ºC (R) are presented in Table 4.6.3.

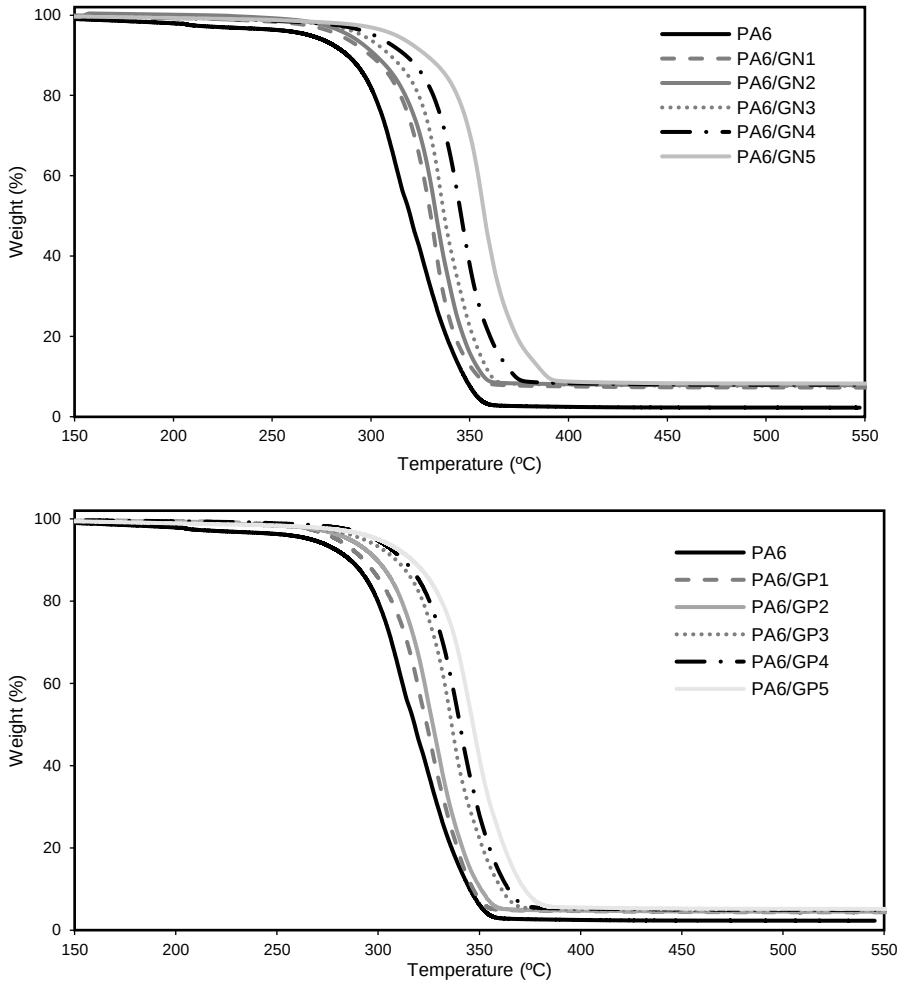

Figure 4.6.3. Thermogravimetric analysis curves of PA6 nanocomposites reinforced with **(a)** GN and **(b)** GP.

A typical TGA curve is observed for PA6. There is an initial weight loss occurs below 240 ºC due to decomposition of the lower molecular weight polymer, with a continuous weight loss between 250 ºC and 350 ºC due to decomposition of the higher molecular weight polymer[35]. After this temperature, there is a complete polymer degradation, as shown by the thermal pattern.

It can be seen that the values of the above parameters are improved with increasing GNP content, indicating that the incorporated GNP improves the thermal stability of PA6. The main cause of the improved thermal stability is due to the formation of a mass transfer barrier, which prevents the diffusion of degradation products to the outer surface of the polymer[36]. GNP in the polymer matrix are able to create a tortuous path that acts as a barrier structure for gases formed during degradation from the interior of the composite to the polymer surface[37]. This retards degradation and improves thermal stability. On the other hand, GNP restrict the mobility of the polymer chain, increasing the energy required for degradation and producing a more thermally stable nanocomposite

Table 4.6.3. TGA results of PA6, and its nanocomposites reinforced with GNP.

Samples	$T_{5\%}$, ºC	$T_{10\%}$, ºC	$T_{50\%}$, ºC	R (wt.%)
PA6	266.9	286.2	317.9	2.1
PA6/GN1	284.1	299.8	330.3	7.3
PA6/GN2	288.9	302.3	333.1	7.9
PA6/GN3	295.5	309.7	337.1	7.7
PA6/GN4	301.6	317.6	345.7	8.0
PA6/GN5	312.5	328.1	357.5	8.3
PA6/GP1	279.8	292.9	324.0	4.3
PA6/GP2	285.9	299.4	327.0	4.5
PA6/GP3	293.0	308.8	336.3	4.7
PA6/GP4	298.9	312.5	340.4	4.8
PA6/GP5	300.1	316.8	346.8	5.1

The degradation onset parameters of the nanocomposites increased with the addition of GNP. For PA6/GN1, $T_{10\%}$ was increased up to 13.6 ºC relative to PA6, while for PA6/GP1 it was increased by 6.7 ºC. As observed, both nanocomposites showed an increase in thermal stability, but GN showed a more efficient thermal stability compared to GP. It is worth noting that the particle size of GNP plays a key role in this context. Smaller GNP showed a better dispersion within the polymer matrix, thus improving the thermal stability.

4.3. Mechanical behaviour

Tensile tests were performed to evaluate the influence of GNP on the mechanical properties (Figure 4.6.4).

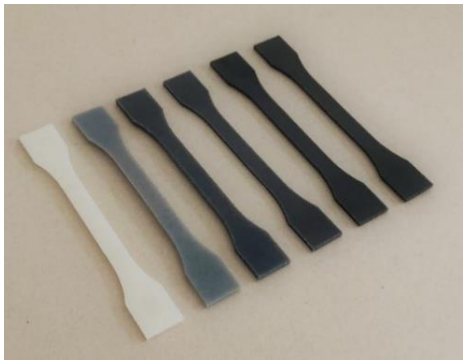

Figure 4.6.4. Representative specimens for tensile tests. From right to left: PA6, PA6/GN1, PA6/GN2, PA6/GN3, PA6/GN4 and PA6/GN5.

Tensile strength (σ_{max}), elongation at break (ε_{max}) and Young modulus (E) as a function of the GNP content are plotted in Figure 4.6.5. The tensile data of these materials, and their standard deviations are given in Table 4.6.4.

Table 4.6.4. Tensile properties of PA6 and nanocomposites.

Samples	σ_{max} (MPa)	ε_{max} (%)	E (GPa)
PA6	63.5 ± 2.1	14.3 ± 3.5	2.6 ± 0.3
PA6/GN1	72.0 ± 11.3	14.4 ± 6.2	4.2 ± 0.8
PA6/GN2	73.9 ± 11.9	16.0 ± 12.8	4.2 ± 0.7
PA6/GN3	77.0 ± 9.3	33.4 ± 8.8	4.4 ± 0.7
PA6/GN4	79.0 ± 5.2	44.4 ± 2.1	4.2 ± 0.9
PA6/GN5	76.7 ± 5.3	13.9 ± 1.2	3.9 ± 0.3
PA6/GP1	63.4 ± 4.9	15.2 ± 4.4	3.3 ± 0.7
PA6/GP2	68.1 ± 5.5	13.4 ± 8.8	3.5 ± 0.3
PA6/GP3	72.4 ± 6.1	28.3 ± 7.3	3.8 ± 0.5
PA6/GP4	74.6 ± 8.8	35.3 ± 14.8	4.1 ± 0.7
PA6/GP5	75.1 ± 9.6	21.6 ± 9.1	3.7 ± 0.6

It is observed that for both types of GNP the tensile strength and Young's modulus increase with GNP loading. This is due to the high modulus of the GNP which causes an improvement in the stress transfer at the interface between the reinforcing phase and the polymer matrix. The improved tensile properties are attributed to the increase in stiffness which enhances the interaction between the GNP and the PA6 matrix. The tensile strength increased from a minimum of 63.5 ± 2.1 MPa for PA6 to approximately 79.0 ± 5.2 MPa for PA6/GN4. A slight increase in stiffness was observed with the addition of GNP to the polymeric matrix. PA6 showed a Young's modulus of 2.6 ± 0.3 GPa. It increased to 4.4 ± 0.7 GPa (~63%) for PA6/GN3 nanocomposite, while a maximum value of 4.2 ± 0.7 GPa (~61%) was reported for PA6/GP4. Compared to the PA6 matrix, the elongation at break is increased by ~210% and ~174% for PA6/GN4 and PA6/GP4, respectively.

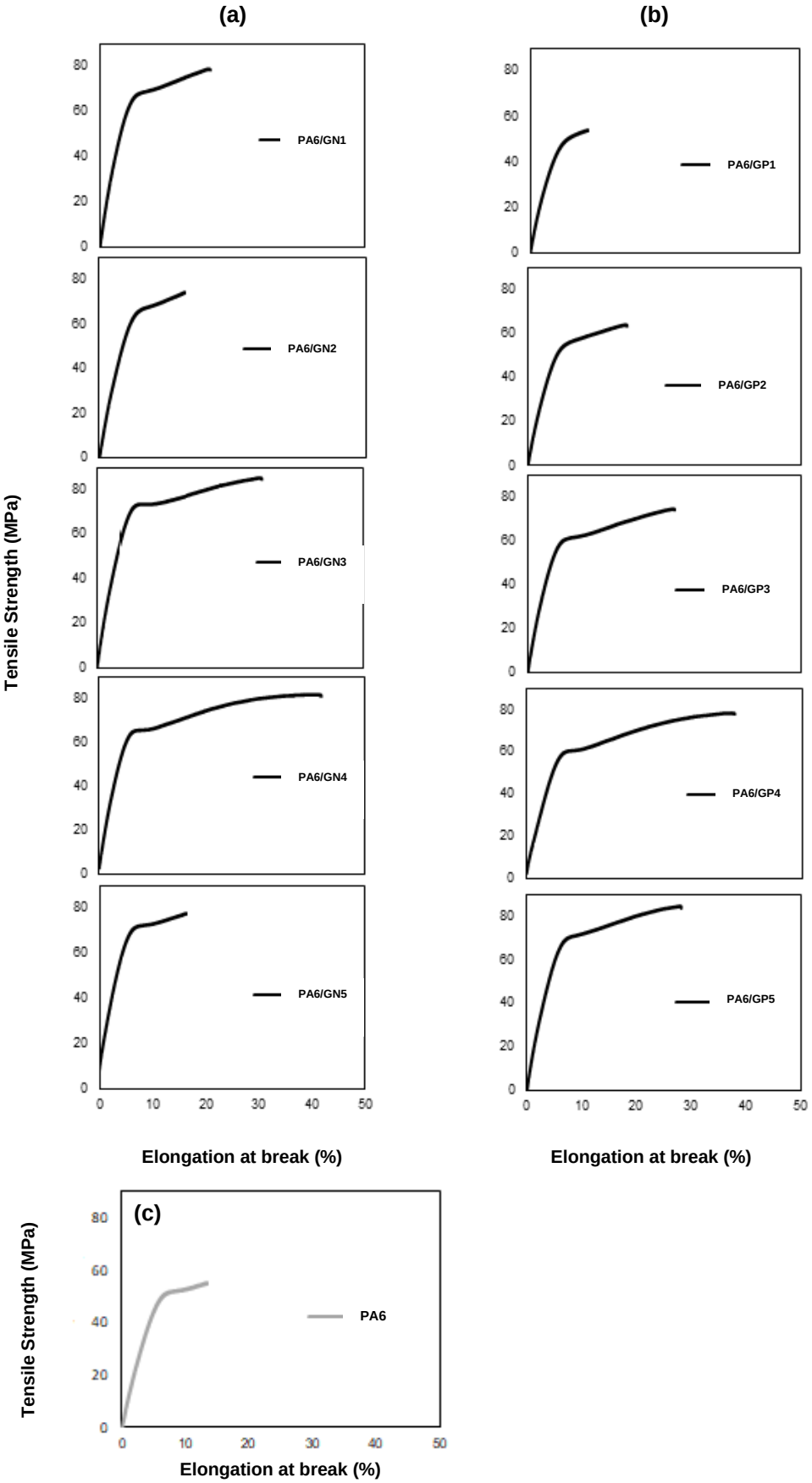

Figure 4.6.5. Tensile stress-strain curves of: **(a)** PA6/GN, **(b)** PA6/GP samples and **(c)** PA6.

When the GNP loading reached 1.0 wt.%, the mechanical properties showed a decrease. In general, the mechanical properties of the nanocomposites improve significantly with the addition of different loadings, but an excess of GNP can form small agglomerates, thus reducing the molecular interaction and leading to a reduction in tensile strength[38]. Another possible explanation for this reduction is that agglomerates can act as stress concentration sites.

Overall, tensile strength, elongation at break and Young's modulus improved with the addition of GNP. However, it is important to note that these properties were always higher for the nanocomposites containing the GN grade of GNP. Reducing the thickness of the sheet increases the efficiency of the reinforcement, as the reduction in thickness will promote interfacial bonding between PA6 and GNP, causing a further reduction in agglomeration. As the mechanical properties are inversely proportional to the size of the reinforcing phase[39].

The influence of GNP content on flexural properties is sketched in Figure 4.6.6 and the corresponding data are reported in Table 4.6.5.

Table 4.6.5. Flexural properties of PA6 and nanocomposites.

Samples	σ_{max} (MPa)	ε_{max} (%)	E (GPa)
PA6	125.1 ± 6.2	8.4 ± 0.5	2.7 ± 0.5
PA6/GN1	132.2 ± 4.5	6.4 ± 0.4	4.2 ± 0.7
PA6/GN2	157.5 ± 7.3	7.9 ± 0.4	4.0 ± 0.3
PA6/GN3	157.0 ± 9.7	7.4 ± 0.2	4.4 ± 0.2
PA6/GN4	178.5 ± 10.5	7.5 ± 0.3	4.9 ± 0.8
PA6/GN5	189.0 ± 9.4	7.7 ± 0.8	4.8 ± 0.8
PA6/GP1	126.2 ± 8.2	6.8 ± 0.1	3.3 ± 0.3
PA6/GP2	131.7 ± 3.6	7.0 ± 0.3	3.7 ± 0.4
PA6/GP3	139.6 ± 3.5	6.8 ± 0.2	3.9 ± 0.8
PA6/GP4	132.9 ± 1.7	6.8 ± 0.1	3.9 ± 0.3
PA6/GP5	134.8 ± 2.0	7.3 ± 0.3	3.4 ± 0.2

PA6 showed a flexural strength of 125.1 ± 6.2 MPa, which increased by approximately 26% and 12% respectively when only 0.1% w/w GN and GP were loaded. With a further increase in GNP content, the flexural properties of the samples showed an increasing trend. Compared to the flexural modulus of PA6, an increase of 80% was obtained for PA6/GN4 and 46% for PA6/GP4. In general, the influence of GNP was more noticeable in GN samples than in GP, showing that GN is more effective in reinforcing the polymer than that of GP. Similar behaviour was also obtained for the tensile properties. The causes of the improvement in flexural properties are attributed to the same mechanisms as previously discussed.

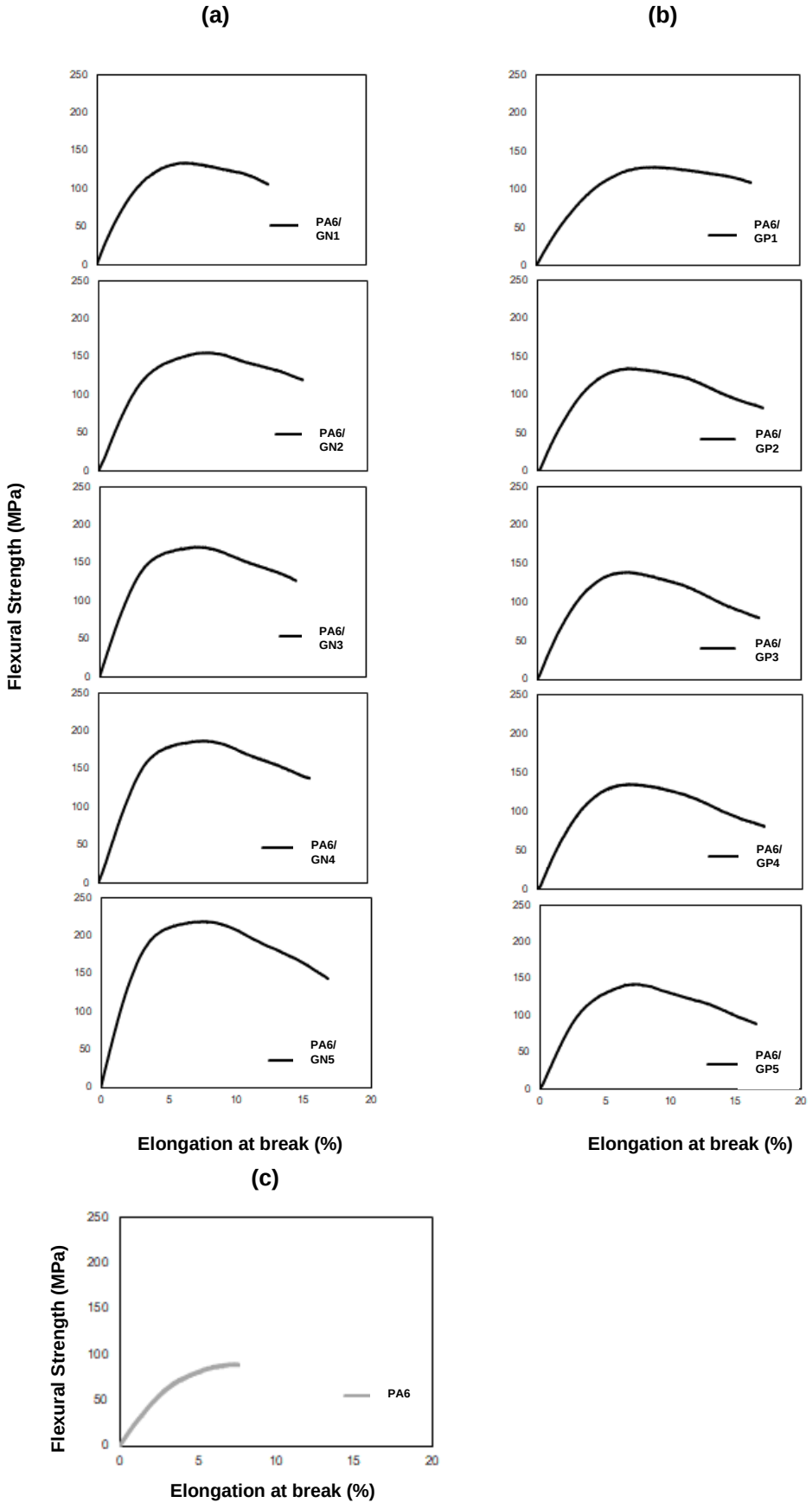

Figure 4.6.6. Flexural curves of: **(a)** PA6/GN, **(b)** PA6/GP samples and **(c)** PA6.

4.4. Morphological analysis

SEM analyses were performed on the fractured surface of PA6 matrix and PA6 nanocomposites to assess morphology and homogeneity (Figure 4.6.7). PA6 (Figure 4.6.7a) presents a well-defined surface typical of this polymer.

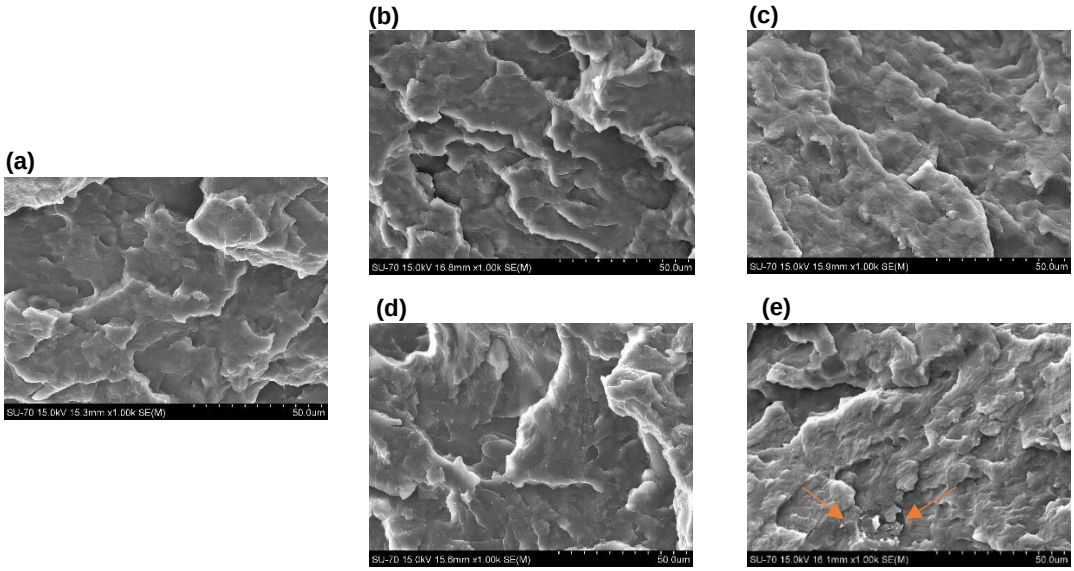

Figure 4.6.7. SEM imagens of **(a)** PA6; **(b)** PA6/GN1; **(c)** PA6/GN5; **(d)** PA6/GP1 and **(e)** PA6/GP5.

From Figure 4.6.7(c-d), it can be seen that there is a satisfactory dispersion, and the platelets are uniformly stacked throughout the PA6 matrix. Phenomena such as buckling do not exist for the nanocomposite due to the smaller size of the GN. This increases the reinforcement efficiency and dispersion and reduces agglomeration. With respect to GP nanocomposites (Figure 4.6.7e-f), the observed surfaces are rougher compared to PA6/GN. This is due to the larger size of the GNP flakes and the agglomeration of the GNP structure caused during processing. At low loadings the nanoparticles completely cover the polymeric matrix, but at high loadings the surface becomes uneven and larger stacks are formed (indicated by the narrows). A larger fraction of the platelets are unable to adhere to the polymer matrix and remain as large particles in the mixture, restricting the polymer surface. These results support those obtained from mechanical analysis.

5. Conclusion

The present work demonstrated an effective approach to PA6 and PA6 nanocomposites production by *in situ* polymerization through T-RTM technology. The effect of GNP content on the different properties of PA6 are thoroughly studied, as well as the effect of GNP particle size.

Different GNP loadings slightly affected the T_m of PA6 towards lower values. The crystallization temperature shifted to higher temperatures, as well as X_c that increases with increasing GNP loading. The addition of GNP has a nucleating effect on PA6. The initial thermal decomposition of PA6/GNP nanocomposites was higher than that of PA6, indicating the strong interaction between GNP and PA6. The GN nanocomposites exhibited higher thermal stability compared to GP nanocomposites.

The degradation process was enhanced with the smaller particle size, once having the ability to transfer heat throughout the nanocomposite.

Even very low loadings of GNP promote a relevant increase in both tensile and flexural tests, compared to the PA6 polymer matrix. The tensile strength of PA6 was found to increase with the addition of GN and GP. A significant increase in Young's modulus was also observed for both GNP. The flexural properties also showed an improvement in properties with increasing GNP content. In general, it was clearly observed that GN was more effective in reinforcing the polymer matrix than GP.

Based on the results, GNP have been successfully incorporated into low viscosity raw materials using T-RTM technology. The improvement in mechanical properties at low loadings of GNP, offer great promise of this technology applications to produce PA6/GNP nanocomposites for automotive applications. Therefore, the particle size of GNP also has a significant effect on the performance efficiency of the final nanocomposites, and it is recommended to use the smaller GNP for all-round performance.

Acknowledgements

This work was partially supported by Simoldes Group. This work was also developed within the scope of the project CICECO-Aveiro Institute of Materials, UIDB/50011/2020 & UIDP/50011/2020 & LA/P/0006/2020, financed by national funds through the FCT/MEC (PIDDAC). Authors would also want to knowledge Suzana Peripolli for helping during SEM analysis.

References

1. Serman, L. M. Thermoplastics Take On All Comers in Expanded Automotive Applications. *Plastics Technology* (2017).
2. Elmarakbi, A., El-Safty, S., Martorana, B. & Azoti, W. Nanocomposites for Automotive: Enhanced Graphene-based Polyer Materials and Multi-Scale Approach. *International Journal of Automotive Composites* **2**, 155–166 (2017).
3. Louisy, E., Samyn, F., Bourbigot, S., Fontaine, G. & Bonnet, F. Preparation of glass fabric/poly (L-lactide) composites by Thermoplastic Resin Transfer Molding. *Polymers (Basel)* **11**, 339 (2019).
4. Miranda Campos, B., Bourbigot, S., Fontaine, G. & Bonnet, F. Thermoplastic matrix-based composites produced by resin transfer molding: A review. *Polym Compos* **43**, 2485–2506 (2022).
5. Sibikin, I. & Karger-Kocsis, J. Toward industrial use of anionically activated lactam polymers: Past, present and future. *Advanced Industrial and Engineering Polymer Research* **1**, 48–60 (2018).
6. Ageyeva, T., Sibikin, I. & Karger-Kocsis, J. Polymers and related composites via anionic ring-opening polymerization of lactams: Recent developments and future trends. *Polymers (Basel)* **10**, 357 (2018).
7. Valente, M., Rossitti, I., Biblioteca, I. & Sambucci, M. Thermoplastic Composite Materials Approach for More Circular Components: From Monomer to In Situ Polymerization, a Review. *Journal of Composites Science* **6**, 132 (2022).
8. Zaldua, N. *et al.* Nucleation and crystallization of PA6 composites prepared by T-RTM: Effects of carbon and glass fiber loading. *Polymers (Basel)* **11**, 1680 (2019).

9. Murray, J. J. *et al.* Thermoplastic RTM: Impact Properties of Anionically Polymerised Polyamide 6 Composites for Structural Automotive Parts. *Energies (Basel)* **14**, 5790 (2021).
10. Wilhelm, M., Wendel, R., Aust, M., Rosenberg, P. & Henning, F. Compensation of water influence on anionic polymerization of ε-caprolactam: 1. Chemistry and experiments. *Journal of Composites Science* **4**, 7 (2020).
11. Liu, H., Hou, L., Peng, W., Zhang, Q. & Zhang, X. Fabrication and characterization of polyamide 6-functionalized graphene nanocomposite fiber. *J Mater Sci* **47**, 8052–8060 (2012).
12. Li, J., Tian, L., Pan, N. & Pan, Z. Mechanical and electrical properties of the PA6/SWNTs nanofiber yarn by electrospinning. *Polym Eng Sci* **54**, 1618–1624 (2014).
13. Wang, Y., Liu, S., Zhang, Q. & Meng, Q. In situ polymerization to prepare graphene-toughened monomer cast nylon composites. *J Mater Sci* **50**, 6291–6301 (2015).
14. Fu, X., Liu, Y., Zhao, X., Zhao, D. & Yang, G. A commercial production route to prepare polymer-based nanocomposites by unmodified multilayer graphene. *J Appl Polym Sci* **132**, (2015).
15. Huang, X., Qi, X., Boey, F. & Zhang, H. Graphene-based composites. *Chem Soc Rev* **41**, 666–686 (2012).
16. Sham, A. Y. W. & Notley, S. M. A review of fundamental properties and applications of polymer–graphene hybrid materials. *Soft Matter* **9**, 6645–6653 (2013).
17. Lee, S.-K., Rana, K. & Ahn, J.-H. Graphene films for flexible organic and energy storage devices. *J Phys Chem Lett* **4**, 831–841 (2013).
18. Lee, C., Wei, X., Kysar, J. W. & Hone, J. Measurement of the elastic properties and intrinsic strength of monolayer graphene. *Science (1979)* **321**, 385–388 (2008).
19. Jin, J., Rafiq, R., Gill, Y. Q. & Song, M. Preparation and characterization of high performance of graphene/nylon nanocomposites. *Eur Polym J* **49**, 2617–2626 (2013).
20. Li, C., Xiang, M. & Ye, L. Intercalation structure and highly enhancing tribological performance of monomer casting nylon-6/graphene nano-composites. *Compos Part A Appl Sci Manuf* **95**, 274–285 (2017).
21. Zhuang, Y. F. *et al.* Monomer casting nylon/graphene nanocomposite with both improved thermal conductivity and mechanical performance. *Compos Part A Appl Sci Manuf* **120**, 49–55 (2019).
22. Perumal, S., Atchudan, R. & Cheong, I. W. Recent Studies on Dispersion of Graphene–Polymer Composites. *Polymers (Basel)* **13**, 2375 (2021).
23. Sanes, J., Sánchez, C., Pamies, R., Avilés, M.-D. & Bermúdez, M.-D. Extrusion of polymer nanocomposites with graphene and graphene derivative nanofillers: An overview of recent developments. *Materials* **13**, 549 (2020).
24. Yu, X., Dong, X., Song, Z. & Gui, J. Fabrication of polyamide 6 nanocomposites reinforced by the exfoliated graphene. *Plastics, Rubber and Composites* **49**, 281–288 (2020).
25. Vasiljević, J. *et al.* Characterization of polyamide 6/multilayer graphene nanoplatelet composite textile filaments obtained via in situ polymerization and melt spinning. *Polymers (Basel)* **12**, 1787 (2020).
26. Kashani Rahimi, S. & Otaigbe, J. U. Polyamide 6 nanocomposites incorporating cellulose nanocrystals prepared by In situ ring-opening polymerization: Viscoelasticity, creep behavior, and melt rheological properties. *Polym Eng Sci* **56**, 1045–1060 (2016).
27. Meng, F. *et al.* In situ intercalation polymerization approach to polyamide-6/graphite nanoflakes for enhanced thermal conductivity. *Compos B Eng* **117**, 165–173 (2017).
28. Xiang, M., Li, C. & Ye, L. In situ synthesis of monomer casting nylon-6 / reduced graphene oxide nanocomposites : Intercalation structure and electrically conductive properties. *Journal of Industrial and Engineering Chemistry* **50**, 123–132 (2017).

29. Lagarinhos, J., Santos, L. & Oliveira, J. Effect of Catalyst and Activator on Properties of Polyamide 6 Prepared by Thermoplastic Resin Transfer Molding Technology. *J Mater Eng Perform* **31**, 7098–7103 (2022).
30. Lagarinhos, J. & Oliveira, M. *Dispersibility of Graphene Nanoplatelets in ε-Caprolactam* . (2023).
31. Cartledge, H. C. Y. & Baillie, C. A. Studies of microstructural and mechanical properties of nylon/glass composite Part I The effect of thermal processing on crystallinity, transcrystallinity and crystal phases. *J Mater Sci* **34**, 5099–5111 (1999).
32. Zhang, X., Fan, X., Li, H. & Yan, C. Facile preparation route for graphene oxide reinforced polyamide 6 composites via in situ anionic ring-opening polymerization. *J Mater Chem* **22**, 24081–24091 (2012).
33. Gong, L., Yin, B., Li, L. P. & Yang, M. B. Nylon-6/Graphene composites modified through polymeric modification of graphene. *Compos B Eng* **73**, 49–56 (2015).
34. Mayoral, B. *et al.* Melt processing and characterisation of polyamide 6/graphene nanoplatelet composites. *RSC Adv* **5**, 52395–52409 (2015).
35. Patole, A. S. *et al.* A facile approach to the fabrication of graphene/polystyrene nanocomposite by in situ microemulsion polymerization. *J Colloid Interface Sci* **350**, 530–537 (2010).
36. Gu, J. *et al.* Thermal conductivities, mechanical and thermal properties of graphite nanoplatelets/polyphenylene sulfide composites. *RSC Adv* **4**, 22101–22105 (2014).
37. Cui, Y., Kundalwal, S. I. & Kumar, S. Gas barrier performance of graphene/polymer nanocomposites. *Carbon N Y* **98**, 313–333 (2016).
38. Wang, J., Song, F., Ding, Y. & Shao, M. The incorporation of graphene to enhance mechanical properties of polypropylene self-reinforced polymer composites. *Mater Des* **195**, 109073 (2020).
39. Fu, S.-Y., Feng, X.-Q., Lauke, B. & Mai, Y.-W. Effects of particle size, particle/matrix interface adhesion and particle loading on mechanical properties of particulate–polymer composites. *Compos B Eng* **39**, 933–961 (2008).

Chapter 5

Development of an automotive component prototype – a case study

This chapter is dedicated to the design and development of an automotive prototype. It culminates with the outcomes presented in the preceding chapters.

5.1 Development of an automotive component prototype – a case study

Joana Lagarinhos[1,2] and Martinho Oliveira[1,2]

[1]EMaRT Group – Emerging: Materials, Research, Technology, School of Design, Management and Production Technologies, University of Aveiro, Estrada do Cercal 449, 3720-509 Oliveira de Azeméis, Portugal

[2]CICECO – Aveiro Institute of Materials, University of Aveiro, Campus Universitário de Santiago, 3810-193 Aveiro, Portugal

To be submitted to Journal of Thermoplastic Composite Materials

Abstract

The study and development of Thermoplastic Resin Transfer Moulding (T-RTM) technology at an industrial scale are necessary for an efficient and high-volume production adapted for the automotive industry. A specific car body component was selected as the target part for this study.

Polyamide 6 (PA6) and PA6 reinforced graphene nanoplatelets (GNP) at 0.5 wt.% were prepared using T-RTM prototype equipment. The selection of these formulations was based on previous investigations aimed at optimizing the material concentrations and processing conditions, as well as the thermal and mechanical properties. This work also demonstrates the importance of key parameters, such as temperature and pressure, in achieving high quality parts.

A preliminary assessment of the environmental impact of the finished parts was also carried out. The results showed that parts produced by T-RTM technology had a lower environmental impact in 11 of the 16 categories assessed. Overall, the results of this work demonstrated the potential of these materials in automotive applications.

Keywords

Polyamide 6; thermoplastics; T-RTM technology; graphene nanoplatelets; three-dimensional parts; automotive industry

Contributions

The author had contributed to the planning and execution of all the experiments and procedures presented herein, as well as on the discussion, interpretation, and preparation manuscript. Martinho Oliveira contributed to the conceptualization, review and editing of the data presented.

1. Introduction

The automotive industry has undergone a significant transformation in terms of the materials used in its structural components. From a dependence on traditional metals, the modern automotive landscape has embraced new lightweight solutions. This shift has been driven primarily by stringent environmental regulations that aim to reduce weight in order to improve fuel efficiency and meet regulatory standards[1,2]. To meet these requirements, automotive manufacturers are exploring various strategies, one of which is to replace traditional materials with plastics. This strategic shift offers benefits such as reduced weight, ease of processing and corrosion resistance, all of which are highly desirable attributes for automotive components. Moreover, rapid production cycles are essential to meet the high volume requirements of the automotive sector[3]. Robust materials that can withstand substantial impact loads are required for the automotive industry. High molecular weight thermoplastics generally offer greater toughness than thermosets. Consequently, the use of such thermoplastics as matrix materials in composites is expected to provide improved resistance to impact damage. In addition, improved energy absorption over an extended period of time can reduce the deceleration forces of projectiles, thereby reducing the potential for injury to vehicle occupants[4].

Recent advances in reactive processing have paved the way for the liquid moulding of thermoplastic composites[5,6]. Among the many technologies available for the production of thermoplastic materials, Thermoplastic Resin Transfer Moulding (T-RTM) has emerged as a promising technique[3,7]. This method allows the production of materials with shorter production cycles compared to traditional resin transfer moulding (RTM) methods. T-RTM is characterized by a rapid anionic polymerization reaction being suited to the required mass production of lightweight materials for this high-demand market[3,7–12]. In the literature, there are several studies that have investigated the development of polyamide 6 (PA6) using an industrial approach by anionic ring-opening polymerization (AROP)[3,7,13–15]. These studies have investigated the effects of catalyst and activator dosages, as well as the parameters of the moulding process. However, these studies have predominantly used a two-dimensional mould shape, similar to a plate. The mould plays a key role in defining both the geometry and the quality of the final parts. A recent paper by Boros and co-workers[13] extensively investigated the design concept of a T-RTM mould. However, this work mainly presented a theoretical and conceptual mould design, which was characterized by its adaptability to different features (neat polymer parts, fibre-reinforced composites, or sandwich structures) and thicknesses (ranging from 2 to 12 mm). However, to effectively address the specific requirements of typical automotive applications, a mould with distinct geometries and shapes is essential. To the best of our knowledge, there has been few studies focusing on three-dimensional (3D) mould geometries. Moreover, the evaluation of the final properties of the produced parts using 3D moulds for automotive components is an unexplored facet within the field of AROP.

The main goal and motivation of the current case study is to investigate the feasibility of producing a 3D part using both PA6 and PA6 reinforced with graphene nanoplatelets (GNP). This investigation aims to bridge the existing gap in research regarding 3D mould shapes and their

potential applicability in the field of automotive parts production. To achieve these goals, a careful part selection process was undertaken, focusing on a structural body component that meets the key requirements of the automotive industry. The chosen component is the side impact reinforcement located under the car seat, an area that requires robust structural integrity and effective energy absorption capabilities. The target component (Figure 5.1) was selected with the support of Simoldes Plásticos.

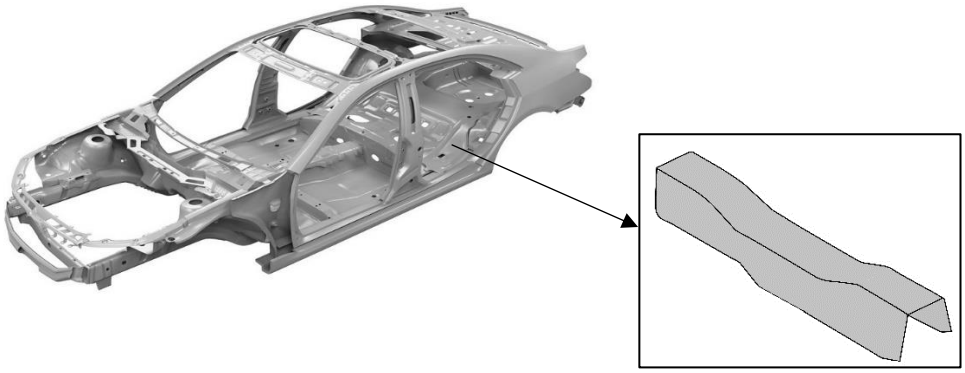

Figure 5.1. From seat rear cross member component.

In parallel, a comprehensive explanation of the concept and design of the 3D T-RTM mould was provided. The key findings are presented, with the choice of parameters for this case study based on previous optimization studies. In addition to these aspects, this study also seeks to provide a comparative preliminary environmental analysis between T-RTM and traditional RTM technologies. This comparative study analyses the potential of thermoplastic composites as opposed to thermoset parts. This comprehensive analysis aims to provide valuable insights for both the automotive industry's optimization of structural components and a wider understanding of the environmental impact of these manufacturing processes.

2. T-RTM mould – the concept and specifications

The design process was driven by the goal of simplification, taking into account a number of key factors such as weight considerations, ease of processability, ease of assembly, and compliance with mechanical specifications. Based on these factors, the part shown in Figure 5.1 was modified and the geometry shown in Figure 5.2 was defined. This design process resulted in the definition of a U-shaped geometry characterized by a uniform thickness of 2mm.

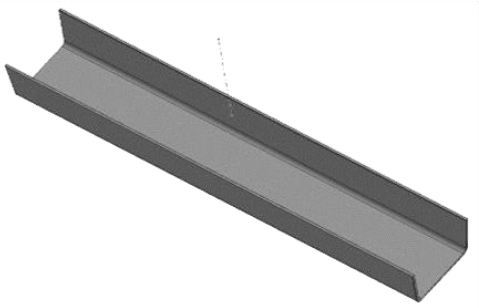

Figure 5.2. Final target geometry.

The mould has a cavity with a U-shaped geometry, as shown in Figure 5.3. The mould was machined from two aluminium blocks, each measuring 450 mm x 400 mm x 40 mm.

The choice of aluminium as the mould material was primarily driven by practical considerations, including cost-effectiveness, ease of machinability, and its relatively lighter weight compared to steel. In addition, aluminium has a high thermal conductivity, which meets the requirements of the moulding process.

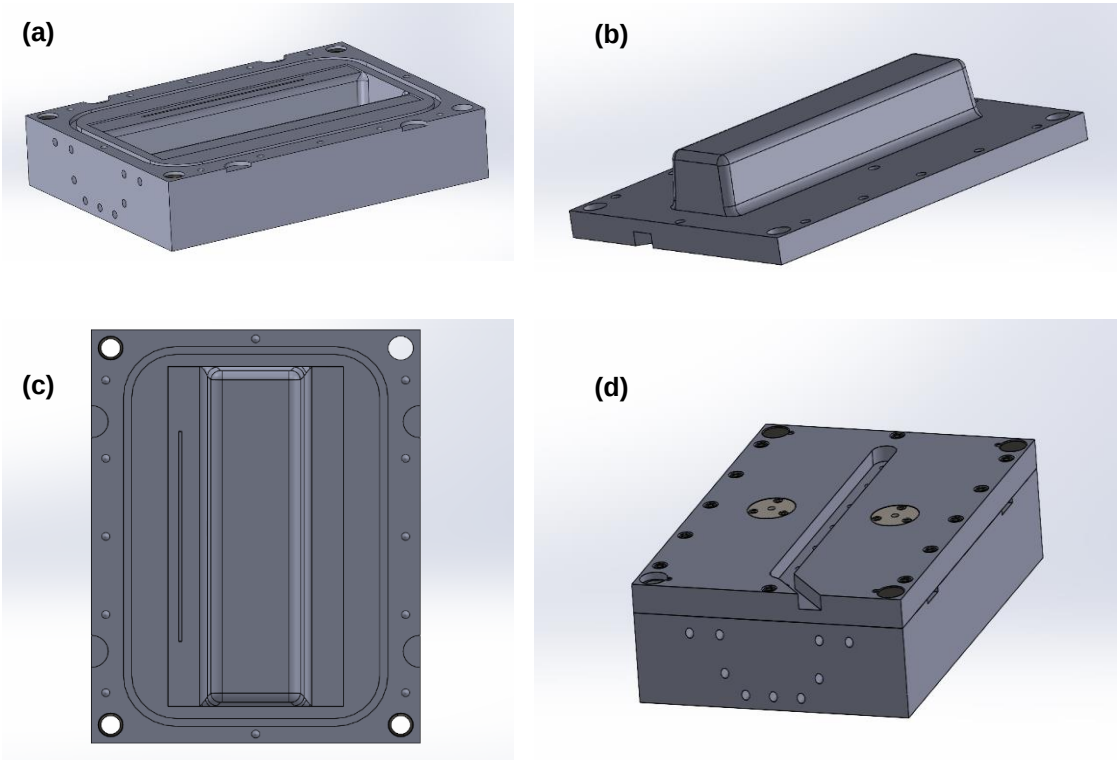

Figure 5.3. Mould geometry **(a)** Lower part; **(b)** upper part; **(c)** detail lower part and **(d)** general view.

The injection point is strategically placed in the centre of one of the side flaps of the upper part of the mould to improve process stability. To facilitate easy demoulding, the inlet and outlet holes have been angled to allow easy removal of the runners alongside the parts. To ensure consistent and uniform heating, the placement of temperature resistors was carefully arranged throughout the mould. Cartridge resistances were thoughtfully distributed with 18 in the lower mould part and 7 in the upper mould part.

Given the elevated temperature range used during the polymerization reaction (150-160ºC), perfluoroalkoxy (PFA) and silicone rubber (VMQ) seals were selected for their ability to function effectively in environments reaching temperatures of approximately 300ºC. To secure the mould closure, a total of 12 screws were meticulously positioned across the mould, complemented by four guides strategically placed at the corners to ensure accurate alignment and closure of the mould components.

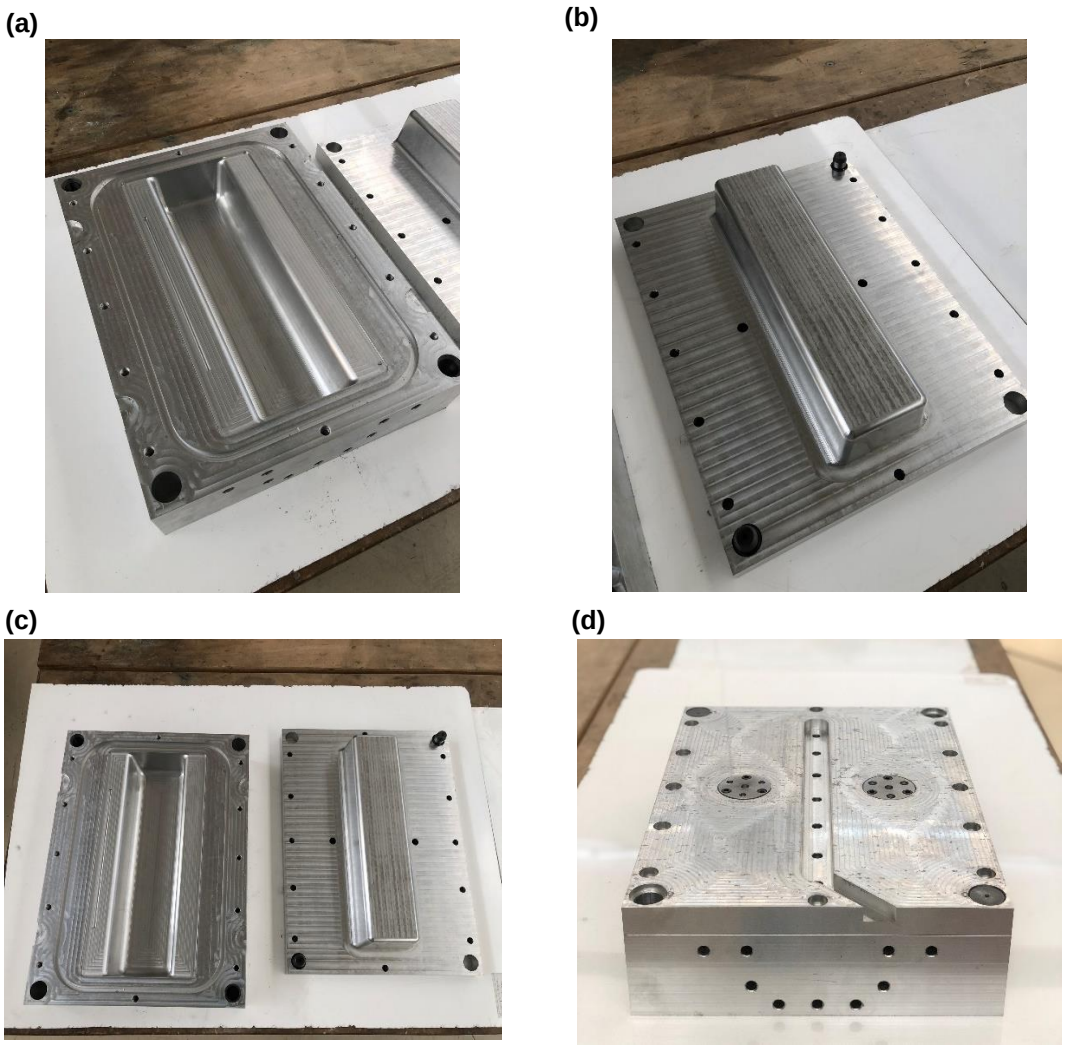

Figure 5.4. Final aluminium mould **(a)** Lower part; **(b)** upper part; **(c)** both parts and **(d)** general view.

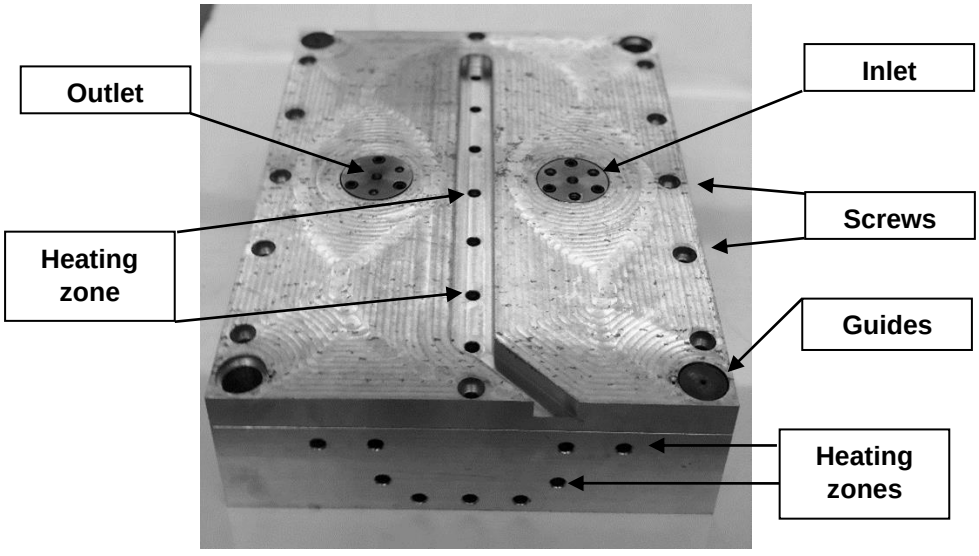

Figure 5.5. Final prototype mould.

The mould shown in Figure 5.5 has a total weight of 50 kg, of which the upper part weighs 36 kg and the lower part 14 kg. The dimensions of the mould are 455 mm in length, 345 mm in width and 120 mm in height.

3. Methodology

3.1. Materials

The ε-CL monomer (AP-NYLON® caprolactam) was used together with Bruggolen® C10 as catalyst and Bruggolen® C20P as activator for the AROP of PA6[16,17]. These materials were purchased from L. Brüggemann GmbH and Co. KG, Germany. Graphene nanoplatelets (GNP) with two different particle sizes, namely 0.5-1 μm (referred to as GN) and 1-2 μm (referred to as GP), were purchased from NanoXplore in Canada.

3.2. PA6 and PA6/GNP preparation

The formulation procedure for preparing PA6 and PA6/GNP used in this case study has been previously reported elsewhere[16,18]. AP/GNP formulations with 0.5 wt.% GN (AP/GN) and 0.5 wt.% GP (AP/GN) were selected. The choice of these specific formulations was based on the thermal and mechanical characterizations already reported in previous studies[17].

3.3. T-RTM parameters

Samples were prepared using the T-RTM laboratory equipment developed inhouse. T-RTM parameters used in this case study are presented in Table 5.1:

Table 5.1. Parameters used on T-RTM experiments.

Dosing unit temperature (ºC)	90
Dosing volume (g)	350
Mould temperature (ºC)	160
Polymerization time (min)	6
Pressure (bar)	3

The mould temperature and pressure were defined based on previous experiments[16,19]. The polymerization time was set at 6 minutes, instead of 2 minutes[19] as this is insufficient to polymerize the higher amount of material required to fill the three-dimensional mould. The volume of the mould cavity was used to calculate the dosage of material to be injected.

3.4. Mechanical analyses

Tensile tests were performed using a Shimadzu AG-IS 10 kN universal testing machine at a constant crosshead speed of 1 mm·min^{-1}. The tests were performed in accordance with ISO 527-2 (Type 1BA). Standard specimens of both PA6 and PA6/GNP were cut from the parts produced in the 3D T-RTM mould[19]. The elongation of each specimen was measured using video extensometer (Shimadzu DVE 101/201) in a range of 25 mm. For flexural tests, samples were

prepared according to ISO 178 with a span of 32 mm. The tests were performed at a room temperature with a constant crosshead speed of 1 mm·min^{-1} was used for all specimens.

A minimum of five specimens (from 3 different parts) were tested for each composition, for both tensile and flexural tests.

3.5. Preliminary environmental impact analysis

A preliminary environmental impact analysis was conducted using The Eco Impact Calculator 2023[20]. The relevant background datasets were taken from SimaPro 9.3.0.3 software databases, using reference data from Ecoinventoin[21], the European reference Life Cycle Database (ELCD)[22] and those developed by Plastics Europe[23]. This tool calculates the environmental factors related to the production of composite parts during the "*cradle to gate*" phase, which includes the production of raw materials, the transportation to the manufacturer and the component production. Two different manufacturing scenarios (shown in Figure 5.6) were considered:

a) Scenario 1: Production of PA6 using the T-RTM technology. In this scenario, the final part is produced using a low viscosity thermoplastic via T-RTM technology.

b) Scenario 2: Production of epoxy resin using resin transfer moulding (RTM) technology. This type of thermoset resin is not recyclable and can contribute to landfill waste[24,25].

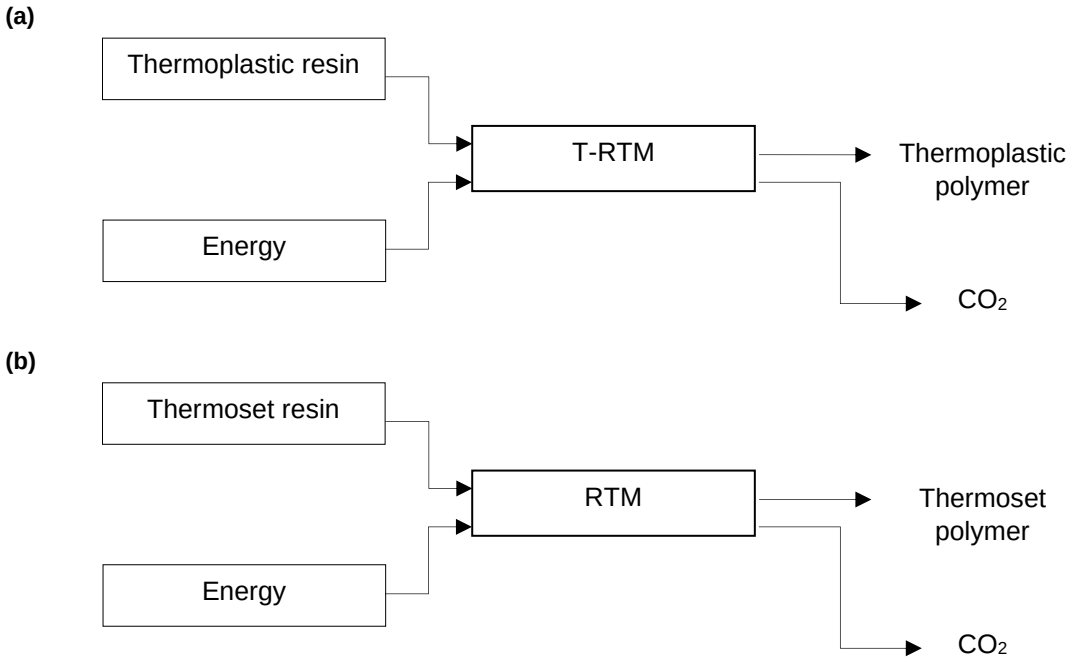

Figure 5.6. System boundary considered for **(a)** T-RTM and **(b)** RTM to polymer production.

The main inputs in the Eco Impact Calculator were the manufacturing process and the material formulation, including the type and amount of the raw materials used to produce the final component matrix composition, whether thermoplastic or thermoset resin. The quantities of raw materials, which include the monomer, activator, and catalyst, have been determined based on the tests performed. The final weight of the thermoplastic part was 0.250 kg. Since epoxy resin

has a slightly higher density (1.25 g·cm^{-3}) than PA6 (1.14 g·cm^{-3}), it was assumed that the part produced with epoxy resin would have a proportionally higher weight (as shown in Table 5.2). The datasets used for the two different processes were set as default (energy and streams).

Table 5.2. Inventory data of both scenarios used for the calculations.

Scenarios	Materials	Quantity
T-RTM	Thermoplastic part – PA6	250 g
RTM	Thermoset part – Epoxy resin	274 g

* Quantity values have been calculated on the assumption of the same final mould volume.

4. Results and Discussion

4.1. Processing trials

The produced 3D parts using the T-RTM equipment can be seen in Figures 5.7 to 5.10. From Figure 5.7 and 5.8, that corresponds to the trials involving PA6 and PA6/GN, respectively, it becomes evident that the injection pressure applied (3 bar) was insufficient to completely fulfil the mould cavity. Voids and defects are present. Previous studies by Shaharuddin *et al.*[26] and Bright at *al.*[27] have highlighted the importance of injection pressure and speed as key parameters affecting the quality of the final parts. Therefore, it is recommended higher injection speeds and pressures to achieve complete parts with dimensional accuracy.

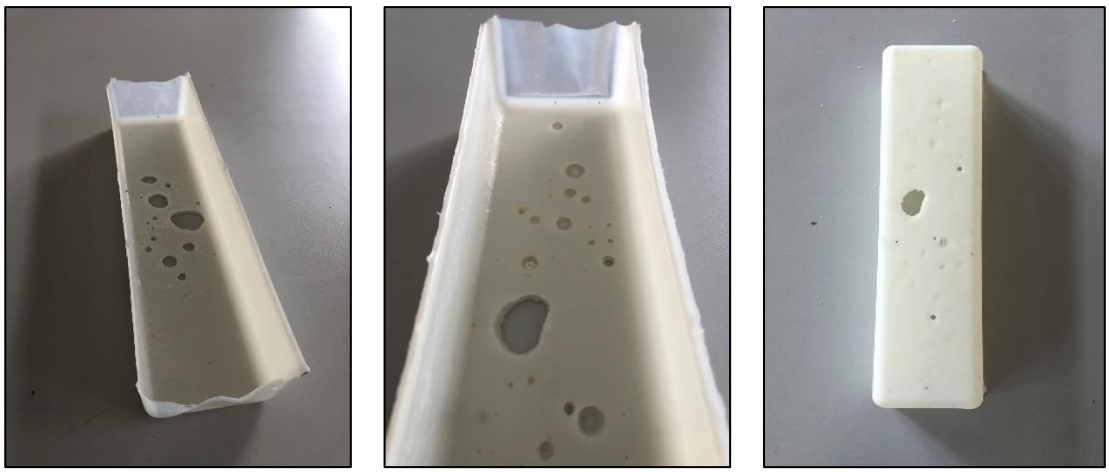

Figure 5.7. PA6 samples produced by T-RTM using 3 bar injection pressure.

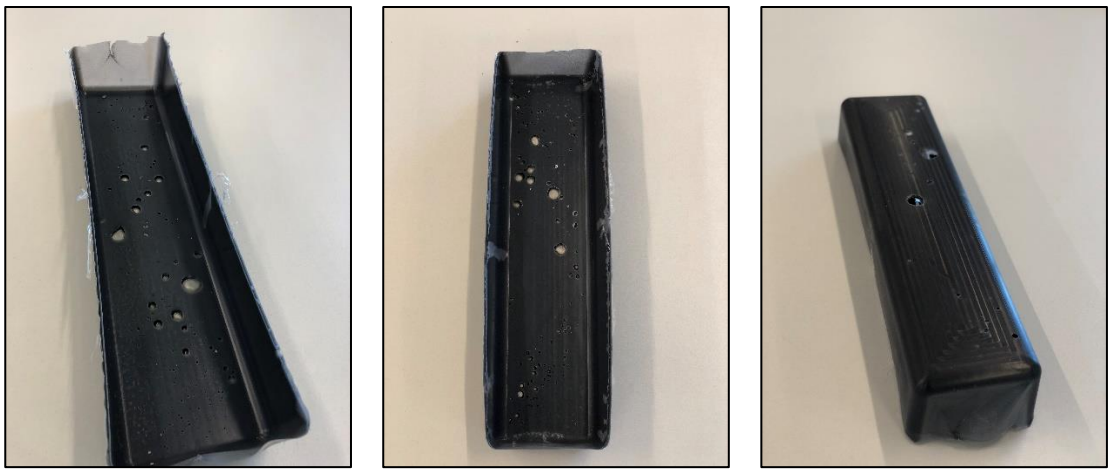

Figure 5.8. PA6/GN samples produced by T-RTM using 3 bar injection pressure.

Several studies were conducted to overcome the challenges observed in the previous figures. In this sense, the injection pressure was systematically varied until a complete part is reached. The injection pressure was then increased to 5 bar, which is the maximum allowable pressure for the prototype T-RTM equipment used in the study. Figures 5.9 and 5.10 provide a clear evidence that the mould cavity was almost completely filled at the increased injection pressure of 5 bar.

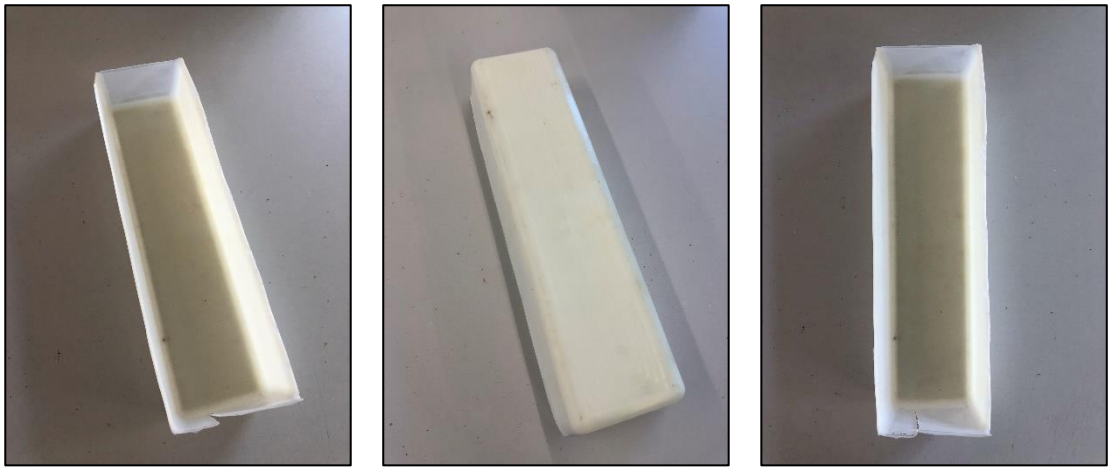

Figure 5.9. PA6 samples produced by T-RTM using 5 bar injection pressure.

Figure 5.10. PA6/GN samples produced by T-RTM using 5 bar injection pressure.

4.2. Mechanical and morphological analyses

However, despite the limitations of the equipment, the mechanical properties of the samples obtained at 5 bar, were evaluated by tensile and flexural tests. The results are summarized in Table 5.3:

Table 5.3. Mechanical properties.

		Samples		
		PA6	**PA6/GN**	**PA6/GP**
Tensile	**σ (MPa)**	58.9 ± 1.8	78.1 ± 6.6	68.8 ± 4.0
	ε (%)	8.1 ± 3.7	23.8 ± 2.4	19.3 ± 2.3
	E (GPa)	3.1 ± 0.1	4.2 ± 0.3	3.4 ± 0.3
Flexural	**σ (MPa)**	101.1 ± 5.0	188.3 ± 9.8	137.6 ± 6.2
	ε (%)	7.0 ± 0.3	7.4 ± 0.1	7.2 ± 0.3
	E (GPa)	2.4 ± 0.3	4.9 ± 0.6	3.5 ± 0.2

Tensile strength and Young's modulus increased with the addition of GNP. The PA6/GN showed an increase of 33% in tensile strength and 35% in Young modulus compared to PA6. The PA6/GP showed an increase of 17% in tensile strength and 9% in Young modulus. This observation in tensile strength and modulus with the addition of GNP could be attributed to the uniform dispersion of the nanoplatelets within the polymer matrix, resulting in an effective stress transfer between the polymer matrix and the nanofiller[28,29]. In addition, PA6/GN samples showed improved tensile and modulus parameters compared to PA6/GP. These results showed that the size of the graphene flakes can significantly affect the tensile strength of the composites, as observed in a previous study[17]. As shown in Table 5.3, a significant increase in elongation at break was observed with the addition of GNP to the polymer matrix. This increase was interpreted by considering that the dispersed GNP in PA6 may prevent premature fracture of the specimen and may also mean that the GNP behaved as a reinforcement in the PA6 matrix.

Regarding the flexural results, it can be observed that the flexural strength increases with the addition of GNP, from 101.1 to 188.3 and 137.6 MPa for PA6/GN and PA6/GP respectively. The influence of GNP was again more noticeable in PA6/GN samples than in PA6/GP, showing that GN is more effective in reinforcing the polymer than GP[17].

The results presented in Table 5.3 show a good agreement between the tensile and flexural results of the 3D parts and those documented in previous studies for 2D shaped samples[17,18].

In general, it can be concluded that the three-dimensional mould geometry does not have a significant influence on the mechanical properties of the final parts. However, it is important to recognise that certain improvements need to be made in the future.

4.3. Preliminary environmental impact

Each scenario's results were evaluated using two distinct methods: greenhouse gas protocol (GHG) V1.01/CO_2 eq (kg) and cumulative energy demand V1.09/CED (MJ). The GHG metric quantifies the carbon footprint associated with each production process. This measure focuses on the emissions and removals generated over the life cycle of a product, excluding any actions taken to mitigate or avoid emissions, and is expressed in kilograms of carbon dioxide equivalent. On the other hand, Cumulative Energy Demand (CED) represents the total use of energy resources throughout the life cycle, including both renewable and non-renewable energy sources. This indicator is expressed in megajoules[30].

Figure 5.11 shows the results of the Eco Impact Calculator. The data show a lower carbon footprint associated with the use of the RTM process compared to T-RTM. This finding can be explained by the historical use and refinement of equipment optimized for thermosets, which may not be fully adaptable to the unique characteristics of thermoplastics.

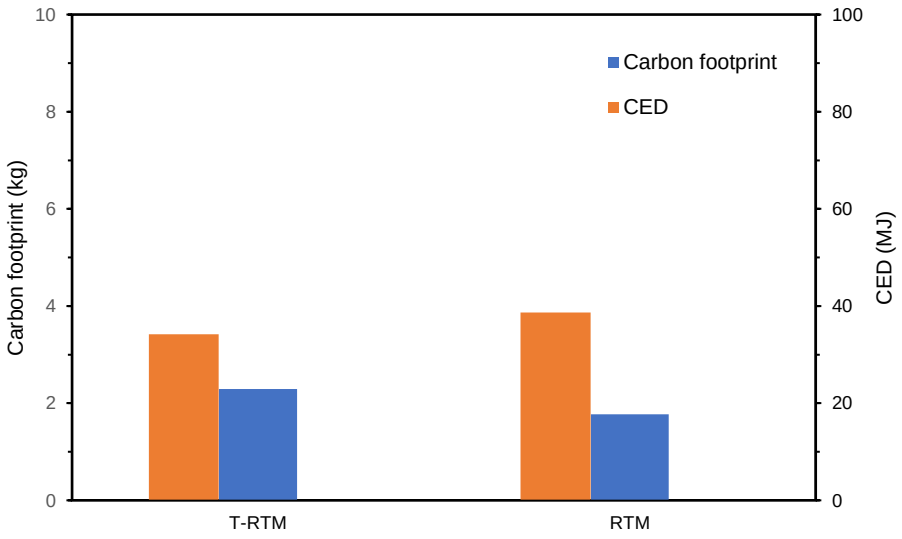

Figure 5.11. Environmental impact results of two materials obtained through different scenarios.

These emissions can be categorized according to different environmental impact categories since the pollutant emissions resulting from the production of the selected part were identified.

Each impact category highlights the specific environmental impact of individual pollutant emissions[31]. The summary of information on the total impact of each process is summarized in Table 5.4.

The data analysis shows that the thermoplastic part, produced by T-RTM, has a lower environmental impact in 11 of the 16 impact categories assessed. However, it is worth noting that the impact categories where the thermoplastic part has a higher impact include ionizing radiation, freshwater eutrophication, land use and mineral fossil and ren resource depletion. These differences in impact, while significant, are primarily due to the current non-optimized recycling process.

Table 5.4. Summary of the impact of the final target obtained through the two processes.

Impact category	Unit	T-RTM	RTM
Climate change	kg CO_2 eq	2.26	1,73
Ozone depletion	kg CFC^{-11} eq	9,48 x 10^{-9}	2,55 x 10^{-7}
Human toxicity (non-cancer effects)	CTUh	2,07 x 10^{-8}	1,81 x 10^{-7}
Human toxicity (cancer effects)	CTUh	1,58 x 10^{-8}	3,12 x 10^{-8}
Particulate matter	kg PM2.5 eq	8,96 x 10^{-4}	1,05 x 10^{-3}
Ionizing radiation HH	kBq U235 eq	9,16 x 10^{-3}	6,40 x 10^{-2}
Ionizing radiation E (interim)	CTUe	7,11 x 10^{-8}	5,12 x 10^{-7}
Photochemical ozone formation	kg NMVOC eq	4,75 x 10^{-3}	4,78 x 10^{-3}
Acidification	mol H^+ eq	9,44 x 10^{-3}	8,17 x 10^{-3}
Terrestrial eutrophication	mol N eq	1,96 x 10^{-2}	1,56 x 10^{-2}
Freshwater eutrophication	kg P eq	6,13 x 10^{-5}	6,36 x 10^{-5}
Marine eutrophication	kg N eq	2,83 x 10^{-3}	1,40 x 10^{-3}
Freshwater ecotoxicity	CTUe	1,01	3,54
Land use	Kg C deficit	1,84 x 10^{-1}	1,81
Water resource depletion	m^3 water eq	3,06 x 10^{-3}	9,04 x 10^{-3}
Mineral, fossil and ren resource depletion	kg Sb eq	2,00 x 10^{-5}	4,15 x 10^{-5}

It is important to note that the analysis carried out in this study focuses exclusively on the raw material sourcing and transformation stages leading to the final product . The life cycle phase of the product has been excluded from this analysis, in particular to the final disposal phase. A closer look at the disposal phase reveals the cyclic nature of the materials used, and this comparison between thermoset and thermoplastic resins might potentially favour thermoplastics.

Thermoplastic resins provide a significant advantage in recyclability owing to their reversible melting process. This inherent characteristic makes them more accessible for recycling when compared to thermosetting matrices[32]. This facilitates the continued use of these materials across various contexts, reducing the demand for new resources[33]. In contrast, recycling thermosetting matrices is energy-intensive due to their irreversible curing process. Despite this limitation, thermosetting composites often show greater durability, particularly in specific applications, potentially resulting in a longer lifespan compared to thermoplastics[34,35]. However, it is important to recognise that the thermal decomposition of thermosetting materials can be problematic, potentially releasing harmful compounds, thereby introducing a significant environmental consideration[36].

In summary, the selection between thermoplastic and thermosetting matrices demands a critical equilibrium of recyclability, energy efficiency, mechanical characteristics, and environmental effects. Each type offers unique benefits and challenges, requiring a comprehensive assessment based on the precise needs and concerns of the intended application and overall sustainability objectives. Furthermore, the study does not consider the potential environmental impacts associated with the inclusion of GNP. The lack of a significant number of specific datasets on GNP makes it difficult to compile consistent and reliable data for an inventory of this process.

5. Conclusions

This case study focused on a specific automotive component located underneath the car seats. The objective was to design and develop a 3D concept mould suitable for T-RTM technology. This mould was designed to enable the production of both pure polymer parts and reinforced polymer parts.

The results demonstrated the successful production of 3D parts. However, it became apparent that higher injection pressures were essential to achieve complete and well-formed parts. Despite this, the mechanical properties of the parts were not significantly affected by the three-dimensional mould geometry. The mechanical results obtained with the three-dimensional shape were comparable to those obtained with a two-dimensional shape, suggesting that mould geometry does not significantly affect mechanical properties.

A preliminary environmental impact assessment was also carried out for two different production scenarios. The data showed a lower carbon footprint associated with the use of the RTM process compared to T-RTM. However, it is important to note that the process conditions for RTM are already well defined, whereas the process conditions for T-RTM are still at the optimization stage (pilot scale). Nevertheless, the thermoplastic part produced by T-RTM had a lower environmental impact in 11 of the 16 categories assessed.

This case study not only provides a pioneering exploration of the use of 3D moulds and the use of GNP as a reinforcement phase, but also lays the groundwork for future industrial solutions. It adds a 3D approach to the limited existing literature on T-RTM technology. In addition, the trials conducted provide valuable insights for an industrial perspective, identifying key challenges and barriers in the industrialisation process and suggesting potential strategies to overcome these challenges.

Acknowledgements

The authors would like to acknowledge the partial financial support from Simoldes Plásticos, S.A. This work was developed within the scope of the project CICECO-Aveiro Institute of Materials, UIDB/50011/2020, UIDP/50011/2020 & LA/P/0006/2020, financed by national funds through the FCT/MEC (PIDDAC). Authors would also want to knowledge Helder Morais and Ricardo Torcato for mould design and assembly.

References

1. Mallick, P. K. Thermoplastics and thermoplastic–matrix composites for lightweight automotive structures. in *Materials, design and manufacturing for lightweight vehicles* 187–228 (Elsevier, 2021).
2. Mallick, P. K. Advanced materials for automotive applications: An overview. *Advanced materials in automotive engineering* 5–27 (2012).
3. Ageyeva, T., Sibikin, I. & Karger-Kocsis, J. Polymers and related composites via anionic ring-opening polymerization of lactams: Recent developments and future trends. *Polymers (Basel)* **10**, 357 (2018).
4. Pradeep, S. A., Iyer, R. K., Kazan, H. & Pilla, S. Automotive applications of plastics: past, present, and future. in *Applied Plastics Engineering Handbook* 651–673 (Elsevier, 2017).
5. Murray, J. J., Robert, C., Gleich, K., McCarthy, E. D. & Brádaigh, C. M. Ó. Manufacturing of unidirectional stitched glass fabric reinforced polyamide 6 by thermoplastic resin transfer moulding. *Mater Des* **189**, 108512 (2020).
6. Murray, J. J. *et al.* Thermoplastic RTM: Impact Properties of Anionically Polymerised Polyamide 6 Composites for Structural Automotive Parts. *Energies (Basel)* **14**, 5790 (2021).
7. Semperger, O. V. & Suplicz, A. The Effect of the Parameters of T-RTM on the Properties of Polyamide 6 Prepared by in Situ Polymerization. *Materials* **13**, 4 (2020).
8. Maazouz, A., Lamnawar, K. & Dkier, M. Chemorheological study and in-situ monitoring of PA6 anionic-ring polymerization for RTM processing control. *Composites Part A* **107**, 235–247 (2018).
9. Höhne, C. *et al.* Hexaphenoxycyclotriphosphazene as FR for CFR anionic PA6 via T-RTM : a study of mechanical and thermal properties. *Fire Mater* **41**, 291–306 (2016).
10. Wu, B., Gong, Y. & Yang, G. Non-isothermal crystallization of polyamide 6 matrix in all-polyamide composites: Crystallization kinetic, melting behavior, and crystal morphology. *J Mater Sci* **46**, 5184–5191 (2011).
11. Ben, G. & Sakata, K. Fast fabrication method and evaluation of performance of hybrid FRTPs for applying them to automotive structural members. *Compos Struct* **133**, 1160–1167 (2015).
12. Laurenzi, S. & Marchetti, M. Advanced composite materials by resin transfer molding for aerospace applications. in *Composites and their properties* 197–226 (IntechOpen, 2012).

13. Boros, R., Sibikin, I., Ageyeva, T. & Kovács, J. G. Development and Validation of a Test Mold for Thermoplastic Resin Transfer Molding of Reactive PA-6. *Polymers (Basel)* **12**, 976 (2020).
14. Wilhelm, M., Wendel, R., Aust, M., Rosenberg, P. & Henning, F. Compensation of water influence on anionic polymerization of ε-caprolactam: 1. Chemistry and experiments. *Journal of Composites Science* **4**, 7 (2020).
15. Rijswijk, K. Van, Bersee, H. E. N., Jager, W. F. & Picken, S. J. Optimisation of anionic polyamide-6 for vacuum infusion of thermoplastic composites : choice of activator and initiator. *Compos Part A Appl Sci Manuf* **37**, 949–956 (2006).
16. Lagarinhos, J., Santos, L. & Oliveira, J. Effect of Catalyst and Activator on Properties of Polyamide 6 Prepared by Thermoplastic Resin Transfer Molding Technology. *J Mater Eng Perform* **31**, 7098–7103 (2022).
17. Joana Lagarinhos & Martinho Oliveira. The effect of graphene-based materials in polyamide 6 obtained by in situ thermoplastic resin transfer moulding (T-RTM) polymerization. in *Proceedings 20th European Conference on Composite Materials - Composites Meet Sustainability* 152–159 (Lausanne, 2022).
18. Lagarinhos, J., Magalhães da Silva, S. & Martinho Oliveira, J. Non-Isothermal Crystallization Kinetics of Polyamide 6/Graphene Nanoplatelets Nanocomposites Obtained via In Situ Polymerization: Effect of Nanofiller Size. *Polymers (Basel)* **15**, (2023).
19. Lagarinhos, J., Magalhaes, S. & Oliveira, M. *Optimization of Processing Conditions in Thermoplastic Resin Transfer Moulding for PA6 Production*. (2023).
20. EuCIA 2023. Eco Impact Calculator. http:// ecocalculator.eucia.eu/ - Accessed on 03/10/2023.
21. Weidema, B. P. *et al.* Overview and methodology: Data quality guideline for the ecoinvent database version 3. (2013).
22. European Commission. International Reference Life Cycle Data System (ILCD) handbook: Framework and requirements for life cycle impact assessment models and indicators. (2010).
23. Plastics Europe. Plastics Europe 2022. https://plasticseurope.lca-data.com/.
24. Kaynak, C. & Kas, Y. O. Effects of Injection Pressure in Resin Transfer Moulding (RTM) of Woven Carbon Fibre/Epoxy Composites. *Polymers and Polymer Composites* **14**, 55–64 (2006).
25. Robertson, F. C. Resin transfer moulding of aerospace resins—a review. *British Polymer Journal* **20**, 417–429 (1988).
26. Shaharuddin, S. I. S. & Salit, M. S. A review of the effect of moulding parameters on the performance of polymeric composite injection moulding. *Turkish Journal of Engineering and Environmental Sciences* **30**, 23–34 (2006).
27. Bright, P. F. & MW, D. Factors influencing fibre orientation and mechanical properties in fibre reinforced thermoplastics injection mouldings. (1981).
28. Gaska, K., Xu, X., Gubanski, S. & Kádár, R. Electrical, Mechanical, and Thermal Properties of LDPE Graphene Nanoplatelets Composites Produced by Means of Melt Extrusion Process. *Polymers (Basel)* **9**, 11 (2017).
29. El Achaby, M. *et al.* Mechanical, thermal, and rheological properties of graphene-based polypropylene nanocomposites prepared by melt mixing. *Polym Compos* **33**, 733–744 (2012).
30. Scheepens, A., van der Flier, A., Romeo-Hall, A. & Veugen, R. EuCIA Eco Impact Calculator Background Report. *EY CCaSS* (2020).
31. Sala, S., Crenna, E., Secchi, M. & Pant, R. Global normalisation factors for the environmental footprint and life cycle assessment. *Publications Office of the European Union: Luxembourg* 1–16 (2017).
32. Biron, M. Thermoplastic Composites. in *Thermoplastics and Thermoplastic Composites* 769–829 (William Andrew, 2012).

33. Jagadeesh, P. *et al.* Sustainable recycling technologies for thermoplastic polymers and their composites: A review of the state of the art. *Polym Compos* **43**, 5831–5862 (2022).
34. Post, W., Susa, A., Blaauw, R., Molenveld, K. & Knoop, R. J. I. A Review on the Potential and Limitations of Recyclable Thermosets for Structural Applications. *Polymer Reviews* **60**, 359–388 (2020).
35. Morici, E. & Dintcheva, N. Tz. Recycling of Thermoset Materials and Thermoset-Based Composites: Challenge and Opportunity. *Polymers (Basel)* **14**, 4153 (2022).
36. Ibarra, R. M. Recycling of thermosets and their composites. in *Thermosets* 639–666 (Elsevier, 2018).

Chapter 6

Concluding remarks and future perspectives

This chapter summarizes the overarching findings and outcomes of this thesis, providing a reflective analysis of the initial objectives outlined in the introductory section. Recommendations for further improvements that may be pursued in the future to address gaps in the current study, and others to improve the technology to a commercially viable manufacturing are given.

6 Concluding remarks and suggestions for future work

The main objective of this work was to develop a thermoplastic material by T-RTM, and subsequently, to introduce nanoparticles to facilitate efficient and high-volume production of automotive parts. The synthesis of PA6 and its potential for use in thermoplastic nanocomposites through reactive liquid processes has been thoroughly investigated. It is noteworthy that these objectives have been successfully addressed by achieving the objectives set out in Chapter 1.

6.1. PA6

The successful manufacturing of PA6 through AROP using laboratory prototype equipment has been achieved, resulting in PA6 with improved chemical, thermal, and mechanical properties.

The concentration of catalyst and activator, polymerization temperature and time, and atmosphere were identified as significant factors influencing polymerization.

A commercial catalyst and activator combination, C10-C20, was selected as the most suitable for T-RTM for high-rate production. The effects of different concentrations of the three reactants (monomer, catalyst, and activator) were extensively studied. Higher concentrations of activator result in a large number of chains, a lower M_η, and a slower reaction rate. Higher amounts of catalyst also promote an increase in oligomer content, which reduces the DC of the reaction. Lower concentrations of catalyst and activator will promote a higher M_η and DC, which will contribute to a higher material toughness. Faster reaction rates can also be achieved with lower concentrations of catalyst and activator. Mechanical analyses have shown that PA6 revealed the desired properties for the proposed application. The most suitable combination was 95% CL, 3% catalyst and 2% activator for a mould temperature of 160ºC during ≈5 min. The produced PA6 by T-RTM exhibited a T_m of around 217ºC and a X_c of 36%. In terms of mechanical performance, PA6 presented values of tensile and flexural strength and moduli of around ~66 and 126 MPa and 2.7 and 2.6 GPa, respectively.

A particular aspect of this process is that polymerization and crystallization occur simultaneously if the processing temperature is below the crystallization temperature. Mould temperature appears to be the most important parameter during AROP, influencing the X_c and M_v. The effect of mould temperature (between 130 ºC and 170 ºC) and polymerization time (between 2 to 10 minutes) were analysed. Samples revealed higher monomer conversion and improved thermal stability at higher mould temperatures (150 ºC and 160 ºC) compared to lower mould temperatures. In addition, the mechanical properties (tensile and flexural) were influenced by X_c and M_v. At 160 ºC, PA6 showed the best balance between the mechanical and the thermal behaviour. In the case of polymerization time, it was observed that this processing parameter did not significantly affect the thermal and mechanical performance, compared to the mould temperature. From this work, it was established a mould temperature of 160 ºC and a polymerization time of 2 minutes as the optimal processing conditions.

The potential for mass production of PA6 by T-RTM is particularly compelling for the automotive industry. The developments detailed in this thesis further enhance the application of T-RTM for future lightweight material production.

6.2 PA6/graphene-based nanocomposites

The successful incorporation of GBM into PA6 using T-RTM technology is a significant achievement with great potential for automotive applications. This development not only fills a gap in the existing literature but also promises to open up new avenues in both the scientific and industrial communities.

The objective of developing PA6/graphene-based nanocomposites was achieved by selecting two different GNP with different particle sizes, namely D90 < 50 µm (defined as GN) and D90 <70 µm (defined as GP). This approach aimed to fully understand how the structure of the GNP could affect the chemical and mechanical properties of the final nanocomposites. The results revealed that considerable progress had been made in terms of the dispersion process of the reinforcing phase. The dispersion patterns of the GNP within the polymer matrix were found to have a significant influence on the properties of the nanocomposites. To address this, a systematic study was carried out using two dispersion techniques, namely mechanical stirring and sonication. The dispersion of GNP in molten PA6 monomer by sonication was found to be an effective method of achieving a homogeneous dispersion and reducing the size of the agglomerates formed as evidenced by POM images. The results also showed that the larger size GNP required more time to achieve adequate dispersion when compared to the smaller size GNP.

The nucleation activity of GNP in PA6 during a non-isothermal crystallization process was investigated using 0.1 wt.% of GN and GP. Both GNP showed a nucleation activity of less than 1, revealing their role as surface active agents within the polymeric matrix, promoting the crystallization process. For a complete kinetic analysis, a comprehensive study was carried out to analyse the influence of GNP size on the non-isothermal crystallization behaviour of PA6/graphene-based nanocomposites. The addition of GNP increased the crystallization rate of PA6, and the GNP with a smaller diameter exhibited a faster crystallization rate when compared to the larger diameter GNP. Overall, these results are indicative that less energy is required for the crystallization to occur in the presence of GNP.

The effect of GNP size and loading rates (0.1, 0.25, 0.5, 0.75 and 1.0 wt.%) on various physicochemical properties of nanocomposites with PA6 was also evaluated. The size of the GNP also played a role in the thermal stability and mechanical properties of the samples. Nanocomposites prepared with smaller GNP exhibited superior thermal stability and mechanical performance compared to those prepared with larger size. Tensile tests showed that the incorporation of GNP resulted in a significant increase in tensile strength (21% increase over pure PA6) and Young's modulus 21% increase over pure PA6) and reaching values of 79 MPa and 4.4 GPa, respectively. In addition, the elongation at break was also improved by the addition of GNP. In general, the results were more pronounced for GN, revealing the effect of GNP size. As a result, the use of smaller GNP is recommended.

The resulting nanocomposites exhibited unique characteristics and properties that have the potential to drive the development of innovative solutions and products for the automotive industry.

In summary, the unique characteristics and properties exhibited by the developed nanocomposites have significant potential to drive innovation within the automotive industry. The enhanced mechanical performance improved thermal stability, and tailored crystallization behaviour of these nanocomposites are relevant for the creation of new solutions and products. These advances could lead to the development of lighter, stronger, and more durable automotive components, ultimately contributing to improved vehicle performance, safety, and efficiency.

6.3 Case-study

A case-study was conducted to validate the optimal processing parameters defined previously in the production of a 3D-shape component prototype by the T-RTM technology. By selecting a U-shaped structure located under the car seats, the study aimed to understand how the process and material properties would be affected by the change in geometry.

Higher injection pressures were required to ensure that the entire mould cavity was adequately filled with the polymer mixture. Despite this difference, a comparison of the results obtained from two-dimensional and three-dimensional approaches showed a consistent and similar behaviour in terms of the polymerization mechanism. This finding suggests that even with increased amounts of material and changes in geometry, the fundamental characteristics of the polymerization process remain largely unchanged. It can therefore be suggested that the transition to an industrial-scale T-RTM process is likely to show a similar behaviour.

The preliminary environmental impact assessment showed that the T-RTM technology offers advantages in terms of reduced environmental impact in several categories. A lower carbon footprint was achieved for the RTM process compared to T-RTM. RTM is a technology with well-defined process conditions, whereas T-RTM process conditions are still being optimized. The thermoplastic part produced by T-RTM had a lower environmental impact in 11 of the 16 categories assessed. The main factor contributing to this result is the fact that the thermoplastic matrix can be re-used through the recycling process, which is not possible with the incineration process of the thermoset target product.

The impact of the possible incorporation of GNP on the life cycle of the target product was not included in this study. When comparing the T-RTM process with the RTM process, there is not enough data to support the analysis.

6.4 Suggestions for future work

The overall objective of this thesis was to investigate the production of PA6 and PA6/graphene-based materials for potential use in the automotive industry. From the conclusions drawn in the previous sub-sections, several topics for future research have emerged. It is worth noting that the initial stages of this project involved continuous modifications to the laboratory equipment to improve process and quality.

- **Improving technology for process reproducibility:** One of the main challenges identified is the lack of a reliable equipment to ensure both the quality of the parts produced and the process reproducibility, particularly in terms of reaction control. The complexity of the polymerization reaction has an impact on the robustness of the system, which affects part quality and process reliability. To meet this challenge, equipment improvements are being investigated in several areas:
  - Dosing and Injection unit: Developing solutions that ensure melting, accurate dosing, and optimal mixing of raw materials is crucial. Simulation techniques can help to select appropriate injection systems by analysing resin flow;
  - Mixing unit: Ensuring proper homogenization of raw materials and controlling temperature and pressure during mixing are essential. Novel mixing solutions, possibly integrated into the moulding area, can be explored to promote homogenization, and avoid void formation;
  - Mould unit: The mould unit plays a key role in the T-RTM process. Optimizing mould geometry for material flow or introducing a dynamic mould can have a significant impact on part quality. Simulation software can assist in mould design and process optimization.
- **Additives Investigation:** The investigation of additives and their effect on PA6 properties, such as liquid catalysts and impact modifiers, can contribute to tailoring material characteristics. Different catalysts and activators can significantly influence the properties of the final material. NYRIM® C1 is a liquid catalyst that works at low moulding temperatures. Its unique properties can influence the polymerization process and potentially lead to desired material properties. Bruggolen® C540 is also a catalyst that acts as an impact modifier, improving the Charpy impact strength of the finished material.
- **Moisture content control:** Moisture content can have a significant effect on the properties, such as thermal or mechanical, of PA6 and its composites. Close monitoring and control of moisture during storage and processing is therefore essential to better understand its influence and to optimise the manufacturing process for consistent and high quality results.
- **Graphene-based materials:** Based on the conclusions of the previous section, further research is needed to further improve the dispersion of fillers within the polymer matrix. Therefore, several future work plans and research objectives are proposed:
  - Modification of GNP: Exploring various modification techniques for GNP could significantly affect their dispersion within the polymer matrix. Investigation of methods such as controlled thermal treatment without chemical agents could lead to improved properties and cost-effective production. The modification process should be carefully optimized to balance dispersion improvement with potential changes in graphene properties;
  - Synergistic fillers: Investigating the synergistic effects of combining different types of nanofillers, such as GNP and clay, is a promising work. Understanding

how these different fillers interact within the matrix can lead to composite materials with improved properties. Research should focus on identifying filler combinations that provide improved mechanical, thermal and electrical performance.

- **Environmentally friendly materials:** As industries strive to reduce their environmental impact, the development and implementation of sustainable materials are becoming increasingly important. The production of bio-based composites, which combine bio-based thermoplastics with natural fibres (ramie, hemp, sisal, kenaf, etc.) or recyclable reinforcements, is the starting point for the production of green composites.

Appendices

Appendix A

Materials selection and description

For successful implementation of anionic ring-opening polymerization of ε-caprolactam to PA6, it's crucial to carefully select a suitable catalyst and activator that can interact effectively with the monomer. In addition, proper storage of raw materials is of paramount importance due to the sensitivity of anionic polymerization to moisture and the inherent hydrophilic nature of these materials. Special precautions should be taken to prevent any exposure of the raw materials to moisture.

The material selection of CL, catalyst and activator system were made based on availability and material information from the suppliers. Many material suppliers offer CL monomer suitable for anionic polymerization (Table A1):

Table A1. Suppliers for CL monomer.

Supplier	Product name	Form
Brüggemann Chemical	AP-Nylon®	Flakes
BASF	Caprolactam	Liquid
Lanxess	AP caprolactam	Flakes

CL monomer plays a key role in the anionic ring-opening polymerization process for the production of PA6. It is therefore essential to handle the CL monomer under conditions that ensure its moisture-free state, such as in an inert atmosphere and under vacuum conditions.

In the context of material characterization and process development, the CL monomer chosen was AP-NYLON® from Brüggemann GmbH & Co. KG (Germany), which has a moisture content of less than 150 ppm. Preliminary tests have shown that Brüggemann Chemical's CL monomer, due to its low moisture content of 0.01% (100 ppm), allows faster processing when combined with suitable catalysts and activators. This CL monomer is supplied in the form of flakes (as shown in Figure A1) with a diameter of 2-4 mm and a flake thickness of 0.6 mm, packed in 25 kg aluminium-lined bags. An overview of some properties of AP-Nylon® Caprolactam flakes from Brüggemann GmbH can be found in Table A2:

Table A2. Properties of AP-Nylon®.

Property	Value
Solidification temperature (dry)	≈ 69 °C (ISO 7060)
Moisture content	max. 0.01 % (m/m)
Purity Caprolactam (dry)	min. 99.9 % (m/m)
Density	1.01 g/cm^3
Molecular weight	≈ 113 g/mol

For the selection of the catalyst and activator system, products offered by Brüggemann GmbH & Co. KG were chosen. The same reasoning as for the monomer selection was applied. The choice was based on the availability of the solid catalyst (Bruggolen® C10) and the activator (Bruggolen® C20P). This reactive system has proven to be highly effective in producing uniform PA6 parts of consistently high quality. The process has short production cycles with demoulding in less than 10 minutes. In addition, the process operates at low casting temperatures, with a melt temperature range of 110 to 140ºC and a mould temperature range of 130 to 170ºC.

An additional advantage of this system is that Bruggolen® C20P contains a blocked diisocyanate, which prevents the diisocyanate from reacting with substances other than caprolactam (CL). This feature ensures the stability and specificity of the polymerization process, contributing to the overall reliability and reproducibility of the production of high quality PA6 parts.

By using this catalyst and activator system from Brüggemann GmbH, the anionic polymerization process becomes well controlled, efficient, and conducive to the generation of consistently superior PA6 products.

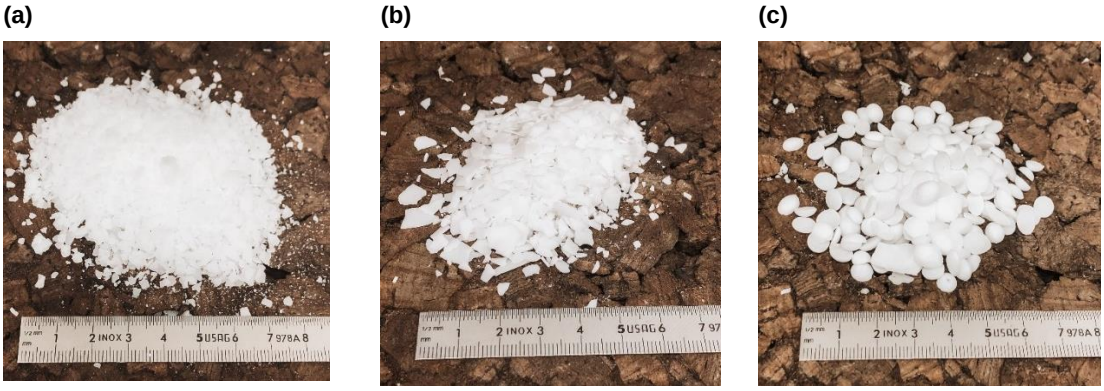

Figure A1. Flakes of **(a)** CL; **(b)** catalyst C10 and **(c)** activator C20P.

Preliminary tests showed that the use of liquid forms of catalyst and activator had a tendency to react and solidify when exposed to ambient air. Table A3 provides a summary of typical properties associated with the selected catalyst and activator:

Table A3. Typical properties of Bruggolen® C10 catalyst and Bruggolen® C20P activator.

	Bruggolen® C10[1]	**Bruggolen® C20P[2]**
Composition	17-19% sodium caprolactamate in caprolactam	17% blocked diisocyanate in caprolactam with a cyanate (NCO)
Melting temperature	≈ 68 ºC	> 60 ºC
pH value	≈ 13.3	≈ 5.6
Density	1.1 g/cm^3	1.2 g/cm^3
Molecular weight	≈ 135 g/mol	≈ 394 g/mol

[1] BrüggemannChemical. Product data sheet C10. Available at: https://www.brueggemann.com/.
[2] BrüggemannChemical. Product data sheet C20P. Available at: https://www.brueggemann.com/.

Appendix B

T-RTM laboratory equipment

The research and experimental work was carried out using the equipment described in this section. An internally developed semi-automatic T-RTM laboratory apparatus was designed and constructed (Figure B1)[3].

The project started with the creation of a CAD design using Solidworks 2016 software, followed by computerized numerical control (CNC) machining to develop the equipment. After assembly, an ongoing process of optimization testing was carried out. This laboratory equipment allows precise compaction of the mixture in the mould, uniform mixing of the reactive mixture and careful control of the quantity and ratio of reagents used.

The aim of this prototype is to promote a deeper understanding of the process and to enable laboratory scale experimentation. In the future, it could serve as a blueprint for industrial-scale installations.

The laboratory T-RTM setup includes a dosing unit with two tanks, a mixing head, a mould heating system and a pressure and vacuum control system.

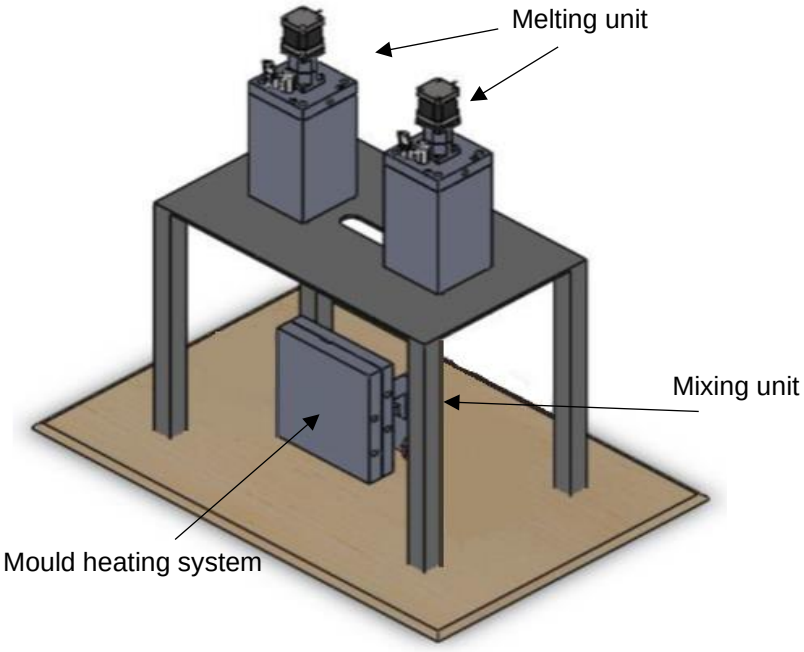

Figure B1. CAD image of T-RTM laboratory equipment employed.

A schematic diagram of the T-RTM system used in this work is shown in Figure B2. The system consists of two tanks, one for the activator/monomer (A), and another one for the catalyst/monomer (B), which meet at the mixing head.

Each tank is equipped with a heating system and a stirrer. Following melting the components, A and B flow through separate inlets into the mixing head while being subjected to controlled

[3] Martins, F. Materiais compósitos de matriz termoplástica processados por T-RTM - Master Thesis. (University of Aveiro, 2017).

pressure (3bar) and vacuum conditions (150 mbar absolute). Here, the components merge and mix before entering the mould. The two components mix as they pass through the mixing head.

As shown in Figure B2, each tank is connected to a nitrogen line. A nitrogen line is connected to each tank for purging the moisture from tanks, and injection lines, and to flush the system after injection to prevent the occurrence of polymerization within the heated parts.

Using impingement, the reactive mixture is introduced into a pre-heated mould at a temperature determined by experimental parameters. The mould has a vacuum inlet connected to the outlet of the mould to facilitate the removal of air.

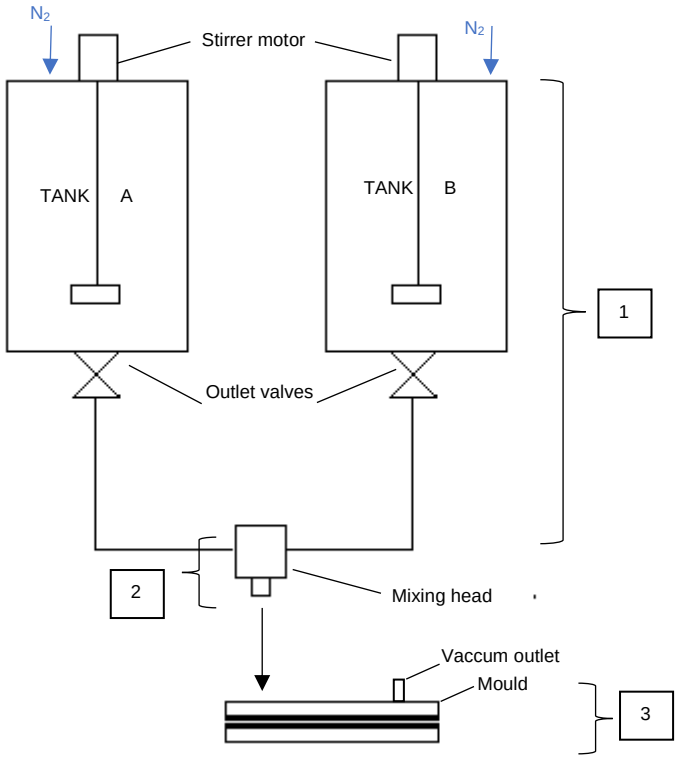

Figure B2. Schematic diagram of the flow network for the T-RTM lab equipment.

Temperature control within the system is achieved using four PID RS ESM-9920 temperature controllers, which are responsible for managing the temperatures of the tanks, mixing head and mould.

The temperature in the tanks and pipes (1) can be adjusted within the range of 80-90°C. The mixing head cylinders (2) can reach temperatures between 100-120°C. The mould polymerization unit (3) operates within a temperature range of 130-170°C to facilitate the polymerization reaction.

An Arduino Mega 2560 R3 is used to program and control the motors. This Arduino unit is connected to a Big Easy Drive, which has the role of transmitting the necessary commands to the motors, allowing precise control of their operation.

Melting unit

To initiate the reaction, the raw materials must be heated to temperatures above their respective melting points. As shown in Appendix A, the monomer has the highest melting point of the three raw materials. It is therefore essential that the materials are heated to temperatures above 69°C.

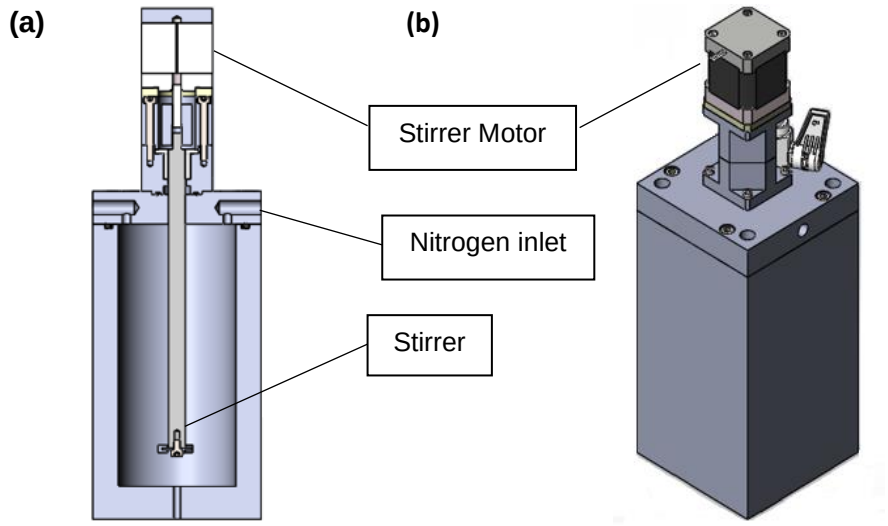

Figure B3. Isometric view **(a)** and sectional view **(b)** of a tank.

The design of each tank (Figure B3) prioritized easy disassembly for efficient cleaning procedures. These tanks, have a storage capacity of 1.2L, and were fabricated from aluminium and feature a detachable cover. A mechanical stirrer and nitrogen connection are incorporated into each tank. The CL monomer was divided equally between the two tanks. To one tank, the catalyst (C10) was introduced, while the activator (C20P) was added to the other. The melt temperature in each tank was set at 90 ºC with stirring. The relatively low melt viscosities of the raw materials required minimal mixing within each tank to achieve a uniform mix. It's important to note that the raw materials are highly hygroscopic, which underlines the need for moisture protection during the processing phase.

Since atmospheric air naturally contains moisture, it's essential to either remove the air or use an inert gas, such as nitrogen or argon, with a well-regulated moisture content. This approach creates a gas-free environment, effectively mitigating moisture-related concerns.

Mould

The polymerization reaction takes place inside the mould. Image of CAD model and actual images of the mould are shown in Figure B4. The mould cavity is designed with plate-like dimensions measuring 280mm x 150mm x 2mm. These dimensions were chosen to facilitate the production of mechanical test specimens in accordance with various testing standards.

The selection of aluminium as the mould material, as opposed to stainless steel, is primarily guided by practical considerations such as ease of machining, lower cost, and reduced weight. Aluminium, particularly the 3003 alloy, has a high thermal conductivity (190 W/mK), in contrast to

steel (16 W/mK)[4]. As a result, aluminium is more effective at conducting heat than steel. However, there are certain drawbacks associated with aluminium's high thermal conductivity, which can result in heat energy being dissipated into the environment. While this may not pose a significant issue at the laboratory scale, it can lead to substantial heating power costs in larger scale production. Another limitation of aluminium is its relatively lower hardness in comparison to steel, making it more susceptible to dents and scratches during the demoulding process.

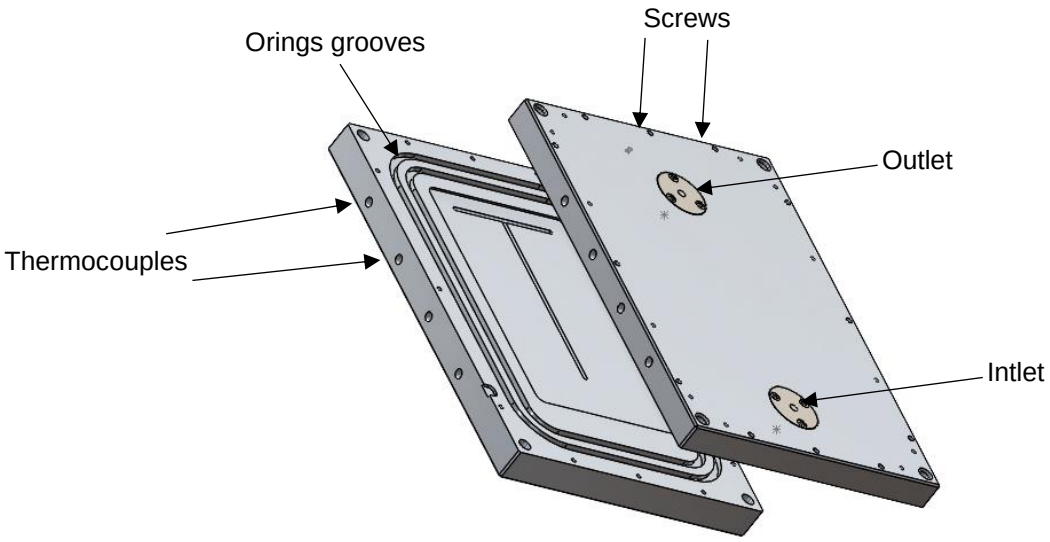

Figure B4. CAD image of the mould.

The mould is composed of two distinct parts: the upper and lower sections (Figure B4). The upper part contains the injection line, which is machined to allow direct and uniform filling of the compound. The lower part of the mould contains the mould cavity.

In the lower part of the mould, two grooves have been incorporated to accommodate o-rings. These o-rings play a vital role in providing a reliable seal for the mould. In particular, PFA-VMQ (Vinyl Methyl Silicone) o-rings were used for this sealing function. These o-rings (Figure B5) are constructed with a silicone (VMQ) rubber core encapsulated in a fluoroplastic material. This choice gives them exceptional temperature resistance, capable of withstanding temperatures up to 260ºC and even temporary exposure to 300ºC without compromising their inherent properties.

FKM Viton® and PTFE o-rings were also tested as part of the process. However, certain problems were encountered with both materials. FKM Viton® o-rings showed a tendency to permanent deformation, accompanied by swelling and an increase in weight. On the other hand, PTFE o-rings, while possessing rigidity, were not suitable for providing an effective seal due to their inflexible nature.

[4] Biswas, S. et *al., Int. J. Energy Res.* **42**, 3977–3986 (2018).

Figure B5. PFA-VMQ orings used in mould cavity.